University of
South-Eastern Norway

Ashish Shrestha

Estimation of the energy-mix proportion for the secure operation of converter dominated power system

Dissertation for the degree of Ph.D
Process, Energy and Automation

Faculty of Technology, Natural Sciences and Maritime Studies

University of
South-Eastern Norway

Ashish Shrestha

Estimation of the energy-mix proportion for the secure operation of converter dominated power system

A PhD dissertation in
Process, Energy and Automation Engineering

Dedication

To my teachers, family, and friends without whom I could not complete this work.

Acknowledgments

Abstract

The modern power system has undergone significant transformations driven by the necessary for environmental sustainability, technological progress, and evolving energy demands. A notable distinction between the modern power system and its conventional complement lies in the increased integration of renewable energy sources (RESs). This shift towards RESs, such as solar photovoltaics (PV), wind turbines, and hydropower, has significantly reduced carbon emissions and emphasized environmental sustainability. The modern power system also encompasses technological advancements in power electronic converters (PECs) and smart grid infrastructure, as well as a focus on decentralization and distributed energy resources (DERs) at the local level.

Despite these advancements, the integration of inverter-based resources (IBRs) contains challenges to grid stability, supply-demand balance, and system frequency control. One of the key challenges is the reduced system inertia caused by the high penetration of IBRs such as wind turbines and solar PV. System inertia, represented by the kinetic energy of rotating masses in conventional generators, helps maintain stable voltage levels and frequency during contingencies. However, the low inertia of PEC-based technologies limits the system's ability to withstand disturbances and maintain stable frequency. This reduced inertia and the intermittent nature of RES generation can lead to frequency fluctuations and instability in the power grid.

Furthermore, the uncertainties introduced by the stochastic nature of RES generation complicate the stability and secure operation of IBR-dominated power systems. Fluctuations in RES output, coupled with varying consumer demand, require effective balancing mechanisms to ensure a reliable power supply and avoid grid instability. Addressing these uncertainties necessitates the development of advanced control strategies and system-wide coordination mechanisms to maintain stability and security in IBR-dominated power systems.

This thesis investigates the stability and secure operation of power systems dominated by IBRs. It explores the unique dynamic characteristics and operational complexities introduced

by the high penetration of RESs and reliance on PECs. The research focuses on addressing challenges related to reduced system inertia, frequency stability, and uncertainties in the demand/supply chain. It emphasizes the development of advanced modeling techniques, control algorithms, and optimization methods tailored to IBR-dominated power systems.

The research also emphasizes the significance of day-ahead and online estimation of power system parameters and time-series data analysis. Online estimation enables continuous monitoring and estimation of the energy-mix proportion, allowing operators to proactively manage the system, optimize its performance, and effectively integrate the technologies and RESs. This thesis utilizes techniques such as deep reinforcement learning (DRL) and online simulation to develop innovative strategies, control mechanisms, and optimization frameworks for the secure operation of converter-dominated power systems.

Through comprehensive studies and simulations, this PhD thesis provides valuable insights, practical strategies, and control mechanisms for enhancing the stability, reliability, and security of IBR-dominated power systems. The findings contribute to the ongoing efforts of decarbonization, renewable energy integration, and the transition to a sustainable energy future. By effectively addressing stability challenges, optimizing resource utilization, and leveraging advanced technologies, this research paves the way for a secure, reliable, and resilient power system.

Keywords: Power System Dynamics; Power Electronic Converter; Inverter Based Generators; Machine Learning.

List of papers

Following is the list of main publications that were completed during this PhD study.

Article 1

Shrestha, A., Mohammed A.M. Y., Sharma, B. and Gonzalez-Longatt, F. A narrative review highlighting challenges and opportunities for making 100% renewable grid. [Submitted, Renewable and Sustainable Energy Reviews]

Article 2

Shrestha, A. and Gonzalez-Longatt, F., 2021. Frequency stability issues and research opportunities in converter dominated power system. Energies, vol. 14, issue 14, pp. 4184. doi: 10.3390/en14144184

Article 3

Shrestha, A. and Gonzalez-Longatt, F., 2021. Parametric sensitivity analysis of rotor angle stability indicators. Energies, vol. 14, issue 16, pp. 5023. doi: 10.3390/en14165023

Article 4

Shrestha, A., Ghimire, B. and Gonzalez-Longatt, F., 2021. A Bayesian model to forecast the time series kinetic energy data for a power system. Energies, vol 14, issue 11, pp. 3299. doi: 10.3390/en14113299

Article 5

Shrestha, A., Rajbhandari, Y. and Gonzalez-Longatt, F., 2024. Day-ahead estimation of energy-mix proportion for the secure operation of converter dominated power system. International Journal of Electrical Power and Energy Systems, vol 155, part B, no. 109560. doi: 10.1016/j.ijepes.2023.109560

Article 6

Shrestha, A., Marahatta, A., Rajbhandari, Y. and Gonzalez-Longatt, F., 2023. Deep reinforcement learning method in estimation of electricity-mix proportion for the secure operation of converter dominated power system. [Revised, Energy Reports]

The list of other publications that were produced as a result of research collaborations during the PhD period is provided below. Although some of the published articles may not have a direct connection to the PhD research work, they did help and advance the necessary knowledge and abilities to complete this PhD study.

Article 7

Shrestha, A. and Gonzalez-Longatt, F., 2022. Parametric sensitivity analysis of rotor angle stability indicators: Simulation case. Energy Reports, vol. 8, pp. 727-735. doi. 10.1016/j.egyr.2021.11.233

Article 8

Rajbhandari, Y., Marahatta, A., **Shrestha, A**., Gachhadar, A., Thapa, A., Gonzalez-Longatt, F., Guerrero, J.M. and Korba, P., 2022. Load prioritization technique to guarantee the continuous electric supply for essential loads in rural microgrids. International Journal of Electrical Power & Energy Systems, 134, p.107398. doi: 10.1016/j.ijepes.2021.107398

Article 9

Yassin, M., **Shrestha, A.,** Rabie S., 2023. Digital twin in power system research and development: Principle, scope, and challenges. Energy Reviews, vol. 2, issue 3, no. 100039. doi. 10.1016/j.enrev.2023.100039

Article 10

Malla, T.B., Bhattarai, A., Parajuli, A., **Shrestha, A.,** Chhetri, B.B., Chapagain, K., 2022. Status, Challenges and Future Directions of Blockchain Technology in Power System: A State of Art Review. Energies, vol 13, issue 22, pp. 8571. doi. 10.3390/en15228571

Article 11

Sharma, B., **Shrestha, A.,** Terriche, T., Lashab, A., Guerrero, J. M., 2022. Sharing sequence components of reactive power in a three-phase four-wire islanded microgrid. Electric Power Systems Research, vol 213, no. 108675. doi. 10.1016/j.epsr.2022.108675

Article 12

Sharma, B., Pankaj, P. K., Terriche, T., Saim, A., **Shrestha, A.,** Su, C., Guerrero, J. M., 2023. Power Sharing in Three-Level NPC Inverter Based Three-Phase Four-Wire Islanding Microgrids With Unbalanced Loads. IEEE Access, vol 11, pp. 20725-20740. doi. 10.1109/ACCESS.2023.3250219

Article 13

Marahatta, A., Rajbhandari, Y., **Shrestha, A.,** Phuyal, S., Thapa, A., Korba, P., 2022. Model predictive control of DC/DC boost converter with reinforcement learning. Heliyon, vol. 8, no. 11416. doi. 10.1016/j.heliyon.2022.e11416

Article 14

Rajbhandari, Y., Marahatta, A., Ghimire, B., **Shrestha, A**., Gachhadar, A., Thapa, A., Chapagain, K. and Korba, P., 2021. Impact study of temperature on the time series electricity demand of urban nepal for short-term load forecasting. Applied System Innovation, vol. 4, issue 3, pp. 43. doi. 10.3390/asi4030043

Article 15

Marahatta, A., Rajbhandari, Y., **Shrestha, A.,** Singh, A., Thapa, A., Gonzalez-Longatt, F., Korba, P. and Shin, S., 2021. Evaluation of a lora mesh network for smart metering in rural locations. Electronics, 10(6), p.751. doi. 10.3390/electronics10060751

Article 16

Rajbhandari, Y., Marahatta, A., **Shrestha, A**., Gachhadar, A., Thapa, A., Gonzalez-Longatt, F., Korba, P., 2023. Enhanced Demand Side Management for Solar-Based Isolated Microgrid System: Load Prioritization and Energy Optimization. IET Smart Grid.

$$\overline{}$$
x

List of tables

List of figures

Table of contents

1 Introduction

1.1 Background

The modern power system has witnessed significant changes and advancements compared to conventional power systems. This transformation has been driven by various factors, including the obligation for environmental sustainability, technological progress, and evolving energy demands. A comparison between the modern power system and its conventional counterpart sheds light on the achievements made and the challenges encountered in the energy sector [1-3].

A noteworthy distinction between the modern power system and the conventional power system lies in the increased integration of renewable energy sources (RESs). Conventional power systems heavily rely on fossil fuel-based generation, such as coal and natural gas, which contribute to greenhouse gas emissions and environmental degradation. In contrast, the modern power system emphasizes the utilization of RESs like solar photovoltaics (PV), wind turbines, and hydropower to produce clean and sustainable electricity. This shift towards RES has resulted in a significant reduction in carbon emissions and an amplified focus on environmental stewardship [3, 4].

Moreover, the modern power system is marked by technological advancements, particularly in power electronic converters (PECs) and smart grid infrastructure. PECs, such as inverters and converters, play a crucial role in integrating RES into the grid, enabling efficient energy conversion, and facilitating grid stability. Smart grid technologies, encompassing advanced sensors, communication systems, and automation, have revolutionized power system management and control [5, 6].

Another key aspect of the modern power system is the increasing emphasis on decentralization and distributed energy resources (DERs). Conventional power systems typically rely on large-centralized power plants, with electricity transmitted over long distances to end consumers. In contrast, the modern power system incorporates DERs like rooftop solar panels, small wind turbines, and energy storage systems at the local level. This

decentralized approach allows for greater energy independence, grid resilience, and localized power generation, reducing transmission losses and enhancing overall system flexibility [7-9].

Despite these advancements, the modern power system faces several challenges. The integration of inverter-based resources (IBRs) such as solar and wind introduces issues related to grid stability, supply-demand balance, and system frequency control. Additionally, managing a diverse energy mix, addressing grid congestion, and mitigating cybersecurity risks are complex tasks for the modern power system. Efforts are underway to develop advanced control strategies, energy storage technologies, and grid infrastructure upgrades to overcome these challenges and ensure the secure and reliable operation of the modern power system [7, 10-13].
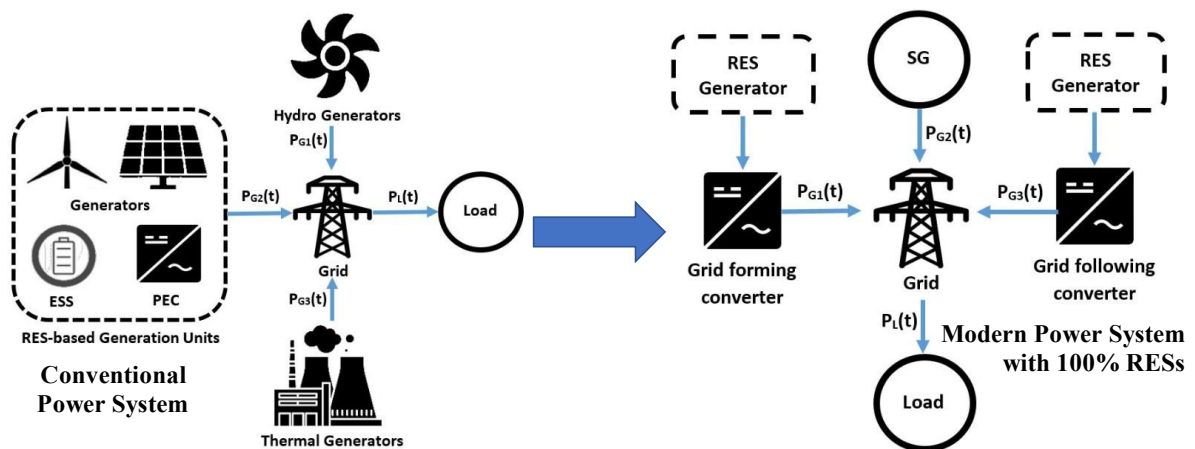
Figure 1.1: Schematic representation of power system transformation.

Figure 1.1 presents an overview of the transformation of a conventional power system into a modern power system. This Figure shows that the modern power system is characterized by the increased integration of RESs, advancements in PECs and smart grid technologies, and a shift towards decentralization and DERs. While notable progress has been made in achieving a cleaner and more sustainable energy sector, challenges continue in areas such as grid stability, irregular generation, and system management. Ongoing research and development endeavors are focused on tackling these challenges and further enhancing the efficiency, reliability, and resilience of the modern power system.

1.2 Problem Statement

The stability and secure operation of IBR-dominated power systems present significant challenges in the modern energy landscape. With the increasing integration of RESs and PECs, ensuring the reliable and resilient operation of these systems becomes crucial. IBR-dominated power systems, characterized by a high penetration of RESs and a reliance on PECs, exhibit unique dynamic characteristics and operational complexities that can impact system stability and security [14].

A major challenge in IBR-dominated power systems is the reduced system inertia caused by the high penetration of IBRs such as wind turbines and solar PV. The low inertia of PEC-based technologies limits the system's ability to withstand disturbances and maintain stable voltage levels [15]. Similarly, frequency stability is essential for the reliable and secure delivery of electricity to consumers [3]. The intermittent nature of RES generation further adds complexity to maintaining frequency stability, as variations in RES output can interrupt the balance between power supply and demand [16].

The stochastic nature of RES introduces uncertainties in the demand/supply chain, further complicating the stability and secure operation of IBR-dominated power systems. Fluctuations in RES output, coupled with varying consumer demand, require effective balancing mechanisms to ensure a reliable power supply and avoid grid instability. Developing efficient control strategies and system-wide coordination mechanisms to address these uncertainties is crucial for maintaining stability and security in IBR-dominated power systems [17-19].

Furthermore, the increasing complexity of power system dynamics and the integration of new technologies necessitate the exploration of innovative approaches for stability analysis, control, and operational planning. Traditional methods and tools used in conventional power systems may not be sufficient to address the unique challenges posed by IBR-dominated systems. Therefore, there is an insistent need for research that focuses on developing advanced modeling techniques, control algorithms, and optimization methods specifically adapted to the requirements of IBR-dominated power systems [20].

The problem statement emphasizes the challenges associated with the stability and secure operation of IBR-dominated power systems. The reduced system inertia, uncertainties introduced by RES, and the need for advanced modelingand control techniques are critical issues that require attention. Conducting research in this field is essential for developing effective strategies, algorithms, and operational frameworks that enhance the stability, reliability, and security of IBR-dominated power systems, paving the way for a sustainable and resilient energy future.

1.3 Motivation

To successfully transition to a sustainable and low-carbon energy landscape, it is crucial to understand and tackle the stability challenges presented by power systems dominated by IBRs. The integration of RESs offers a substantial reduction in greenhouse gas emissions and environmental impact when compared to conventional fossil fuel-based generation. However, the dynamic characteristics of IBRs and their interaction with the power grid introduce stability challenges that must be resolved for the power system to operate reliably and sustainably.

Ensuring grid resilience and reliability is of utmost importance. Power systems must maintain stable frequency, voltage, and power flow to guarantee the dependable delivery of electricity to consumers. As IBRs become more prevalent, the reduced system inertia and intermittent nature of RES generation create obstacles to grid stability. By addressing these stability issues in IBR-dominated systems, the power grid's resilience and reliability can be enhanced [3].

Optimizing resource utilization also serves as a key driver for research in this field. IBR-dominated power systems comprise a diverse mix of energy resources, including irregular RESs and controllable PECs. Achieving the most effective utilization of these resources requires the development of advanced control strategies and coordination mechanisms to maintain system stability while maximizing the integration of renewable generation [21].

Similarly, technological advancements play a pivotal role in advancing research efforts. With the progress made in power electronic devices, smart grid technologies, and control systems,

new opportunities arise to improve the stability of IBR-dominated power systems [22]. Leveraging these technological advancements enables the development of innovative modeling techniques, control algorithms, and operational strategies that effectively address the unique challenges posed by IBRs.

Moreover, the transition to a decentralized energy system is a significant motivation for researching power system stability. The increasing penetration of IBRs and DERs facilitates the establishment of a more decentralized and resilient energy system [23]. However, this transition introduces complexities in terms of system operation, coordination, and stability [24]. By conducting this research work, solutions can be developed to integrate and operate DERs while maintaining grid stability.

The motivation for conducting this research work arises from the growing significance of RESs and the shift towards a cleaner and more sustainable power system. Addressing the challenges associated with frequency stability is essential for the reliable functioning of frequency-sensitive devices and ensuring overall power system reliability and resilience. The motivation to conduct research lies in the need to devise effective strategies, control mechanisms, and mitigation measures. It is aimed to explore innovative solutions that enhance power systems' ability to accommodate high levels of RES integration while maintaining stability.

Additionally, the economic implications of power system instability should not be ignored. Power system operators and market participants must consider the costs associated with abnormalities and the provision of ancillary services [16]. Conducting new research can facilitate the development of cost-effective solutions that optimize RES utilization, enhance system efficiency, and reduce reliance on expensive ancillary services.

The motivation to conduct this research work, particularly in power systems dominated by IBRs, arises from the vital of addressing the unique challenges presented by the integration of RESs and PECs. By understanding and mitigating stability issues, it becomes possible to ensure

the reliable, resilient, and sustainable operation of IBR-dominated power systems, thus contributing to the global transition towards a clean energy future.

1.4 Research Objectives

The main objective of this PhD study revolves around developing an estimation methodology to ensure the secure operation of power systems dominated by IBRs under normal conditions and contingencies. The study comprises three specific objectives that were pursued throughout the PhD.

a. To create a methodology that can calculate the minimum proportion of technologies (i.e., synchronous generators, grid-forming converters, grid-following converters, and flexible demand) to guarantee frequency stability.
b. To create a system architecture and information model suitable for the created methodology.
c. To evaluate the developed methodology and validation.

The first objective focuses on creating a methodology capable of calculating the minimum proportion of various technologies, including synchronous generators, grid-forming converters, grid-following converters, and flexible demand, necessary to maintain frequency stability. This methodology aims to determine the optimal mix of these technologies to ensure the system operates within the desired frequency range. By accurately assessing the required proportions, the methodology contributes to maintaining stable frequency conditions.

The second objective centers around developing a system architecture and information model that are well-suited for the aforementioned methodology. The information model is designed to capture and integrate data from diverse sources within the power system, providing a comprehensive overview of its operation. This architecture and model facilitate the effective implementation and utilization of the developed estimation methodology. Integrating data from different levels and considering historical information enhances the precision and dependability of the estimation process.

The third objective involves conducting simulations and testing the developed systems to validate their effectiveness. Day-ahead and online-simulation techniques are employed to evaluate the suitability and performance of the proposed methodology. The study adheres to relevant standards and grid codes to assess various system parameters, ensuring that the developed systems meet the required criteria and operate effectively in practical scenarios.

In summary, this PhD study's scope encompasses the development of an estimation methodology, supported by a suitable system architecture and information model, to enable the secure operation of IBR-dominated power systems. The methodology determines the minimum proportions of power-generating technologies necessary for maintaining frequency stability. The information model integrates online and historical data from different levels of the power system, contributing to estimation. By fulfilling these objectives, the study contributes to advancing secure and reliable operation in IBR-dominated power systems.

1.5 Overall Thesis Layout

This thesis represents the result of the research works conducted during the PhD study. It encompasses a collection of six scientific publications that are organized and presented across different chapters. These publications serve as the core foundation for the thesis. Additionally, other publications result from collaborative research efforts during the PhD period. While some of these publications may not directly link to the specific research conducted for the PhD, they have played a valuable role in advancing the necessary knowledge and skills required to complete this study successfully.

The remaining sections of this thesis are organized as follows:

1.5.1 Chapter 2

This chapter aims to analyze various scenarios, challenges, historical and current research activities, and potential solutions related to power system dynamics, PECs, and the modern power system. The insights drawn primarily from **Article 1, Article 2,** and **Article 3** contribute

valuable knowledge to the research field and underscore the importance of studying RES-based power systems and their secure operation in the present context.

1.5.2 Chapter 3

This chapter focuses on short-term forecasting of kinetic energy in converter-dominated power systems. It presents a method using a Bayesian model to estimate the kinetic energy of the power system by forecasting univariate time-series data. The chapter demonstrates the effectiveness of the Bayesian model in accurate forecasting and analyzing kinetic energy, which can be leveraged to estimate system inertia and other dynamic characteristics. The content of this chapter is primarily based on **Article 4**, highlighting the significance of time-series data analysis, specifically kinetic energy, for ensuring the secure operation of converter-dominated power systems. It serves as a valuable resource for understanding the importance of time-series data analysis in such systems.

1.5.3 Chapter 4

This chapter presents the findings from the research conducted in **Article 5**, emphasizing the effectiveness of the proposed approach in addressing various challenges related to reliability, system dynamics, stability, control efficiency, and security in IBR-dominated power systems. It emphasizes the importance of day-ahead estimation for decarbonization and renewable energy integration, aiming for a sustainable and environmentally friendly energy landscape.

1.5.4 Chapter 5

This chapter emphasizes the significance of online simulation in overcoming challenges associated with integrating IBRs and managing the dynamic behavior of power systems. The insights presented in this chapter, derived from the research conducted in **Article 6**, demonstrate the effectiveness of the proposed approach in addressing crucial challenges in IBR-dominated power systems. This chapter serves as a valuable resource, underscoring the importance of online estimation of power system parameters in ongoing efforts toward decarbonization and the integration of RESs.

1.5.5 Chapter 6

This chapter primarily focuses on the comprehensive discussion of the results obtained throughout the PhD research work. It delves into the relevance of these results and their contribution to the field and presents an overall conclusion. The chapter thoroughly discusses and synthesizes the findings, highlighting their significance and implications. It discusses the research journey, summarizing the key outcomes and drawing conclusions based on the conducted investigations.

2 Literature Review

Conventional generators incorporate governor controls that monitor machine speed, allowing adjustments to the input valve to regulate their speed and maintain system frequency. These controls ensure that the mechanical power input is adjusted during normal operation and minor imbalances, restoring the speed and system frequency to their nominal values. In the case of major disturbances, the governor control minimizes frequency deviations from the nominal value. Additional control systems and dispatch instructions further assist the system operator in the real-time management of the generation-demand balance. To mitigate frequency disturbances, a wide range of frequency control services from generators, loads, and other devices are deployed over different time intervals. After a significant system disturbance or imbalance, such as a sudden loss of generation, the frequency can deviate rapidly from its nominal value [25, 26].

However, the integration of RESs into the modern power system introduces new challenges. RESs, such as solar and wind, rely on weather conditions and environmental factors, leading to intermittent and unpredictable energy generation [27]. As power system developers strive to accommodate a significant share of RESs in the grid, PECs become fundamental components. Yet, the integration of RESs and PECs; IBRs pose stability concerns for the power system. Without appropriate modifications, a system heavily reliant on IBRs becomes vulnerable and unsustainable, ultimately impacting power system operation [28].

In today's technology-driven and automated era, ensuring a stable power supply has become increasingly critical. Frequency fluctuation stands out as a key factor that can disrupt the normal operation of the power system, potentially causing widespread blackouts. As the power system grows more complex due to the rapid expansion of PEC-based technologies and the prevalence of non-synchronous generators, it becomes essential to thoroughly investigate the underlying causes and consequences of an unstable power system. Additionally, exploring control techniques to address these issues is of paramount importance [29, 30].

To gain a comprehensive understanding of power system dynamics, PECs, and the modern power system, this chapter aims to analyze various scenarios, challenges, historical and current research activities, and potential solutions. The content draws primarily from **Article 1, Article 2** [3], and **Article 3** [31] providing valuable insights into this research domain and highlighting the significance of studying power system stability in today's context.

2.1 RES-based Future Power System

In this PhD research work, the author is delving into an IBR-dominated power system, one that hypothesized, is entirely powered by RESs. This raises an important question with far-reaching implications for the common future: Can a power system that's 100% powered by RESs be realistically achieved? This question needs deep research and analysis, transcending just academic interest.

If a global energy system can be created fully powered by RESs, it would be a significant step towards reducing carbon emissions and fighting climate change. This could be a pivotal point towards a more sustainable future. However, envisioning a 100% RES-based power system brings several questions and challenges to the forefront: Are renewable energy technologies reliable enough to meet global energy demand? How can the intermittency of certain RESs be addressed to ensure power grid stability? What might be the impact on the existing power infrastructure? To what extent do political decisions and social viewpoints influence this transition?

These are not just academic questions but urgent practical issues. The responses to these questions will shape the strategies to counter climate change and achieve sustainable development. In this section, it is aimed to argue on these queries, drawing from recent research and technological advancements. The goal, through a systematic review, is to assess the feasibility of a fully RES-based power grid, considering the technological, social, political, and geographical challenges involved. This sub-section mainly focuses on these discussions, using insights from **Article 1.**

The expedition to decipher the multifaceted implications of fully RESs in power generation necessitates a comprehensive journey through scholarly and institutional texts. This expedition unfolds in two primary phases. The initial phase encompasses the selection and gathering of academic articles that focus solely on RES-powered power systems, giving precedence to those available in complete English texts for straightforward analysis. The subsequent phase includes a thorough evaluation of these compiled articles, drawing on their insights to guide the discourse.
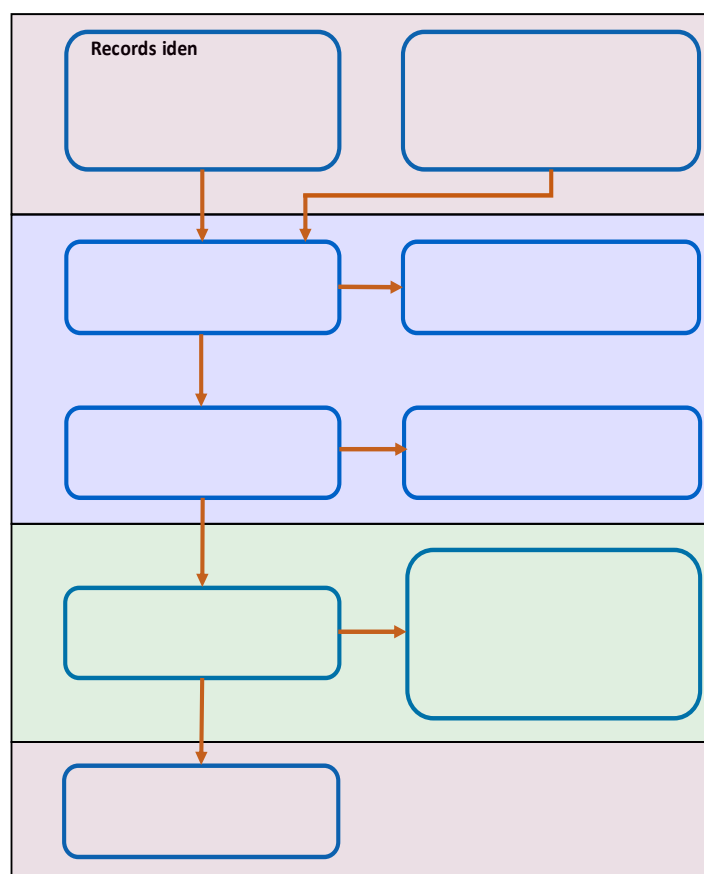
Figure 2.1: Process followed to identify the reference documents.

The investigation primarily addressed four central research questions as discussed. Figure 2.1 depicts the strategies employed throughout the analysis. The literature survey embraces a comprehensive approach, utilizing a meticulous keyword search method. The search parameters, such as "100% Renewable*" AND "power system*" OR "100% Renewable*" AND "energy system*", aid in identifying articles with these subjects appearing in the title, abstract,

or keywords. The intention is to uncover scholarly works that address renewable energy systems and their various subfields. The research influences respected literature databases like Web of Science and Scopus to accumulate publications related to the chosen keywords. A July 19, 2023 search yielded 359 and 696 records from Web of Science and Scopus, respectively.

Moreover, this study incorporates reports issued by various governmental and non-governmental bodies, such as the International Energy Agency (IEA), International Renewable Energy Agency (IRENA), National Renewable Energy Laboratory (NREL), Resources for the Future (RFF), Norwegian Center for Renewable Energy (SFFE), and others. The incorporation of governmental policies, guidelines, and regulations is crucial when appraising the viability of a wholly RES-based power grid. Information from relevant governmental reports supplements the findings to enhance understanding of the regulatory frameworks governing these technologies worldwide.

The initial engagement with the substantial collection of documents sourced from academic databases involves an exacting screening process. This process aims to eliminate potential redundancy in records across the databases. Given the extensive search across two primary databases, some overlap is imagined. Thus, the initial task is to meticulously sift through each entry, comparing and discarding identical documents to ensure the distinctiveness of each record in the dataset.

After the screening process, the unique set of documents undergoes an intensive review. This process transcends a cursory read-through; it involves an exhaustive inspection of each document. Each document's title, abstract, and keywords are examined to identify resources appropriate to the research objectives. This complex process requires a clear comprehension of the research questions and the selectivity to gauge whether each document could offer valuable insights or data. Titles offer a concise overview of the content, abstracts provide a study summary, and keywords help identify primary themes undertaken. This intense examination facilitates the refining of the document collection, ultimately yielding a manageable subset of 143 articles aligned with the research theme.

___

The filtered collection undergoes further refinement to pinpoint the most beneficial resources for the investigation. Several eligibility criteria guide this process: (a) relevance to the research questions, (b) type of the study, (c) technological focus, (d) time frame, and (e) credibility of the publishers. Each document must meet these specific requirements to be included in the study. Adhering to these stringent criteria results in a final compilation of 84 documents. Selected for their quality and relevance, these documents form the foundation of the research, granting a more intricate and profound understanding of the research topic. Figure 2.2 visually represents the key terms extracted from our chosen documents. The likelihood that a given word will appear increases as the size of the font increases.

Figure 2.2: Word cloud based on the terms used in the published publications.

These 84 documents serve as the primary references for deliberations on the feasibility of a 100% RES-based power system. The information from these sources facilitates a multifaceted exploration of the topic from technological, socio-economic, political, geographical, and policymaking perspectives. Each document uniquely highlights different aspects of RESs, offering valuable insights that guide discussions and shape understanding of the topic. The selection and analysis of these documents reveal both the challenges and prospects associated with transitioning to a fully RES-based power system.

Additionally, this chapter presents a detailed discussion of the INPS as a case study, connecting discussed points with a practical power system. The INPS has proven to be a successful project advancing towards a 100% RES goal. The data related to INPS, particularly in this study, are derived from documents produced by Nordic TSOs, governmental and non-governmental organizations, and research institutions.

2.1.1 Technical feasibility of 100% RES-based power system

The BP Statistical Review of World Energy documented that fossil fuels accounted for the largest chunk of the world's energy in 2020, contributing 61.3% of the total. The rest was generated by nuclear power (10.1%), hydroelectric power (16.1%), wind energy (5.9%), solar power (3.2%), and other renewable sources (0.9%) [32]. From a humble beginning, renewable energy is making strides in the electricity generation market due to substantial investment in RES technologies. The rise in renewable investments from 2004 to 2016 testifies to the promising emphasis on solar and wind technologies [33, 34]. Consequently, the discourse concerning the potential of renewables to completely surpass the existing power grid is intensifying.

In this dissertation, a joint statement by 47 renowned scientists from esteemed institutions and businesses posited that a quick transition to 100% renewable energy is conceivable, with the power sector possibly converting by 2030 and other sectors shortly after [35]. This notion is supported by a study by Zappa et al., who, through the simulation of seven scenarios for the European power system for 2050, suggested a fully renewable system could operate as effectively as the current one [36].

In contrast, Heard et al. expressed skepticism about models predicting a renewable future due to the absence of historical and empirical evidence. They further argued that an electricity system entirely dependent on renewable energy conflicts with urgent climate change mitigation measures [37]. Diesendorf et al. pointed out flaws in the critiques of a 100% RES-based system, including doubtful assumptions, inconsistencies, omissions, errors, and exaggerations. They contended that a complete transition to renewable energy is technically

and economically feasible, even though obstructed by political challenges and misinformation [38].

The Technological Momentum theory asserts that technological progress, which significantly shapes social evolution, is time-dependent [39]. It underscores the crucial role of engineers, scientists, and technically oriented managers in system innovation and development. The Concept of Progress further illuminates how new technologies can address social issues and contribute to progress and integrity [40]. The rapid pace of technological advancements, as proposed by Moore's Law in 1965, differs from Eugene E. Selk's linear progression theory [41, 42]. The idea of continual technological evolution is beautifully captured in a metaphor by Hartshorne and Weisse, emphasizing the dynamic nature of our perceptions and technological advancements [43].

The energy sector is transforming from conventional power systems primarily dependent on non-renewable energy sources to PEC-based systems incorporating RESs such as wind, solar, and hydroelectric power. Owing to their solid-state electronics, PECs offer efficient power conversion and improved control flexibility [3, 44, 45]. This shift is transforming power generation and revolutionizing transmission, distribution, and utilization sectors, laying the groundwork for a more sustainable and robust energy system.

However, RESs face challenges such as high energy costs, inefficiencies in transmission and storage, and issues with system dynamics and security [37, 46, 47]. Some researchers propose these challenges can be overcome by employing diverse grid topologies, energy resources, and control mechanisms [48-50]. Yet, integrating PEC-based RESs into the grid can increase the system's complexity and vulnerability, potentially leading to blackouts [3].

Several studies have examined the technical viability of achieving a 100% RES-based power system across different countries and regions, considering various renewable energy sources and storage technologies. For instance, Turkey has delineated a two-phase plan to transition from fossil fuels to solar PV and wind power [51]. Similarly, the Middle East/ North Africa

(MENA) region, Saudi Arabia, Denmark, the Maldives, and China have also demonstrated the technical and economic viability of a full RES [52-57].

Market design options for a 100% RES-based power system must consider investment incentives and operational factors to ensure cost recovery and effective resource allocation [58]. Countries like Barbados, China, Ireland, Sweden, and several European nations offer examples of how a 100% renewable energy system can be realized, considering system costs, technology integration, flexibility options, policy, and forecasting models for green electricity targets [59-63].

Battery technology is necessary for transitioning to terawatt levels of PV, as it can defend fluctuations and foster higher PV adoption rates [31, 64, 65]. Nigeria and California have highlighted the viability of a blend of natural gas and RESs for achieving 100% electrification and a 100% renewable electricity supply, respectively [66, 67]. Likewise, Australia has shown how spatial and temporal configurations, energy storage, and dispatchable RESs can boost the feasibility of a 100% national renewable energy supply [68].

Synchronous generators in hydropower, thermal, geothermal, and nuclear plants contribute to system inertia, providing resilience in emergencies [31, 65]. The optimization of hydroelectric reservoirs and secondary voltage control can help ensure a balanced and reliable energy system [69]. Countries with plentiful hydropower resources, like Norway, Iceland, Paraguay, Costa Rica, Tajikistan, Nepal, and Bhutan, are closer to achieving the goal of 100% RESs [70]. However, reaching this goal will necessitate substantial time, transformation, and technological advancement for countries with limited hydropower resources.

2.1.2 Social acceptability of 100% RES-based power system

The successful integration and long-term persistence of renewable energy projects significantly axis on social acceptance, as evidenced by several studies [52, 71]. The acceptability factor covers myriad determinants that shape society's stance towards a system and technology. In the realm of RESs and the prospect of a fully RES-powered grid, social perspectives play a pivotal role. Interestingly, most Lithuanians exhibit awareness and support

for renewable energy adoption [71]. African rural areas' receptivity towards RES depends on a blend of technical, economic, and social factors [72]. Another research underscores that socio-political, market, and community considerations predominantly shape Colombian perspectives towards RESs, thereby confirming that policies centered on energy justice and economic benefits substantially affect the social acceptance of these initiatives [73, 74].

In 2019, approximately 9.916% of the world's population lacked electricity access, predominantly residing in rural parts of developing and impoverished nations [75]. This brings to light a major challenge in RES implementation - achieving energy justice. Despite their considerable potential for renewable energy (around 45% by 2050) [76], Sub-Saharan Africa could only provide electricity to 46.75% of its population as of 2019 [75].

As environmental concerns accelerate, RESs are emerging as viable alternatives for decarbonization, especially in countries like the Nordic nations aiming for decarbonization by 2050. This suggests that environmental considerations might drive global RES deployment in the foreseeable future. The Convergence theory, derived from the Stage of Development Theory, can aid in overcoming energy equity and economic barriers [77]. Case studies, like that of Saudi Arabia, spotlight sector integration and potential social impact and advocate the efficient use of water resources via seawater reverse osmosis (SWRO) to augment public acceptability [53]. Research in the MENA region [52] emphasizes that job creation and economic diversification linked to a renewable energy transition can boost social acceptability.

Moreover, a global transition to 100% RES may generate around 35 million jobs by 2050, particularly in solar photovoltaic, battery storage, and wind power technology sectors [78]. For instance, a transition strategy for Denmark to achieve 100% decarbonization by 2045 [54] suggests social costs don't necessarily need to rise during this process, contributing significantly to social acceptance. The support from the public also strengthens with the projected job increase and the prospect of economic growth.

According to the Technological Determinism theory, the progression of technology shapes societies' structure and inherent values [79], a notion accepted by modern society that sees technology as a change catalyst. The transition towards sustainable energy systems must address community acceptability and energy justice to avoid issues related to social exclusion, community conflict, and environmental degradation [80]. Favorable regulatory frameworks backed by the government are indispensable for the social acceptance of RESs [81].

Promoting community participation, transparency, and inclusive planning processes can amplify social acceptance. Research indicates community ownership and participation in renewable energy projects may boost social acceptance by fostering local ownership, bringing economic benefits, and enhancing community engagement. Therefore, social acceptability is an indispensable factor in developing and implementing a fully RES-powered power system.

2.1.3 Geographical complexities for 100% RES-based power system

Establishing a power infrastructure entirely dependent on RESs presents considerable challenges driven by geographical constraints. Investigations have illuminated how the availability of resources, such as hydro, wind, solar, and even fossil resources, display distinct variances across geographical landscapes [51, 52]. For instance, the Middle East region demonstrates considerable solar potential and moderate wind potential, although it has limited resources for hydropower [70, 82]. On the contrary, most European countries show lower potential for solar energy. Figure 2.3 and Figure 2.4 illustrate the worldwide electricity distribution generated from diverse sources in 2020. Figure 2.3 scales the share of hydroelectric power from 0 to 100%, indicating that some nations are entirely reliant on hydropower.

On the other hand, the share of wind power is scaled up to 60%, suggesting that it accounts for only a minor part of the overall supply. Similarly, Figure 2.4 scales the fossil fuel power share from 0 to 100%, illustrating that certain nations rely entirely on fossil fuels. On the other hand, the power share for solar energy is scaled up to 5%, indicating it provides only a tiny proportion of the total supply. According to the data, some countries are exclusively

dependent on a single source, such as hydropower or fossil fuels, while others utilize a blend of various sources. These variations can be attributed to factors such as energy resource scarcity, political divide, or a combination of both [70, 82].

(a) Share of electricity that comes from hydropower

No data 0%   20%   40%   60%   80%   100%

(b) Share of electricity that comes from wind

No data 0%   1%   5%   10%   20%   30%   60%
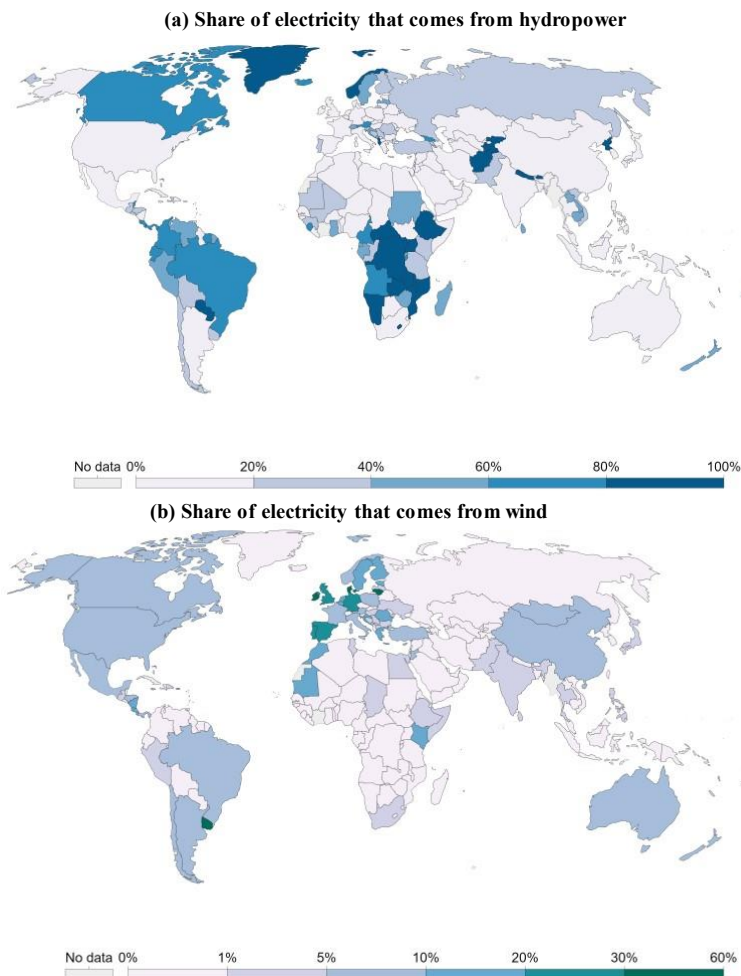
Figure 2.3: The share of electricity comes from hydro and wind resources [32, 33].

Geographical constraints also introduce unique challenges and opportunities. The Maldives, a low-lying archipelago nation, faces land scarcity, emphasizing the necessity to explore floating offshore technologies [56]. A study in Australia examines the potential geographical configurations for a reliable, cost-effective renewable energy system, taking into account the availability and unpredictability of wind and solar resources [68]. Research on Barbados acknowledges the need for imported biodiesel due to specific wind and sunlight patterns, underscoring the crucial influence of resource availability on system design [59]. China focuses

on the spatial distribution of wind, solar, biomass, and hydropower resources, which significantly influences the feasibility and scale of renewable energy deployment [60]. Scotland's grid largely benefits from wind power due to the country's abundant wind resources and favorable geographical position [83]. Cameroon's high solar resource potential and advantageous geographical location make PV the most promising technology for establishing a sustainable energy system [81].

(a) Share of electricity that comes from solar

(b) Share of electricity that comes from fossil fuels
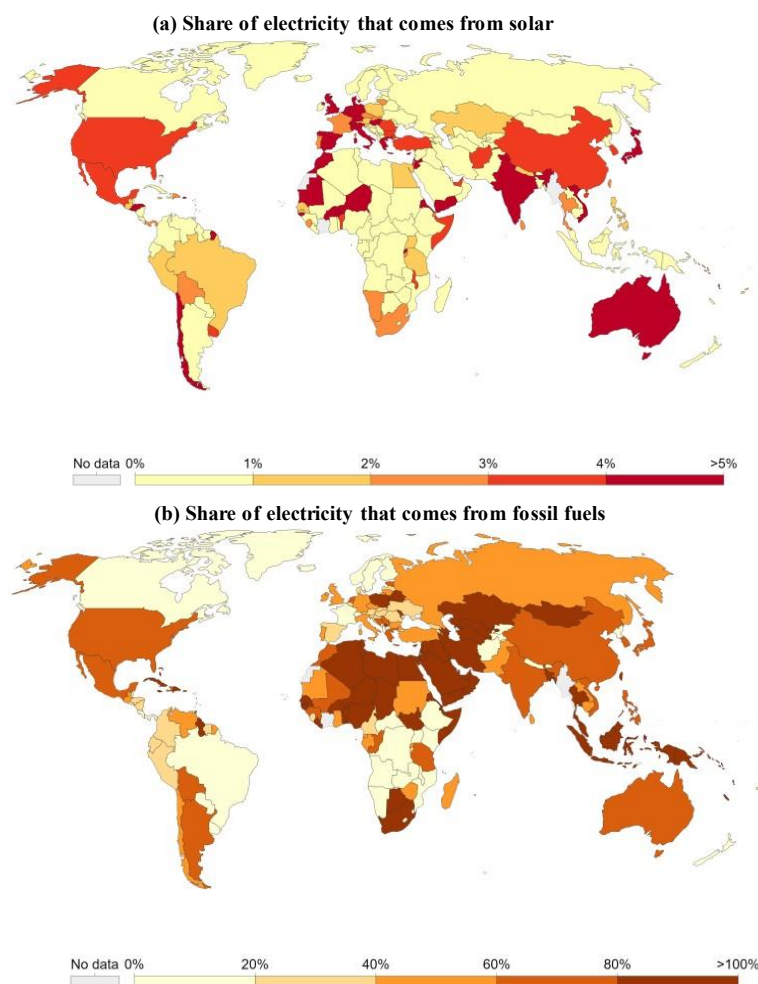
Figure 2.4: The share of electricity comes from solar sources and fossil fuels [32, 33].

In Denmark, the roadmap for a decarbonized society considers geographical characteristics like wind resource availability when constructing a renewable energy system [54]. A case study of an abandoned island underscores the significance of location and conditions for determining the optimal mode of energy delivery [84]. Geographical variations affect the

feasibility of integrating renewable energy systems at a European level, underscoring the need for enhanced transmission capacity and cross-border collaboration [36].

Overcoming geographical limitations and establishing a sustainable transition to RES-based power systems require customized solutions encompassing a range of renewable energy technologies, international collaboration, and supportive policies. Strategies such as identifying suitable sites for RESs, enhancing the efficiency of transmission networks, and exploring various energy storage options to mitigate fluctuations and mismatches between supply and demand are imperative to circumvent geographical restrictions.

2.1.4 Role of political support for 100% RES-based power system

Transitioning to a fully RES-based power system is a complex process that is significantly influenced by various political factors. Among these factors, regulatory frameworks, policy incentives, and the availability of political will are the most obvious. Governments and policymakers have a crucial role in creating policies and regulations that stimulate the deployment of renewable energy and its seamless integration into the existing power grid. A stable and clear regulatory framework is a prerequisite in this regard [36, 56].

However, this process is not devoid of political challenges. For instance, the cooperation of several governments, the conclusion of international agreements, and the consideration of geopolitical factors can pose hurdles. Infrastructure development, such as that needed for cross-border data transmission, requires coordination among various political entities [36, 56].

The path towards a RES-based system is not devoid of obstacles. Resistance from mandatory industries, barriers to renewable energy deployment, a lack of supportive policies and incentives, and the complexities of integrating RES into current power systems can impede the transition [84]. To overcome these barriers, sustained political commitment, stability, and a conducive policy environment are required [81]. Such an environment should stimulate RES investments and advance the licensing process. Hence, a decisive public investment and a

clear policy direction are paramount in driving the transition. Without these, the transition could be hindered, regardless of its technical feasibility [54].

Various studies provide evidence of the importance of supportive policy frameworks and political commitment. Saudi Arabia's Vision 2030 aims to reduce the nation's dependence on oil and diversify the economy, emphasizing the importance of strong political will and supportive policies for a successful transition [53]. Similarly, research in the MENA region points out the necessity of regional collaboration and political stability for large-scale integration of RESs [52]. Studies focused on Indonesia's power system transition underline the need for significant investments, increased use of solar PV and BESS technologies, and comprehensive planning that considers geographical constraints and technical possibilities [85].

Various technologies like carbon capture and storage and nuclear power need political backing along with clear policy objectives [60]. These elements can drive the necessary transformations and investments across all sectors of the energy system. Including policymakers, stakeholders, and the general public in debates and decision-making processes, education on the benefits of RESs; and building consensus are key strategies to overcome political barriers [80]. Aligning energy policies and goals with broader political contexts and priorities is essential for a successful transition [86].

Political issues and partisanship can significantly impact the adoption of renewable energy technologies in certain regions, notably in some countries that are heavily dependent on fossil fuels [87]. However, evidence suggests that an understanding of basic science and cognitive sophistication can foster pro-science attitudes and mitigate the impact of political disputes on perceptions of scientific disciplines [88]. This suggests that even in politically contentious issues, familiarity with fundamental science can promote pro-science sentiments, thus highlighting the role of basic scientific knowledge in shaping attitudes toward science [89].

2.1.5 Case study of Integrated Nordic Power System (INPS)

2.1.5.1 The 2020 target

The Nordic-grid nations, encompassing Denmark, Finland, Norway, and Sweden, have committed to EU Directives, including the Renewable Energy Directive (RED). This directive aims to ensure that RES constitutes 20% of the EU's total energy and 10% of the transportation sector specifically by 2020. Figure 2.5 illustrates the proportions of RESs used in these countries from 2004 to 2020, following their National Renewable Energy Action Plans (NREAPs) set for 2020. The Nordic grid, a collaborative venture involving Finland, Sweden, Norway, and Denmark, has significantly reduced the region's overall carbon footprint [90].

Transmission system operators (TSOs), such as Fingrid, Energinet, Statnett, and Svenska Kraftnat, are responsible for the competitive nature of the regional power market. The collaborative mechanism of the Nordic grid members has enabled them to achieve their RES targets ahead of the scheduled timeline. This region's substantial evolution as an energy-intensive area can be partially attributed to the abundant natural resources, like wind, timber, minerals, and hydroelectric potential, playing a significant role in its progression [90].

The diverse energy mix and regional cooperation have enabled Denmark to reach its overall RES target in 2015, Finland and Norway in 2014, and Sweden as early as 2013, as indicated in Figure 2.5 [90]. The TSOs in the Nordic grid employ their forecasts to ensure the uninterrupted operation of the energy system. They devise and implement effective strategies for managing the generation and transmission of renewable energy. Other stakeholders, such as demand aggregators and energy suppliers further utilize these projections.

2.1.5.2 The energy transition toward 2030 and 2050 targets

Building on the prior target of 20% renewable energy by 2020, the RED 2018/2001/EU, issued in 2018, set a renewed goal of at least 32% renewable energy by 2030. This objective surpassed the European Green Deal adopted in December 2019. On July 14, 2021, the European Commission announced revised climate targets for 2030, aiming to increase the renewable energy target to 40% of the EU's energy mix. Subsequently, on May 18, 2022, the

Commission introduced the REPowerEU plan to expedite the green transition and reduce dependence on Russian fossil fuels, intending to diversify energy supplies within the EU. The plan includes measures to reduce energy consumption, encourage clean energy sources, and reach a target of 45% renewable energy in the transport, power generation, and industrial sectors by 2030 [91].
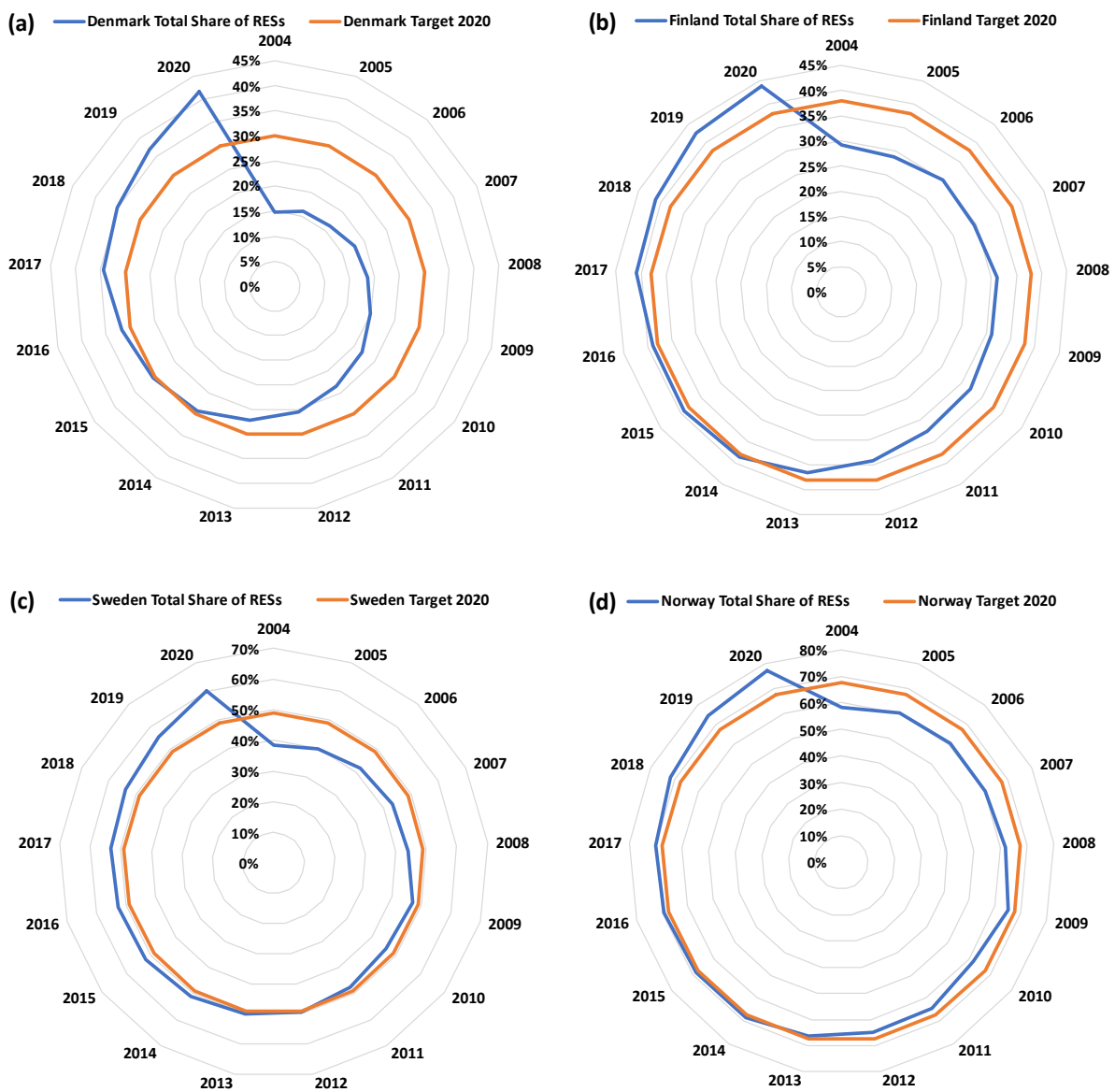
Figure 2.5: Overall share of energy from RESs between 2004-2020 along with NREAP targets, (a) Denmark, (b) Finland, (c) Sweden, and (d) Norway.

In light of these global developments and objectives, the four Nordic TSOs unveiled the Nordic Grid Development Perspective (NGDP) 2021 report [92]. The report emphasizes the ambitions of these four Nordic countries, where Finland aims to achieve carbon neutrality by 2035, Sweden by 2045, Denmark by 2050, and Norway aspires to become a low-emission society by 2050, as shown in Table 2.1. The report also denotes an increase in energy consumption in all Nordic countries, along with efforts to enhance renewable electricity production and decrease dependence on traditional thermal plants. The 2050 target is to achieve decarbonization across all Nordic countries, with nations rapidly escalating renewable energy production capacity and investing in necessary infrastructure.

Table 2.1: Trend of electrical power generation and consumption in Nordic countries** [92]

Components	Finland	Sweden	Denmark	Norway
Hydroelectric power	≈	≈	≈	+
Onshore wind power	+++	+++	+	+
Offshore wind power	+(+)	+(+)	+++	++
Solar power and energy storage	+	+	++	+
Nuclear power	≈	≈(-)	≈	≈
Other thermal power	-	-	-	-
Electricity consumption	+++	++	+++	+++
P-2-X	+++	+++	+++	+
Demand-side response (excluding P-2-X)	+	+	+	+
Electricity balance	Balanced	Moderate export	Export	Moderate export
Decarbonization year (sector/society)	2035/2035	2040/2045	2030/2050	2040/2050

* Decarbonisation in terms of the overall energy sector includes all forms of energy consumption like electricity, cooking, transportation, industries, heating, cooling, and so on.

** + increase, - decrease, ≈ remain at a similar level. The categories for different countries should not be compared to each other.

In 2022, the Nordic TSOs published a report [93], which delivers an exhaustive analysis of strategies and actions required to address the climate challenge by 2030. The green energy strategy outlined in the report covers four interconnected elements: electrification, increased generation from variable and renewable wind power sources; flexibility to manage the

variability of renewable energy, and sector integration, optimizing the energy system across different infrastructures, promoting synergy and efficiency.

To project the percentage of RESs in Nordic countries, the Nordic Energy Research platform offers critical insights, as depicted in Figure 2.6 [94]. This graph exhibits two scenarios: the Carbon Neutral Nordic (CNN) and the Nordic Powerhouse (NPH). The CNN scenario contemplates the most cost-effective route while considering current governmental plans, strategies, and ambitions. It visualizes the outcomes of stated tactics and goals that are yet to be implemented. The forecast indicates the need for increased production of renewable energy and heat to satisfy the demand for clean energy in various sectors.
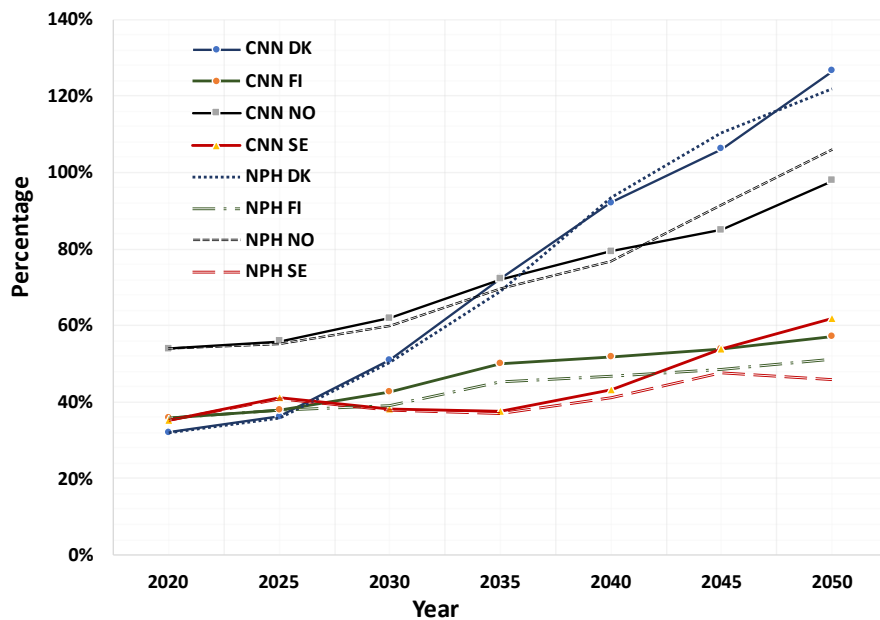
Figure 2.6: Forecast of the total share of RESs in Nordic countries.

The NPH scenario investigates the potential of the Nordic countries to play a more substantial role in the broader European energy transformation. It visualizes the Nordic countries as providers of affordable clean energy, hosts of more low-carbon businesses and services, exporters of low-carbon goods and energy sources, and increased exports of carbon-free steel and aluminum. Applying these scenarios, it is projected that Denmark will lead the transition to a green economy, with a projected 100% share of RES by around 2042, followed by Norway around 2048-2050. Finland and Sweden are projected to account for between 40% and 60%

of their respective RES shares by 2050 [96]. These projections underscore the potential for significant progress in the transition to renewable energy in Nordic countries.

2.1.5.3 INPS toward 100% RES

The transition towards a RES-powered grid system requires thoroughly examining the demand-supply balance. Climate change and the construction of more small hydropower plants are expected to increase Norway's annual hydropower output. Meanwhile, in Finland and Sweden, where large-scale hydropower use is not feasible, there is an uptick in onshore wind power generation, with Sweden's growth rate potentially slowing down. Land-based wind energy offers the most substantial return on investment among RESs in these countries. However, local opposition has slowed the growth of the onshore wind industry in Denmark and Norway. These countries instead focus on offshore wind development opportunities. The PV has a slower development rate than wind farms across the Nordic countries, and future capacity will likely come from rooftop and commercial installations [95]. Figure 2.7(b) presents TSOs' predictions for RES energy generation until 2040 under the CNN Scenario, showing the significant contributions of wind and photovoltaics to overall production [92].

The growing interest in electric vehicles (EVs) and government goals to eliminate fossil fuel use is anticipated to drive the increased adoption of electric vehicles [96]. Moreover, the Nordic countries' access to clean, economic power and advanced infrastructure makes them attractive locations for data centers. Various sectoral changes, such as the electrification of both direct and indirect processes, could impact power demand. However, overall consumption is still expected to rise, despite the use of P2X and Vehicle-to-Grid (V2G) technologies to meet peak demand. Figure 2.7(a) portrays the breakdown of energy use in Nordic countries by industry, with transportation, heating, data centers, and P2X applications projected to be the main drivers of future demand [92].

The Nordic countries' transition to renewable energy is met with public and government support, recognizing the importance of RES, and reducing carbon footprints. The Nordic Council of Ministers' Nordic Co-operation Program on Energy Policy 2022-24 aims to make the

Nordic region the world's most sustainable and integrated region by 2030, promoting well-being, inclusion, equality, interconnection, cultural exchanges, and connectivity [97].
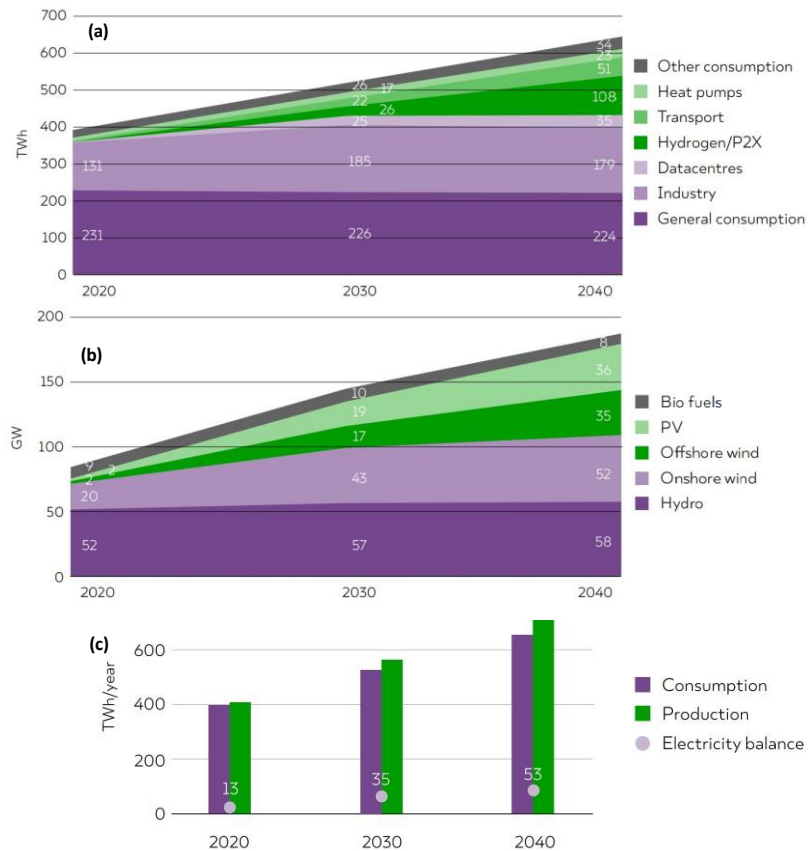
Figure 2.7: (a) Nordic electricity consumption, (b) Nordic renewable electricity production capacity, and (c) Nordic electricity balance from 2020 to 2040 under CNN Scenario [92].
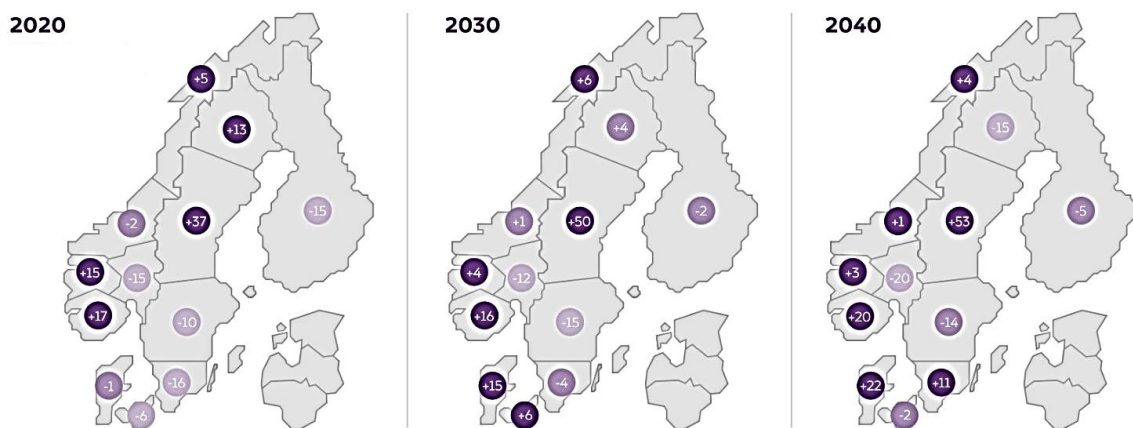
Figure 2.8: Projected electricity balance (TWh) in the Nordic bidding zones in 2030 and 2040 under the Climate Neutral Nordics Scenario [92].
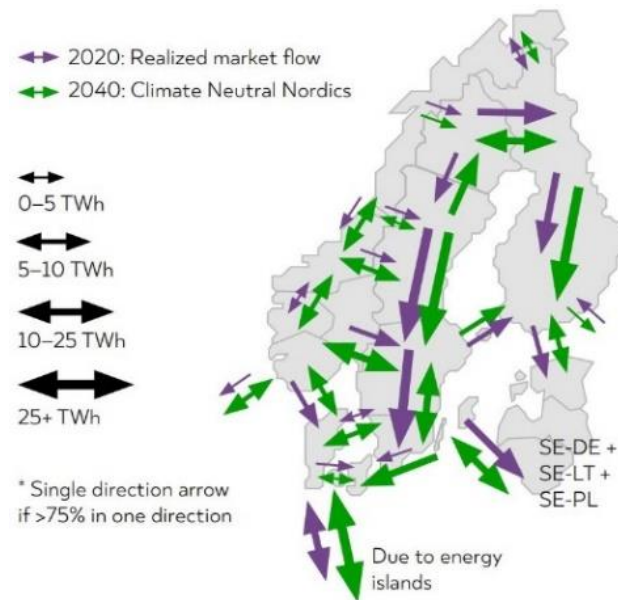
Figure 2.9: Power flows (TWh) among Nordic bidding zones in 2020 and projected values for 2040 under the Climate Neutral Nordics Scenario [92].

The geographic diversity of the Nordic countries dictates their renewable energy potentials. While Norway and Sweden have substantial hydropower potential, Denmark and Finland have limited access to this type of energy. Nevertheless, Denmark has excelled in harnessing wind energy and has become an industry leader. Figure 2.8 displays the power balance for 2020, with projections for the electricity balance in 2030 and 2040 in the Nordic bidding zone under the Climate Neutral Nordics Scenario [92]. Despite these geographical variations, the Nordic countries have managed to maintain interconnected and synchronized electricity grids, facilitating a balance between supply and demand. This example of international cooperation showcases the fruitful outcomes that can be achieved through collaborative efforts. Figure 2.9 provides anticipated values for 2040, and the power flows in 2020 between the Nordic bidding zones, highlighting the successful cooperation between the Nordic TSOs and their crucial role in ensuring a secure and functioning power system [92].

2.1.6 Is it feasible?

The complexity of transitioning to a fully RES-based power system necessitates an integrated approach that addresses technical, social, political, and geographical considerations.

Technological advancements and continuous innovation are critical for harnessing a diverse array of RES, ensuring grid stability, and addressing the intermittency of renewable energy. In parallel, social and political factors play an instrumental role, requiring strong political will, supportive policies, and robust regulatory frameworks that promote the deployment of RES.

Incorporating RES into power systems is a technical endeavor and a socio-political process. The engagement of public stakeholders and the creation of supportive regulatory environments are pivotal to navigating through political and social resistance. At the same time, the geographical disparities and regional variations in resource availability demand that the transition strategies be tailored to the unique contexts of each region.

The Nordic countries' electricity grid demonstrates the feasibility of a 100% RES-based power system. Through collaborative efforts and inter-regional projects, they have shown that an integrated synchronous grid system can accommodate diverse geographical and political contexts and still be effective. Such alliances illustrate how countries can overcome geographical and resource constraints when working together towards a common goal.

In conclusion, the path towards a 100% RES-based power system is layered with challenges that demand concerted efforts, innovative technological advancements, and dedicated international collaboration. Despite the difficulties, its profound benefits in terms of cost reduction, socio-economic development, and environmental sustainability make it a compelling and necessary goal. The task ahead is formidable, involving significant investment, technological progression, and careful planning. But with a multifaceted approach that addresses the technical, social, political, and geographical aspects, the goal of a 100% RES-based power system can be realized, contributing to a sustainable future for generations to come.

2.2 Previous Studies

The operation of power systems has become increasingly complex with the introduction of IBRs and evolving policies. In order to ensure secure and reliable power system operation, it is crucial to identify techno-economic approaches and technologies. Previous research has

proposed different concepts to tackle these challenges; however, the intricate nature of the framework and potential uncertainties can lead to impractical outcomes and implementation difficulties in real-world settings [98, 99]. Therefore, there is a need for a comprehensive study of unique and practical methods to overcome existing and future challenges associated with upgrading power system structures and operational approaches.

The modern power system emphasizes integrating techno-economic operations while considering environmental constraints. Operational constraints can be enhanced by either replacing the control system with an optimized approach or incorporating an optimized supervisory system without modifying the main system [100]. The latter option is more practical and popular in rapidly growing systems. However, the increasing integration of IBRs presents new challenges, such as unbalanced frequency resilience and low grid inertia [101]. Consequently, practical tools are needed to dynamically monitor, analyze, improve, and visualize system characteristics [102]. It is evident that conventional control technologies are insufficient for a modern power system, necessitating a new approach.

Previous studies have utilized the concept of Battery Energy Storage Systems (BESS) to regulate power system frequency [103, 104]. Another study proposed a self-tuning PID controller using fuzzy logic and thyristor-controlled series compensation (TCSC) to enhance transient stability [105]. Similarly, a controller based on fuzzy logic and a neural network was suggested in [106]. To improve the first swing stability of a power system, compensators like the Static VAR Compensator (SVC) and Static Compensator (STATCOM) were employed with a discontinuous control strategy [107, 108]. In [109], a controller was discussed to enhance transient stability through synchronous generator extraction. Teng et al. introduced the integration of Electric Vehicles (EVs) to improve the frequency response of the Great Britain power system [110], while Liu et al. investigated the effects of EV integration on secondary frequency control [111]. The integration of EVs as Distributed Energy Resources (DERs) is widely adopted in modern power systems to enhance frequency quality. Additionally, studies have explored the application of demand-side management (DSM) concepts for power system

security [112-114]. Various techniques have been proposed to address stability issues in IBR-based power systems, taking into account multiple variables.
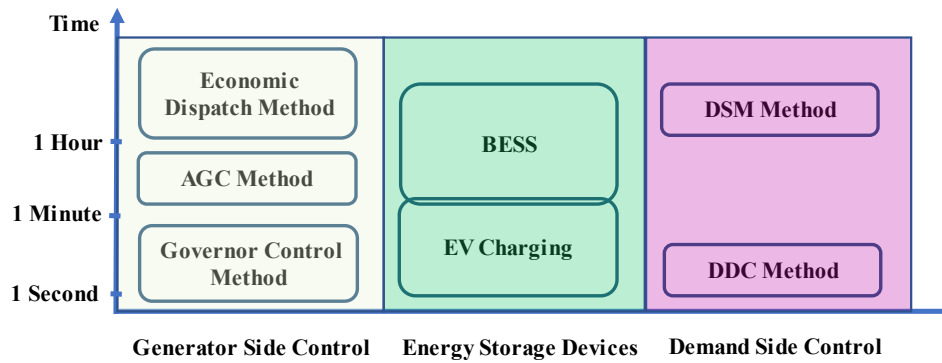
Figure 2.10: General techniques for regulating the frequency in RES-based power systems.

Figure 2.10 illustrates the classification of frequency control techniques. The regulation of power system frequency has been extensively studied, with Automatic Generation Control (AGC) being a traditional method through generator control. AGC adjusts the rate of generation based on frequency monitoring to maintain regulation. Researchers have applied optimization tools and objective functions to identify optimal parameters for AGC controllers, such as the Harmony Search (HS) algorithm and Integral Square Time Square Error (ISTSE) [115]. Additionally, the implementation of Superconducting Magnetic Energy Storage (SMES) in conjunction with AGC has been explored to analyze controller performance and power system behavior [116]. The stability of the system and optimization of controller parameters have been investigated using Lyapunov's second law [117]. Detailed transient analysis of individual AGC within a multi-source power system has also been conducted. Artificial Neural Network (ANN) techniques have been employed to analyze AGC problems [118]. Novel approaches, including the combination of the Tilted Integral Derivative (TID) controller and the Teaching Learning Based Optimization and Pattern Search (hTLBO-PS) approach, have been suggested for AGC in a deregulated environment [119]. Furthermore, an Ecological Population Cooperative Control (EPCC) strategy based on a Multi-Agent System Stochastic Consensus Game (MAS-SCG) has been proposed for AGC in an islanded smart grid [120]. Parameter-plane approaches have been used to identify optimal controller parameters, and

sensitivity analysis has been performed to examine stability via AGC [121]. A hybrid technique combining the Firefly Algorithm and Pattern Search Method has been proposed for AGC in multi-area power systems [121]. AGC is a general technique for regulating system frequency through control of generator-side parameters, operating in the secondary response, and taking a few minutes.

The Model Predictive Control (MPC) method has also gained popularity in power system control. Various studies have utilized MPC for different applications in power systems. For instance, Cui et al. proposed a Multimodal Long Short-Term Memory (M-LSTM) deep learning approach for Composite Load Modeling(CLM) to determine time-varying variables [122]. An MPC-based method with Superconducting Magnetic Energy Storage (SMEA) units was developed to enhance transient stability [123]. MPC has also been used for frequency regulation in wind energy integrated power systems [124], power system stability improvement through a hybrid control system combining MPC and Neural Network [125], and control of thyristor firing angle for transient stability improvement [126]. The concept of Transient Energy Function (TEF) has been combined with MPC to achieve multiple Unified Power Flow Controller (UPFC) operations and enhance system stability [127]. MPC has been implemented in various applications, including TCSC control, damping oscillated power in an HVDC system, managing distributed generated energy, and stabilizing the grid after contingencies [128-131]. MPC offers a plug-and-play structure that enables easy redesign and evaluation of the controller structure.

Similarly, Dynamic Demand Control (DDC) has been proposed as an approach for regulating grid frequency. Shrot et al. introduced DDC as a technique for frequency stabilization [132]. Zhu et al. investigated Robust Load Frequency Control (RLFC) along with DDC for power system regulation [133]. Qingxin et al. proposed a Thermostatic Load Control (TLC) strategy based on DDC, utilizing thermostatic loads such as HVAC units and Electric Water Heaters (EWHs) [134]. A hybrid DDC concept has been introduced to provide rapid and steady regulation of primary and secondary frequency [135]. Various studies have examined the effects of DDC on frequency and highlighted the need for randomization to minimize oscillatory instabilities

[132, 136, 137]. DDC is valued for its fast response, flexible operation, and economic efficiency.

Researchers have developed ideas and strategies to address associated issues as grids evolve and new technologies are integrated. While efforts have been focused on maintaining stable voltage, rotor angle, and frequency, research on online or real-time management of instability, a major cause of blackouts, has been limited [138, 139]. Effective and reliable techniques for resolving frequency management problems in low-inertia systems have been discovered through research experiments. Inertial support has been identified as a promising approach, but long-lasting and practically applicable solutions are still needed [140]. The management features and operating principles of revolving power systems have the potential to solve problems in modern power systems through the development of new technologies or the proper planning, management, and implementation of operational strategies.

The advancements in regulating PECs have emphasized the significance of components and technological progress. Grid-forming (GFM) converters can adjust frequency and voltage amplitude at the Point of Common Coupling (PCC) and offer advantages over grid-following (GFL) converters, particularly in weak power systems [5, 6]. However, challenges arise in studying GFM due to limited current in the PEC during significant disturbances [141]. The potential of versatile GFM in addressing power system issues is being investigated, requiring further research to understand its features, reactions, and effects. GFL, while limited by its reliance on grid synchronization, can play a crucial role in resolving challenges when implemented with the planning approach [142-145]. Operational strategies, including comprehensive recovery strategies, have been discussed to preserve power system reliability. The literature highlights the need for solutions related to IBRs and low-inertial systems.

2.3 Power System Stability

The stability of electrical power systems is a critical concern, and various stability issues can arise. Traditionally, stability issues were classified into three types: rotor angle instability, frequency instability, and voltage instability. Rotor angle stability is essential for system

synchronization and requires quick resolution for transient-state and steady-state stability. Effective solutions for rotor angle instability include Power System Stabilizers (PSS), PEC-based exciters, and generator-tripping protection mechanisms. Frequency stability refers to maintaining the operating frequency within an acceptable range and can be restored in a few seconds to several minutes. Voltage stability plays a vital role in keeping the receiving end voltage within an acceptable range and requires a similar time frame for restoration. Restoration of long-term voltage stability requires HVDC interconnections, adjustable tap transformers, and generator excitation current limiters [146]. Short-term voltage stability can be addressed by Automatic Voltage Regulators (AVR), excitation systems, and induction motors.
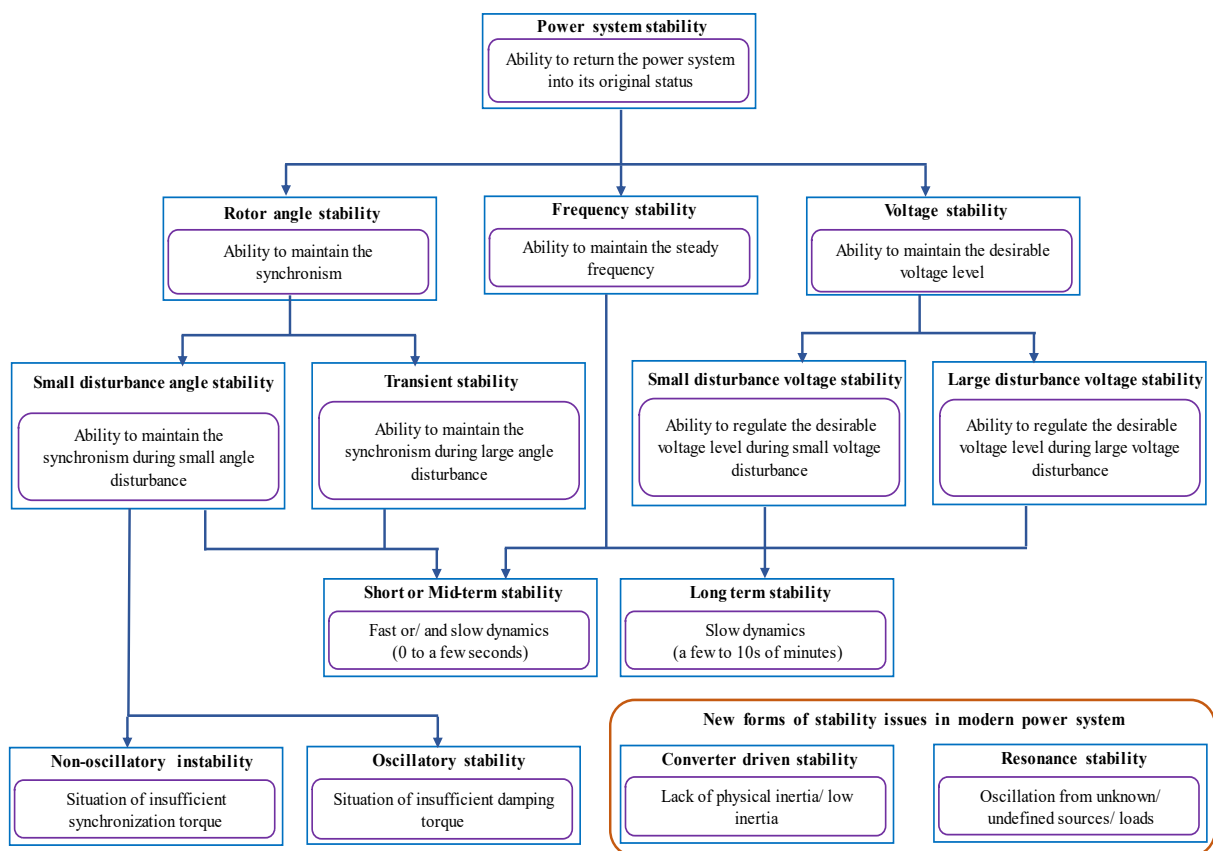
Figure 2.11: Power system stability classification.

In modern power systems, integrating PEC-based technologies introduces two additional stability issues: converter-driven stability and resonance stability. Converter-driven stability pertains to oscillations caused by cross-coupling between dynamic electromechanical devices

and transients in the grid networks. Resonance stability occurs due to insufficient energy dissipation within the system, leading to periodic oscillations [1, 147-149].

The integration of IBRs in the power system introduces instability due to two primary factors. Firstly, the high penetration of PEC-based resources like solar photovoltaics (PV) and wind turbines reduces system inertia, posing a challenge in balancing the demand-supply chain. Addressing this factor is crucial for system stability. Secondly, RESs exhibit unpredictable patterns, making predicting the time series values of demand and generation difficult. The presence of non-synchronous generators with PECs diminishes system inertia and increases the risk of unstable frequency. A system with low inertia can lead to frequency fluctuations and power system blackouts. Upgrading protection equipment with conventional operation settings becomes necessary to accommodate the significant integration of PEC-based technologies [17-19].

2.3.1 Rotor Angle Stability

Rotor angle stability is a crucial aspect of power system operation, ensuring the dependability and stability of the grid. It involves maintaining relative rotor angles within acceptable limits, even in the face of disturbances or variations in the power system. Power systems' smooth and secure operation relies on rotor angle stability, as it directly impacts the dynamic behavior of generators and their ability to withstand system-wide disturbances. Consequently, rotor angle stability is one of the most critical factors in ensuring the reliability of power systems [150].

The dynamics of power systems are experiencing significant changes due to the increasing integration of IBRs. These changes introduce new challenges to rotor angle stability, primarily stemming from the reduced fraction of synchronous generators and evolving power generation and control methods. The introduction of variable and intermittent power generation from RES, like wind turbines and solar photovoltaic systems, adds unpredictability to the system. Combined with the lower inertia of RES-based generators, this unpredictability can lead to variations in rotor angles, potentially undermining rotor angle stability. In addition,

the utilization of PEC technologies for regulating active and reactive power on both the generation and load sides has further effects on the dynamics of the rotor angle [15, 151].

Understanding rotor angle stability and taking measures to improve it are crucial for modern power systems' reliable and secure functioning. Rotor angles can deviate from their steady-state values when disturbances occur, such as sudden load changes or network malfunctions. Excessive rotor angle deviations can trigger unstable oscillations and system-wide instabilities, posing significant risks to power system stability and reliability. Researchers and industry professionals can pave the way for innovative solutions that preserve stability and drive the transition towards a sustainable and resilient power grid by investigating the complex relationships and factors influencing rotor angle dynamics.

2.3.1.1 *Parametric Sensitivity of the Rotor Angle Stability Indicators*

The evaluation and monitoring of rotor angle stability indicators are crucial for assessing the stability of power systems. These indicators provide valuable insights into the dynamic behavior of synchronous generators, helping identify potential stability issues that can impact the safe and reliable operation of the grid. By analyzing rotor angle stability indicators, system operators and engineers can take proactive measures to preserve stability, prevent cascading failures, and optimize the utilization of power system resources. These indicators are typically derived from analyzing the dynamics of generator rotor angles and related system variables, such as electrical power outputs, voltages, and currents. They offer quantitative metrics that indicate the proximity of the power system to instability. Commonly used indicators include the critical fault clearing time (CCT), damping ratio (ζ), and eigenvalues [15].

The rotor angle stability index considers the rotor angles of generators and the corresponding power flows to quantify the system's proximity to instability. It provides a numerical value representing the stability margin, enabling system operators to identify potential stability limits. The CCT represents the time required for a disturbance to be considered eliminated from the system to prevent instability. It provides valuable information for emergency control actions and decision-making during fault conditions. Whereas the damping ratio (ζ) reflects the rate at which oscillations diminish over time, indicating the system's ability to recover and

maintain stable operation. Eigenvalues also contribute to and demonstrate the stability of the system. Mathematical expressions, as shown in Equation 2.1, Equation 2.2, and Equation 2.3, represent the CCT, overall system frequency, and damping for a power system, respectively [31, 65, 152].

Here in Equations, H_{sys} is the inertia constant of the system, ω_s is the angular frequency, P_{max} is the maximum rated power, δ_{CCT} is the critical power angle, δ_0 is the initial power angle, and K_D is the damping constant for the equivalent system.

$$T_{CCT} = \sqrt{\frac{4H_{sys}}{\omega_s P_{max}} (\delta_{CCT} - \delta_0)} \text{ [in s]} \qquad \text{Equation 2.1}$$

$$\omega_{sys} = \sqrt{\frac{\omega_s P_{max} \cos \delta_0}{2H_{sys}}} \text{ [in rad/s]} \qquad \text{Equation 2.2}$$

$$\zeta = \frac{1}{2} K_D \sqrt{\frac{\omega_s}{2H_{sys} P_{max} \cos \delta_0}} \qquad \text{Equation 2.3}$$

As a case study, the IEEE 39 Bus New England power system is investigated to demonstrate how important it is for power systems to maintain rotor angle stability. Ten generators make up this power system, along with 39 buses and 33 connecting lines. As shown by the blue lines in Figure 2.12, the system can be conceptually broken up into three distinct sections based on its location: west, north, and south. The West region is an aggregated power system that has several machines (G1), the North region contains three generators (G8, G9, and G10), and the South region consists of six generators (G2, G3, G4, G5, G6, and G7). In Figure 2.12, Generator buses are indicated with red points, PQ buses are blue points, and transmission wires are yellow lines. To model and simulate the various components of the power system, DigSILENT PowerFactory software, in conjunction with the DigSILENT Programming Language (DPL) [153, 154] is used. To do a sensitivity analysis of the inertia constant, three different scenarios have been considered, each with six different sub-cases. The various possibilities are outlined in Table 2.2. In the first possible scenario, the inertia level of the West and South areas is typical, whereas the North area's inertia level is considered quite low. In the second scenario, the level of inertia in the South area is low; in the third scenario, the level of inertia is low in both the

North and South areas. The nominal values of the inertia constants are received from the source [155], and we investigate the system's response to low inertia values in six sub-cases: base case H, 0.9H, 0.8H, 0.7H, 0.6H, and 0.5H.
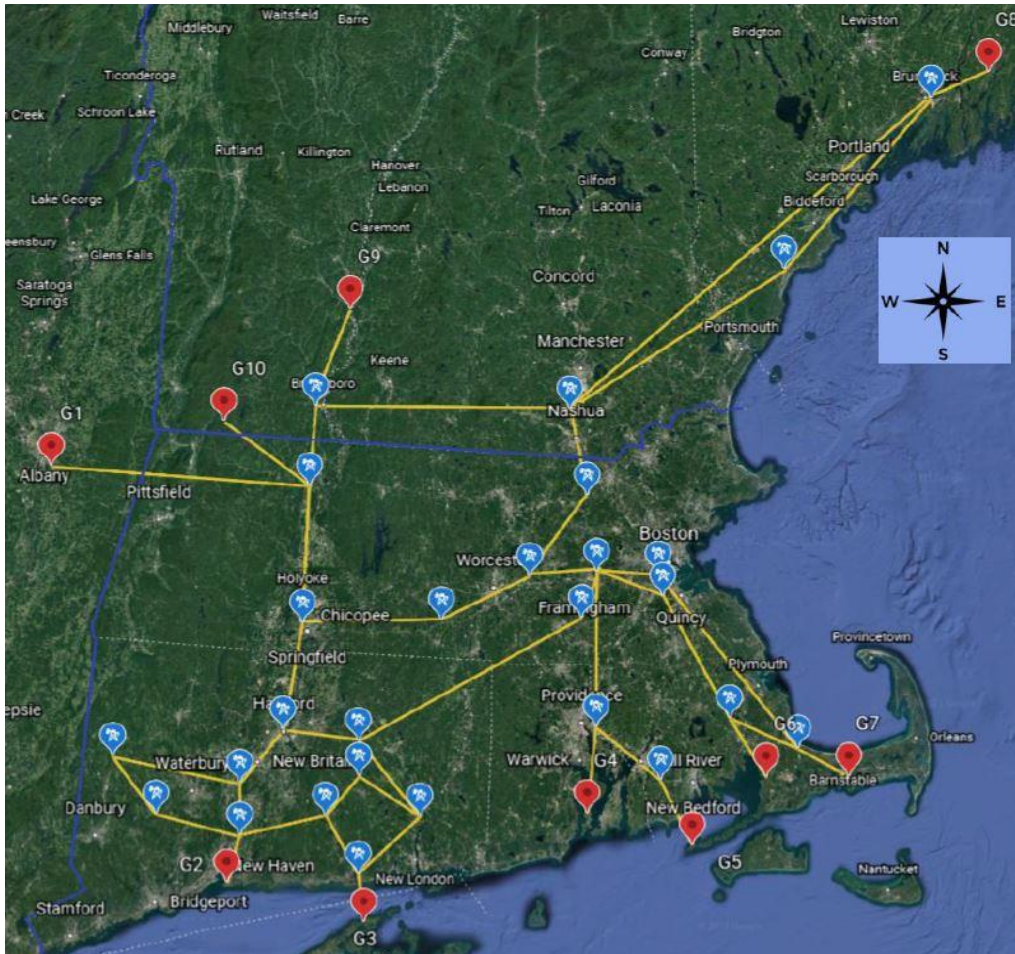
Figure 2.12: IEEE 39 Bus New England electricity system with three zones.

Table 2.2: Assumed cases for the sensitivity analysis.

Scenarios	West	North	South
a	Normal	Low	Normal
b	Normal	Normal	Low
c	Normal	Low	Low
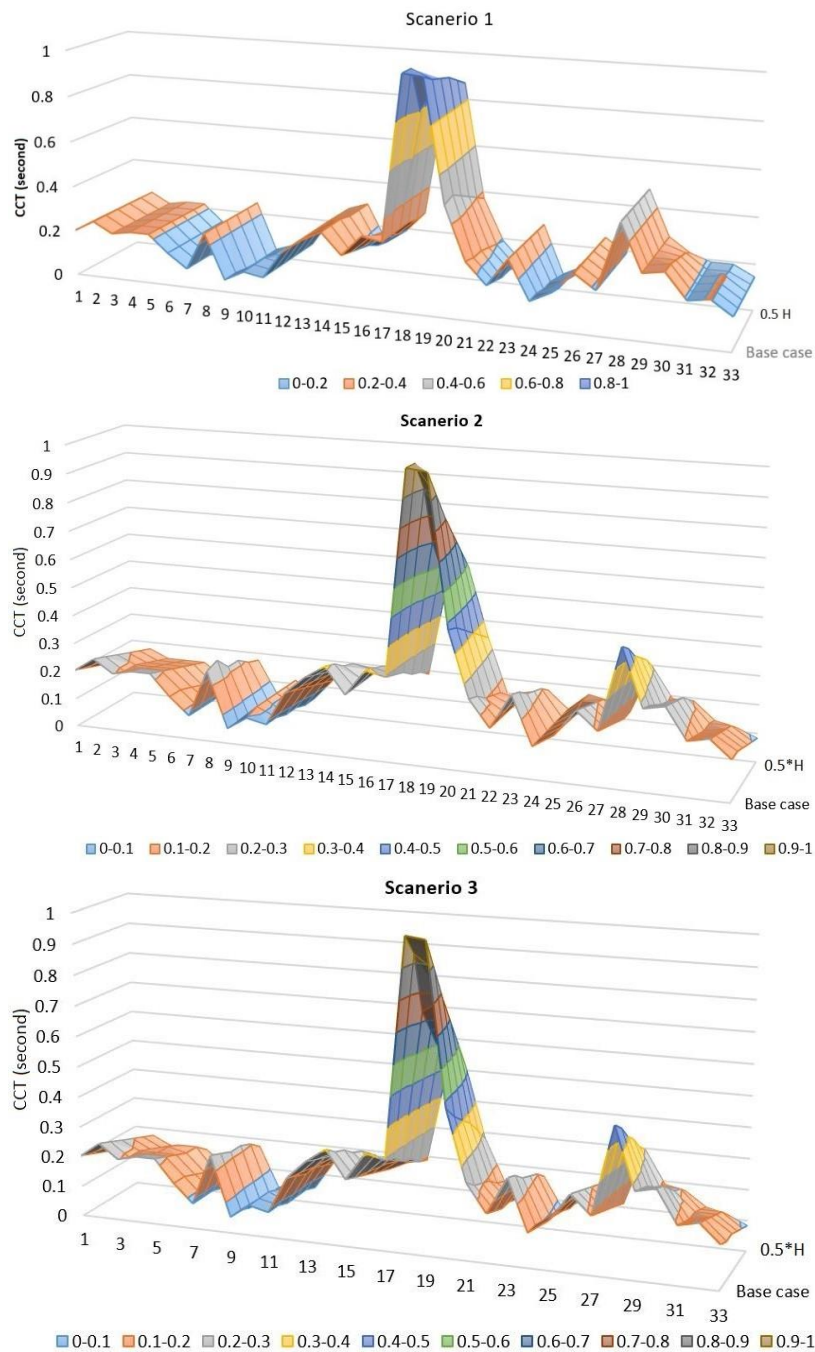
Figure 2.13: Sensitivity analysis of inertia constant with the CCTs for three scenarios.

During the analysis process, a fault is deliberately introduced into a transmission line, and the CCTs for each transmission line are observed. Figure 2.13 illustrates the CCTs obtained for different values of the inertia constant across the three scenarios outlined in Table 2.2. It is evident from the figure that the CCTs generally decrease as the inertia constant decreases.

Notably, scenario 'c' exhibits a higher rate of difference compared to the other two scenarios due to the overall reduction in system inertia ($H_a > H_b > H_c$). The slope of the graph in Figure 2.13 indicates the difference rate of CCTs among the scenarios, with scenario 'c' displaying the highest difference rate. Furthermore, the transmission lines near G1 consistently exhibit higher CCTs compared to others. To investigate this further, the CCTs in different areas of the power system are examined across various scenarios and sub-cases; detailed information on the CCTs can be found in Table 2.3.

Table 2.3: CCTs in different areas for different scenarios.

Scenarios		a (s)	b (s)	c (s)
West	Base case	0.9960	0.9960	0.9960
	0.9H	0.9810	0.9505	0.9090
	0.8H	0.8790	0.8560	0.7575
	0.7H	0.8790	0.7195	0.6740
	0.6H	0.8785	0.6285	0.5905
	0.5H	0.8330	0.5680	0.4995
North	Base case	0.2033	0.2033	0.2033
	0.9H	0.1986	0.1966	0.1901
	0.8H	0.1911	0.1873	0.1741
	0.7H	0.1817	0.1778	0.1608
	0.6H	0.1693	0.1663	0.1446
	0.5H	0.1589	0.1531	0.1276
South	Base case	0.2415	0.2415	0.2415
	0.9H	0.2415	0.2265	0.2255
	0.8H	0.2415	0.2093	0.2083
	0.7H	0.2405	0.1951	0.1941
	0.6H	0.2405	0.1761	0.1701
	0.5H	0.2405	0.1580	0.1549

Table 2.3 reveals that in all cases, the CCT values decrease from top to bottom and left to right in correspondence with the decreasing inertia constant. In scenario 'a', where only the inertia of the North area is reduced, Table 2.3 demonstrates that the decreased inertia affects the CCTs throughout the entire power system. However, the North area experiences a higher rate of difference, whereas the other two scenarios exhibit lower rates. Similarly, in scenario 'b',

the South area shows a higher difference rate due to the reduced inertia in that region. Notably, scenario 'c' has a more significant impact since the reduced inertia is greater in comparison to the other scenarios (involving decreased inertia in both the North and South areas). This highlights the dependency of CCTs on the location within the power system. Furthermore, the CCTs for all components demonstrate a consistent reduction with varying inertia at specific locations. This data unequivocally shows that the CCTs decrease as the inertia decreases in any section of the multi-machine power system, albeit with a more pronounced effect in local areas and a lesser impact in neighboring regions.
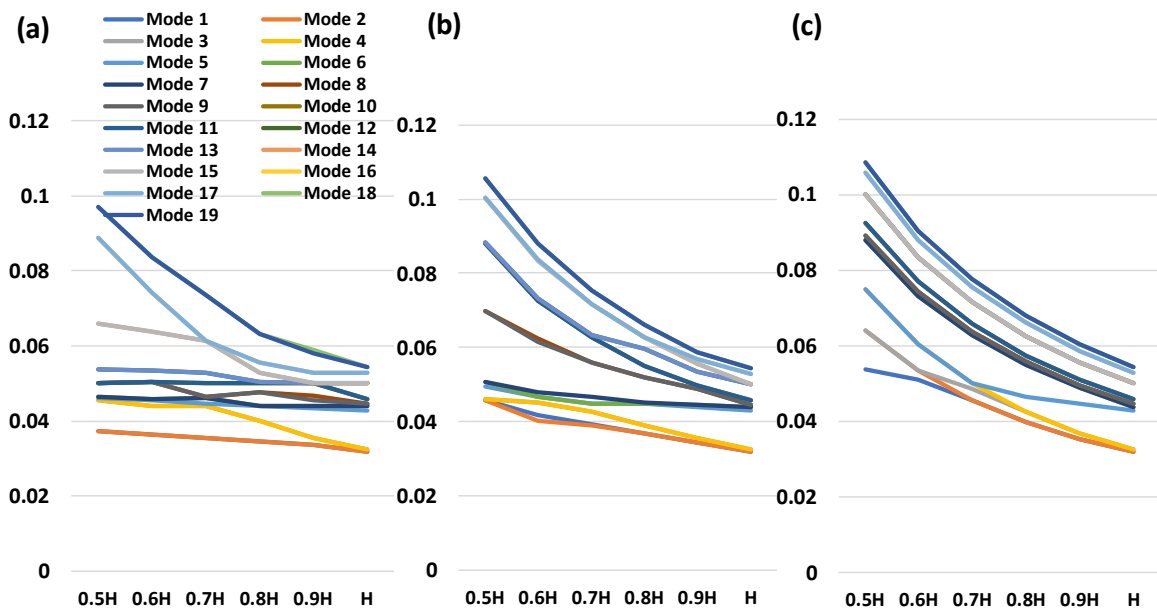
Figure 2.14: Damping with the increasing order of inertia constant for three scenarios.

This is only one illustration of how a low moment of inertia might influence a transmission line. However, when a bus system is regarded in place of a transmission line, it has the same impact as the transmission line. Like how increasing inertia has significant impacts on frequency and voltage variations, lowering inertia does the same. Figure 2.14 illustrates the sensitivity of the damping with respect to the inertia constant for the various situations that were assumed. According to the findings, there is a negative correlation between the rise in the inertia constant and the damping. In addition to this, it has been seen that the slope of

the drop is steeper in scenario 'b' than it is in scenario 'a,' and scenario 'c' also has a steeper drop than the other three scenarios.

2.3.1.2   Rotor Angle Stability in IBR-dominated Power System

In traditional power systems, the shape, frequency, and damping factor of rotor oscillations are highly affected by the number and type of synchronous generators that are connected to the grid. However, as the number of IBRs increases, the number of synchronous generators decreases. This means that the system has little or no inertia. Because of this, there are clear changes in the way the power system works and looks, which leads to several problems. PEC technologies, which are built into IBR systems, make it possible to handle active and reactive power on both the generation and load sides, which can help keep the rotor angle and frequency stable. Still, the lower system inertia that comes with IBRs can make it hard to keep frequency balance when there are big changes in output or load that happen quickly. To solve the problems caused by rotor angle stability in an IBR-dominated power system, it is important to do a complete study and assessment.

As mentioned in Subsection 2.2.1.1, the analysis shows that CCT values rely greatly on the power system's inertia constant. As the inertia constant goes down, the CCT values of all parts of the multi-machine power system go down noticeably. This effect is more noticeable in the local area than in nearby areas. The third of the cases looked at shows big differences in performance due to a big drop in system inertia. Even though all scenarios and sub-cases show stability, a drop in the inertia constant has a big effect on all indicators of rotor angle stability. Notably, as the inertia constant goes down, voltage, frequency, and generator speed all change in noticeable ways, in conclusion, it is important to think about rotor angle stability in an IBR-dominated power system. The drop in system inertia and the stability problems that come with it are big problems that need to be solved well.

2.3.2 Frequency Stability

Maintaining stable frequency is essential for a power system's reliable and efficient operation. The frequency of a power system is carefully controlled within an acceptable range to balance

the generation capacity with the total load, ensuring a consistent supply of electrical power. However, imbalances between generation and demand can lead to frequency deviations, which can significantly affect power system operation, reliability, and security. These deviations can impact load performance, cause transmission line overloading, result in protection failures, and reduce equipment efficiency [146].

Frequency fluctuations occur when the system has a difference between the supplied and demanded power. Mathematically, this can be expressed as $P_M(t) \neq P_L(t)$, where $P_M(t)$ represents the mechanical or generated power and $P_L(t)$ represents the electrical load at a specific moment in time. The system's frequency is directly proportional to the speed of the generator. An increase in rotor speed leads to an increase in system frequency, while a decrease in rotor speed corresponds to a decrease in frequency. When the system demand increases, the rotor speed gradually decreases, causing a decrease in frequency (i.e., $P_M(t) < P_L(t)$). Conversely, when the system load decreases, the rotor speed and frequency increase (i.e., $P_M(t) > P_L(t)$). Therefore, to prevent frequency deviations, the generated power must match the sum of the demand power and power losses. This relationship between frequency and power deviation can be mathematically expressed using the swing equation, as shown in Equation 2.4.

Practical cases have shown frequency sensitivity to various factors, highlighting the need to understand the dynamics through specific examples. One such example is the Royal Wedding of Prince William and Catherine on April 29, 2011, which provides insights into the relationship between electricity demand and system frequency. The event witnessed significant fluctuations in electricity demand, leading to drastic changes in frequency. The operation of numerous electronic appliances during the event resulted in a high load demand, causing a sudden rise of 2,300 MW within a few minutes, followed by a drop of 3,100 MW. These sharp fluctuations in demand pose challenges in maintaining frequency within acceptable limits, highlighting the importance of frequency stability even during infrequent special events. The change in electricity demand and system frequency for that day can be shown in Figure 2.15.

$$\frac{2H}{\omega_s}\frac{d^2\delta}{dt^2} = P_M - P_L \text{ (in per unit)}$$

Equation 2.4
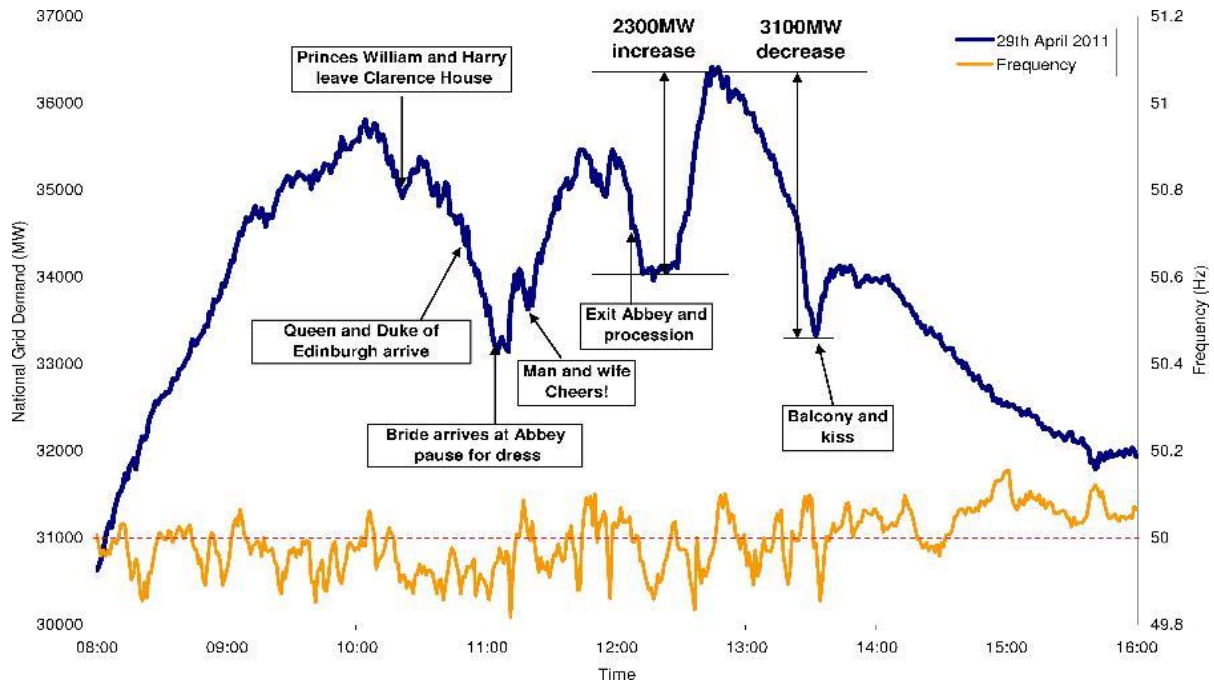
Figure 2.15: Change in electricity demand and system frequency in Great Britain's power system during the Royal Wedding of Prince William and Catherine on 29 April 2011 [156].
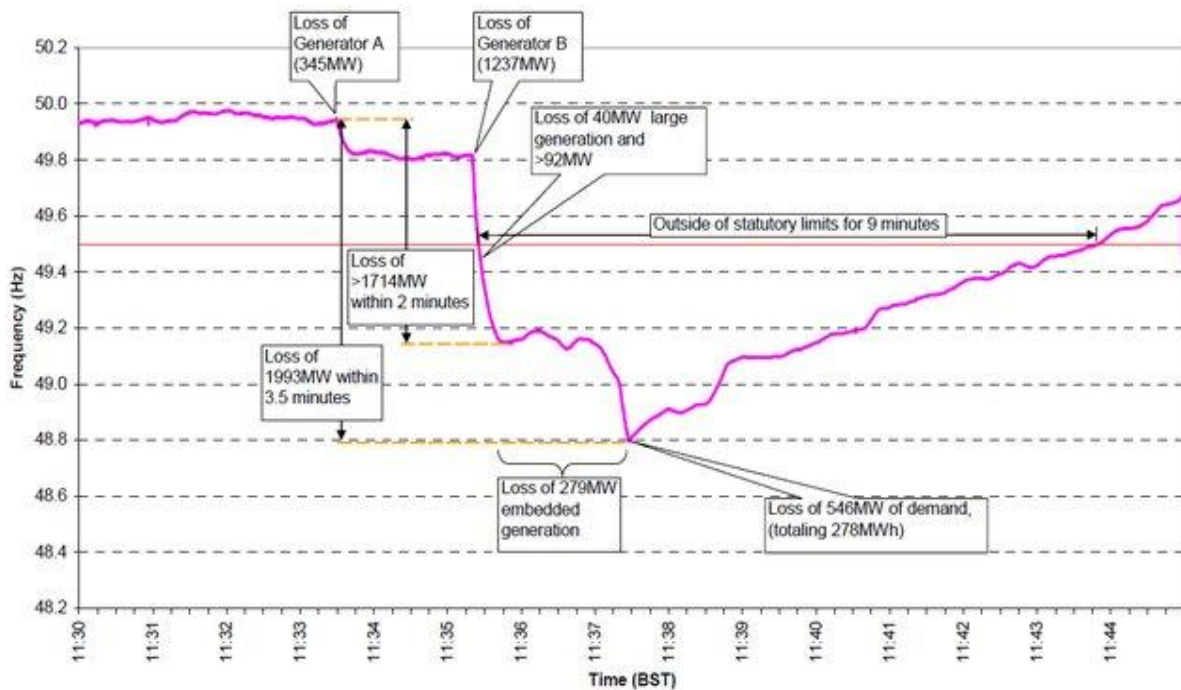
Figure 2.16: Frequency fluctuation in the British power system during the failure of the Sizewell B nuclear power plant on 28 May 2008 [156].

Another example that demonstrates the significance of frequency stability is the failure of the Sizewell B nuclear power plant on May 28, 2008, in the Great Britain power system. The incident resulted in three power system failures and one embedded generation failure, leading to a total failure of 1,993 MW within a short period of 3.5 minutes. The capacity of the failed power system exceeded the actual reserve capacity, making it difficult to balance generation and demand. As a consequence, the frequency exceeded the acceptable limit, necessitating a controlled power cut-off of 546 MW in a specific part of the city for stability maintenance. This incident highlights the importance of considering frequency stability and the challenges associated with significant generation changes within a short time frame. The frequency fluctuation in the British power system during the failure of the Sizewell B nuclear power plant can be shown in Figure 2.16.

Overall, these specific examples emphasize the critical role of frequency stability in the proper operation of a power system. Fluctuations in electricity demand, whether due to special events or unexpected failures, can lead to drastic changes in frequency, posing challenges to system stability. Understanding the dynamics and factors influencing frequency stability is essential for system operators and engineers to implement measures that ensure reliable and secure power system operation. Further research in this area can focus on developing advanced monitoring and control techniques to enhance frequency stability and mitigate the risks associated with significant demand fluctuations and unexpected failures.

2.3.2.1 Frequency Response and Regulation Techniques

To ensure the maintenance of an acceptable frequency range, the power system relies on the injection and withdrawal of generated power. This process must be responsive and rapid to accommodate dynamic load changes and achieve supply-demand balance. The power system incorporates flexible power generation that can be adjusted according to load variations, thereby regulating the system frequency [157]. This regulation is an ongoing and continuous process. In the context of the Great Britain power system, Figure 2.15 demonstrates significant

fluctuations in demand, with a sudden rise of 2,300 MW and a subsequent drop of 3,100 MW within a short period.

Nevertheless, the system managed to maintain its frequency within the range of 49.8 Hz to 50.2 Hz. This process is known as frequency regulation within a power system. Each power system has a predefined normal operating frequency band (NOFB) that it aims to maintain. The restrictions may vary from nation to country, but a general idea of the nominal frequency interval and the critical frequency interval can be seen in Table 2.4.

Table 2.4: Nominal and critical frequency intervals in the power systems.

Country	Nominal frequency (Hz)	Critical frequency (Hz)	References
Great Britain	49.5-50.5	47-52	[158-160]
Germany	49.5-50.5	47-52	[160-162]
France	49.5-50.5	47-52	[160, 161]
Belgium	49.5-50.5	47-52	[160]
Austria	49.5-50.5	47.5-51.5	[160]
Australia	49.75-50.25	47-52	[163-165]
Ireland	49.8-50.2	47-52	[160]
Italy	49.1-50.1	47.5-51.5	[160]
Poland	49.5-50.5	47-52	[160]
Denmark	49.9-50.1	47.5-51	[166-168]
China	49.8-50.2	48-51	[169]

Frequency instability in power systems arises due to disparities between electric generation and demand, leading to power deviations. To ensure effective operation, power systems employ various means to balance the demand-supply chain. For extensive systems, a significant reservoir can be utilized, while Battery Energy Storage Systems (BESS) are suitable for smaller systems [170]. However, relying solely on these approaches may not be sufficient to maintain equilibrium in real-time scenarios. Hence, generating plants must possess flexible generation capabilities, which support instant balancing and mitigate potential failure risks [170, 171]. Moreover, critical issues can emerge from significant deviations occurring within short periods, necessitating proper management for overall system protection. Consequently, power systems implement control mechanisms at different levels to maintain the NOFB and

safeguard the entire system. These control levels include: (a) primary control, (b) secondary control, (c) tertiary control, and (d) emergency control. Figure 2.17 illustrates conventional power system frequency control techniques aimed at minimizing frequency deviations within an acceptable range to ensure secure and reliable operation.

Additionally, Figure 2.18 presents the frequency response of the power system under various control actions, showcasing their respective characteristics. The primary control action depicted in Figure 2.18 is the initial and fastest response, while secondary and tertiary control actions exhibit slower activation times. It should be noted that the specific response times and control actions may vary across different nations and power systems.
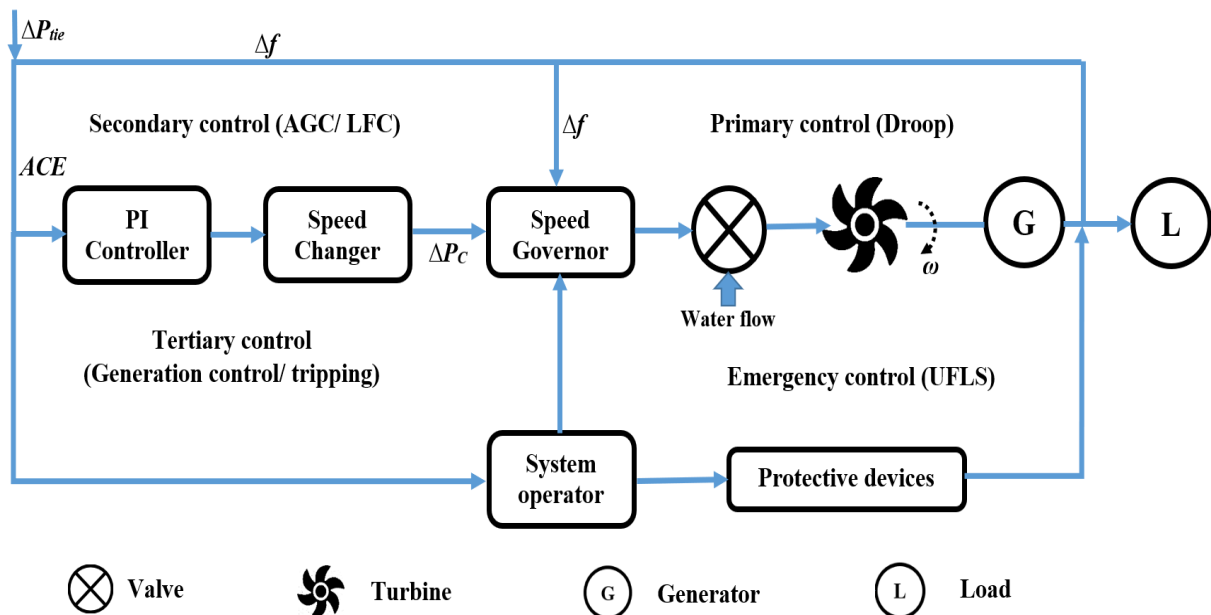
Figure 2.17: Frequency control techniques/ loops in a power system.

Frequency control is a crucial aspect of maintaining the stability and reliability of a power system. In conventional power systems, frequency is directly related to the angular velocity of the rotor, which means that controlling the rotor speed is essential for frequency control. The primary frequency control technique, implemented through the governor mechanism, regulates the flow of water/steam based on rotor speed sensing to maintain the speed of the turbine-generator set. This technique is responsible for correcting low speed and frequency deviations within seconds, acting as the initial line of defense in frequency control [172].
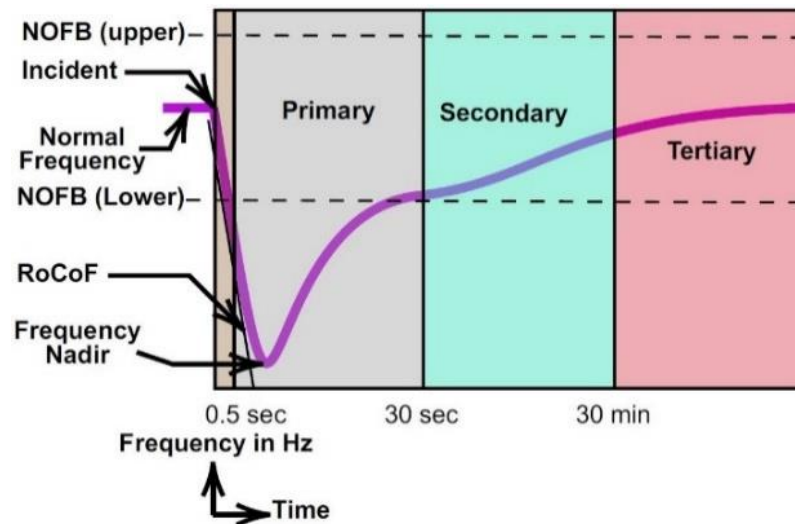
Figure 2.18: Frequency response of the power system under different control actions.

However, in cases where frequency deviations exceed a certain threshold, the primary frequency control alone may not be sufficient to restore system frequency. This calls for implementing the secondary frequency control technique, also known as Load Frequency Control (LFC). The secondary control technique utilizes spinning and non-spinning reserve capacities to balance the load and control the frequency. It employs automatic and centralized controls, utilizing the system's reserve capacity to restore the frequency within a few minutes to several minutes. The secondary control technique consists of unit-level and system-level controls, with unit-level controllers monitoring system variables and requiring action from the primary control, while the Automatic Generation Control (AGC) system coordinates power generation adjustments among all power generators. AGC and LFC aim to maintain system frequency by coordinating power exchange with neighboring control areas, aiming for a lower Area Control Error (ACE) value in each power plant area [173-177].

The tertiary stage of frequency control comes into play during severe supply-demand imbalances caused by sharp frequency deviations. It involves manual or automatic control techniques to adjust the working rate of power generation. Tertiary control encompasses adjustment, rescheduling, and deployment of new power generators, and it takes a longer duration, ranging from tens of minutes to hours, to restore the secondary control reserves. Tertiary control can be seen as an economic dispatch method and is typically employed in a

fully deregulated market framework. It supports the secondary control by coordinating reserves and relieving the secondary control response to approach a lower value of ACE. In situations where frequency deviations exceed acceptable limits and control techniques fail, standby supplies or emergency actions such as Under Frequency Load Shedding (UFLS) schemes or disconnection of generation stations may be necessary to prevent cascading faults and system blackouts [177-179].

In conclusion, frequency control in power systems involves multiple stages: primary frequency control for immediate correction of small deviations, secondary frequency control for longer duration frequency restoration utilizing reserve capacities, and tertiary frequency control for managing severe supply-demand imbalances. These control techniques are vital for maintaining system stability and reliability, and their proper implementation ensures the smooth operation of power systems even in the face of disturbances and fluctuations in load and generation. Future research in this area can focus on developing advanced control strategies and coordination techniques to enhance the efficiency and effectiveness of frequency control in modern power systems.

2.3.2.2 *Frequency Stability in IBR-dominated Power System*

The modern power system is undergoing significant transformations in generation, transmission, distribution, and utilization, driven by the rapid growth of PEC-based technologies and the integration of IBRs. These transformations involve the extensive integration of PEC-based RESs, such as solar PV and wind turbines, in the generation, as well as the dependence on PECs for appliances and control methods in other sectors. However, these advancements have also introduced challenges related to short-term frequency instability in the power system for two reasons. Firstly, the high penetration of PEC-based RESs reduces system inertia, and secondly, the unpredictable patterns of RESs make it challenging to balance the demand-supply chain [180].

The modern power system is undergoing significant transformations driven by the integration of PEC-based technologies and the increasing penetration of RESs. The integration of RESs,

such as solar PV and wind turbines, has led to challenges related to short-term frequency instability in the power system. Two main reasons contribute to this instability: the reduction of system inertia due to the high penetration of PEC-based RESs and the unpredictable nature of RESs, which makes it challenging to balance the demand-supply chain. These rapid changes have made the modern power system more complex [180]. Solar and wind resources exhibit stochastic characteristics, with variable power generation trends occurring over different timescales. Similarly, power demand in the system also exhibits stochastic behavior with continuous variations. The modern power system experiences short-term variations in both generation and load within minutes and hours. Various studies have been conducted to forecast solar and wind power generation to reduce uncertainty in the power system. However, forecasted results may not be highly accurate on an exact timescale, leading to significant deviations in system frequency, especially in low-inertia power grids. The increasing penetration of PECs amplifies the stochastic variations in active power generation, which can result in unpredictable situations within the system [181-188].

In a conventional power system, synchronous generators contribute to system inertia, which is essential for maintaining system frequency. The rotation of synchronous machines is directly linked to the system frequency, and the inertia these machines provide helps minimize initial frequency deviations. The total mechanical inertia of the system exhibits resistive properties against changes in machine rotation, ensuring frequency stability. Equation 1 highlights how a slight imbalance between power generation and load can lead to frequency deviations in a power system. A more detailed representation of Equation 4 is provided in Equation 2.5 and Equation 2.6, considering the inertia constant (H), system frequency (f), rated power of the machine (S), kinetic energy (E_{kin}), equivalent inertia of the entire power system (H_{sys}), system base power (S_{sys}), and the inertia (H_i) and rated power (S_i) of ith machines [189].

The relationship between system inertia and the kinetic energy of machines in the power system is evident from the equations provided. The system inertia increases in direct proportion to the kinetic energy of the machine, assuming a constant rated power. In

conventional power systems, synchronous generators serve as both a source of kinetic energy and system inertia. However, the modern power system exhibits reduced kinetic energy and inertia due to the increasing adoption of IBRs. These technologies are widely utilized in appliances and equipment control mechanisms, significantly reducing inertia. The rate of IBR integration is rising steadily, leading to a steep decline in system inertia [190].

$$H = \frac{(J\omega_0{}^2)/2}{S} = \frac{E_{kin}}{S} = \frac{H_i S_i}{S_{sys}}$$

Equation 2.5

$$H_{sys} = \frac{E_{kin,sys}}{S_{sys}} = \frac{\sum_{i=1}^{n} H_i S_i}{S_{sys}}$$

Equation 2.6

Maintaining synchronism and uniform frequency is crucial in a power system with multiple generators. However, significant power deviations can cause individual generators to lose synchronization, resulting in fluctuating motion around the Centre of Inertia (COI) (see Equation 2.7 and Equation 2.8). Each unit's frequency may differ, leading to oscillatory behavior. The extent of oscillation depends on the power deviation between generations. $P_M(t)$ and load $P_L(t)$, as depicted in Equation 2.4. However, the frequencies of individual units are close to the COI, and the damping and inertial forces among the units strive to restore system-wide synchronization. A control mechanism must be activated if these forces fail to maintain the system's stability [191, 192].

Equation 2.8 and Equation 2.9 highlight the direct relationship between system frequency, its rate of change, and the inertia of the power grid. Reduced system inertia results in higher frequency fluctuations. Figure 2.19 (a) and (b) visually analyze these issues, illustrating frequency dynamics at different inertial constants and power deviations. Figure 2.19 (a) demonstrates that lower system inertia leads to higher frequency deviations, potentially resulting in an unstable power system. Similarly, Figure 2.19 (b) showcases the dynamic characteristics of the frequency with changing power deviations—the analysis employed transfer function constants obtained from a reference book [146].

$$f_{COI} = \frac{\sum_{i=1}^{n} H_i S_i f_i}{\sum_{i=1}^{n} H_i S_i}$$

Equation 2.7

$$f_{COI(t)} = 1 + \frac{\Delta P}{2H_{sys}} t$$

Equation 2.8

$$RoCoF = \frac{\Delta P}{2H_{sys}}$$

Equation 2.9
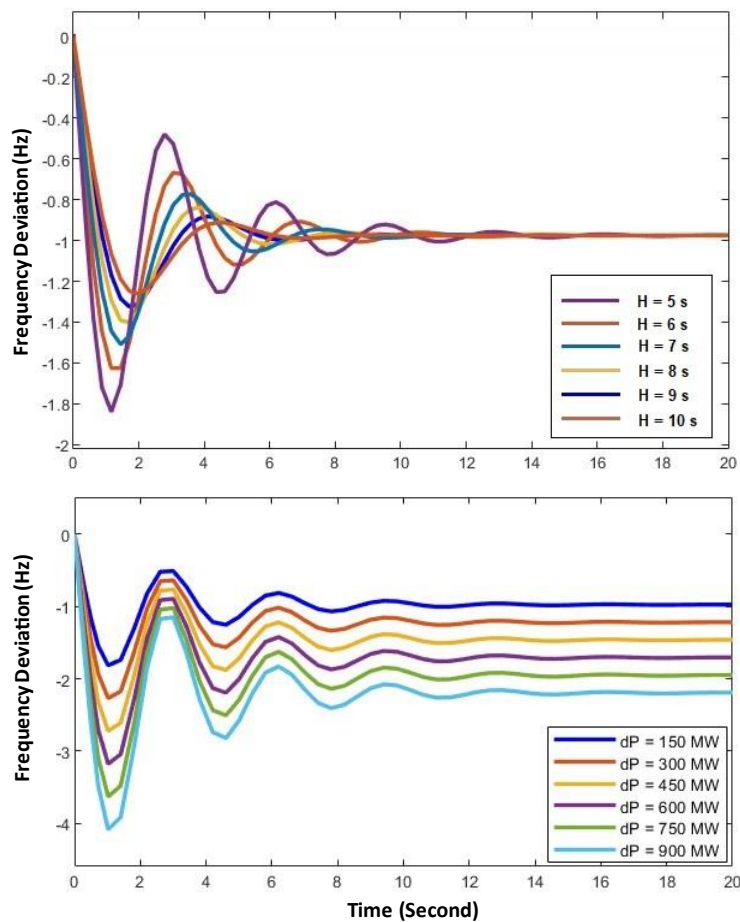
Figure 2.19: Frequency dynamics at different (a) inertial constant, and (b) power deviation.

The integration of IBRs in a power system not only affects frequency stability but also gives rise to other stability issues. The synchronous generators linked to the grid directly affect the system's stability in terms of rotor angle and small signals [193]. When there are more IBRs in the power system, there are fewer synchronous generators. This can change the form, frequency, and damping factor of rotor oscillation [149]. Also, power system stabilizers that are tied to synchronous generators can not be used with the power system. As disturbances

increase, transient instability may occur due to changes in power flow through tie-lines [194]. Rotor angle stability is closely related to frequency stability, as the rotor speed of generators is adjusted in response to system frequency [15]. PEC-based technologies, capable of controlling active and reactive power on both the generation and load sides, can be utilized to address rotor angle stability and frequency stability concerns [195, 196]. Moreover, low inertia power systems may struggle to maintain frequency balance during significant deviations resulting from rapid generation/load changes [197].

2.3.3 Voltage Stability

Voltage stability is a critical aspect of power systems, ensuring reliable and secure electrical network operation. It refers to a power system's ability to maintain acceptable voltage levels within predetermined limits under normal conditions and in the face of disturbances. If not properly managed, voltage instability can lead to voltage collapse, causing widespread blackouts and severe damage to electrical equipment. Reactive power plays a crucial role in understanding voltage stability; it is essential for maintaining voltage levels and supporting the transmission and distribution of electrical energy [194].

Voltage instability happens when a disturbance, an increase in load demand, or a change in the system causes the voltage to drop in a way that can not be stopped. The primary factor contributing to instability is the power system's inability to meet the demand for reactive power. Voltage stability issues often arise in heavily stressed systems, where factors such as the strength of the transmission network, power transfer levels, generator reactive power/voltage control limits, load characteristics, and reactive compensation devices significantly impact the system's stability [194].

Voltage stability can be broadly defined as the system's ability to maintain steady, acceptable voltages at all buses following a disturbance or contingency. It is affected by the power system's ability to meet the demand for active and reactive power flow through the transmission network. Small disturbance voltage stability refers to the system's ability to maintain steady-state stability, where voltages near the loads remain close to their pre-

disturbance values. Analysing voltage stability typically involves simulating the power system using nonlinear differential-algebraic equations [198].

Several indices are employed to assess voltage stability and measure a power system's overall stability. These include the voltage stability margin (VSM) and the voltage stability index (VSI). These indices help evaluate the system's proximity to voltage collapse and provide valuable insights into its stability characteristics. Ensuring voltage stability is crucial for the reliable and secure operation of power systems. Achieving a balance between reactive power supply and demand is essential to avoid deviations that can result in voltage instability and potential system collapse. Robust analysis techniques, such as monitoring eigenvalues and employing appropriate voltage control devices like capacitor banks at different buses, are essential for maintaining voltage stability in both transmission and distribution systems [199].

In summary, voltage stability plays a vital role in power system operation, enabling the maintenance of acceptable voltage levels. By understanding and managing reactive power, analyzing voltage stability through various indices, and implementing appropriate control measures, power system operators can ensure the reliable and secure operation of electrical networks while mitigating the risks associated with voltage instability.

2.3.3.1 *Voltage Stability in IBR-dominated Power System*

Keeping the voltage stable in an IBR-dominated power system is a unique problem that needs creative solutions. As more and more RESs like solar and wind power connect to the power grid through IBRs, keeping the voltage stable is important for the system to work well. Reactive power is mostly made by synchronous machines in standard power systems, but IBRs don't have the ability to make reactive power on their own [200]. This makes the balance between reactive power supply and demand a very important issue.

One of the biggest problems with power systems that are mostly made up of IBRs is that their output can change and isn't always predictable. Solar and wind resources can vary depending on the weather and how often they are used. This can cause real-world power output to change quickly. These changes in real power generation have a direct effect on reactive power

usage, which causes voltage changes and could make voltage stability less stable. Because of this, effective plans are needed to lessen these effects and keep the voltage stable.

It is important to fix gaps in reactive power in IBR-dominated power systems. Coordinated reactive power control is a potential way to handle both traditional and IBR-based reactive power sources in a coordinated way. Advanced control methods and communication infrastructure allow the best use of available reactive power resources to meet the system's demand, which helps keep the voltage stable. Coordinated control can use real-time tracking and control systems to make sure that the reactive power output of IBRs and other compensating devices is adjusted on time, which reduces the risk of voltage instability [201].

In IBR-dominated power systems, keeping the voltage stable is a big job for voltage control and compensation equipment. Devices like on-load tap changers and shunt capacitors make it possible to control voltage and compensate for gaps in reactive power. These devices give you more options for controlling voltage levels, making up for reactive power demand, and improving the general stability of the system. Voltage regulation devices can compensate for voltage changes caused by changes in IBR output by changing tap positions on the fly and adding or taking away reactive power as needed [202].

Integration of BESS is a creative way to improve voltage stability in power systems that are controlled by IBR. BESS can act as a buffer by keeping extra energy when production is high and releasing it when demand is high or when IBR output changes. By giving reactive power support quickly, BESS can help control voltage levels and stop voltage changes caused by changes in IBR output. Implementing BESS along with IBRs and other types of generation sources can make it much easier for the system to keep the voltage stable even when working conditions change [203].

In IBR-dominated power systems, proactive voltage stability management is only possible with the help of advanced tracking and control systems. When real-time measurements are combined with predictive algorithms, voltage changes, and possible instability can be detected early on. These systems make it easy to take corrective steps quickly, like changing

the settings for reactive power control or turning on voltage regulation devices, so that voltage instability doesn't happen. Power system operators can deal with problems with voltage stability in IBR-dominated environments by using insights from data and smart control methods [7, 204].

In the end, voltage stability in power systems that are controlled by IBR needs careful thought and the use of new strategies. Keeping the voltage stable requires coordinated control of reactive power, devices that change the voltage, BESS, and advanced tracking and control systems. As the use of renewable energy continues to grow, more research and development are needed to improve voltage stability techniques and make sure that IBR-dominated power systems work reliably and safely. By managing reactive power balance well and using current control technologies, the stage for a future with sustainable energy while keeping the power grids stable can be settled.

2.3.4 Converter-driven Stability

In recent years, there has been a lot of growth in the use of RESs like wind power and photovoltaics (PVs). This has been made possible by PECs, which turn the changeable output of RESs into stable electrical energy for the power grid. However, the presence of IBRs in the system introduces new challenges, particularly in terms of converter-driven stability. Modal resonances and interactions between different IBRs and weak grids cause these problems. These things can worsen dynamic performance and threaten the whole system's security. Due to the wide use of Voltage Source Converter (VSC) technology, converter-driven stability in RES integration is very different from that of traditional synchronous engines. IBRs use control loops and methods with fast response times, such as phase-locked loops (PLL) and inner-current control loops. However, because these controls have a long-time scale, they can cross-couple with the electrical dynamics of machines and the electromagnetic transients of the network. This can cause oscillations that are unstable over a wide range of frequencies [205-207]. Stability effects caused by the converter can be put into two groups: fast interactions and slow interactions. Dynamic problems caused by the control systems of devices that use power electronics and their interactions with fast-response components are what make fast

interactions happen. On the other hand, slow interactions happen when there are interactions with parts of the power system that respond slowly. The parts that follow give more information about these groups:

2.3.4.1 Fast-Interaction Converter-Driven Stability

This group includes instability caused by interactions between power electronic-based systems, like converters, HVDC, and FACTS, and fast-response components, like transmission networks and synchronous generators. Harmonic instability, multi-resonance, and high-frequency oscillations caused by switches and control interactions are some examples.

(a) Instability in harmony: Harmonic instability is a type of instability caused by fast, dynamic reactions between power electronic converters and passive system components. High-frequency waves are caused by these interactions between the fast inner-current loops of converters and passive components [208, 209]. Harmonic instabilities can be caused by resonances in parallel or series, switching at high frequencies, or interactions between converters that are linked to the grid [209-211]. There are some case studies and findings of harmonic instability in different power systems [212-214].

(b) High-Frequency Oscillations: High and very high-frequency oscillations have been seen in large wind power plants linked to VSC-HVDC systems, which makes stability hard to achieve [215]. The paper talks about the waves' frequency range, what causes them, and how they might be stopped [213, 216]. It also shows how important well-tuned control strategies, like virtual synchronous machine controllers, are for lowering the number of fast oscillations [213].

2.3.4.2 Slow-Interaction Converter-Driven Stability

This group focuses on the instability caused by the dynamic interactions between power electronic devices and slow-response components, such as the electromechanical dynamics of synchronous generators. Low-frequency waves and weak systems are two good examples.

___

(a) Low-frequency oscillations: Slow-Interaction Converter Driven Stability involves slow dynamic interactions between the controls of the converter and the electromechanical dynamics of synchronous engines or weak grids. Low-frequency waves that aren't stable can happen when converter control loops and other system parts interact [209]. [217] shows case studies of low-frequency oscillations in power systems with converter-based generators, like windmills with direct-drive permanent-magnet generators (PMGs). Similarly, [218] talks about how the system's strength, the PLL's tuning, and the control methods affect low-frequency oscillations.

(b) Weak System Stability: Weak system stability looks at the problems with power transfer limits and how converters can change their phase in weak networks [17-20]. Stability is looked at in terms of how converter control loops, PLL performance, and power transfer limits affect it. Research articles [217, 219], talk about possible methods, such as coordinated control of multiple converters and control strategies that make a grid.

In conclusion, converter-driven stability includes a wide range of dynamic phenomena and problems that happen when converter-based systems, like CIGs, are added to the power grid. Understanding both fast and slow interactions is important for making effective control methods that can fix these problems and make power systems more stable and reliable. The goal of ongoing studies and improvements in converter control technologies is to find ways to deal with these problems and make the power grid more stable and reliable.

2.3.5 Resonance Stability

Resonance stability within an IBR-based power system refers to the occurrence of periodic energy exchange in an oscillatory manner. This phenomenon amplifies voltage, current, and torque parameters while hindering the dissipation of energy, resulting in significant oscillations that can affect both electrical and mechanical components. There are two distinct types of resonance stability: (a) torsional resonance, and (b) electrical resonance. Torsional resonance is primarily observed in conventional power systems with synchronous generators, whereas electrical resonance is more prevalent in systems utilizing IBRs, particularly variable-

speed induction generators found in wind turbines. These resonances pose challenges by causing disturbances in current, voltage, and electrical torque, impacting the overall system performance [193, 207].

The occurrence of resonance in a power system stems from inadequate dissipation of energy, leading to periodic energy exchange in an oscillatory fashion. This amplifies voltage, current, and torque magnitudes, and when these magnitudes surpass certain thresholds, resonance instability arises. Resonance stability encompasses subsynchronous resonance (SSR), which can manifest as either electromechanical resonance or purely electrical resonance. SSR can occur in two forms: resonance between series compensation and the mechanical torsional frequencies of the turbine-generator shaft and resonance between series compensation and the electrical characteristics of the generator. The former, known as the Induction Generator Effect, arises from interactions between the series compensated electrical network and the mechanical modes of torsional oscillations on the turbine-generator shaft [193, 207].

SSR occurs when there is significant energy exchange between the network and a turbine generator at one or more of the natural sub-synchronous torsional oscillation modes within the combined turbine generator mechanical shaft [220]. These oscillations can exhibit poor damping, no damping, or even negative damping, posing a threat to the mechanical integrity of the turbine-generator shaft. Device-dependent subsynchronous oscillations occur due to the interaction between fast-acting control devices, such as HVDC lines, static VAR compensators, static synchronous compensators, and power system stabilizers with the torsional mechanical modes of nearby turbine-generators [220, 221]. It is important to note that Device-dependent subsynchronous oscillations can have both detrimental and beneficial interactions, as some interactions enhance torsional damping [222].

SSR mainly involves torsional interactions and resonance in power systems employing conventional turbine-generators, with the Induction Generator Effect not observed in actual power systems utilizing conventional synchronous generation. However, it was predicted that variable-speed induction generators used in doubly-fed induction generators would be highly susceptible to Induction Generator Effect SSR [223]. This susceptibility arises due to the direct

grid connection of a variable-speed doubly-fed induction generators generator, making it an induction generator capable of experiencing electrical resonance with series compensation [207]. Self-excitation SSR occurs when the series capacitor forms a resonant circuit at sub-synchronous frequencies, with the effective inductance of the induction generator [224]. If the total negative resistance surpasses the positive resistance near the resonant frequencies, self-excitation SSR takes place. This resonance primarily leads to large current and voltage oscillations that can damage electrical equipment within the generators and transmission system and may also result in mechanical damage to the turbine-generator assembly, such as the gear box [207, 224]. Incorporating additional controllers into the doubly-fed induction generator converter controls has been demonstrated to mitigate and dampen resonant oscillations [207, 225].

3 Time-series analysis of kinetic energy in power system analysis

Estimating kinetic energy from time-series data is a crucial aspect of energy research and power system management. Kinetic energy, representing the energy associated with object movement, holds significant importance in various sectors, such as renewable energy integration, grid stability, and demand forecasting. Accurate estimation of kinetic energy using time-series data enables improved planning, operation, and control of power systems. By analyzing historical patterns and trends in kinetic energy, researchers and practitioners gain valuable insights into the behavior and dynamics of energy systems. This knowledge aids in optimizing renewable energy generation and consumption, enhancing grid reliability, and mitigating potential risks and uncertainties. Understanding the temporal variations of kinetic energy empowers stakeholders to make informed decisions regarding energy infrastructure investments, load balancing, and integrating intermittent renewable sources into the grid.

Furthermore, accurate estimation of kinetic energy through time-series analysis facilitates short-term and long-term forecasting, which is vital for efficient energy management. Forecasting kinetic energy patterns assists in planning energy generation and storage capacities, optimizing energy dispatch, and managing demand response programs. It also supports the development of strategies for grid stability, frequency regulation, and reliable power supply, particularly in converter-dominated power systems with high levels of intermittent renewable energy sources. The study of time-series data estimation of kinetic energy also contributes to the advancement of data-driven models and algorithms. It involves developing and applying statistical and machine learning techniques to analyze and predict energy patterns accurately. These models can capture the complex interactions and dependencies within energy systems, leading to more precise estimations and improved system operation. Moreover, the findings from such studies can inform the development of predictive control strategies, enabling real-time adjustments and optimization of energy resources. By accurately forecasting and analyzing kinetic energy patterns, power system

operators can make informed decisions, develop effective strategies, and pave the way for a more sustainable and resilient energy future.

This chapter focuses primarily on the short-term forecasting of kinetic energy in converter-dominated power systems, and its main objective is to analyze the importance of time-series data analysis of kinetic energy in power system analysis, especially the modern power system dominated by IBRs. This sub-section presents the prospective for estimating power systems' dynamic characteristics by forecasting time-series kinetic energy data. The content of this chapter is primarily derived from **Article 4** [190].

3.1 Methodology used to forecast the time-series data sets

3.1.1 Data sets

The main objective of this sub-section is to analyze the importance of time-series data on kinetic energy in power system analysis. The time-series data on kinetic energy obtained from the Integrated Nordic Power System (INPS) is utilized for that. The kinetic energy data for the INPS in 2019 is obtained from FINGRID's web portal [226]. A total of 525,604 samples were collected, with measurements taken every minute. Upon reviewing the raw datasets, it was discovered that some entries were of the NaN (not a number) type. These observations served as an initial indication of outliers within the collected data. Ensuring high-quality data is crucial for accurate analysis and proper visualization of results. Presenting flawed visualizations resulting from poor data can lead to audience misinterpretation. Therefore, the raw data underwent initial processing to minimize potential errors by filtering and addressing missing values. Out of the 525,604 samples, 9,273 samples (approximately 1.76%) are missing and replaced with the corresponding column's mean values. The minimum and maximum values recorded for kinetic energy in 2019 were 126 GWs and 273 GWs, respectively. Similarly, the mean and median values of the entire sample set are determined to be 194.1 GWs and 191 GWs, with a standard deviation of 27.6. Figure 3.1 displays the frequency characteristics over the entire year, while Figure 3.2 illustrates the kinetic energy of the Nordic grid. Both figures are provided below for reference.
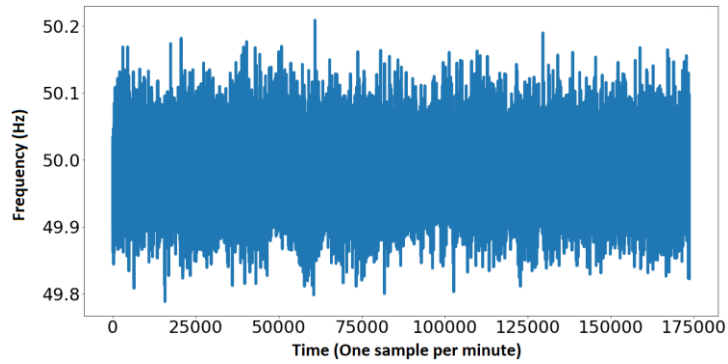
Figure 3.1: Plot of the datasets of frequency for one year.
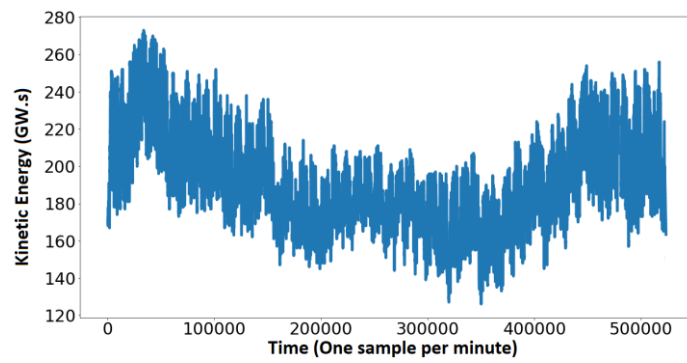
Figure 3.2: Plot of the datasets of kinetic energy for one year.
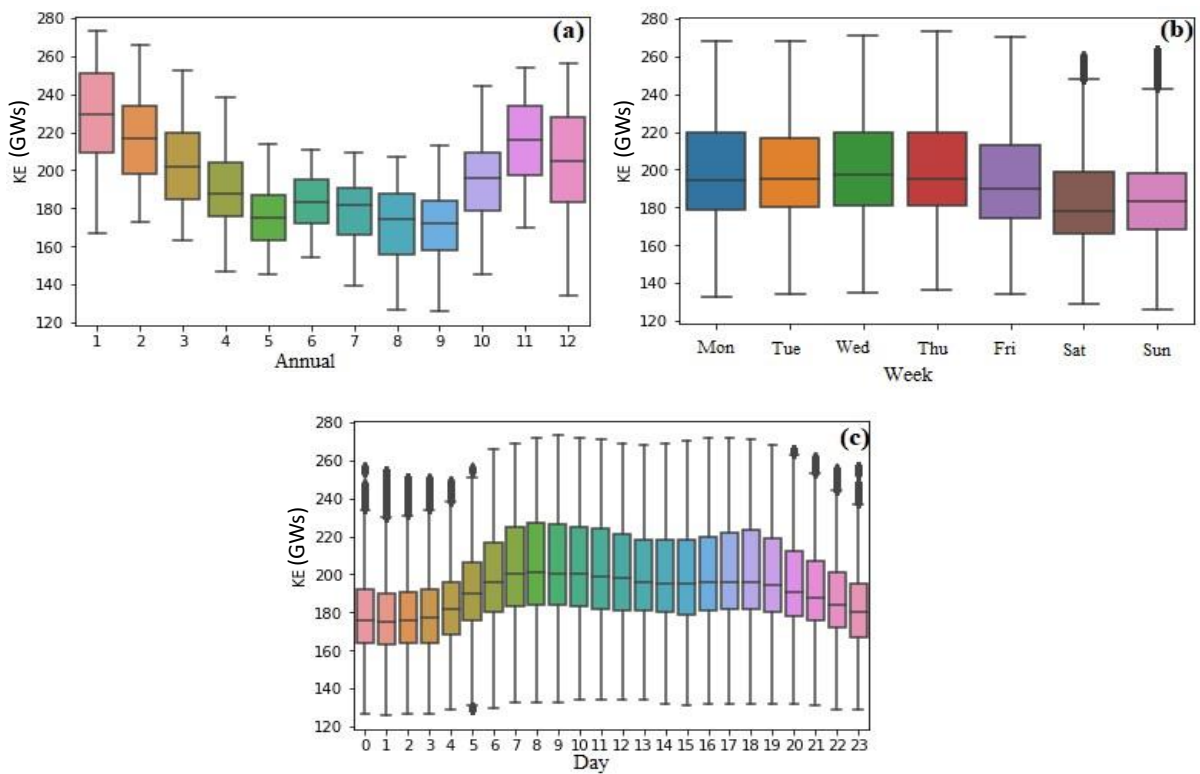
Figure 3.3: Seasonal variations of KE: (a) annual, (b) weekly, and (c) daily.

To gain a deeper understanding of the data, box plots can be employed to visualize its characteristics. As depicted in Figure 3.3 (a), the case study results indicate that the amount of kinetic energy depends on prevailing weather conditions. Higher values are observed during the winter, while lower values are observed during the summer. Figure 3.3 (b) and (c) present the weekly and daily variations in kinetic energy. Interestingly, these figures demonstrate that kinetic energy is higher than the average during office hours but lower during non-working hours and holidays. This disparity can be attributed to the fact that kinetic energy production is directly proportional to the duration of productive activity.

3.1.2 Bayesian model

Bayes' theorem is a crucial principle in probability theory that enables us to adjust our beliefs and determine the probability of an event based on new evidence. It establishes a mathematical connection between the conditional probability of an event given another event and the prior probability of the events in question. Utilizing Bayes' theorem allows us to integrate fresh information and update our initial assumptions, resulting in more precise and well-informed probabilistic forecasts. This theorem has broad applications across disciplines such as statistics, machine learning, and data science, empowering us to make improved decisions and derive significant insights from observed data [227, 228].

In Bayes's theorem, the probability of event X occurring, given the occurrence of event Y, can be calculated using Equation 3.1 when X and Y are two events. Equation 3.1 represents the joint probability of the two events and does not exhibit symmetrical characteristics. Within Equation 3.1, the terms are defined as follows: P(X|Y) is referred to as the posterior probability, P(X) as the prior probability, P(Y|X) as the likelihood, and P(Y) as the evidence. If the prior probability, likelihood, and evidence values are known, the posterior probability can be easily determined.

$$P(X/Y) = \frac{P(X \cap Y)}{P(Y)} = \frac{P(X).P(Y|X)}{P(Y)}$$

Equation 3.1

In traditional linear regression estimation, Equation 3.2 is employed along with a normally distributed error term (ϵ_t ~ Normal (0, σ^2)). However, the accuracy of estimation can be improved by utilizing Bayes' theorem. By applying Bayes' theorem to linear regression, Equation 3.3 presents the updated posterior distribution, while Equation 3.4 represents the likelihood function. In these equations, β refers to the coefficient and σ^2 denotes the variance. This incorporation of Bayes' theorem allows for more precise estimation in linear regression analysis.

$$Y_t = BX_t + \epsilon_t$$

Equation 3.2

$$H(\beta,\ \sigma^2/Y_t) \propto F(Y_i|\beta,\ \sigma^2) * P(\beta,\ \sigma^2)$$

Equation 3.3

$$F(Y_t|\beta,\ \sigma^2) = (2\pi\sigma^2)^{-T/2}\ e^{-\frac{(Y_t-\beta X_t)^T\ (Y_t-\beta X_t)}{2\sigma^2}}$$

Equation 3.4

As given by Equation 3.1, the probability of conditional events can be identified if the values of the other three parameters are available. However, Stan's LM-BFGS [229] is used as the optimization algorithm in this study. By using Stan's Limited Memory Broyden-Fletcher-Goldfarb-Shanno (LM-BFGS), the new value (x_{t+1}) can be obtained as given in Equation 3.5 [230], where α_t is the step length that should be satisfy the Wolfe conditions, ∇f_t is the gradient, and H_t is the updated Hessian approximation (*n**n symmetric) at the iteration.

$$x_{t+1} = x_t - \alpha_t H_t \nabla f_t$$

Equation 3.5

The accuracy and efficiency of the LM-BFGS model in estimation heavily rely on the sensitivity of the Hessian approximation, denoted as H_t. This approximation involves replacing the vector pair (s_i, y_i) with the most recent pair (s_t, y_t) at each new iteration, which is then updated accordingly. For instance, if the current iterate is x_t, the set of vector pairs at the tth iteration will be (s_i, y_i) where *i* ranges from *(t – m)* to *(t – 1)*. The initial Hessian approximation, H_t^0, is considered and continuously updated up to the tth iteration until H_t satisfies the

condition described in Equation 3.6. The workflow followed for LM-BFGS in this study is depicted in Figure 3.4.

$$H_t = (V_{t-1}^T \ldots\ldots V_{t-m}^T) \, H_t^0 \, (V_{t-m} \ldots\ldots V_{t-1}) + \rho_{t-m} \, (V_{t-1}^T \ldots\ldots V_{t-m+1}^T) \, s_{t-m}$$
$$s_{t-m}^T \, (V_{t-m+1} \ldots\ldots V_{t-1}) + \rho_{t-m+1} \, (V_{t-1}^T \ldots\ldots\ldots V_{t-m+2}^T) \, s_{t-m+1} \, s_{t-m+1}^T \qquad \text{Equation 3.6}$$
$$(V_{t-m+2} \ldots\ldots\ldots\ldots V_{t-1}) + \ldots\ldots\ldots + \rho_{t-1} \, s_{t-1} \, s_{t-1}^T$$

$$\rho_t = \frac{1}{y_t^T \, s_t} \qquad\qquad \text{Equation 3.7}$$

$$V_t = I - \rho_t s_t^T y_t \qquad\qquad \text{Equation 3.8}$$

$$s_t = x_{t+1} - x_t \qquad\qquad \text{Equation 3.9}$$

$$y_t = \nabla f_{t+1} - \nabla f_t \qquad\qquad \text{Equation 3.10}$$
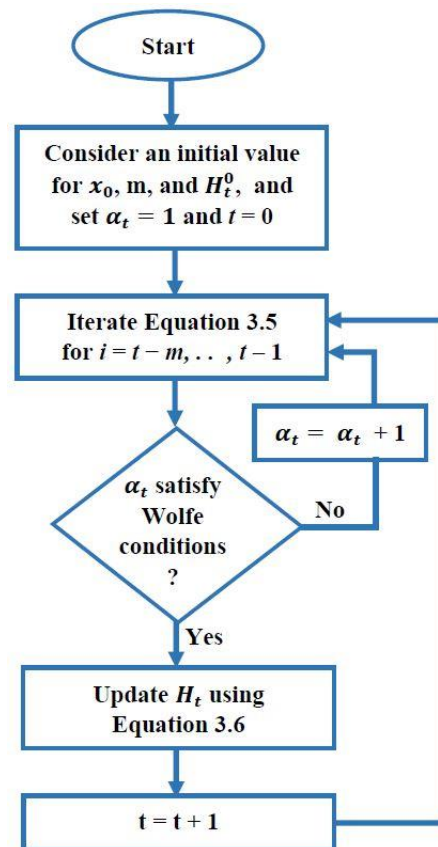
Figure 3.4: Flow chart of the LM-BFGS algorithm.

3.1.3 Optimization

Time-series data refers to a collection of observations, often taken at regular time intervals, although this is not always the case. Unlike models that consider the temporal dependence in the data, the described model approaches the forecasting problem as a curve-fitting exercise. It assumes that the factors influencing the data are functions of time since the data itself is a function of time. These factors are not treated separately since the model disregards temporal dependencies and focuses solely on the time component of the output. To optimize this model, one strategy is to experiment with different training datasets.

```
                          ┌─────────┐
                          │  Start  │
                          └─────────┘
                               │
              ┌────────────────────────────────────┐
              │ Set the number of training data set = 0 │
              └────────────────────────────────────┘
                               │
              ┌────────────────────────────────────┐
              │ Increase the number of training data set by 15 │◄──┐
              └────────────────────────────────────┘              │
                               │                                  │
              ┌────────────────────────────────────┐              │
              │ Extract the defined number of training data set │  │
              └────────────────────────────────────┘              │
                               │                                  │
              ┌────────────────────────────────────┐              │
              │           Train the model          │              │
              └────────────────────────────────────┘              │
                               │                                  │
              ┌────────────────────────────────────┐              │
              │      Compute and save the RMSE     │              │
              └────────────────────────────────────┘              │
                               │                                  │
              ┌────────────────────────────────────┐              │
              │      a = number of training data   │              │
              └────────────────────────────────────┘              │
                               │                                  │
              ┌────────────────────────────────────┐              │
              │     b = length (training data set) │              │
              └────────────────────────────────────┘              │
                               │                                  │
                            ◇ if a == b ? ◇──── No ───────────────┘
                               │
                             Yes
                               │
                          ┌─────────┐
                          │  Stop   │
                          └─────────┘
```
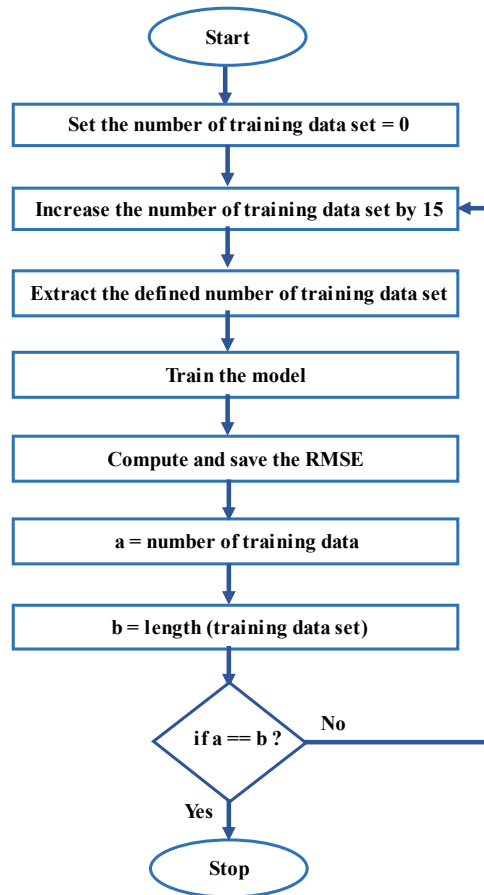
Figure 3.5: Flow chart of the optimization process.

The specific question being addressed is how many training datasets are required for short-term forecasting of kinetic energy with the least margin of error. An optimization model is developed to address this question, and the flow chart for this model is presented in Figure 3.5. The available data consists of a total of 525,604 observations. Initially, this data is divided

into a training set and a test set. The test set comprises the most recent 30 minutes of data, organized at minute intervals, while the training set consists of the remaining data and serves as the main dataset for training.

Using the training dataset, the model predicts the kinetic energy for the subsequent half an hour. The RMSE is then computed by comparing the predicted output with the test dataset. The number of training datasets is gradually increased by 15, and the aforementioned process is repeated. At each stage, the calculated RMSE is logged and plotted against the total number of training samples. Ultimately, the number of samples that yield the lowest RMSE value is considered the best option. This iterative procedure helps determine the optimal number of training datasets for achieving the most accurate short-term kinetic energy forecasts.

3.1.4 Performance evaluation index

It is crucial to evaluate and validate the performance of a developed model. The data undergo training using optimal regression coefficients and are then used for in-sample forecasting. A subset of samples is allocated for validation to assess the accuracy of the results. To evaluate the performance of the model and understand the nature of kinetic energy, popular measures such as Mean Absolute Percentage Error (MAPE), Mean Absolute Error (MAE), Root Mean Square Error (RMSE), and Mean Absolute Scaled Error (MASE) are employed.

$$\text{MAPE} = \frac{1}{n} \sum_{i=1}^{n} \left| \frac{y_i - \hat{y}_i}{y_i} \right| \qquad\qquad \text{Equation 3.11}$$

$$\text{MAE} = \frac{1}{n} \sum_{i=1}^{n} |y_i - \hat{y}_i| \qquad\qquad \text{Equation 3.12}$$

$$\text{RMSE} = \sqrt{\frac{1}{n} \sum_{i=1}^{n} (y_i - \hat{y}_i)^2} \qquad\qquad \text{Equation 3.13}$$

$$\text{MASE} = \frac{\frac{1}{j} \sum_{0}^{j} |e_j|}{\frac{1}{T-1} \sum_{t=2}^{T} |y_i - y_{i-1}|} \qquad\qquad \text{Equation 3.14}$$

These measures, described in the above equations, utilize the actual values (y_i), forecasted values ($\hat{y}_i$), and the corresponding errors ($e_j = y_i - \hat{y}_i$) at the jth iteration for time t (t = 1, 2,..., T), where the training set is considered. For the evaluation and validation of the kinetic energy datasets, a platform called EXPLORATORY [231] is utilized. This platform facilitates the assessment of performance and validation of the model's results.

3.2 Characteristics of the model and relevance of this study

Figure 3.6 focuses primarily on the characteristics of the forecasted values and the training datasets of kinetic energy used for evaluation. Figure 3.6 (a) illustrates the data nature of training, testing, and forecasting using the Bayesian model, while Figure 3.6 (b) shows the same data nature using the ARIMA model, which was used for comparison purposes. Comparing the two figures, it is observed that the forecasted and testing variables for the Bayesian model exhibit close alignment, indicating good accuracy. In contrast, the forecasted variables in the ARIMA model display similar characteristics. Still, the accuracy is not as good compared to the Bayesian model, as there are some discrepancies between the testing and forecasted values.
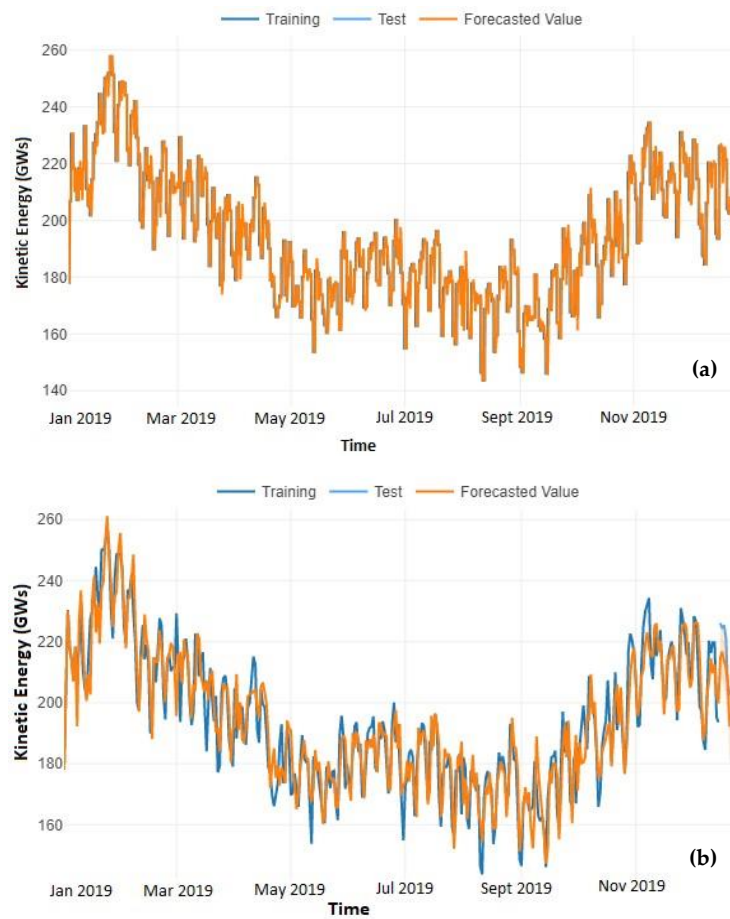
Figure 3.6: Results showing the nature of training, testing, and forecasted values for (a) the Bayesian model and (b) the ARIMA model.

Furthermore, Figure 3.7 (a) depicts the current trend of kinetic energy and its development pattern for the datasets. The application of the Bayesian model does not show any trend-altering points, indicating its strong performance in accurately capturing the trend. However, the ARIMA model illustrates the point at which the trend shifts, albeit with some points for improvement, as shown in Figure 3.7 (b). Both figures suggest that the presented Bayesian model performs better than the ARIMA model.
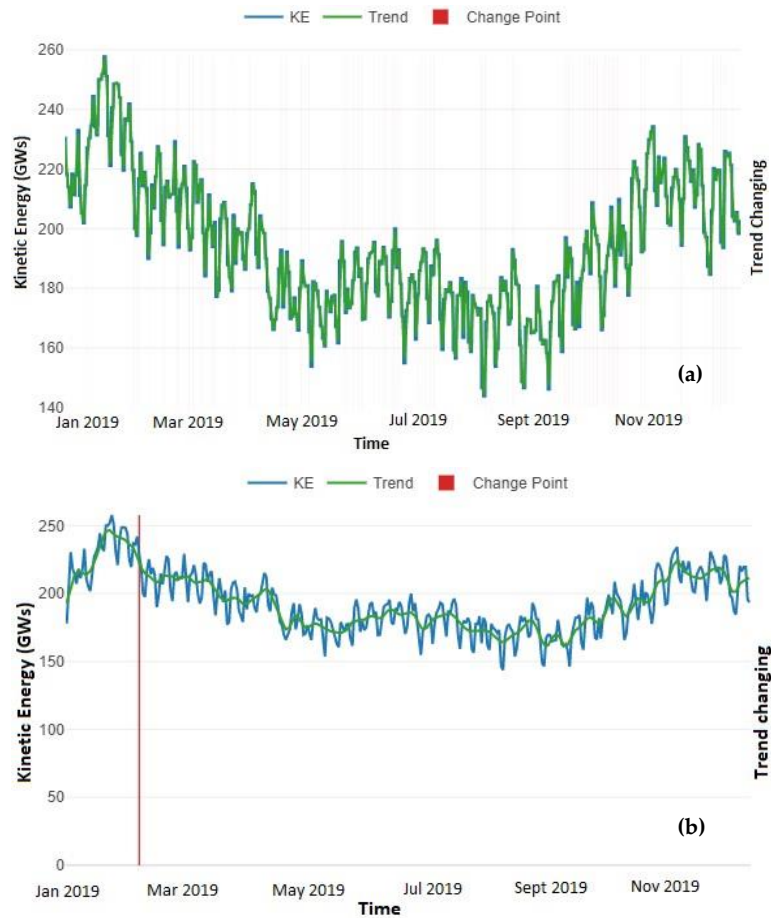
Figure 3.7: Results showing the trend and trend-changing pattern for (a) the Bayesian model and (b) the ARIMA model.

The performance metrics of the Bayesian model are calculated as follows: RMSE (4.67), MAE (3.865), MAPE (0.048), and MASE (8.15). In contrast, the ARIMA model yielded the following performance metric values: RMSE (6.15), MAE (4.680), MAPE (0.069), and MASE (12.34). The comparison between the two models confirms that the Bayesian model outperforms the ARIMA model in terms of accuracy. It is worth noting that these values could potentially be further improved by increasing the number of MCMC samples. Figure 3.8 provides the performance metrics for the Bayesian model at different MCMC sample numbers, demonstrating that the optimal value is achieved with 200 MCMC samples for analysis.
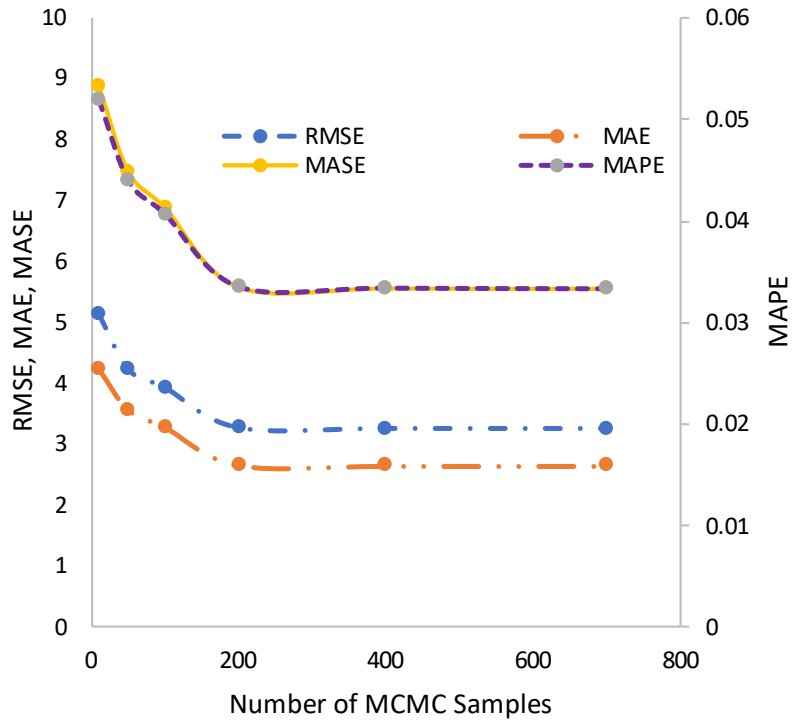
Figure 3.8: Effect of the Bayesian inference on the performance metrics
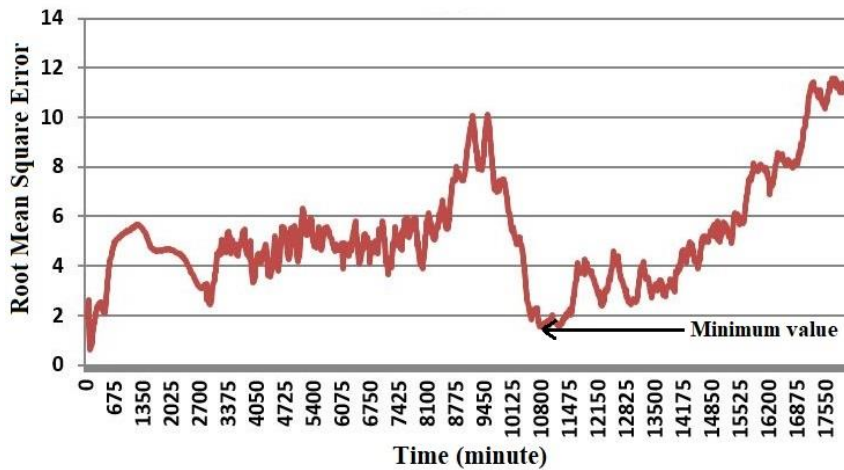
Figure 3.9: RMSE at different numbers of training sets during short-term forecasting

Finally, Figure 3.9 displays the RMSE for different numbers of training sets used to compute predictions for the next 30 minutes. The minimum RMSE value of 1.54504 is attained when utilizing a total of 10,830 minutes (or 180.5 hours) of training samples. This result indicates that the training dataset of 10,830 minutes is sufficient for predicting kinetic energy

(specifically for the considered case study and the datasets) with an accuracy of 1.54504 RMSE for short-term outcomes (i.e., 30 minutes).

3.3 Importance of time-series analysis in power system analysis

Estimating kinetic energy from time-series data is a crucial aspect of energy research and power system management. Kinetic energy, representing the energy associated with object movement, holds significant importance in various sectors, such as renewable energy integration, grid stability, and demand forecasting. Accurate estimation of kinetic energy using time-series data enables improved planning, operation, and control of power systems. By analyzing historical patterns and trends in kinetic energy, researchers and practitioners gain valuable insights into the behavior and dynamics of energy systems. This knowledge aids in optimizing renewable energy generation and consumption, enhancing grid reliability, and mitigating potential risks and uncertainties. Understanding the temporal variations of kinetic energy empowers stakeholders to make informed decisions regarding energy infrastructure investments, load balancing, and integrating intermittent renewable sources into the grid.

Furthermore, precise estimation of kinetic energy through time-series analysis facilitates short-term and long-term forecasting, which is vital for efficient energy management. Forecasting kinetic energy patterns assists in planning energy generation and storage capacities, optimizing energy dispatch, and managing demand response programs. It also supports the development of strategies for grid stability, frequency regulation, and reliable power supply, particularly in converter-dominated power systems with high levels of intermittent renewable energy sources. The study of time-series data estimation of kinetic energy also contributes to the advancement of data-driven models and algorithms. It involves developing and applying statistical and machine learning techniques to analyze and predict energy patterns accurately. These models can capture the complex interactions and dependencies within energy systems, leading to more precise estimations and improved system operation. Moreover, the findings from such studies can inform the development of predictive control strategies, enabling real-time adjustments and optimization of energy resources. By accurately forecasting and analyzing kinetic energy patterns, power system

operators can make informed decisions, develop effective strategies, and pave the way for a more sustainable and resilient energy future.

4 Day-ahead estimation of the energy-mix proportion

The day-ahead estimation of power system parameters plays a crucial role in the context of IBRs and the global transition towards a sustainable future. As countries increasingly incorporate RESs into their power grids to address environmental concerns and achieve net-zero emissions, integrating IBRs presents technical challenges related to reliability, system dynamics, stability, and control efficiency. Using IBRs complicates the power grid and reduces system inertia, which can impact overall performance and stability. Additionally, the stochastic nature of RESs like solar and wind introduces demand and supply chain complexities. Therefore, efficient day-ahead estimation of power system parameters becomes vital in managing short-term demand-supply imbalances caused by the variability of RESs. By utilizing historical time-series data and employing data-driven models, day-ahead estimation enables the identification of optimal energy-mix proportions and the scheduling of power producers, considering constraints and objective functions related to generation costs, reserve scheduling, system strength, and overall security. Such estimation practices contribute to the reliable and sustainable operation of power systems in compliance with regulatory requirements, facilitating a greener and more resilient energy future.

With the objective of ensuring the secure functioning of converter-dominated power systems, this chapter focuses on estimating the optimal day-ahead energy-mix proportion of the power-generating technologies. It utilizes time-series data obtained from the TSOs of the Nordic grid to estimate day-ahead values using a data-driven model. These estimated values are then used to determine the optimal scheduling of power-generating technologies, considering different power-generating technologies such as synchronous generators, grid-following converters, and grid-forming converters. Based on the research conducted in **Article 5** [232]**,** the findings presented in this chapter highlight the proposed approach's effectiveness in addressing the IBR-dominated power systems. This chapter is a valuable resource to underscore the significance of day-ahead estimation of power system parameters in the ongoing efforts of decarbonization, renewable energy integration, and combatting global warming.

4.1 Methodology used for day-ahead estimation

This section provides a detailed exploration of the chosen approaches and the underlying assumptions made to support the investigation. Methodologies, including a power system model, data-driven forecasting model, and optimal energy-mix generation and reserve scheduling model, have been carefully considered. Figure 4.1 provides an overview and summary of this approach. The power system model encompasses all the necessary components to meet grid standard requirements. Real-world data collected from power systems worldwide serves as a valuable source of independent and variable time series data, including power production and consumption. A data-driven forecasting model is employed to forecast the time series data for the following day based on the available time series data used for estimating day-ahead values. The model for optimal energy-mix generation and reserve scheduling considers the power system's constraints and anticipated time series data related to power generation and consumption. The most efficient scheduling of power-generating technologies is determined by analyzing the reactions of different power-generating technologies. Techno-economic impact evaluations aid in determining the optimal distribution of components, while the reserve schedule ensures the uninterrupted and secure operation of the power system.
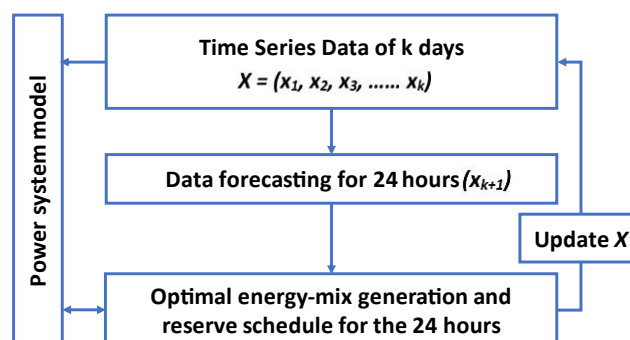
Figure 4.1: An overview of the adopted approach.

4.1.1 Power system components

An approach is utilized to investigate day-ahead scheduling with an optimal energy-mix proportion for the secure operation of a converter-dominated power system, as depicted in

Figure 4.1. This model serves as the basis for exploring and analyzing the day-ahead scheduling strategies with an optimal energy-mix. The primary network under investigation is the IEEE 9 bus power system, illustrated in Figure 4.2. Table 4.1 provides the ratings for the generators and load centers incorporated in the IEEE 9 bus power system. Furthermore, it is assumed that the primary network operates at a voltage of 230 kV and a frequency of 50 Hz. For a more comprehensive understanding of the power system model, the book authored by P.M. Anderson [233], contains all the necessary information. Specifically, it is assumed that the first generator represents a synchronous generator (a hydroelectric plant), the second generator includes a Battery Energy Storage System (BESS) with a grid-following converter, and the third generator encompasses a wind turbine with a grid-forming converter. Figure 4.3 provides an overview of the system under analysis, giving a holistic view of its configuration and components.
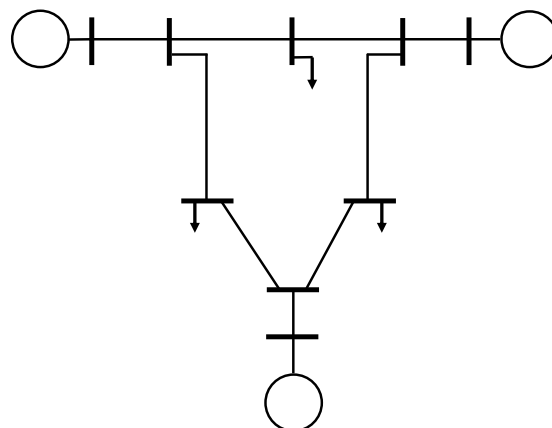
Figure 4.2: Single line diagram of IEEE 9 bus system.
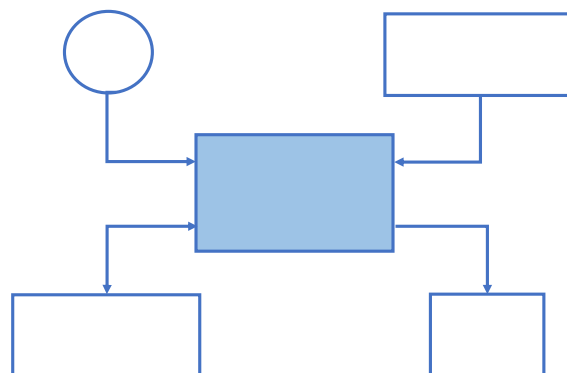
Figure 4.3: Overview of the considered power system.

Table 4.1: Rating of the generators and the loads in the considered power system

Parameters	Values
Generator 1	163 MW (1.025 pu) at 18 kV
Generator 2	72.19 (1.04 pu) at 16.5 kV
Generator 3	85 MW (1.025 pu) at 13.8 kV
Load 1	100 MW/ 35 MVAR
Load 2	125 MW/ 50 MVAR
Load 3	90 MW/ 30 MVAR

The model for the synchronous generator used can be defined by Equation 4.1 and Equation 4.2. Equation 4.1 relates to the mechanical power $P_{m,i}$ and the damping torque coefficient D_i of the ith generator. Similarly, δ_i represents the rotor angle in radians, ω_i denotes the shaft speed in per unit (pu), ω_0 is the nominal speed in pu, and H_i represents the inertia constant in MJ/MVA. The derivative with respect to time is denoted by the symbol (˙). Additionally, r_a represents the armature resistance, $i_{q,i}$ and $i_{d,i}$ represent the q- and d-axis components of stator current, while $v_{q,i}$ and $v_{d,i}$ denote q-axis and d-axis components of the voltage [234].

$$\dot{\delta}_i = \omega_0(\omega_i - 1) \qquad \text{Equation 4.1}$$

$$2H_i\omega_i\dot{\omega}_i = -D_i\omega_0(\omega_i - 1) + P_{m,i} - (v_{q,i}i_{q,i} + v_{d,i}i_{d,i} + r_a i_{d,i}{}^2 + r_a i_{q,i}{}^2) \qquad \text{Equation 4.2}$$

Similarly, the grid-forming converter employs the grid-forming virtual emulator described in [235]; the mathematical representation of this emulator is expressed by Equation 4.3 and Equation 4.4. Here in these Equations, P_i represents the active power output of the ith generator, while ω_i and θ_i denote the frequency and voltage angles. Additionally, the positive parameters $\tilde{m}_i$ and $\tilde{d}_i$ are referred to as the virtual inertia constant and virtual damping constant, respectively.

$$\dot{\theta}_i = \omega_i \qquad \text{Equation 4.3}$$

$$\tilde{m}_i \; \dot{\omega}_i = -\tilde{d}_i \, \omega_i - P_i \qquad\qquad \text{Equation 4.4}$$

Conversely, the mathematical representation of the grid-following converter can be expressed as Equation 4.5 and Equation 4.6 [235]. In these equations, τ_i represents the filter time constant, while $K_{P,i}$ and $K_{I,i}$ are the proportional and integral gain constants, respectively, for the component. The symbol (ˆ) indicates that the value is estimated.

$$\dot{\hat{\theta}}_i = \widehat{\omega}_i \qquad\qquad \text{Equation 4.5}$$

$$\tau_i \dot{\widehat{\omega}}_i = -\widehat{\omega}_i - K_{P,i} v_{q,i} - K_{I,i} \int v_{q,i} \; dt \qquad\qquad \text{Equation 4.6}$$

4.1.2 Data sets

To conduct the analysis, actual data on hydropower production, wind power output, and load consumption are utilized. The data initially collected for the INPS is subsequently reduced in size to comply with the specifications of the IEEE 9 bus standard. The data on hydropower output specifically originates from Finland but is considered valid for all Nordic countries, as the seasonal streamflow trends for different rivers in these countries exhibit comparable patterns [236, 237]. However, the wind power and load consumption data are taken for INPS from the FINGRID's web portal [226]. The data spans from January 1, 2021, to December 31, 2021, with a resolution of three minutes.

Upon examining the raw datasets, it is observed that some entries are of the NaN type (indicating missing or invalid values), while others appeared to be sourced from incorrect columns. These observations indicate the presence of extreme values within the collected datasets. To better understand the data distribution and conduct a thorough analysis, histograms based on normal distributions are employed, as shown in Figure 4.4. The hydropower histogram demonstrates that most values fall within the range of zero to 3,688.96 MW. Similarly, load consumption ranges from 4,245.98 to 15,006.4 MW, and wind power ranges from zero to 2,915.54 MW. Outliers that fall outside these range boundaries are identified.
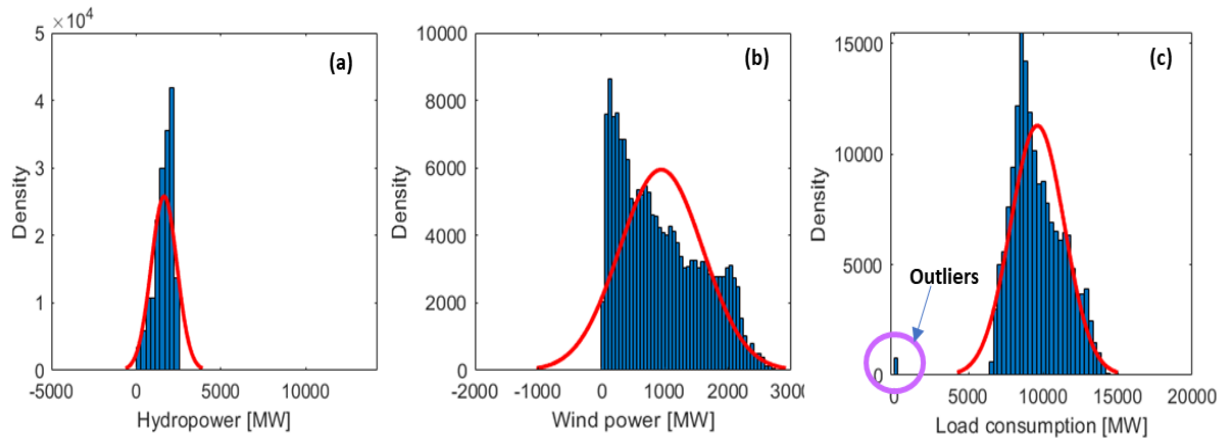
Figure 4.4: Normal distribution of datasets for (a) hydropower, (b) wind power, and (c) load consumption.

During the analysis process, a total of 763 outliers were identified in the hydropower dataset, one outlier in the wind power dataset, and 768 outliers in the load consumption dataset, out of 174,988 samples in total. These outliers are subsequently replaced with the mean values of their respective columns: 944.27 MW for wind power, 1,609.8 MW for hydropower, and 9,668 MW for load consumption.

Before proceeding with the analysis, the data undergo pre-processing to refine outliers and are then scaled down to adhere to the specifications of the IEEE 9-bus standard. Normalization technique is applied to achieve the desired data form, as shown in Equation 4.7 [238].

$$Z_i = \frac{X_i - \min(X)}{\max(X) - \min(X)} * Q \qquad \text{Equation 4.7}$$

In this equation, X_i represents the ith value, $max(X)$ denotes the maximum value, and $min(X)$ represents the minimum value for the respective datasets. The maximum values (Q) derived from the power ratings of the generators and load consumption (as indicated in Table 4.1) are used for normalization. The scaling down of the data occurs as part of this pre-processing step. The scaled datasets are subsequently utilized in conjunction with the forecasting model to provide values for the parameters one day in advance, specifically for wind power and load consumption.

Given that hydropower production is heavily influenced by the water flow, which typically exhibits minimal changes over short time periods (assuming no significant weather variations, such as rainfall), it is reasonable to consider the water discharge as a constant value for the entire day when performing day-ahead estimation. Monthly forecasting can be utilized for hydropower production, taking into account its dependency on the water flow. Conversely, as wind power and load consumption are subject to random variations, accurate predictions are crucial in studying these phenomena. Therefore, the importance of forecasting the next day's wind power production and load demand is emphasized in this study, with a primary focus on this aspect of forecasting.

4.1.3 Operation and reserve scheduling model

For optimization purposes, cost is considered as the objective function, which is mathematically represented by Equation 4.8. This allowed them to identify the most efficient allocation of energy-generating technologies. The objective functions in this study are categorized into four aspects: (a) the cost of energy generation, including the charging and discharging cost of the BESS; (b) the service fee provided by power generators to enhance the power system's strength; (c) the cost of generator start-up and shutdown; and (d) the cost of energy reserve.

$$
min \sum_{t \in \mathcal{T}} \left[\begin{array}{l} \sum_{g \in \mathcal{G}} \left(C_{g,t}^{p} \cdot p_{g,t} + C_{g,t}^{Up} \cdot u_{g,t}^{Up} + C_{g,t}^{Down} \cdot u_{g,t}^{Down} + C_{g,t}^{reserve} \cdot p_{g,t}^{reserve} \right) \\ + \sum_{e \in \mathcal{E}} \left(C_{e,t}^{Dis} \cdot p_{e,t}^{Dis} - C_{e,t}^{Charge} \cdot p_{e,t}^{Charge} \right) \end{array} \right] \qquad \text{Equation 4.8}
$$

In Equation 4.8, the cost parameters for energy, generator start-up, generator shut-down, and reserve are denoted as $C_{g,t}^{p}$, $C_{g,t}^{Up}$, $C_{g,t}^{Down}$, and $C_{g,t}^{reserve}$, respectively. Similarly, $p_{e,t}^{Dis}$ and $p_{e,t}^{Charge}$ denote the energy supplied/consumed, while $C_{e,t}^{Dis}$ and $C_{e,t}^{Charge}$ represent the cost parameters during the discharging and charging process of the BESS. The energy generated by the generators at time t is represented by $p_{g,t}$, and the reserved energy is denoted as $p_{g,t}^{reserve}$. Furthermore, $u_{g,t}^{Up}$ and $u_{g,t}^{Down}$ are binary variables indicating the start-up and shutdown of the

generating units, respectively. The $C_{g,t}^p$ signifies the cost parameters for energy generated by different power producers.

These cost parameters vary for each power generator based on their resources and characteristics. For example, the energy cost generated by RESs is relatively higher than non-renewable sources due to incentives provided by society towards RESs. Synchronous generators are often the preferred choice when discussing RESs, as they are easy to start and shut down and offer reliable supply and system security. Grid-forming converters and virtual inertia are effective methods to enhance system strength and stability. Similarly, the BESS can serve as an additional frequency service provider. Considering each energy producer's distinct characteristics and contributions to the overall power system quality, it is crucial to conduct a comprehensive cost analysis that considers the individual service costs of multiple generators. The distribution of cost parameters for generated energy is presented in Equation 4.9 and Equation 4.10, where $C_{g,t}^{gp}$ represents the real cost parameter for energy generation from various generators, and C_g^{ss} is the cost parameter for the service provided by different generators to improve system strength, C_{price}^{ss} is unit price and LF^{ss} is location factor, respectively. These parameters contribute to the calculation of the total cost of generated energy.

$$C_{g,t}^p = C_{g,t}^{gp} + C_g^{ss} \qquad\qquad \text{Equation 4.9}$$

$$C_g^{ss} = C_{price}^{ss} \left(\frac{\$}{MVA}\right) \times LF^{ss} \times p_g^{ss}\ (MVA) \qquad\qquad \text{Equation 4.10}$$

4.1.4 Constraints

To ensure the secure operation of the considered power system and identify accurate optimization of the cost function, several constraints need to be considered. Equation 4.11 represents the relationship between variables associated with generator operation, start-up, and shut-down, while Equation 4.12 imposes constraints on the variables related to start-up and shut-down. The variables, $U_{G,t}^{on}$, $U_{G,t}^{Up}$ and $U_{G,t}^{Down}$ correspond to unit commitment, start-up,

and shutdown of the generating technology at time t. It is crucial for generators to operate within a reasonable range and comply with grid requirements during start-up and shutdown.

$$u_{g,t}^{on} - u_{g,t-1}^{on} = u_{g,t}^{Up} - u_{g,t}^{Down}$$ Equation 4.11

$$u_{g,t}^{Up} + u_{g,t}^{Down} \leq 1$$ Equation 4.12

Likewise, Equation 4.13 establishes the relationship between the power generated by the generator and the maximum and minimum ramp rates at which the generator can operate. The upper and lower bounds for the ramp rates are denoted as $RP_{g,t}^{Up}$ and $RP_{g,t}^{Down}$, respectively, while $p_{g,t}$ represents the power generated by each power-generating technology at time t. Furthermore, Equation 4.14 sets a constraint on the amount of energy that should be reserved to ensure sufficient supply. The minimum, maximum, and available reserve bounds are denoted by p_g^{min}, p_g^{max}, and $p_{g,t}^{reserve}$, respectively.

$$u_{g,t}^{on} RP_{g,t}^{Down} \leq p_{g,t} - p_{g,t-1} \leq u_{g,t}^{on} RP_{g,t}^{Up}$$ Equation 4.13

$$p_g^{min} \leq p_{g,t} + p_{g,t}^{reserve} \leq p_g^{max}$$ Equation 4.14

Ensuring the stability of the phase angle is addressed in Equation 4.15, where the minimum and maximum limits of the phase angle are represented by θ_g^{min} and θ_g^{max}, respectively, and $(\theta_g - \theta_{sg})$ represents the phase angle differences. Additionally, Equation 4.16 outlines the prerequisites that must be met before any generators can begin producing active electricity.

$$\theta_g^{min} \leq \theta_g - \theta_{sg} \leq \theta_g^{max}$$ Equation 4.15

$$u_{g,t}^{on} p_g^{min} \leq p_{g,t} \leq u_{g,t}^{on} p_g^{max}$$ Equation 4.16

4.1.5 Indicator of power system strength

The system non-synchronous penetration (SNSP) ratio is considered as a crucial indicator of system strength to identify the secure operating level of the IBR-dominated power system. It serves as a measure to assess the integration of non-synchronous generators into the power

system and is calculated by using Equation 4.17 [239]. While analyzing, various scenarios were simulated to determine the secure operating level of the power system, considering load and PEC-based generation disturbances. The worst-case scenario involved adjusting the generation dispatch until satisfactory results are obtained. The SNSP ratio is then calculated to establish the maximum limit for the SNSP ratio, expressed as a percentage. The relationship between the maximum threshold and secure operational SNSP ratios depends on the contingency event with the most significant impact on RoCoF and frequency control. Figure 4.5 provides a detailed overview of the procedures used to determine these limits.

$$SNSP\ (\%) = \frac{Non\text{-}Synchronous\ Generation + Net\ Interconnector\ Imports}{Demand + Net\ Interconnector\ Exports} \times 100 \qquad \text{Equation 4.17}$$
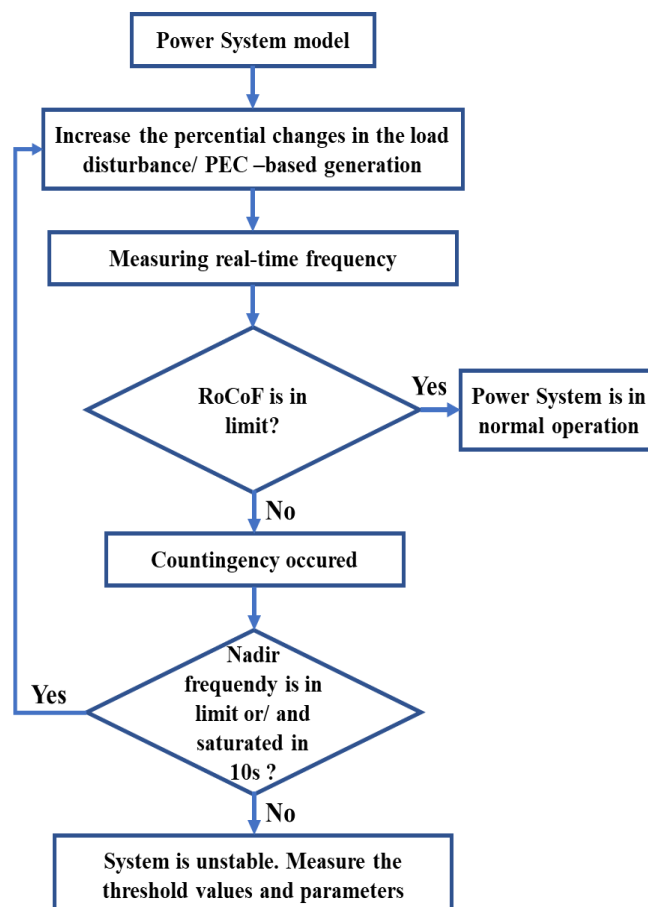
Figure 4.5: Processes to identify the threshold values and secure function conditions of the considered power system model.

4.1.6 Data-driven model for day-ahead forecasting

The primary objective is to estimate the energy-mix proportions for the next day, ensuring the reliable functioning of the power system. To achieve this, Long Short-Term Memory (LSTM) is considered a suitable option due to its ability to handle complex datasets and patterns. LSTM, an improvement over Recurrent Neural Networks (RNN), addresses the challenge of learning long-term dependencies. Developed by Google DeepMind, LSTM incorporates an extended memory function, enabling it to retain information over longer periods. The addition of four gates - input, forget, update, and output - is a crucial modification that enhances LSTM's performance. The forget gate controls the update of the memory cell and the transfer of data to existing and new memory cells. The update gate determines whether the memory cell should be updated and the information it acquires from the previous step. Lastly, the output gate determines the values of the subsequent hidden layer. The expressions of these four gates are given below [240].

$$\Gamma_i = \sigma\big(W_i\big[a^{\langle t-1\rangle}, X^{\langle t\rangle}\big] + b_i\big) \qquad \text{Equation 4.18}$$

$$\Gamma_f = \sigma\big(W_f\big[a^{\langle t-1\rangle}, X^{\langle t\rangle}\big] + b_f\big) \qquad \text{Equation 4.19}$$

$$\Gamma u = \tanh\big(W_u\big[a^{\langle t-1\rangle}, X^{\langle t\rangle}\big] + b_u\big) \qquad \text{Equation 4.20}$$

$$\Gamma_0 = \sigma\big(W_0\big[a^{\langle t-1\rangle}, X^{\langle t\rangle}\big] + b_0\big) \qquad \text{Equation 4.21}$$

Here in these Equations, the weight matrices and bias vectors of the recurrent network are represented by W and b, respectively, while the states of the neurons are denoted by a and X. The activation function is represented by σ. In this process, Equation 4.22 allows to determine the current state of the time-series model, and Equation 4.23 calculates the output value using the four gates.

$$h_t = \tanh(W_{hh}h_{t-1} + W_{xh}x_t) \qquad \text{Equation 4.22}$$

$$y_t = W_{hy}h_t \qquad \text{Equation 4.23}$$

Here in these Equations, the current state is denoted as $h_t \in (-1,1)^h$, the previous state as h_{t-1}, the output as $y_t \in R^t$, and the input as $x_t \in R^t$. The weight of the recurrent neuron is represented by $W_{hh} \in R^{h*t}$, the weight of the input neuron by W_{xh}, the weight of the output neuron by W_{hy}, and the bias vector parameters to be learned during model training by $b \in R^h$. Figure 4.6 provides an overview of the LSTM model architecture used in this study, where the inputs are the recorded data of power production and load consumption, and the output is a day-ahead estimation of the parameters.

Input values of wind power (p_w) and load consumptions (l) for k days

$$X = \begin{bmatrix} p_{w,1}, p_{w,2}, p_{w,3}, p_{w,4} \cdots \cdots p_{w,k} \\ l_1, l_2, l_3, l_{,4} \cdots \cdots \cdots \cdots \cdots \cdots l_k \end{bmatrix}$$

$$Y = \begin{bmatrix} p_{w,k+1} \\ l_{k+1} \end{bmatrix}$$

Output values of wind power (p_w) and load consumptions (l) for k+1 day
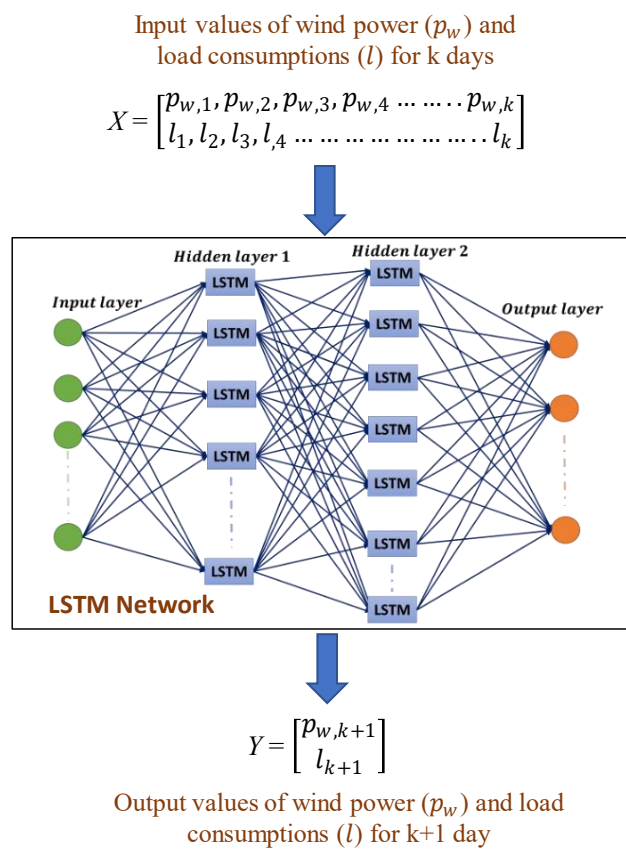
Figure 4.6: Overview of the data-driven model.

4.1.6.1 Hyperparameter tuning

In the realm of neural network analysis, selecting appropriate values for hyperparameters is vital for achieving optimal performance. These hyperparameters have a significant impact on the network's learning behavior and capacity. However, determining suitable hyperparameter values is often challenging and requires meticulous fine-tuning. To address this issue, the

Bayesian optimization algorithm is adopted as a highly effective method for determining the values of network hyperparameters. This approach utilizes objective function evaluations to educate a Gaussian process model, and it is leveraged with the deep learning application integrated with MATLAB software for optimization [241].

During the hyperparameter tuning process, an optimization function called *valErrorFun(optVars)*, specifically designed for tuning the variables, is employed. Table 4.2 provides a comprehensive overview of the specified ranges for the other parameters involved. When developing the model architecture, crucial considerations included determining the number of hidden layers and the number of neurons within each layer. The choice of activation function played a vital role in introducing non-linearity and determining the activation of specific neurons based on weighted sums and biases. Similarly, the optimal learning rate varied based on the presented data and the network being trained. To prevent underfitting and overfitting, regularization played a significant role. Various hyperparameter values are explored, taking into account their respective weights and their impact on the optimization process.

Table 4.2: Hyperparameters ranges/ types for tuning

Parameters	Value/ types
Number of hidden layers	$\mathbb{Z}$ [1, 5]
Number of units in the hidden layer	$\mathbb{Z}$ [10, 200]
Activation function	[tanh, relu, sigmoid]
Learning rate	$\mathbb{R}$ [0.00001, 1]
Dropout value	$\mathbb{R}$ [0.1, 0.7]
L2 Regularization	$\mathbb{R}$ [1e-10, 1e-2]

Figure 4.7 graphically demonstrates the relationship between the objective function's minimal values and the function evaluation when Bayesian optimization is employed to obtain the optimal hyperparameter values. The observed and estimated values of the objective function, after conducting the simulation for one hundred epochs, are found to be 0.055348 and 0.0892, respectively. The significant hyperparameters are identified through the output of Bayesian optimization. A comprehensive listing of all the employed hyperparameters for the

presented LSTM model can be found in Table 4.3. These endeavors aimed to ensure that the neural network model could operate at its best performance level by determining appropriate hyperparameter values through Bayesian optimization.

Table 4.3: Hyperparameters for the presented LSTM model

Parameters	Value/ types
Optimizer	Adam
Maximum Epoch	100
Mini batch size	32
Dropout value	0.5
Number of hidden layers	2
1st hidden layer	197 hidden units, tanh activation function, uniform initializer
2nd hidden layer	197 hidden units, sigmoid activation function, uniform initializer
Initial learning rate	0.001
Learn rate schedule	piecewise
L2 Regularization	0.00518
Input weight initializer	Glorot, with LR 1 and L2 factor 1
Recurrent weight initializer	Orthogonal, with LR 1 and L2 factor 1
Bias Initializer	Unit-forget-gate, with LR 1 and L2 factor 0

Figure 4.7: Minimum objective vs. number of function evaluations.

4.1.6.2 Performance evaluation

Figure 4.8 illustrates the model's error progression with increasing epochs, indicating an improvement in training performance. At 100 epochs, the RMSE is measured as 0.1352, while the loss function yields a value of 0.0183. Both indicators exhibit significant initial decreases, but the subsequent rate of change becomes minor, resulting in a steady decline. Considering the negligible rate of change beyond this point, a total of 100 epochs is selected for their model analysis.
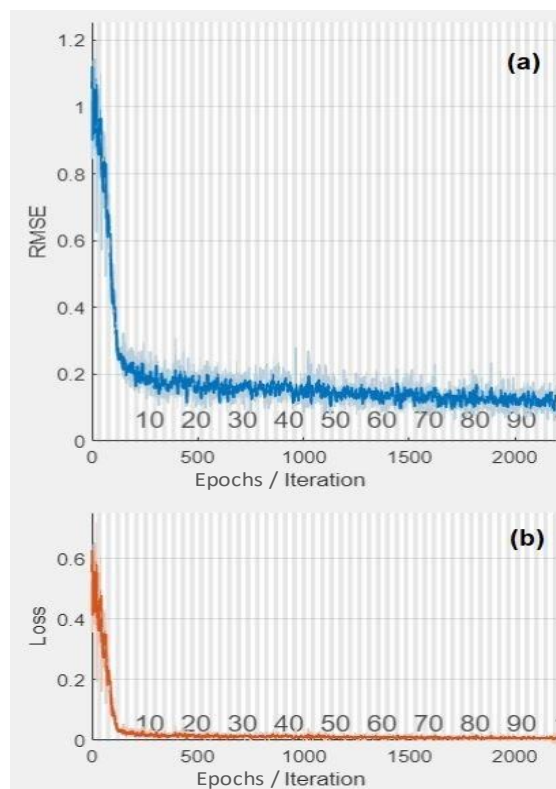
Figure 4.8: Loss function with epochs/ iterations.

To assess the model's performance, regressions are conducted on the training, testing, and overall datasets for both wind power output and load consumption. These regressions are performed on two separate sets of data. Figure 4.9 presents these regression graphs, offering a comprehensive overview. The dataset is split into two parts: training (80%) and testing (20%) using the 'dataPartitioning(opt, data)' method [242]. The train-test split technique is employed to accurately evaluate the model's performance when making predictions on

unseen data, thus providing a robust assessment. The rank correlation values for all examples are found to exceed 0.980, indicating the effectiveness of the provided model. This signifies a strong association between the predicted and actual values, highlighting the model's capability to capture meaningful patterns and accurately estimate wind power output and load consumption.
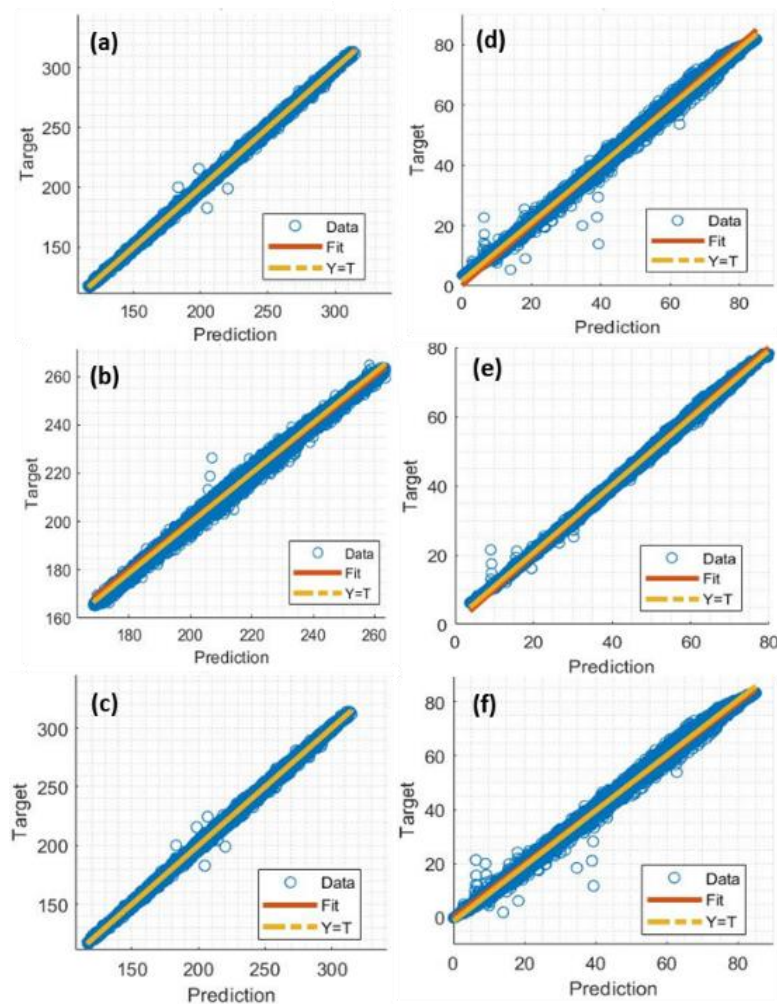
Figure 4.9: Normalized regression of LSTM model for (a) load training data, (b) load testing data, (c) load all data, (d) wind training data, (e) wind testing data, and (f) wind all data.

4.2 Results

The model begins by utilizing data to estimate the factors affecting power generation and consumption for the upcoming day. These estimated values are then input into a dynamic

model of the power system, which incorporates an optimization model. The objective is to determine the optimal proportion of energy-mix for the day ahead. In the scenario being examined here, the power system consists of a SG, wind turbines with GFL, and BESS with GFM. When power-generating technologies operate under their typical conditions, they have certain ratings that apply to their performance. These ratings are taken into account when determining the sizes of these technologies. Figure 4.10 (a) presents the percentage of total installed capacity contributed by each of the three types of power-generating technologies. Considering this aspect, the provided model dynamically optimizes the power ratings of these technologies for the day-ahead scenario and allocates resources accordingly to accommodate any changes. On the other hand, Figure 4.10 (b) illustrates the hourly energy delivery from each of these power-generating technologies for the examined one-day-ahead scenario.
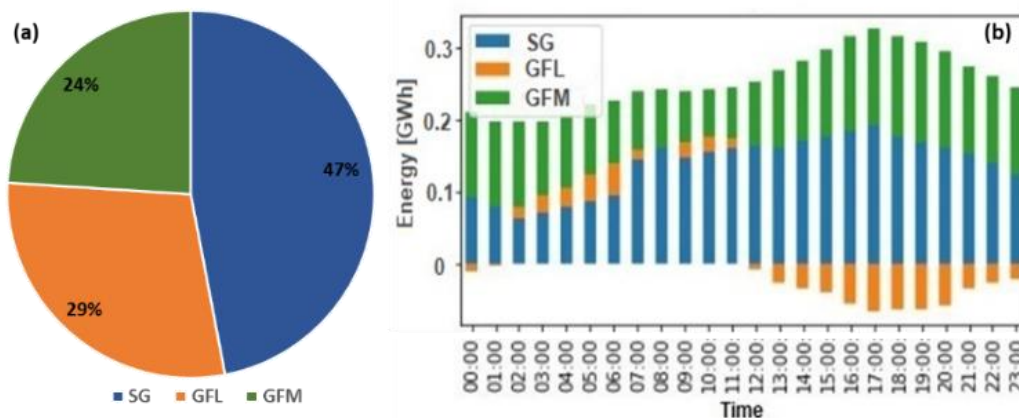
Figure 4.10: (a) proportion of installed capacity of the power-generating technologies, and (b) hourly generated electricity at the day-ahead scenario.

Figure 4.11 (a) illustrates the power quantities supplied and used by these components, along with the optimal power they supply. When the GFL value is positive, it indicates that the BESS is being discharged. Conversely, when the GFL value is negative, the BESS is being charged from the grid using power generated by other sources. Figure 4.11 (b) provides an overview of the SoC level of the BESS system in the day-ahead simulation scenario. The lowest SoC recorded during this specific one-day simulation is forty percent, which falls well within the permissible range, as evident from the figure. Similarly, Figure 4.11 (c) displays the total system frequency, which is measured in this simulation model. The frequency appears to

exhibit less variance under normal operating conditions and remains within the conventional frequency constraints set by Nordic TSOs. This indicates that the frequency is within acceptable limits. Finally, Figure 4.11 (d) illustrates the range of the SNSP ratio observed in the researched condition, spanning from 28% to 64%. These findings pertain to the regular operation of the power system, with the maximum SNSP ratio determined as 64%. Consequently, it is reasonable to conclude that the SNSP value of 64% falls within a safe operating range for the investigated power system.
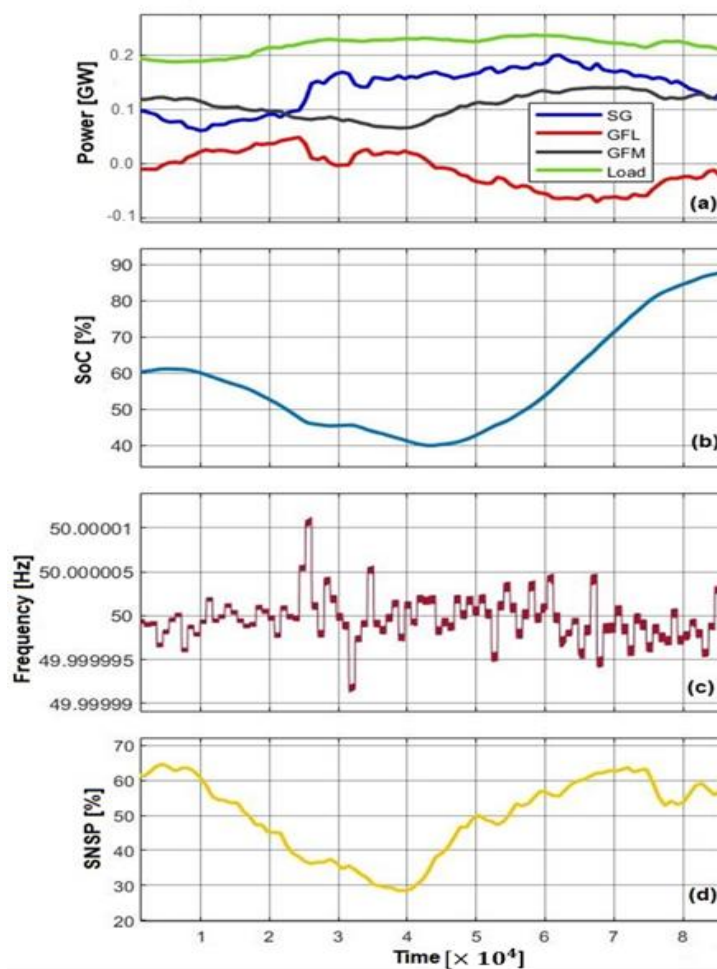
Figure 4.11: (a) Power generated through power-generating technologies, (b) SoC of BESS, (c) system frequency, and (d) SNSP values for 24 hours-time spans (samples per unit of time).

However, the power grid must be prepared to handle unexpected disruptions that can impact the electrical system's performance. Various disturbances can affect a power system, each

exhibiting unique characteristics and symptoms. These disturbances can manifest as different types of faults, including line-to-line faults, line-to-ground faults, multiple-line-to-ground faults, and others. Additionally, sudden changes in load or power generation, such as the addition or removal of a significant load, can adversely affect the overall performance of the power system. Consequently, it becomes imperative to conduct a contingency analysis to assess the system's operation and ensure its safety.
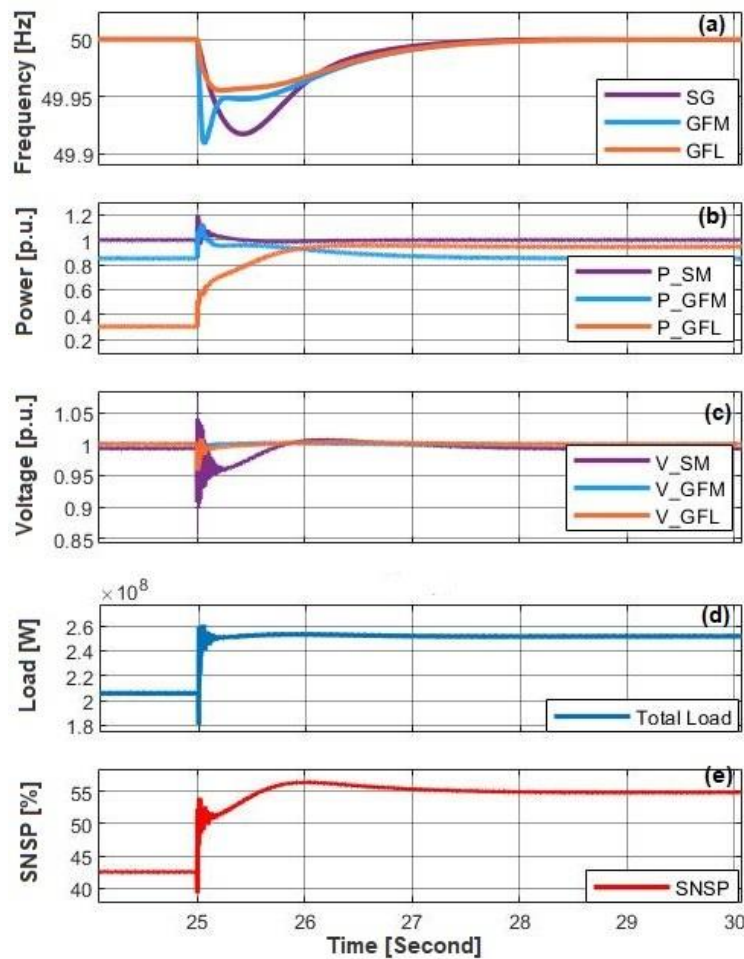
Figure 4.12: System's responses (i.e., frequency, generation, voltage, load, and SNSP) at $\Delta P_L =$ 0.30 pu.

In this study, the power system model is perturbed by introducing an external disturbance, and the time-domain simulation method is employed to analyze the system's response to this disturbance. Figure 4.12 graphically depicts the alterations in the power system's characteristics resulting from a 30% increase in load (i.e., $\Delta P_L =$ 0.30 pu). At the 25-second

mark, when the load is increased, the terminal voltages and frequencies of all generating units begin to decrease, albeit with some variation. This behavior is observed when the load experiences an increase. However, during the same period, the generating units respond by increasing their production to meet the demand reliably. This allows the system to maintain stability and adequately supply demand within seconds. Although it takes slightly longer to reach the saturation level when a significant load increase, such as 30%, most parameters achieve or approach saturation within three seconds, ensuring continued secure supply to the grid. Furthermore, before the disturbance, the SNSP ratio for the considered power system is 43%. However, after the disturbance (applying $\Delta P_L = 0.30$ pu), the SNSP ratio increased to 57%.

In order to conduct a comprehensive investigation, adjustments have been made to the load disturbance level, and maximum values for the SNSP ratio have been determined. The power system model is initially run under normal conditions, and then various load disturbances are introduced for analysis, observing the system's responses to these disturbances. During this analysis, it has been observed that the system becomes unstable when the load disturbance reaches 38% of the total load. This percentage represents the technical limit of the load disturbance for the current investigation. A detailed overview of the procedures followed to establish this limit can be found in Figure 4.5.
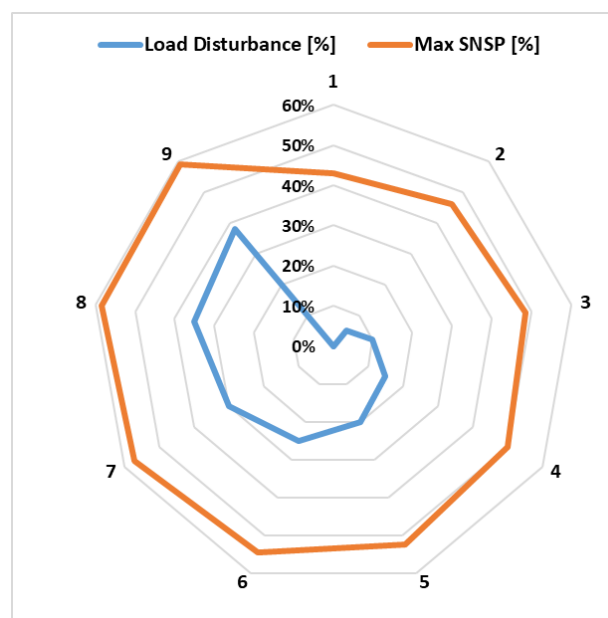
Figure 4.13: Maximum SNSP ratio values at different load disturbances.

Figure 4.13 displays the maximum SNSP ratio values for each load disturbance, which have been determined through extensive analysis. Under normal operating conditions, the SNSP ratio is observed to be 43%, as depicted in the figure. With each increment in the load disturbance, the SNSP ratio gradually increases. It is crucial to maintain this limit to ensure system stability. In the specific operating mode under examination, the maximum load disturbance that can occur without surpassing the stability threshold is 38%. At this level, the highest attainable SNSP ratio is found to be 59%, which can be considered a critical limit for electricity generation technologies.

4.3 Conclusions

In conclusion, day-ahead estimation can play a vital role in ensuring the secure operation of power systems. It involves utilizing data and dynamic models to estimate the factors influencing power generation and consumption for the upcoming day, thereby determining the optimal energy-mix proportion. The insights gained from day-ahead estimation are invaluable in understanding the system's behavior under various scenarios, including load disturbances and external disruptions. This knowledge enables the identification of potential issues and their impact on critical system parameters like terminal voltages, frequencies, and SNSP ratios.

Through contingency evaluations, day-ahead estimation facilitates the assessment of system safety and stability. It helps establish crucial limits, such as maximum load disturbance levels, which must not be exceeded to maintain stability. These insights empower grid operators and decision-makers to make informed choices, implement preventive measures, and mitigate risks, thus ensuring the reliable and secure operation of the power system. Day-ahead estimation serves as an indispensable tool for proactive system management, enabling stakeholders to anticipate and prepare for potential disruptions, optimize resource allocation, and maintain stability and performance within acceptable boundaries. By providing an advanced understanding of the system's behavior, day-ahead estimation significantly contributes to the efficient and secure operation of power systems, even in the face of changing demands and external uncertainties.

5 On-line estimation of the energy-mix proportion

Online simulation has become essential for planning and operating modern power systems. The primary objective is to achieve voltage, rotor angle, and frequency stability, preventing instability and minimizing the risk of blackouts. Through extensive research experiments and simulations, effective techniques have been discovered to manage frequency in low-inertia systems and enhance overall power system reliability.

By connecting the power of online simulation, researchers and operators can develop innovative strategies to overcome the challenges associated with integrating IBRs and dealing with the dynamic behavior of power systems. This includes the development of advanced frequency management techniques and the utilization of cutting-edge PECs. Additionally, machine learning methods provide efficient and robust solutions for estimating the proportion of electricity generated by different sources and ensuring the secure operation of IBR-based power systems.

The insights presented in this chapter, based on the research conducted in **Article 6**, highlight the effectiveness of the proposed approach in addressing key challenges related to reliability, system dynamics, stability, control efficiency, and security in IBR-dominated power systems. This chapter serves as a valuable resource emphasizing the importance of online estimation of power system parameters in ongoing efforts toward decarbonization and RESs integration. By enabling secure and optimized operation of renewable energy-dominated power systems, this approach contributes to the overarching goal of achieving a sustainable and environmentally friendly energy landscape.

5.1 Methodology used for on-line estimation

Ensuring a balanced supply-demand in a power system is crucial for maintaining stable power quality. This requires analyzing simultaneous equations with various variables to determine the proportion of power-generating technologies needed to operate the system safely. However, traditional model-based simulation approaches can be computationally intensive and time-consuming, especially as the size of the case study and the number of variables

increases. To address this issue, this study adopted a deep reinforcement learning (DRL) method that estimates the energy-mix proportion in a converter-dominated power system.

The proposed DRL method utilized a data-driven approach, reducing the computational power and time required for estimation. By considering percentile variations of the load and generations, the threshold values for secure power system operation can be identified. The study aimed to ensure that the power system can operate securely under normal conditions and unforeseen events.
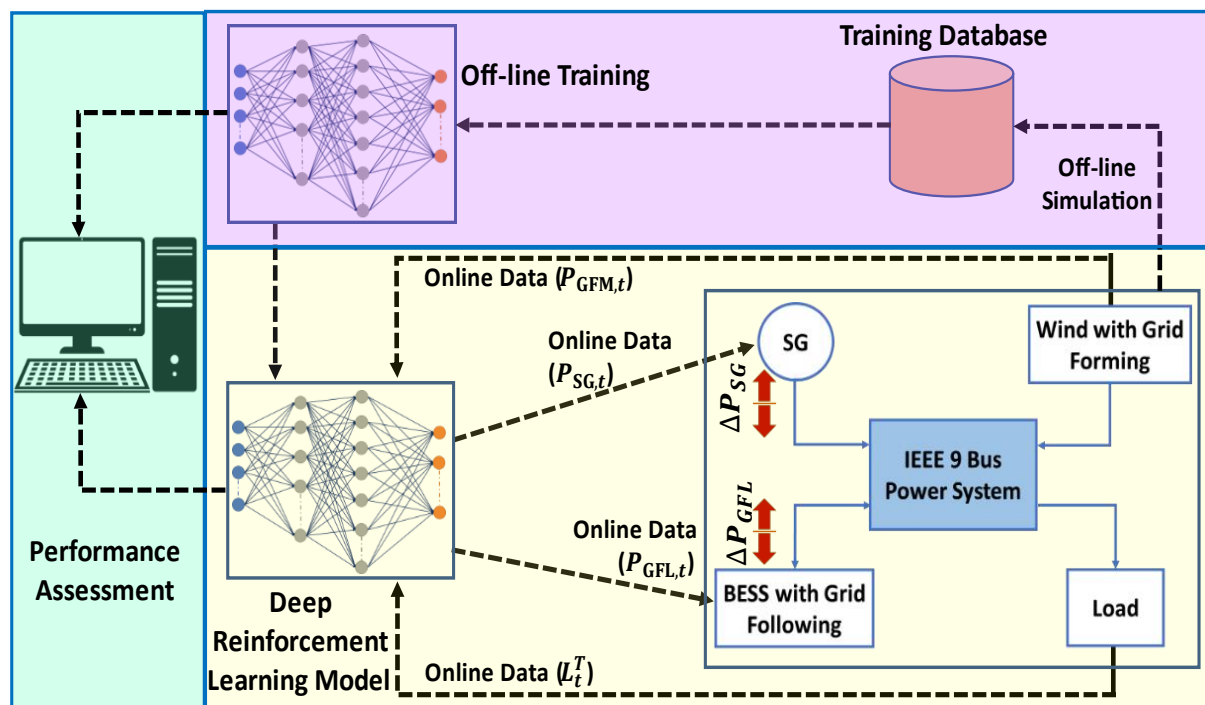
Figure 5.1: Overview of the methodology for online electricity-mix estimation.

Figure 5.1 illustrates the adopted approach involving connecting a benchmark power system to the IEEE 9 bus system as the primary network. A power system model is simulated in MATLAB/Simulink, incorporating various power-generating technologies to generate data for training the DRL model. The data is collected under varied system loads and generations during contingency scenarios, and the simulation results are used to develop a contingency plan. The DRL algorithm runs on Python using OpenAI Gym to create a reinforcement learning environment, while the power system operates within the time-domain framework provided

by MATLAB Simulink. The integration of these two frameworks is achieved using the Python interpreter. The main objective of this integration is to perform online testing and analyze the performance of the proposed methodology, ensuring its validation. The subsequent sections of this chapter delve into the details of the data generation process and the live model used in the study.

5.1.1 Power system components

The power system model and its components, which have been discussed in detail in subsection 4.1.1 of the previous chapter, are utilized in this study without any modifications. The power system model and its network configuration remain the same throughout the research.

5.1.2 Data sets

To gather data for training the DRL model, an offline simulation of the power system model is performed using MATLAB/Simulink. The simulation considered various scenarios with different system loads and generations to account for contingency situations. The parameters related to the power system components are recorded during the simulation and used as a training set for the DRL model.

In the data collection process, particular attention is given to the patterns of variation in the parameters. Rapid load changes are applied, ranging from 1.00 pu to 1.25 pu, while the generation from the GFM varies from 0.75 pu to 1.0 pu, and the generation from the SG changes from 0.75 pu to 1.0 pu. All the setpoints considered in the data collection process are listed in Table 5.1. During the data generation, the switch in the power system model is opened and closed at different time points to observe the system's response. The scope values for the parameters are recorded, and the sampling time and frame for the measurements are defined. The data are collected at a resolution of 10 milliseconds over time periods ranging from 20 to 50 seconds. In total, 792,000 separate data sets were gathered through the sampling process.

Table 5.1: Considered variations on generations and load to collect datasets.

Parameters	Values
Load applied	[1.0, 1.05, 1.10, 1.15, 1.20, 1.25] pu
GFM generation	[0.75, 0.80, 0.85, 0.90, 0.95, 1.0] pu
SG generation	[0.75, 0.80, 0.85, 0.90, 0.95, 1.0] pu
Switching close	[25, 35, 45] second marks
Switching open	[30, 40, 50] second marks

To simulate real-world conditions, white Gaussian noise with a noise power of 5e-6 and a sample time of 0.01 is introduced during the data collection process. The excitation signals for the load disturbances are used to collect the data. Figure 5.2 provides an example of the generated data, depicting a sample scenario with a system load (P_L) of 0.25 pu, an SG generation of 0.85 pu, and a GFM generation of 1.0 pu.
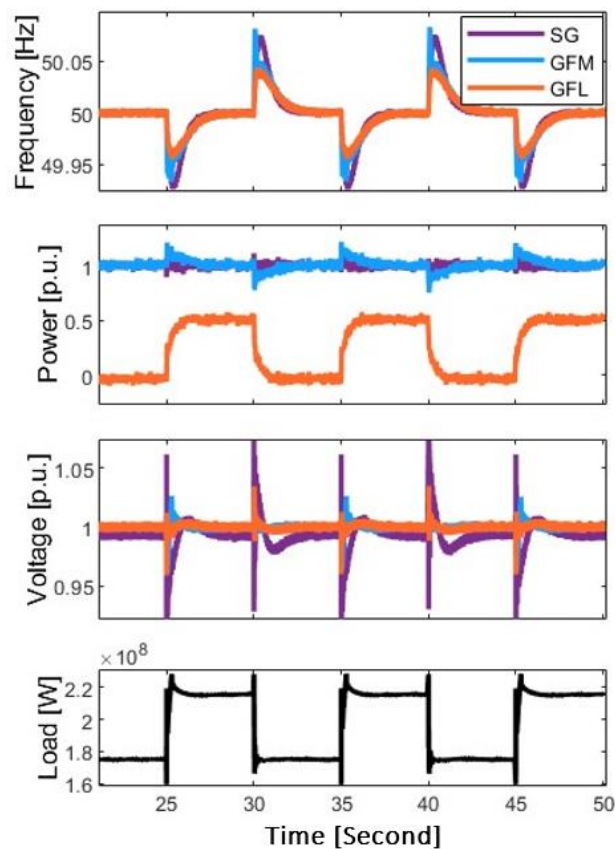

Figure 5.2: Sample of frequency, power generation, voltage, and load for ΔP_L = 0.25 pu at 0.85 pu of SG and 1.0 pu of GFM.

5.1.3 Indicator to assess the power system's robustness

Ensuring power quality and system security are primary concerns in both normal operations and contingencies. To analyze the characteristics of power system components, data patterns with load and power generation variations are collected, focusing on assessing the performance and safe operation during disturbances. The entire creation and operation of the benchmark system adhered to the grid code of the Nordic TSO.

Several significant constraints are considered during power system operation, including variables related to generator operation, ramp rates, energy reserve requirements, phase angle stability, BESS SoC, and short circuit level (SCL) (as discussed in subsection 4.1.4). System strength is employed as an indicator to assess the minimum level of security necessary for the power system.

As the penetration of PEC-based technologies increases, the displacement of SGs within the power system reduces system strength, necessitating a higher level of strength to ensure proper operation. Parameters such as the short circuit ratio (SCR), X/R ratio, and SCL are used to measure the system's secure operating level [243]. In this study, the SCLs are adopted as indicators of power system strength, specifically at the point of interconnections (POI) for each power-generating technology. SCL can be monitored using both natural and artificial disturbances [244]. However, the hybrid approach is used in this study, incorporating white noise as an artificial disturbance and frequent load and generation changes as natural disturbances. The minimum SCL value required for a strong grid is measured, and this value is considered during online testing to identify the energy-mix proportion for system security.

5.1.4 Data-driven model

The approach used in this study is summarized in Figure 5.1, highlighting the significant role of the DRL technique employed. By employing a data-driven methodology, the provided DRL model acts as a decision-making tool to enhance procedural efficiency and generate optimal outcomes. Specifically, this study utilizes the Deep Q-Network (DQN) technology, a form of

DRL that aims to interact with the environment while training an agent to adopt an optimal policy that maximizes expected rewards.

Q-learning, as a model-free reinforcement learning method, employed in this study, offers simplicity compared to other advanced policy gradient techniques. It can be conceptualized as an approach to asynchronous dynamic programming, allowing agents to learn optimal behavior by experiencing the consequences of their actions instead of constructing domain mappings. This perspective enables agents to learn effective behavior in Markovian domains by gaining experience from other domains [245].

The decision-making process is modeled as a set of five tuples denoted by $S, A, P, R,$ and Y. S represents the state space, A represents the action space, P represents the probability of transitioning between states, R represents the reward function, and Y represents the discount factor. The goal of interacting with the environment is to maximize the total reward accumulated during the training process [246, 247]. Equation 5.1 is utilized to determine the optimal action-value function, where each state can be reached from the starting point in a single step [246]. The value $R_{t_{k+1}}$ represents the reward for taking action A to transition from state S to state S', while the discount factor $\gamma \in [0, 1]$ determines the extent to which future rewards are considered valuable.

$$G_t = \sum_{k=0}^{n} \gamma^k * R_{t_{k+1}} \qquad \text{Equation 5.1}$$

The primary objective of DRL is to establish an optimal mapping between states and actions. In this study, this objective is achieved by constructing a Q-value, also known as the "optimal action value," and updating its value as the algorithm explores and learns from the environment. In hypothetical state-action pairings denoted as (S', A'), the state S' corresponds to the highest value associated with the action A for that state (S, A).

Equation 5.2 considers only the immediate and future rewards, without specifying the relative importance of maintaining present benefits versus the impact of future rewards on the

current decision-making process [248]. To address this, a learning rate α is introduced to determine the proportion of current rewards that should be retained. Similarly, the discount factor, denoted by γ, diminishes the influence of future rewards. Considering these factors, the action-value function is updated, resulting in the modified version shown in Equation 5.3.

$$Q_\pi(S,A) = \mathbb{E}[\, R_{t+1} + \gamma \times max_\pi Q(S' + A')] \qquad \text{Equation 5.2}$$

$$Q_\pi(S,A) = (1-\alpha) + \alpha[R_{t+1} + \gamma \times max_\pi Q(S' + A')] \qquad \text{Equation 5.3}$$

In Q-learning, the value function update typically involves using the hard max operator. However, in this work, the Dynamic Boltzmann softmax operator (DBSO), $\forall S \in \mathcal{S}$ defined in Equation 5.4, is employed to optimize and update the value function. In Equation 5.4, β_t represents a state-independent sequence, which is a non-negative variable that needs to be regularly updated. To dynamically update the DBSO, processes like those described in Equation 5.5 and Equation 5.6 were utilized. These Equations specify the procedures for updating and adapting the DBSO in the learning process [249].

$$\text{boltz}_{\beta_t}(Q(S,\cdot)) = \frac{\sum_{A\in\mathcal{A}} e^{\beta_t Q(S,A)} Q(S,A)}{\sum_{A\in\mathcal{A}} e^{\beta_t Q(S,A)}} \qquad \text{Equation 5.4}$$

$$\forall S,A, Q_{t+1}(S,A) \leftarrow \sum_{s'} p(S' \mid S,A)[r(S,A) + \gamma V_t(S')] \qquad \text{Equation 5.5}$$

$$\forall S, V_{t+1}(S) \leftarrow \text{boltz}_{\beta_t}(Q_{t+1}(S,\cdot)) \qquad \text{Equation 5.6}$$

In DRL, an agent interacts with its environment by taking actions and receiving rewards based on the successful completion of state-action pairs. To enable appropriate action selection for experienced conditions, the DRL agent needs to interact with and train itself on specific environmental circumstances. As the environment cannot have an unlimited number of states, a policy is necessary. This study proposes a suitable policy by combining a neural network with optimal values obtained from the Q policy, forming the Deep Q-Network (DQN) approach. This combination allows for the determination of the appropriate policy, as depicted in Figure 5.3, which illustrates the cognitive process underlying the paradigm.
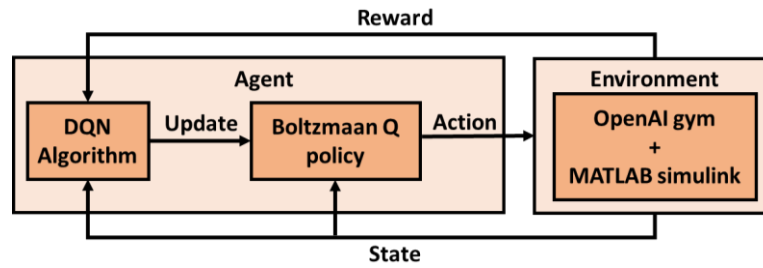
Figure 5.3: Overview of the adopted DQN-learning approach.

The DQN approach improves upon Q-learning by utilizing a neural network to approximate the action-value function $Q_\pi(S, A)$. Through Q-learning, an agent learns to act in a manner that maximizes the projected cumulative reward, $R_{t_0} = \sum_{t=t_0}^{\infty} \gamma^{t-t_0} R_t$, and subsequently applies that knowledge [250]. This involves learning to behave in a way that maximizes the potential for receiving rewards, R_t. By estimating the value of each action in each state using the action-value function $Q_\pi(S, A)$, the action with the highest value is selected. The iterative updating process, known as the Bellman equation (Equation 5.2), considers both the reward obtained from taking an action and the expected future reward from the next state, aiming to maximize the likelihood of achieving the desired outcome.

The DQN algorithm incorporates experience replay, which is a significant advancement [251]. This allows the agent to learn from past mistakes by maintaining a memory buffer of previous experiences in the form of tuples (S, A, R, S'). Random samples from this buffer are used as input for training the neural network. This process continued until the neural network is fully trained. The benefit of this approach is that learning is more consistent, and the correlation between experiences is reduced. Using Huber loss (Equation 5.7 and Equation 5.8) helps minimize errors during batch transitions by taking advantage of the sampled values from the replay memory [252]. In Equation 5.7 and Equation 5.8), δ signifies the temporal difference error.

$$\mathcal{L} = \frac{1}{|B|} \sum_{(S,A,R,S') \in B} \mathcal{L}(\delta) \qquad \qquad \text{Equation 5.7}$$

$$\mathcal{L}(\delta) = \begin{cases} \frac{1}{2}\delta^2 & \text{for } |\delta| \leq 1 \\ |\delta| - \frac{1}{2} & \text{otherwise} \end{cases} \qquad \qquad \text{Equation 5.8}$$

$$\delta = Q_\pi(S, A) - \left(R_{t+1} + \gamma \times max_\pi Q(S' + A')\right)$$ Equation 5.9

Table 5.2: Performance index and hyperparameters for the DQN agent.

Parameters	Value/ types
Optimizer	Adam
Epochs	2000
Batch size	200
Discount factor	0.99
Number of hidden layers	2
1st hidden layer	20 hidden units, tanh activation function, input dimension =3, uniform initializer
2nd hidden layer	20 hidden units, relu activation function, uniform initializer
output layer	1-unit, linear activation function, uniform initializer
Exploration rate	0.99
Learning rate	0.001

Table 5.3: Hyperparameters ranges/ types for tuning.

Parameters	Value/ types
Batch size	[100, 200, 300, 400, 500]
Discount factor	[0.95, 0.96, 0.97, 0.98, 0.99]
Number of hidden layers	[1, 2, 3, 4, 5, 6]
Number of units in 1st hidden layer	[10, 20, 30, 40, 50, 60, 70, 80, 90, 100]
Number of units in 2nd hidden layer	[10, 20, 30, 40, 50, 60, 70, 80, 90, 100]
Activation function	[tanh, relu]
Learning rate	[0.0001, 0.001, 0.01, 0.1]

Furthermore, an enhancement known as the target network, which is a separate neural network with specific parameters used to compute target values, is employed [253]. The neural network took the current state of the environment as input and generated estimated action values for all possible actions. The difference between the predicted action and target values derived from the Bellman equation is used to calculate the loss. The Bellman equation is used to establish the target values. By employing a neural network and obtaining optimal values for the policy from the DBSO, the most effective policy is calculated and successfully implemented, referred to as DQN. Table 5.2 provides an overview of the performance indexes

and hyperparameters adopted for the DQN in this work. The deep learning application provided by the MATLAB software is used for the hyperparameter tuning. Table 5.3 presents the value ranges used in the process of hyperparameter tuning.

5.1.4.1 State, reward, and action spaces

The state spaces in the DRL agent correspond to variables that serve as inputs. In this study, the power system's critical components monitored for secure operation include frequencies, voltages, and SCLs at the POIs, total active load, and active power generated by GFM. These components are considered as inputs, and their associated reward spaces are taken into account. Based on the reward computed, the DRL agent proposes control actions for the power system. The determination of the reward follows the approach outlined in Equation 5.10. When the frequency is close to 50 Hz, a reward is granted, and deductions are applied for more significant deviations.

Similarly, 1.00 pu values represent set points for voltages, and rewards are given for voltage deviations within specific thresholds. The SCLs at each POI are also considered in determining the reward, with secure conditions receiving positive rewards and insecure conditions receiving negative rewards. Given the importance of SCL for system security, it carries more weight in this study's reward calculation.

$$r_f = \begin{cases} 1 & \text{for } |df| \leq 0.1 \text{Hz} \\ 0 & \text{for } 0.1 \leq |df| \leq 0.2 \text{ Hz} \\ -e^{-|df|t} & \text{otherwise} \end{cases} \qquad \text{Equation 5.10}$$

The action spaces, on the other hand, entail incremental adjustments made to the generator set points for SG (ΔP_{SG}) and GFL (ΔP_{GFL}) as a result of training interactions between the DRL agent and the environment. These adjustments pertain to the actual generator set points rather than the ideal set points. Although the training objective is to achieve a secure state in a single step, a well-trained DRL agent is expected to adaptively reach the secure state during the online testing phase through multiple adjustment stages. Therefore, while the training

goal is to attain a secure state in one step, the agent's ability to adapt during online testing reflects its training to achieve such a secure state.

5.1.4.2 Performance evaluation

In the final stage of the modeling framework, this study incorporated an analysis of statistical performance measures to evaluate the model's performance. The indicator used is MAPE, which is employed to assess the accuracy of the model.

5.2 Results

5.2.1 Offline training

An offline training phase was conducted using the available data to prepare the neural network for reinforcement learning. Algorithm 1 outlines the procedure followed in this study. A total of 792,000 samples were collected, each with a resolution of 10 milliseconds, taken over time intervals ranging from 20 to 50 seconds. The samples were then utilized for training and validating the DQN model. The dataset was split into a training set (95% of the data) and a validation set (5%) using random data splitting. The epsilon greedy exploration strategy was employed to allow the DQN model to explore the environment and acquire useful knowledge. The hyperparameters used in training the DQN model are listed in Table 5.2.
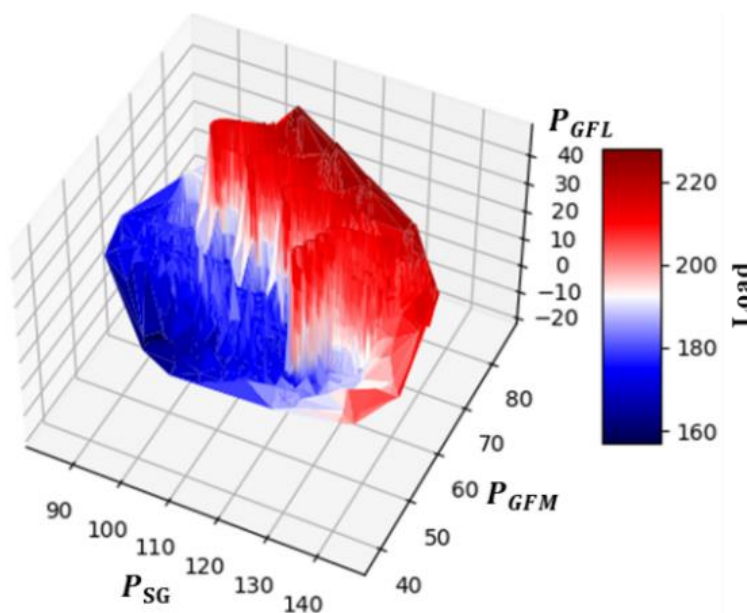
Figure 5.4: Graphical representation of datasets as the function of P_{SG}, P_{GFM}, P_{GFL} and load.

Algorithm 1

1	Initialize the neural network
2	Tune the hyperparameters and train the neural network using previously available data.
3	Create a reinforcement learning environment in OpenAI gym for reinforcement learning.
	A. Initialize action discretization strategy and observation space using gym.
	B. Define a method for dynamic exploration and exploitation rate.
	C. Initialize the communication between reinforcement learning agents in Python and MATLAB Simulink environment.
4	Control the Simulink environment using a reinforcement learning agent and collect the feedback as a reward from the environment.
	A. Give a reward to the associated action based on equation 19.
	B. Optimize the neural network using the Boltzmann optimization method.
5	Repeat step 4 until the training is complete.
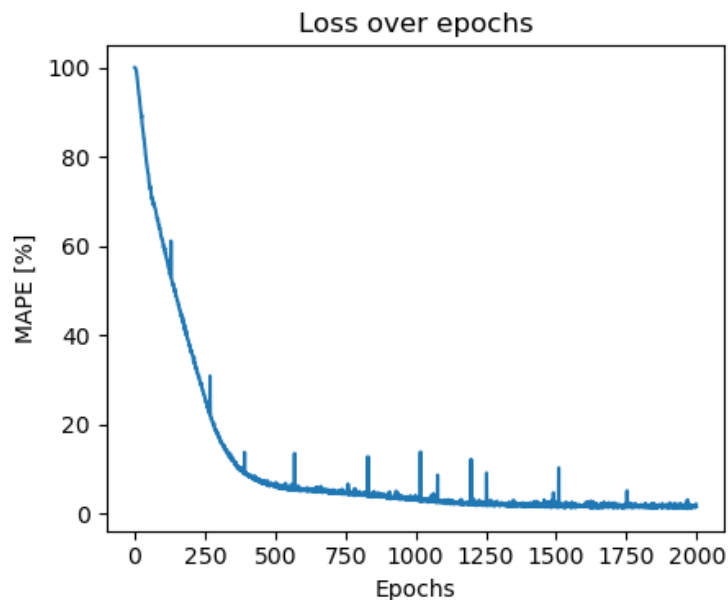
Figure 5.5: Loss function of DNQ model with increasing Epochs.

Figure 5.4 illustrates the datasets, showing the relationship between the load and the power generated by SG, GFL, and GFM. It is evident from the data that SG and GFM provide electricity for lower loads, while all power-generating technologies increase their production as demand increases. GFL serves as a supplementary power source when GFM supply is insufficient or for

heavy loads. SG appears to be the primary power source for all load levels, with GFL contributing more for higher loads.

These datasets are used for training, and the loss function during the training of the DQN model is depicted in Figure 5.5. As the number of epochs increases, there is a significant decrease in the loss function value until it reaches a stable point around 300 epochs. After 400 epochs, the loss function continues to decrease but with slight fluctuations. Figure 5.6 demonstrates the results of applying the regression method to both the training and validation processes. Overall, the DQN model exhibits satisfactory performance considering the datasets and conditions under consideration, as evident from Figure 5.5 and Figure 5.6.
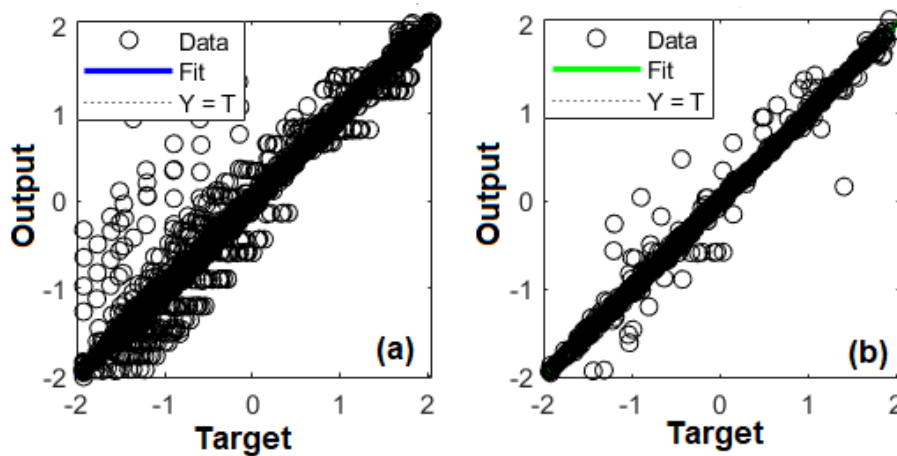
Figure 5.6: Normalized regression plots for P_{GFL}: (a) training, and (b) validation.

5.2.2 Online testing

During online testing, random variations in a portion of the total load are introduced at regular intervals of one second. The online testing was performed in a combined Python and Simulink environment to simulate different scenarios and assess the model's performance. The effects of these load changes on the power system are observed and analyzed. The online testing period spans one minute, allowing for an evaluation of the model's response. The results of the online testing are presented in Figure 5.7.
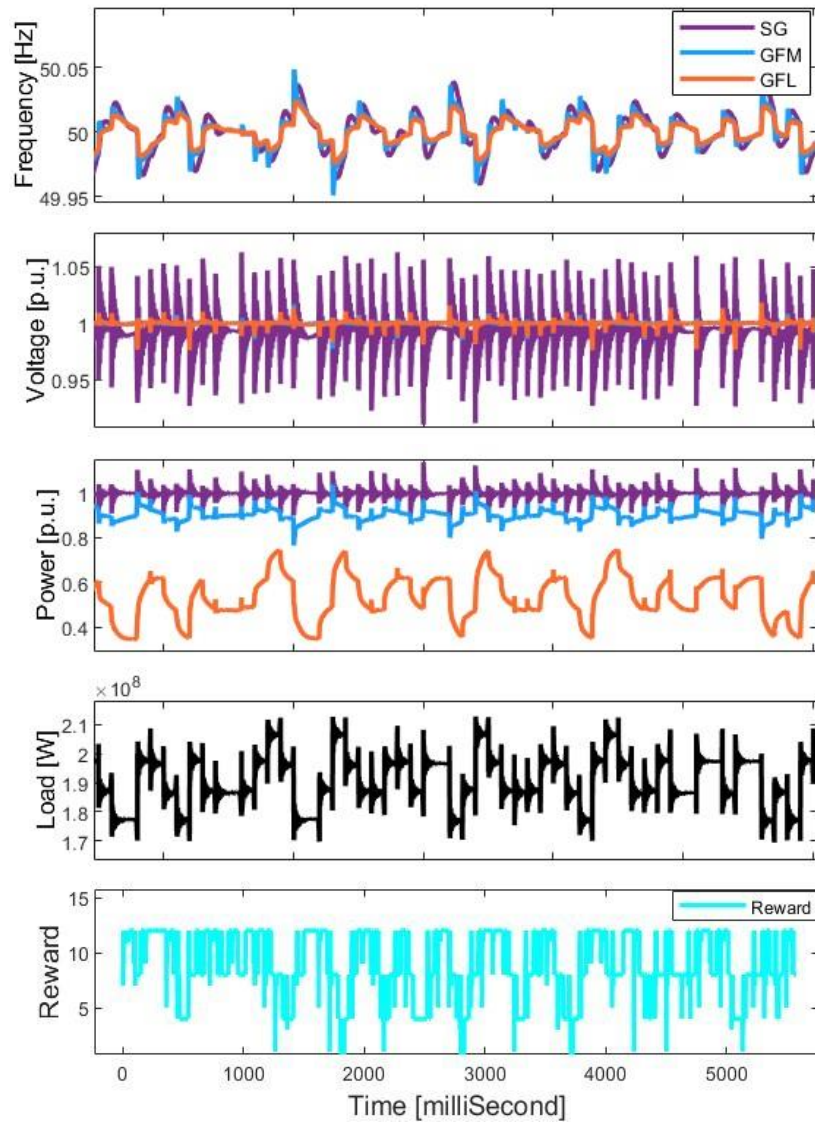
Figure 5.7: Performances of the system for 60 seconds of online testing.

Each power-generating technology exhibits its response in terms of total load, frequency, terminal voltage, and produced power. The model incorporates a reward function to assess the system's performance. As the load changes, the power-generating technologies adjust their generation levels to maintain the supply-demand balance within their operational constraints. The frequency deviation remains within the standard limit specified by the INPS regulation despite fluctuations caused by load variations. The voltage deviation is relatively low for GFM and GFL during rapid load shifts, while SG experiences a larger deviation. When considering the power generated by these technologies, it is important to note the constraints

on increasing or decreasing generation levels and the availability of the sources. GFL appears to play a significant role in maintaining system equilibrium. The environment provides regular rewards to the DQN model, which are considered and illustrated in Figure 5.7. These rewards are based on predefined criteria established for the reward function.
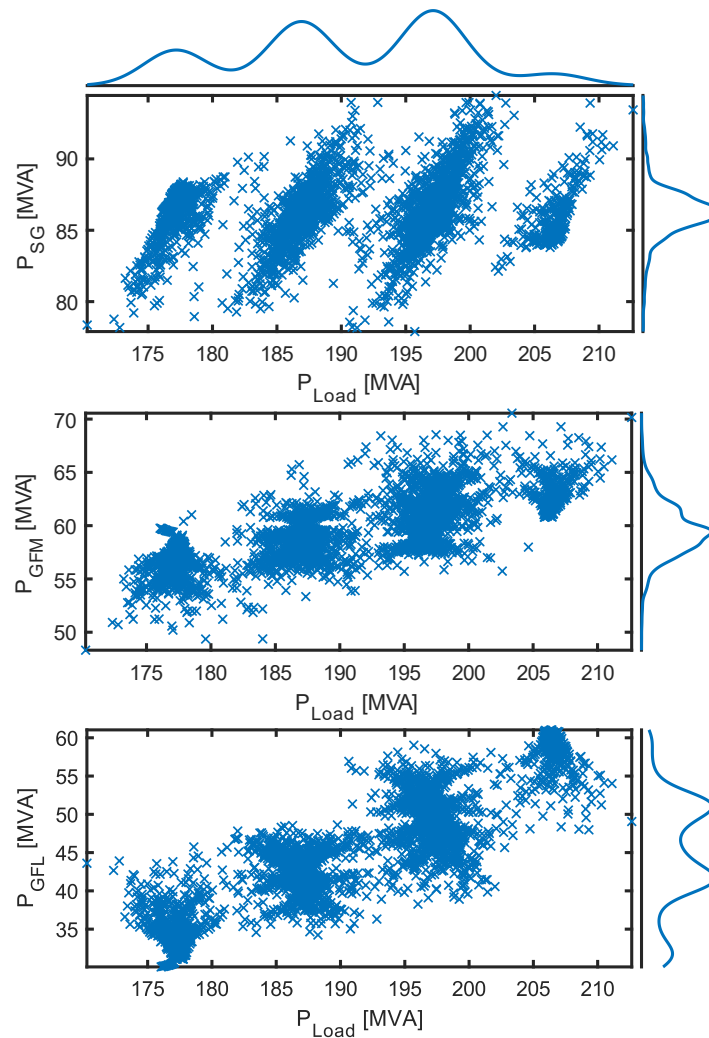
Figure 5.8: Distribution of generations from three power-generating technologies with load for 60 seconds of online testing.

During the one-minute online testing period, the distribution of power generated by the different power-generating technologies concerning the load is shown in Figure 5.8. As mentioned earlier, the load undergoes random and unpredictable shifts at a one-second interval. Figure 5.8 (a-c) depicts the power distribution of the three power-generating

technologies, highlighting their roles in meeting the demand and ensuring system reliability. Among them, the GFL stands out as the most versatile and reliable technology, consistently delivering power even during high-demand periods. This can be observed in Figure 5.9, which displays a distinct distribution pattern for GFL with the load.
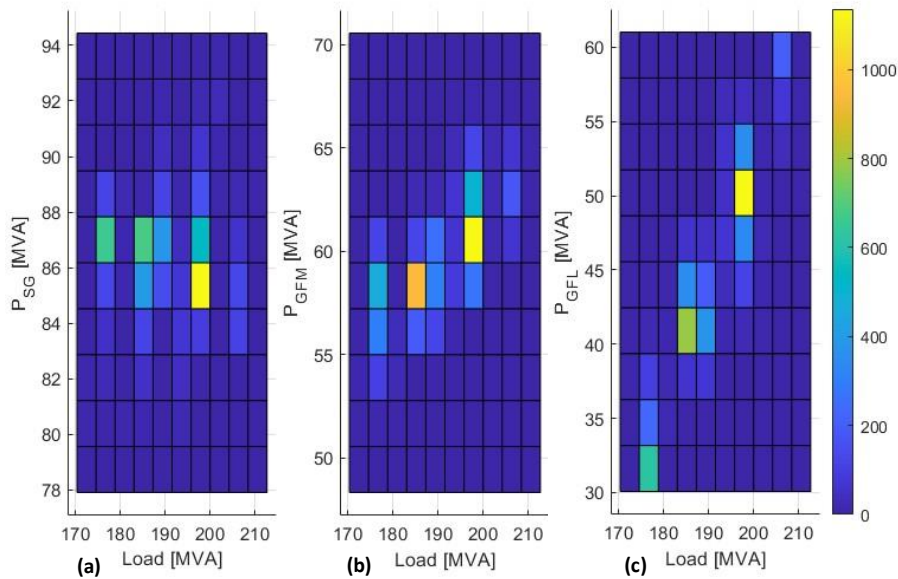
Figure 5.9: Bivariate histogram of generations from three power-generating technologies with respect to total load.
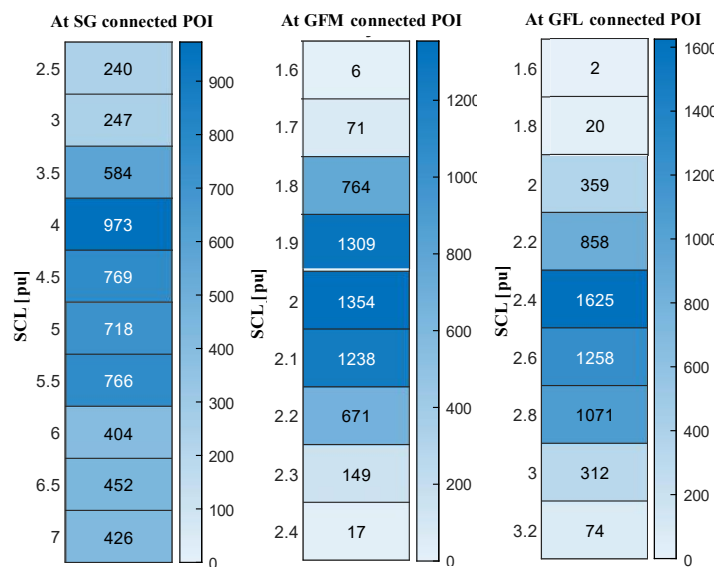

Figure 5.10: Values of SCLs at the POIs connecting (a) SG, (b) GFM, and (c) GFL, for 60 seconds of online testing with 10-millisecond resolutions.

Figure 5.10 illustrates the distribution of the measured SCL values at the POIs of the three power-generating technologies during the one-minute online testing. Each technology contributes to the individual SCL values as the power system operates online. Notably, the SCL value at the POI of SG is higher compared to the other sites. This is due to the relatively higher SCLs provided by SG compared to GFM and GFL. Looking at this figure, it is evident that the SCL values at each POI exceed 1.6 pu, with the majority of the values exceeding 1.9 pu. This reflects the robustness of the evaluated power system during its online operation.

5.3 Conclusion

This chapter identifies that the online estimation of the energy-mix proportion can play a crucial role in ensuring the secure operation of converter-dominated power systems. Researchers and operators can accurately estimate the contribution of different power-generating technologies within the system by utilizing advanced techniques such as DRL. This estimation provides valuable insights into the system's dynamics and enables proactive decision-making to maintain stability and reliability. The importance of online estimation lies in its ability to address the challenges posed by integrating new technologies and the unpredictable nature of RESs and load variations.

The presented framework, utilizing DRL and online estimation, offers significant advantages for the secure operation of converter-dominated power systems. The robustness of the well-trained DRL agent, as demonstrated in the study, ensures optimal performance even in the face of uncertainties and fluctuations. By implementing online estimation of the energy-mix proportion, power system operators gain valuable insights into the behavior and performance of different power-generating technologies. This information enables them to make informed decisions, optimize resource allocation, and implement preventive measures to mitigate risks and ensure reliable and secure operations.

In conclusion, online estimation of the energy-mix proportion is a crucial way to maintain converter-dominated power systems' stability and reliability. It empowers operators to proactively manage the system, optimize its performance, and effectively integrate new

technologies and RESs. By leveraging advanced techniques such as DRL, online estimation offers a promising approach for securing modern power systems in the face of evolving grid topologies and the increasing adoption of renewable energy.

6 Discussion and Conclusions

6.1 Discussion on Results

The overall discussion of this PhD study encompasses the key findings and their significance in the context of power system stability and the integration of IBRs. This study has highlighted the growing importance of RESs and the need to address the challenges associated with frequency stability and system dynamics. One of the primary focuses of this PhD study has been developing effective strategies and control mechanisms to ensure the reliable operation of power systems dominated by IBRs. By exploring innovative solutions, such as advanced frequency management techniques and the utilization of cutting-edge PECs, the research has contributed to enhancing the ability of power systems to adapt to high levels of RES integration while maintaining stability.

In the involved areas of this PhD study, the lines of each article connect to form a comprehensive plot on the potential and challenges of an IBR-dominated power system. The transition towards such a system, powered entirely by RESs, is not simply a scientific pursuit but a fundamental question impacting global sustainability and climate action path. A graphical overview of the interconnections among the presented articles can be seen in Figure 6.1.

Research Hypothesis and Literature Review

Theoritical Foundation and Research Formulations

Article 1

Articel 3

Methodology, Simulation, and Validation

Article 5

Article 6
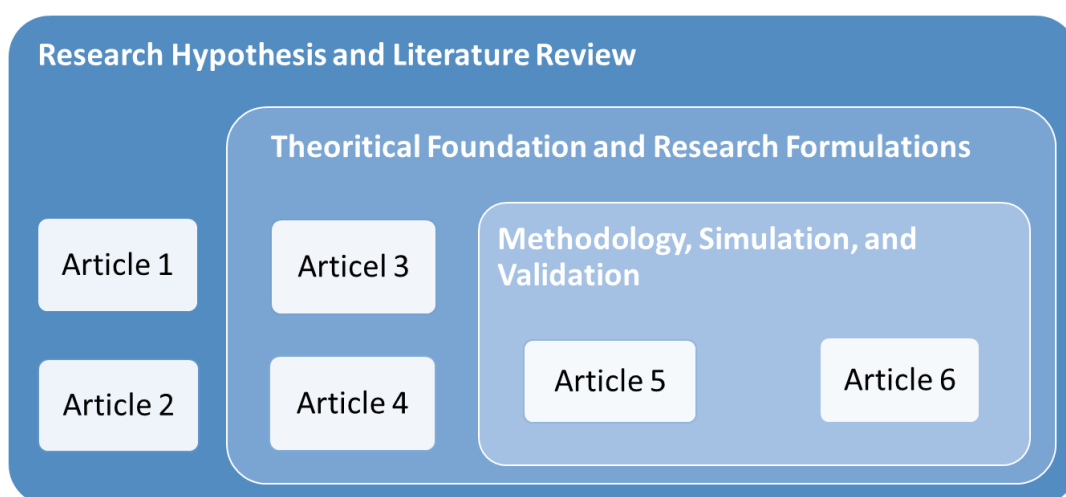
Article 2

Article 4

Figure 6.1: Interconnections and synergies among research articles.

The foundational pillars of this PhD study, **Article 1** and **Article 2**, lay the groundwork by questioning the feasibility and stability of a RES-driven power grid. While **Article 1** explores the broader consequences encompassing technological, social, and political challenges, **Article 2** thoroughly explores stability issues, highlighting the criticality of frequency stability in modern power systems and the strategies to address potential difficulties.

Building upon this foundation, **Articles 3 and 4** take a deeper jump into specific aspects of power system dynamics. **Article 3**, with its extensive analysis of rotor angle stability indicators, illuminates the profound sensitivity of power system stability to system inertia. It underscores the cascading effects that experienced changes in inertia can have on system dynamics, a crucial insight for designing future power systems. Alongside, **Article 4** brings forward the potential of data-driven approaches, especially Bayesian models, for kinetic energy forecasting in converter-dominated systems. It emphasizes the appropriateness of time-series data analysis in shaping a secure operational landscape for such power systems.

The success of this research work is achieved in **Article 5** and **Article 6**, where theory meets application. **Article 5**, leveraging time-series data, pioneers a methodology for estimating the optimal energy mix, a step crucial for ensuring the secure operation of converter-dominated systems. This is further complemented by **Article 6**, which serves as a testimony to the robustness and applicability of the proposed methodologies, emphasizing the potential of online estimations in real-world scenarios.

In essence, this complement of articles dips a complete picture, transitioning from conceptual hypotheses to concrete solutions. The journey from the theoretical foundations in **Article 1** and **Article 2** to the practical applications in **Article 5** and **Article 6** characterizes the tendency of research: to question, to explore, and finally, to resolve. While self-contained in its objective, each article contributes to a larger narrative, emphasizing the interconnection and synergies driving IBR-dominated power systems' evolution. The concluded knowledge from this research promises to help shape the future of power systems, supporting a sustainable, renewable, and stable energy paradigm.

6.2 Strengths of the study

The strength of this PhD study lies in its multi-faceted and comprehensive approach to addressing the challenges and potentialities of an IBR-dominated power system. With a vision rooted in the global obligation of sustainability, this PhD study doesn't merely explore the feasibility of a power system driven entirely by RESs but examines the sophisticated distinctions that motivate such a transition.

First, the study is grounded in a robust foundation, as seen through **Article 1** and **Article 2**. These initial articles ensure that the research is not built on assumptions but is secured in a complete literature review and hypothesis-driven exploration. By questioning the broader implications of a RES-based power system from technological, social, and political perspectives, the research sets a complete stage for subsequent investigations.

Furthermore, the PhD work exhibits a commendable balance between theoretical constructs and practical applications. While **Article 3** and **Article 4** provide a detailed analysis of specific aspects of power system dynamics and its analysis, **Article 5** and **Article 6** transition these insights into actionable methodologies. This flow from concept to application is a feature of impactful research, ensuring that the findings are not confined to academic strips but have real-world implications and utility.

Another strength is the study's emphasis on data-driven approaches, illustrated by the innovative use of data-driven models and time-series data analysis. In an era where data is indicated as the new fuel, this research harnesses it thoughtfully, highlighting its potential in shaping a secure operational landscape for power systems. Such methodologies improve the research's relevance in the modern era and cover the way for future explorations in the domain.

Lastly, the interconnection and synergies evident across the articles bring out the study's coherence. Rather than being isolated pieces, each article contributes to a larger narrative, emphasizing the holistic vision of the PhD Candidate. This coherence ensures readers and

stakeholders can trace the logical progression and appreciate the cumulative knowledge presented.

In conclusion, the PhD study indicates rigorous academic pursuit combined with a vision for sustainable futures. Its strength is reflected in its comprehensive approach, balance between theory and application, innovative methodologies, and cohesive narrative. Such research advances academic understanding and promises to guide the trajectory of global energy systems toward sustainability.

6.3 Limitations of the study

No matter how thoroughly conducted, every comprehensive research inherently has some limitations, and this PhD study is no exception. Recognizing these limitations is crucial not as a sign of weakness but as an acknowledgment of areas that might benefit from further exploration and refinement in future research endeavors.

One of the significant limitations is the validation of the results in a real-time experimental setup, specifically within a laboratory-based environment. While the study extensively utilizes data-driven methodologies and models, the absence of real-time validation means some findings might not translate effortlessly when applied in practical scenarios. Laboratory-based environments provide an invaluable platform to test theories and results under controlled conditions, allowing researchers to capture touches and potential issues that might not be evident in simulations alone. By not leveraging this setup, there's an inherent risk of overlooking practical challenges or system behaviors that could critically impact the implementation of the study's recommendations.

Moreover, the foundational elements of the study, especially as showcased in **Article 1** and **Article 2**, are primarily built upon existing literature. While providing a robust starting point, such an approach also risks inheriting biases or potential gaps from referenced works. The evolving nature of RES technologies and the dynamic global power landscape means that relying heavily on prior research could accidentally miss capturing some existing characteristics.

The specific models and methodologies adopted, as detailed in **Articles 3** through **6**, present their own set of challenges. For instance, the Bayesian model from **Article 4**, while powerful, is contingent on the quality of prior data and foundational assumptions. Any inconsistencies in these initial inputs can lead to forecasts that misalign with the actual system dynamics.

Furthermore, the study's choice to examine specific scenarios and systems, such as the 39 Bus New England power system and IEEE Bus power system, adds depth but potentially sacrifices broader applicability. Power infrastructures across various regions, influenced by inconsistent socio-political, geographical, and infrastructural factors, may not align perfectly with the findings from this specific study.

Another potential limitation could restrict the study's emphasis on data-driven methodologies. While the power of data in modern research is undisputable, over-reliance on it might sometimes doubtful qualitative aspects that are harder to quantify but equally significant. Factors such as social perceptions, political will, or even grassroots movements can play pivotal roles in the adoption and success of RES-driven power systems, and these might not always be captured in numerical models or algorithms.

6.4 Recommendation for future works

This PhD study on IBR-dominated power systems has illustrated several possibilities for future research, particularly in addressing the noted gaps and constraints. Central to these recommendations is the establishment of experimental frameworks in laboratory settings that carefully emulate the complex realities of power systems. Such environments are needed for comprehensive testing of theoretical models and algorithms, thereby confirming their practical applicability and effectiveness in real-world scenarios.

A pivotal recommendation involves the implementation of Virtual Hardware-in-the-Loop (HIL) simulations. These simulations are practiced at recreating complex power system conditions, enabling extensive testing across a field of operational states, some of which might be impractical or hazardous to replicate physically. The utilization of Virtual HIL is key in

thoroughly examining various critical scenarios, ultimately enhancing the durability and adaptability of the proposed models.

Concurrently, advancing the development of sophisticated HIL systems is essential. These systems should encompass not just the electrical aspects of power systems but also their control, communication, and operational dynamics. The integration of artificial intelligence and machine learning within these HIL systems could further augment their capability to simulate unpredictable scenarios and evaluate theoretical models, thereby identifying potential errors and optimizing experimental designs.

Moreover, stochastic considerations in power system research are vital, particularly in managing the variability of power generation from RESs like solar and wind, and in adapting to fluctuating load demands. Developing stochastic models that accurately predict the uncertainties associated with renewable energy generation and load consumption is crucial. These models should employ probabilistic methods to account for the unpredictability inherent in RESs and demand patterns, aiding in the efficient management of power systems and ensuring a harmonious balance between supply and demand.

The rise of distributed prosumers marks a significant shift in energy network dynamics, with power generation becoming increasingly decentralized. This evolution introduces considerable variability and stochastic behavior in power generation and demand. Future research should aim to integrate the role of distributed prosumers into stochastic models for power system analysis, developing algorithms to predict and manage the intermittent and variable energy flow. Investigating the potential of distributed prosumers in enhancing grid resilience, and optimizing their participation through incentives and technological innovations such as smart grid technologies, and AI-driven energy management systems, is also recommended.

Collaboration with industry stakeholders forms another critical component of future research. Engaging with industry partners allows for the incorporation of cutting-edge technology and practical insights, ensuring that research is aligned with contemporary industry standards. A

___

multidisciplinary approach, bringing together expertise from computer science, engineering, and data analytics, is also recommended to develop more comprehensive validation platforms. These platforms would simulate not only the physical aspects of power systems but also their digital and data-driven components, providing a more thorough understanding of modern power system operations. This collaborative and interdisciplinary approach promises to advance power system research, aligning it closely with the evolving demands of modern energy ecosystems.

6.5 Practical implementations

This PhD study is conducted in the domain of IBR-dominated power systems and the possibility of a 100% RES-based energy infrastructure. With the global shift toward RES picking up momentum, such research projects have presented applications with vast and diverse utility.

An understanding of rotor angle stability indicators and the sophisticated relationship between system inertia provides a framework for critical infrastructure investment decisions. This research offers invaluable insights for localities that are at the edge of transitioning to a RES-dominated energy framework. It explains how the extant infrastructure might need recalibration, be it enhancements or modifications, in the face of an evolving energy situation. The dilemma of maintaining grid equilibrium is increased when one considers the intermittent nature of many RESs. For example, by harnessing knowledge about rotor angle stability and the dynamics of kinetic energy, these innovations empower TSOs to perform real-time decisions. Such proactive steps can safeguard a steady energy output and prevent potential grid disturbances.

Furthermore, this research serves as a supportive reference for energy strategists and policymakers. The data regarding the ideal proportions for a day-ahead energy mix presents a tangible blueprint. With this at their disposal, these stakeholders can predict future energy necessities, factor in periodic fluctuations, and carefully integrate both conventional and RESs to provide for these needs. In an era where the world is navigating the elaborate network of ensuring energy reliability while also addressing environmental concerns, this research

emerges as a guide. Regulatory entities can utilize its findings to craft policies that champion the cause of RES adoption. The holistic perspective of this research, which incorporates technological, financial, and social sides, is crucial. It can be the foundation of policies that not only push RES investments but also prioritize the crucial aspect of grid resilience and steadiness.

6.6 Conclusions

This PhD study presents an in-depth exploration of the complexities of power system dynamics, focusing on RES-based and converter-dominated power systems. Through a collection of six scientific publications, this PhD study bridges traditional understanding with current challenges and potential solutions. The study explores the significance of time-series data analysis, day-ahead estimation, and the effectiveness of online simulation in tackling challenges arising from the integration of IBRs. The research also discusses the effectiveness of various methods in ensuring reliability, system stability, and efficient control in IBR-dominated systems. In conclusion, through a comprehensive discussion and synthesis of the findings, this PhD study contributes valuable insights to the academic community and provides a roadmap for sustainable and environmentally conscious advancements in the power system domain.

References

1. Kroposki, B., et al., *Achieving a 100% renewable grid: Operating electric power systems with extremely high levels of variable renewable energy.* IEEE Power and Energy Magazine, 2017. **15**(2): p. 61-73.
2. Verzijlbergh, R., et al., *Institutional challenges caused by the integration of renewable energy sources in the European electricity sector.* Renewable and Sustainable Energy Reviews, 2017. **75**: p. 660-667.
3. Shrestha, A. and F. Gonzalez-Longatt, *Frequency stability issues and research opportunities in converter dominated power system.* Energies, 2021. **14**(14): p. 4184.
4. Saeedian, M., et al., *Emulating Rotational Inertia of Synchronous Machines by a New Control Technique in Grid-Interactive Converters.* Sustainability, 2020. **12**(13): p. 5346.
5. Rocabert, J., et al., *Control of power converters in AC microgrids.* IEEE transactions on power electronics, 2012. **27**(11): p. 4734-4749.
6. Paquette, A.D., et al., *Sharing transient loads: Causes of unequal transient load sharing in islanded microgrid operation.* IEEE Industry Applications Magazine, 2013. **20**(2): p. 23-34.
7. Arraño-Vargas, F., et al., *Challenges and mitigation measures in power systems with high share of renewables—the Australian experience.* Energies, 2022. **15**(2): p. 429.
8. Copp, D.A., et al., *Optimal sizing of distributed energy resources for planning 100% renewable electric power systems.* Energy, 2022. **239**: p. 122436.
9. Pourbabak, H., T. Chen, and W. Su, *Centralized, decentralized, and distributed control for Energy Internet*, in *The Energy Internet*. 2019, Elsevier. p. 3-19.
10. Heuberger, C.F. and N. Mac Dowell, *Real-world challenges with a rapid transition to 100% renewable power systems.* Joule, 2018. **2**(3): p. 367-370.
11. Hodge, B.M.S., et al., *Addressing technical challenges in 100% variable inverter-based renewable energy power systems.* Wiley Interdisciplinary Reviews: Energy and Environment, 2020. **9**(5): p. e376.
12. Shakerighadi, B., et al., *An overview of stability challenges for power-electronic-dominated power systems: The grid-forming approach.* IET Generation, Transmission & Distribution, 2023. **17**(2): p. 284-306.
13. Smadi, A.A., et al., *A Comprehensive survey on cyber-physical smart grid testbed architectures: Requirements and challenges.* Electronics, 2021. **10**(9): p. 1043.
14. Kenyon, R.W., et al., *Stability and control of power systems with high penetrations of inverter-based resources: An accessible review of current knowledge and open questions.* Solar Energy, 2020. **210**: p. 149-168.
15. Meegahapola, L., et al., *Power System Stability with Power-Electronic Converter Interfaced Renewable Power Generation: Present Issues and Future Trends.* Energies, 2020. **13**(13): p. 3441.
16. Meegahapola, L., et al., *Power system stability in the transition to a low carbon grid: A techno-economic perspective on challenges and opportunities.* Wiley Interdisciplinary Reviews: Energy and Environment, 2021. **10**(5): p. e399.

17. Wang, Y., H. Silva-Saravia, and H. Pulgar-Painemal, *Actuator placement for enhanced grid dynamic performance: A machine learning approach.* IEEE Transactions on Power Systems, 2019. **34**(4): p. 3119-3128.

18. Pei, W., et al., *Temporal-spatial analysis and improvement measures of Chinese power system for wind power curtailment problem.* Renewable and Sustainable Energy Reviews, 2015. **49**: p. 148-168.

19. Khadka, N., et al., *Transient Stability in Renewable Energy Penetrated Power Systems: A Review*, in *RESSD 2020 International Conference on Role of Energy for Sustainable Social Development in 'New Normal' Era*. 2020: Nepal.

20. Worighi, I., et al., *Integrating renewable energy in smart grid system: Architecture, virtualization and analysis.* Sustainable Energy, Grids and Networks, 2019. **18**: p. 100226.

21. Alves, E.F., *Optimization of Energy Storage for Frequency Control in Autonomous AC Power Systems–Frameworks for Planning and Operation.* 2023.

22. Ochoa, D.E., et al., *Control Systems for Low-Inertia Power Grids: A Survey on Virtual Power Plants.* IEEE Access, 2023.

23. Majumder, S., et al., *On the Cyber-Physical Needs of DER-based Voltage Control/Optimization Algorithms in Active Distribution Network.* IEEE Access, 2023.

24. Xie, L., et al., *On an Information and Control Architecture for Future Electric Energy Systems.* Proceedings of the IEEE, 2022. **110**(12): p. 1940-1962.

25. Rousis, A.O., et al., *State-of-the-Art Literature Review of System Scarcities at High Levels of Renewable Generation.* Technical Report of European Union's Horizon 2020-EU-SysFlex, 2018.

26. Zhu, J., et al., *Synthetic inertia control strategy for doubly fed induction generator wind turbine generators using lithium-ion supercapacitors.* IEEE Transactions on Energy Conversion, 2017. **33**(2): p. 773-783.

27. Shrestha, A., et al., *Assessment of electricity excess in an isolated hybrid energy system: A case study of a Dangiwada village in rural Nepal.* Energy Procedia, 2019. **160**: p. 76-83.

28. Hou, Q., et al., *Impact of High Renewable Penetration on the Power System Operation Mode: A Data-Driven Approach.* IEEE Transactions on Power Systems, 2019. **35**(1): p. 731-741.

29. Hossain, J. and A. Mahmud, *Renewable energy integration: challenges and solutions*. 2014: Springer Science & Business Media.

30. Energy, U., *the Challenge of Sustainability".* World Energy Assessment, UNDP-WEC, 2000.

31. Shrestha, A. and F. Gonzalez-Longatt, *Parametric sensitivity analysis of rotor angle stability indicators.* Energies, 2021. **14**(16): p. 5023.

32. *BP Statistical Review of World Energy* 2021, BP Statistical Review: London, UK.

33. Hannah, R. and R. Max, *Renewable electricty-generating capacity, 2020*, in *Renewable Energy*, O.W.i. Data, Editor. 2021.

34. Centre/BNEF, F.S.-U., *Global Trends in Renewable Energy Investment 2017*, I.R.E.A. (IRENA), Editor. 2017.

35. Andrew, B., et al., *Joint Declaration of the Global 100% RE Strategy Group*. 2021, The Global 100% RE Strategy Group.

36. Zappa, W., M. Junginger, and M. van den Broek, *Is a 100% renewable European power system feasible by 2050?* Applied Energy, 2019. **233**: p. 1027-1050.

37. Heard, B.P., et al., *Burden of proof: A comprehensive review of the feasibility of 100% renewable-electricity systems.* Renewable and Sustainable Energy Reviews, 2017. **76**: p. 1122-1133.

38. Diesendorf, M. and B. Elliston, *The feasibility of 100% renewable electricity systems: A response to critics.* Renewable and Sustainable Energy Reviews, 2018. **93**: p. 318-330.

39. Hughes, T.P., *Technological momentum.* Does technology drive history, 1994.

40. McCloughan, M.J.B., *Kant's theory of progress*. 2004: University of London, University College London (United Kingdom).

41. Moore, G.E., *Cramming more components onto integrated circuits*. 1965, McGraw-Hill New York.

42. Selk, E.E., *The Idea of Technological Progress and Its Problems.* 1980.

43. Peirce, C.S., *Collected papers of charles sanders peirce*. Vol. 2. 1974: Harvard University Press.

44. Meegahapola, L., et al., *Power system stability with power-electronic converter interfaced renewable power generation: Present issues and future trends.* Energies, 2020. **13**(13): p. 3441.

45. Radaelli, L. and S. Martinez, *Frequency stability analysis of a low inertia power system with interactions among power electronics interfaced generators with frequency response capabilities.* Applied Sciences, 2022. **12**(21): p. 11126.

46. Shrestha, A., et al., *Peer-to-peer energy trading in micro/mini-grids for local energy communities: A review and case study of Nepal.* IEEE access, 2019. **7**: p. 131911-131928.

47. Trainer, T., *'Can renewables meet total Australian energy demand: A "disaggregated" approach.* Energy Policy, 2017. **109**: p. 539-544.

48. Elliston, B., I. MacGill, and M. Diesendorf, *Comparing least cost scenarios for 100% renewable electricity with low emission fossil fuel scenarios in the Australian National Electricity Market.* Renewable Energy, 2014. **66**: p. 196-204.

49. Connolly, D. and B.V. Mathiesen, *A technical and economic analysis of one potential pathway to a 100% renewable energy system.* International Journal of Sustainable Energy Planning and Management, 2014. **1**: p. 7-28.

50. Jacobson, M.Z., et al., *100% clean and renewable wind, water, and sunlight all-sector energy roadmaps for 139 countries of the world.* Joule, 2017. **1**(1): p. 108-121.

51. Kilickaplan, A., et al., *An energy transition pathway for Turkey to achieve 100% renewable energy powered electricity, desalination and non-energetic industrial gas demand sectors by 2050.* Solar Energy, 2017. **158**: p. 218-235.

52. Aghahosseini, A., D. Bogdanov, and C. Breyer, *Towards sustainable development in the MENA region: Analysing the feasibility of a 100% renewable electricity system in 2030.* Energy Strategy Reviews, 2020. **28**: p. 100466.

53.   Caldera, U. and C. Breyer, *The role that battery and water storage play in Saudi Arabia's transition to an integrated 100% renewable energy power system.* Journal of Energy Storage, 2018. **17**: p. 299-310.

54.   Lund, H., et al., *Smart energy Denmark. A consistent and detailed strategy for a fully decarbonized society.* Renewable and Sustainable Energy Reviews, 2022. **168**: p. 112777.

55.   He, J., et al., *Hierarchical optimal energy management strategy of hybrid energy storage considering uncertainty for a 100% clean energy town.* Journal of Energy Storage, 2021. **41**: p. 102917.

56.   Keiner, D., et al., *Powering an island energy system by offshore floating technologies towards 100% renewables: A case for the Maldives.* Applied Energy, 2022. **308**: p. 118360.

57.   Li, L., et al., *Combined multi-objective optimization and agent-based modeling for a 100% renewable island energy system considering power-to-gas technology and extreme weather conditions.* Applied Energy, 2022. **308**: p. 118376.

58.   Weiss, O., et al., *Market designs for a 100% renewable energy system: Case isolated power system of Israel.* Energy, 2017. **119**: p. 266-277.

59.   Harewood, A., F. Dettner, and S. Hilpert, *Open source modelingof scenarios for a 100% renewable energy system in Barbados incorporating shore-to-ship power and electric vehicles.* Energy for Sustainable Development, 2022. **68**: p. 120-130.

60.   Luo, S., et al., *Study on the decarbonization in China's power sector under the background of carbon neutrality by 2060.* Renewable and Sustainable Energy Reviews, 2022. **166**: p. 112618.

61.   Yue, X., et al., *Least cost energy system pathways towards 100% renewable energy in Ireland by 2050.* Energy, 2020. **207**: p. 118264.

62.   Ma, J., et al., *Demand and supply-side determinants of electric power consumption and representative roadmaps to 100% renewable systems.* Journal of Cleaner Production, 2021. **299**: p. 126832.

63.   Nagel, N.O., J.G. Kirkerud, and T.F. Bolkesjø, *The economic competitiveness of flexibility options: A model study of the European energy transition.* Journal of Cleaner Production, 2022. **350**: p. 131534.

64.   Peters, I.M., et al., *The role of batteries in meeting the PV terawatt challenge.* Joule, 2021. **5**(6): p. 1353-1370.

65.   Shrestha, A. and F. Gonzalez-Longatt, *Parametric sensitivity analysis of rotor angle stability indicators: Simulation case.* Energy Reports, 2022. **8**: p. 727-735.

66.   Bamisile, O., et al., *An approach for sustainable energy planning towards 100% electrification of Nigeria by 2030.* Energy, 2020. **197**: p. 117172.

67.   Colbertaldo, P., et al., *Impact of hydrogen energy storage on California electric power system: Towards 100% renewable electricity.* International Journal of Hydrogen Energy, 2019. **44**(19): p. 9558-9576.

68.   Li, M., et al., *The roles of biomass and CSP in a 100% renewable electricity supply in Australia.* Biomass and Bioenergy, 2020. **143**: p. 105802.

69. da Luz, T. and P. Moura, *Power generation expansion planning with complementarity between renewable sources and regions for 100% renewable energy systems.* International Transactions on Electrical Energy Systems, 2019. **29**(7): p. e2817.

70. Agency, I.E., *Hydropower Special Market Report: Analysis and forecast to 2030*. 2021, International Energy Agency.

71. Liobikienė, G., R. Dagiliūtė, and R. Juknys, *The determinants of renewable energy usage intentions using theory of planned behaviour approach.* Renewable Energy, 2021. **170**: p. 587-594.

72. Eder, J.M., C.F. Mutsaerts, and P. Sriwannawit, *Mini-grids and renewable energy in rural Africa: How diffusion theory explains adoption of electricity in Uganda.* Energy Research & Social Science, 2015. **5**: p. 45-54.

73. Rosso-Cerón, A.M. and V. Kafarov, *Barriers to social acceptance of renewable energy systems in Colombia.* Current Opinion in Chemical Engineering, 2015. **10**: p. 103-110.

74. Carley, S. and D.M. Konisky, *The justice and equity implications of the clean energy transition.* Nature Energy, 2020. **5**(8): p. 569-577.

75. WHO, I.I.U., *Tracking SDG 7: The Energy Progress Report*, in *Access to electricity (% of population)*, T.W. Bank, Editor. 2020.

76. Jaganmohan, M., *Global renewable energy potential 2050*. 2021, statista.

77. Cappelen, Å., *11. Convergence, divergence and the Kuznets curve.* Globalization, Economic Development and Inequality, 2007: p. 309.

78. Ram, M., A. Aghahosseini, and C. Breyer, *Job creation during the global energy transition towards 100% renewable power system by 2050.* Technological Forecasting and Social Change, 2020. **151**: p. 119682.

79. Marx, M.R.S.L., *Does technology drive history?: The dilemma of technological determinism*. 1994: Mit Press.

80. Pursiheimo, E., H. Holttinen, and T. Koljonen, *Path toward 100% renewable energy future and feasibility of power -to -gas technology in Nordic countries.* IET Renewable Power Generation, 2017. **11**(13): p. 1695-1706.

81. Manjong, N.B., A.S. Oyewo, and C. Breyer, *Setting the pace for a sustainable energy transition in central Africa: The case of Cameroon.* IEEE Access, 2021. **9**: p. 145435-145458.

82. Program, E.S.M.A., *Global Photovoltaic Power Potential by Country*. 2020, World Bank.

83. Child, M., et al., *Scenarios for sustainable energy in Scotland.* Wind Energy, 2019. **22**(5): p. 666-684.

84. Wang, Z., et al., *Optimal planning of a 100% renewable energy island supply system based on the integration of a concentrating solar power plant and desalination units.* International Journal of Electrical Power & Energy Systems, 2020. **117**: p. 105707.

85. Reyseliani, N. and W.W. Purwanto, *Pathway towards 100% renewable energy in Indonesia power system by 2050.* Renewable Energy, 2021. **176**: p. 305-321.

86. Breyer, C., et al., *Reflecting the energy transition from a European perspective and in the global context—Relevance of solar photovoltaics benchmarking two ambitious scenarios.* Progress in Photovoltaics: Research and Applications, 2022.

87. Brown, K.P. and D.J. Hess, *Pathways to policy: Partisanship and bipartisanship in renewable energy legislation.* Environmental Politics, 2016. **25**(6): p. 971-990.

88. Kunda, Z., *The case for motivated reasoning.* Psychological bulletin, 1990. **108**(3): p. 480.

89. McPhetres, J., B. Bago, and G. Pennycook, *Science beliefs, political ideology, and cognitive sophistication.* 2019.

90. Eurostat, *SHort Assessment of Renewable Energy Sources*. 2022.

91. Commission, E., *The 2030 targets*. 2022.

92. KRAFTINAT, E.F.S.S., *NORDIC GRID DEVELOPMENT PERSPECTIVE 2021*. 2021.

93. KRAFTINAT, E.F.S.S., *SOLUTIONS FOR A GREEN NORDIC ENERGY SYSTEM. Strategies to meet the climate challenge*. 2022.

94. Research, N.E., *Key Performance Indicators*. 2023.

95. Chasanidou;, D., J. Hanson;, and H.E. Normann;, *THE NORWEGIAN SOLAR ENERGY INNOVATION SYSTEM*. Norwegian University of Science and Technology.

96. Outlook, I.N.E. and E. Nordic, *Insights from Leaders in Electric Mobility.* IEA: Paris, France, 2018.

97. *Nordic Co-operation Programme on Energy Policy 2022–24*. 2021, Nordic Council of Ministers

98. Bevrani, H. and T. Hiyama, *Intelligent automatic generation control*. 2017: CRC press.

99. Bevrani, H. and T. Hiyama, *On load–frequency regulation with time delays: design and real-time implementation.* IEEE transactions on energy conversion, 2009. **24**(1): p. 292-300.

100. Milla, F., M.A. Duarte-Mermoud, and N. Aguila-Camacho, *Hierarchical mpc secondary control for electric power system.* Mathematical Problems in Engineering, 2014. **2014**.

101. Chamorro, H.R., et al., *A network control system for hydro plants to counteract the non-synchronous generation integration.* International Journal of Electrical Power & Energy Systems, 2019. **105**: p. 404-419.

102. Hyndman, R.J., X.A. Liu, and P. Pinson, *Visualizing big energy data: Solutions for this crucial component of data analysis.* IEEE Power and Energy Magazine, 2018. **16**(3): p. 18-25.

103. Cheng, M., S.S. Sami, and J. Wu, *Benefits of using virtual energy storage system for power system frequency response.* Applied energy, 2017. **194**: p. 376-385.

104. Lee, S.-J., et al., *Coordinated control algorithm for distributed battery energy storage systems for mitigating voltage and frequency deviations.* IEEE Transactions on Smart Grid, 2015. **7**(3): p. 1713-1722.

105. Kumar, P.S., *Transient stability enhancement of power system using TCSC.* International Journal of Electrical and computer engineering, 2012. **2**(3): p. 317.

106. Wang, M.-H. and H.-C. Chen, *Transient stability control of multimachine power systems using flywheel energy injection.* IEE Proceedings-Generation, Transmission and Distribution, 2005. **152**(5): p. 589-596.

107. Haque, M., *Improvement of first swing stability limit by utilizing full benefit of shunt FACTS devices.* IEEE transactions on power systems, 2004. **19**(4): p. 1894-1902.

108. Murali, D., M. Rajaram, and N. Reka, *Comparison of FACTS devices for power system stability enhancement.* International Journal of Computer Applications, 2010. **8**(4): p. 30-35.

109. Guo, G., et al., *Robust nonlinear controller for power system transient stability enhancement with voltage regulation.* IEE Proceedings-Generation, Transmission and Distribution, 1996. **143**(5): p. 407-412.

110. Teng, F., et al., *Challenges on primary frequency control and potential solution from EVs in the future GB electricity system.* Applied energy, 2017. **194**: p. 353-362.

111. Liu, H., et al., *Optimal dispatch for participation of electric vehicles in frequency regulation based on area control error and area regulation requirement.* Applied Energy, 2019. **240**: p. 46-55.

112. Aghaei, J., et al., *Contribution of emergency demand response programs in power system reliability.* Energy, 2016. **103**: p. 688-696.

113. Babahajiani, P., Q. Shafiee, and H. Bevrani, *Intelligent demand response contribution in frequency control of multi-area power systems.* IEEE Transactions on Smart Grid, 2016. **9**(2): p. 1282-1291.

114. Marahatta, A., et al., *Priority-based low voltage DC microgrid system for rural electrification.* Energy Reports, 2021. **7**: p. 43-51.

115. Behera, A., T.K. Panigrahi, and A.K. Sahoo, *A FO-PID Controlled Automatic Generation Control of Multi Area Power Systems Tuned by Harmony Search.* Recent Advances in Electrical & Electronic Engineering (Formerly Recent Patents on Electrical & Electronic Engineering), 2020. **13**(1): p. 101-109.

116. Tripathy, S., P.C. NAIR, and N. Rao, *Automatic generation control with superconducting magnetic energy storage in power system.* Electric machines and power systems, 1994. **22**(3): p. 317-338.

117. Khamari, D., et al., *Automatic generation control of power system in deregulated environment using hybrid TLBO and pattern search technique.* Ain Shams Engineering Journal, 2019.

118. Zeynelgil, H., A. Demiroren, and N. Sengor, *The application of ANN technique to automatic generation control for multi-area power system.* International journal of electrical power & energy systems, 2002. **24**(5): p. 345-354.

119. Xi, L., et al., *A novel automatic generation control method based on the ecological population cooperative control for the islanded smart grid.* Complexity, 2018. **2018**.

120. Ramakrishna, K. and T. Bhatti, *Automatic generation control of single area power system with multi-source power generation.* Proceedings of the Institution of Mechanical Engineers, Part A: Journal of Power and Energy, 2008. **222**(1): p. 1-11.

121. Sahu, R.K., S. Panda, and S. Padhan, *A hybrid firefly algorithm and pattern search technique for automatic generation control of multi area power systems.* International Journal of Electrical Power & Energy Systems, 2015. **64**: p. 9-23.

122. Cui, M., et al., *Deep Learning-Based Time-Varying Parameter Identification for System-Wide Load Modeling.* IEEE Transactions on Smart Grid, 2019. **10**(6): p. 6102-6114.

123. Kiaei, I. and S. Lotfifard, *Tube-based model predictive control of energy storage systems for enhancing transient stability of power systems.* IEEE Transactions on Smart Grid, 2017. **9**(6): p. 6438-6447.

124. Ersdal, A.M., et al., *Model predictive control for power system frequency control taking into account imbalance uncertainty.* IFAC Proceedings Volumes, 2014. **47**(3): p. 981-986.

125. Ball, S., *Neural Network Predictive Control Applied to Power System Stability*, in *Intelligent Systems Design and Applications*. 2003, Springer. p. 43-51.

126. Venkatesh, C., et al. *Flatness based TCSC controller for transient stability enhancement of power system*. in *2010 Modern Electric Power Systems*. 2010. IEEE.

127. Sun, J., et al., *Energy function-based model predictive control with UPFCs for relieving power system dynamic current violation.* IEEE Transactions on Smart Grid, 2016. **7**(6): p. 2933-2942.

128. Ngamroo, I. and S. Vachirasricirikul, *Coordinated control of optimized SFCL and SMES for improvement of power system transient stability.* IEEE transactions on applied superconductivity, 2011. **22**(3): p. 5600805-5600805.

129. Fuchs, A., et al., *Stabilization of large power systems using VSC–HVDC and model predictive control.* IEEE Transactions on Power Delivery, 2013. **29**(1): p. 480-488.

130. Falahi, M., et al., *Dynamic model predictive-based energy management of DG integrated distribution systems.* IEEE Transactions on Power Delivery, 2013. **28**(4): p. 2217-2227.

131. Bonfiglio, A., et al. *Improving power grids transient stability via model predictive control*. in *2014 Power Systems Computation Conference*. 2014. IEEE.

132. Short, J.A., D.G. Infield, and L.L. Freris, *Stabilization of grid frequency through dynamic demand control.* IEEE Transactions on power systems, 2007. **22**(3): p. 1284-1293.

133. Zhu, Q., et al., *Robust load frequency control with dynamic demand response for deregulated power systems considering communication delays.* Electric Power Components and Systems, 2017. **45**(1): p. 75-87.

134. Shi, Q., et al., *Thermostatic load control for system frequency regulation considering daily demand profile and progressive recovery.* IEEE Transactions on Smart Grid, 2019. **10**(6): p. 6259-6270.

135. Shi, Q., et al., *A hybrid dynamic demand control strategy for power system frequency regulation.* CSEE Journal of Power and Energy Systems, 2017. **3**(2): p. 176-185.

136. Mohsenian-Rad, A.-H., et al., *Autonomous demand-side management based on game-theoretic energy consumption scheduling for the future smart grid.* IEEE transactions on Smart Grid, 2010. **1**(3): p. 320-331.

137. Tchuisseu, E.T., et al., *Effects of dynamic-demand-control appliances on the power grid frequency.* Physical Review E, 2017. **96**(2): p. 022302.

138. Cheng, Y., et al., *Smart frequency control in low inertia energy systems based on frequency response techniques: A review.* Applied Energy, 2020. **279**: p. 115798.

139. Kosmecki, M., et al., *A Methodology for Provision of Frequency Stability in Operation Planning of Low Inertia Power Systems.* Energies, 2021. **14**(3): p. 737.

140. Martinez Romero, S., et al., *Grid Integration Requirements for Variable Renewable Energy*. 2019, The World Bank.

141. Huang, L., et al., *Grid-synchronization stability analysis and loop shaping for PLL-based power converters with different reactive power control.* IEEE Transactions on Smart Grid, 2019. **11**(1): p. 501-516.

142. Gu, Y. and L. Xie, *Early detection and optimal corrective measures of power system insecurity in enhanced look-ahead dispatch.* IEEE Transactions on Power Systems, 2012. **28**(2): p. 1297-1307.

143. Gu, Y. and L. Xie, *Stochastic look-ahead economic dispatch with variable generation resources.* IEEE Transactions on Power Systems, 2016. **32**(1): p. 17-29.

144. Tang, C., et al., *Look-ahead economic dispatch with adjustable confidence interval based on a truncated versatile distribution model for wind power.* IEEE Transactions on Power Systems, 2017. **33**(2): p. 1755-1767.

145. Xie, L., et al., *Short-term spatio-temporal wind power forecast in robust look-ahead power system dispatch.* IEEE Transactions on Smart Grid, 2013. **5**(1): p. 511-520.

146. Bevrani, H., *Robust power system frequency control*. Vol. 85. 2009: Springer.

147. Hatziargyriou, N., et al., *Stability definitions and characterization of dynamic behavior in systems with high penetration of power electronic interfaced technologies.* 2020.

148. Peng, Q., et al., *On the stability of power electronics-dominated systems: Challenges and potential solutions.* IEEE Transactions on Industry Applications, 2019. **55**(6): p. 7657-7670.

149. Hatziargyriou, N., et al., *Definition and Classification of Power System Stability Revisited & Extended.* IEEE Transactions on Power Systems, 2020.

150. Ananthapadmanabha, T., et al., *Rotor angle stability analysis of a distributed generator connected to distribution network.* Journal of Electrical and Electronics Engineering Research, 2010. **2**(5): p. 107-113.

151. Vittal, E., M. O'Malley, and A. Keane, *Rotor angle stability with high penetrations of wind generation.* IEEE transactions on Power Systems, 2011. **27**(1): p. 353-362.

152. Tielens, P., *Operation and control of power systems with low synchronous inertia*, in *Faculty of Engineering Science*. 2017, KU Leuven: Belgium.

153. Gonzalez-Longatt, F., *Ctitical Fault Clearing Transmission Line*. 2021: github.

154. Gonzalez-Longatt, F., *Critical Fault Clearing Bus*. 2021: github.

155. Athay, T., R. Podmore, and S. Virmani, *A practical method for the direct analysis of transient stability.* IEEE Transactions on Power Apparatus and Systems, 1979(2): p. 573-584.

156. Gonzalez-Longatt, F., *Introduction to Power Systems* 2019.

157. Hamon, C., M. Perninge, and L. Soder, *Frequency Control: Operation of Frequency Control Schemes in Power Systems with Large Amounts of Wind Power*. 2016, Energiforsk.

158. ESO, *Grid Code (GC)*, Ofgem, Editor., nationalgridESO.

159. Group, N.G., *The Grid Code Issues 5 Revision 21*. 2017, National Grid Electricity Transmission

160. Luo, X., et al., *Review of voltage and frequency grid code specifications for electrical energy storage applications.* Energies, 2018. **11**(5): p. 1070.

161. Cobben, S., B. Gaiddon, and H. Laukamp, *Impact of Photovoltaic Generation on Power Quality in Urban areas with High PV Population: Results from Monitoring Campaigns.* Intelligent Energy Europe, Brussels, Tech, Rep. EIE/05/171/SI2, 2008. **420208**.

162. Hirth, L. and I. Ziegenhagen, *Control power and variable renewables: A glimpse at German data.* 2013.

163. *Electricity Transmission*, A.E. Regulator, Editor. 2009, Australian Government Australia.

164. Operator, A.E.M., *Black system south australia 28 september 2016.* Report of the Australian Energy Market Operator Limited (AEMO), 2017.

165. Warren, M. *South Australia's blackouts: It's not black or white*. 2017 09/16/2020]; Available from: https://www.energycouncil.com.au/analysis/south-australias-blackouts-not-as-simple-as-it-looks/.

166. Christiansen, W. and D.T. Johnsen, *Analysis of requirements in selected Grid Codes.* Prepared for Orsted-DTU Section of Electric Power Engineering, Technical University of Denmark (DTU), 2006.

167. Cha, S.-T., Q. Wu, and J. Østergaard. *Frequency Stabilizing Scheme for a Danish Island Grid*. in *3rd IEEE PES Innovative Smart Grid Technologies (ISGT) Europe Conference (IEEE PES ISGT Europe 2012)*. 2012. IEEE.

168. Møller Andersen, F., et al., *Analyses of demand response in Denmark*. 2006, Risoe National Lab.

169. *DL T 1040-2007 Grid Operation Guidelines*. 2007, DOC88: China.

170. Handbook, U.O., *Appendix 1: Load-frequency-control and performance.* UCTE Brussels, Belgium, 2004.

171. Lazarev, G., V. Hrustalyov, and M. Garievskij, *1. Non-baseload Operation in Nuclear Power Plants: Load Following and Frequency Control Modes of Flexible Operation.* Nuclear Energy Series, 2018: p. 173.

172. Pandurangan, V., H. Zareipour, and O. Malik. *Frequency regulation services: A comparative study of select North American and European reserve markets*. in *2012 North American Power Symposium (NAPS)*. 2012. IEEE.

173. Undrill, J., *Notes of Frequency Control for the Australian Energy Market Operator*. 2019, Australian Energy Market Commission: Australia.

174. Oshnoei, A., et al., *On the contribution of wind farms in automatic generation control: Review and new control approach.* Applied Sciences, 2018. **8**(10): p. 1848.

175. Tarnowski, G.C., *Coordinated frequency control of wind turbines in power systems with high wind power penetration*. 2012: Technical University of Denmark (DTU).

176. Weckx, S., R. D'hulst, and J. Driesen, *Primary and secondary frequency support by a multi-agent demand control system.* IEEE Transactions on Power Systems, 2014. **30**(3): p. 1394-1404.

177. Committee, P.b.N.R., *Balancing and frequency control: A technical document prepared by the NERC resources subcommittee*. 2011, NERC Technical Report.

178. Perninge, M. and R. Eriksson, *Optimal tertiary frequency control in power systems with market-based regulation.* IFAC-PapersOnLine, 2017. **50**(1): p. 4374-4381.

179. Force, S.T., *Primary Frequency Response Stakeholder Education Part 1 of 2*. 2017, PJM.

180. Hodge, B.M.S., et al., *Addressing technical challenges in 100% variable inverter -based renewable energy power systems.* Wiley Interdisciplinary Reviews: Energy and Environment, 2020: p. e376.

181. Alani, A.Y. and I.O. Osunmakinde, *Short-term multiple forecasting of electric energy loads for sustainable demand planning in smart grids for smart homes.* Sustainability, 2017. **9**(11): p. 1972.

182. Remon, D., et al., *Power system stability analysis under increasing penetration of photovoltaic power plants with synchronous power controllers.* IET Renewable Power Generation, 2017. **11**(6): p. 733-741.

183. Peters, D., et al., *Solar short-term forecasts for predictive control of battery storage capacities in remote PV diesel networks*, in *Transition Towards 100% Renewable Energy*. 2018, Springer. p. 325-333.

184. Xu, Y., et al., *Assessing short-term voltage stability of electric power systems by a hierarchical intelligent system.* IEEE transactions on neural networks and learning systems, 2015. **27**(8): p. 1686-1696.

185. Wang, J., et al., *A short-term photovoltaic power prediction model based on the gradient boost decision tree.* Applied Sciences, 2018. **8**(5): p. 689.

186. Du, P., et al., *A novel hybrid model for short-term wind power forecasting.* Applied Soft Computing, 2019. **80**: p. 93-106.

187. Barbounis, T.G., et al., *Long-term wind speed and power forecasting using local recurrent neural network models.* IEEE Transactions on Energy Conversion, 2006. **21**(1): p. 273-284.

188. Negnevitsky, M., D.H. Nguyen, and M. Piekutowski, *Risk assessment for power system operation planning with high wind power penetration.* IEEE Transactions on Power Systems, 2014. **30**(3): p. 1359-1368.

189. Tielens, P., P. Henneaux, and S. Cole, *Penetration of renewables and reduction of synchronous inertia in the European power system-Analysis and solutions.* 2018.

190. Shrestha, A., B. Ghimire, and F. Gonzalez-Longatt, *A Bayesian Model to Forecast the Time Series Kinetic Energy Data for a Power System.* Energies, 2021. **14**(11): p. 3299.

191. Ulbig, A., T.S. Borsche, and G. Andersson, *Impact of low rotational inertia on power system stability and operation.* IFAC Proceedings Volumes, 2014. **47**(3): p. 7290-7297.

192. Zografos, D., *Power System Inertia Estimation and Frequency Response Assessment*. 2019, KTH Royal Institute of Technology: Stockholm, Sweden.

193. Kundur, P., et al., *Definition and classification of power system stability IEEE/CIGRE joint task force on stability terms and definitions.* IEEE transactions on Power Systems, 2004. **19**(3): p. 1387-1401.

194. Kundur, P., N.J. Balu, and M.G. Lauby, *Power system stability and control*. Vol. 7. 1994: McGraw-hill New York.

195. Mitra, A. and D. Chatterjee, *Active power control of DFIG-based wind farm for improvement of transient stability of power systems.* IEEE Transactions on power systems, 2015. **31**(1): p. 82-93.

196. Munkhchuluun, E., L. Meegahapola, and A. Vahidnia. *The Large Disturbance Rotor Angle Stability with DFIG Wind Farms*. in *2019 9th International Conference on Power and Energy Systems (ICPES)*. 2019. IEEE.

197. Mansouri, N., et al., *Large photovoltaic power plants integration: A review of challenges and solutions.* Energies, 2019. **12**(19): p. 3798.

198. Mondal, D., A. Chakrabarti, and A. Sengupta, *Power system small signal stability analysis and control*. 2020: Academic Press.

199. Ma, J., *Power system wide-area stability analysis and control*. 2018: John Wiley & Sons.

200. Ramasubramanian, D., et al., *Asking for fast terminal voltage control in grid following plants could provide benefits of grid forming behavior.* IET Generation, Transmission & Distribution, 2023. **17**(2): p. 411-426.

201. Kabir, M.N., et al., *Coordinated control of grid-connected photovoltaic reactive power and battery energy storage systems to improve the voltage profile of a residential distribution feeder.* IEEE Transactions on industrial Informatics, 2014. **10**(2): p. 967-977.

202. Safayet, A., P. Fajri, and I. Husain, *Reactive power management for overvoltage prevention at high PV penetration in a low-voltage distribution system.* IEEE transactions on industry applications, 2017. **53**(6): p. 5786-5794.

203. Fedayi, H., et al., *BESS based voltage stability improvement enhancing the optimal control of real and reactive power compensation.* AIMS Energy, 2022. **10**(3): p. 535-552.

204. Hosseinzadeh, N., et al., *Voltage stability of power systems with renewable-energy inverter-based generators: A review.* Electronics, 2021. **10**(2): p. 115.

205. Denholm, P., et al., *The challenges of achieving a 100% renewable electricity system in the United States.* Joule, 2021. **5**(6): p. 1331-1352.

206. Wang, X. and F. Blaabjerg, *Harmonic stability in power electronic-based power systems: Concept, modeling, and analysis.* IEEE Transactions on Smart Grid, 2018. **10**(3): p. 2858-2870.

207. Hatziargyriou, N., et al., *Definition and classification of power system stability–revisited & extended.* IEEE Transactions on Power Systems, 2020. **36**(4): p. 3271-3281.

208. Wang, X., F. Blaabjerg, and W. Wu, *Modeling and analysis of harmonic stability in an AC power-electronics-based power system.* IEEE transactions on power electronics, 2014. **29**(12): p. 6421-6432.

209. Ebrahimzadeh, E., et al., *Harmonic stability and resonance analysis in large PMSG-based wind power plants.* IEEE Transactions on Sustainable Energy, 2017. **9**(1): p. 12-23.

210. Wang, X., et al., *An active damper for stabilizing power-electronics-based AC systems.* IEEE Transactions on Power Electronics, 2013. **29**(7): p. 3318-3329.

211. Liserre, M., F. Blaabjerg, and S. Hansen, *Design and Control of an LCL-Based Three-Phase Active Rectifier.* IEEE Transactions on Industry Applications. **41**(5).

212. Shu, D., et al., *Sub-and super-synchronous interactions between STATCOMs and weak AC/DC transmissions with series compensations.* IEEE Transactions on Power Electronics, 2017. **33**(9): p. 7424-7437.

213. Ierna, R., et al. *Effects of VSM convertor control on penetration limits of non-synchronous generation in the GB power system.* in *15th Wind Integration Workshop.* 2016.

214. Milano, F., et al. *Foundations and challenges of low-inertia systems.* in *2018 power systems computation conference (PSCC).* 2018. IEEE.

215. Kunjumuhammed, L.P., et al., *Electrical oscillations in wind farm systems: Analysis and insight based on detailed modeling.* IEEE Transactions on Sustainable Energy, 2015. **7**(1): p. 51-62.

216. Yu, M., et al. *Use of an inertia-less virtual synchronous machine within future power networks with high penetrations of converters.* in *2016 Power Systems Computation Conference (PSCC).* 2016. IEEE.

217. Fan, L., *Modeling type-4 wind in weak grids.* IEEE Transactions on sustainable energy, 2018. **10**(2): p. 853-864.

218. Papangelis, L., et al. *Stability of a voltage source converter subject to decrease of short-circuit capacity: A case study*. in *2018 Power Systems Computation Conference (PSCC)*. 2018. IEEE.

219. Ramasubramanian, D., et al., *Positive sequence voltage source converter mathematical model for use in low short circuit systems.* IET Generation, Transmission & Distribution, 2020. **14**(1): p. 87-97.

220. Group, I.S.R.W., *Terms, definitions and symbols for subsynchronous oscillations.* IEEE Transactions on Power Apparatus and Systems, 1985. **104**(6): p. 1326-1334.

221. Pourbeik, P., et al., *Vulnerability of large steam turbine generators to torsional interactions during electrical grid disturbances.* IEEE Transactions on power systems, 2007. **22**(3): p. 1250-1258.

222. Pourbeik, P., A. Bostrom, and B. Ray, *Modeling and application studies for a modern static VAr system installation.* IEEE Transactions on Power Delivery, 2005. **21**(1): p. 368-377.

223. Pourbeik, P., et al. *Integration of large wind farms into utility grids (part 2-performance issues)*. in *2003 IEEE Power Engineering Society General Meeting (IEEE Cat. No. 03CH37491)*. 2003. IEEE.

224. Ermis, M., et al., *Self-excitation of induction motors compensated by permanently connected capacitors and recommendations for IEEE std 141-1993.* IEEE Transactions on Industry Applications, 2003. **39**(2): p. 313-324.

225. Larsen, E.V. *Wind generators and series-compensated AC transmission lines*. in *PES T&D 2012*. 2012. IEEE.

226. FINGRID, *Kinetic energy of the Nordic power system- real time data*. 2019.

227. Joyce, J., *Bayes' theorem.* 2003.

228. Efron, B., *Bayes' theorem in the 21st century.* Science, 2013. **340**(6137): p. 1177-1178.

229. Carpenter, B., et al., *Stan: a probabilistic programming language.* Grantee Submission, 2017. **76**(1): p. 1-32.

230. Nocedal, J. and S. Wright, *Numerical optimization*. 2006: Springer Science & Business Media.

231. Nishida, K., *Introduction to Exploratory v6.0*. 2020, Exploratory.

232. Shrestha, A., Y. Rajbhandari, and F. Gonzalez-Longatt, *Day-ahead energy-mix proportion for the secure operation of renewable energy-dominated power system.* International Journal of Electrical Power and Energy Systems, 2024. **155**(109560).

233. Anderson, P.M. and A.A. Fouad, *Power system control and stability*. 2008: John Wiley & Sons.

234. Gibbard, M. and D. Vowles, *IEEE PES task force on benchmark systems for stability controls simplified 14-generator model of the south east Australian power system.* The University of Adelaide, South Australia, 2014.

235. Poolla, B.K., D. Groß, and F. Dörfler, *Placement and implementation of grid-forming and grid-following virtual inertia and fast frequency response.* IEEE Transactions on Power Systems, 2019. **34**(4): p. 3035-3046.

236. Ånund, K., *European Hydropower Capacity – A Study of the Correlation Between the Scandinavian and the Alps Hydropower System*, in *Hydropower'05 - The Backbone of sustainable Energy Supply*. 2005: Stavanger, Norway.

237. EU, E., *River Flow- Projected change in seasonal streamflow for twelve rivers*, E.E. Agency, Editor.

238. ZACH. *How to Normalize Data Between 0 and 100*. 2020; Available from: https://www.statology.org/normalize-data-between-0-and-100/.

239. EirGrid, S., *System non-synchronous penetration definition and formulation*. 2018, Transmission System Operator: Ireland.

240. Staudemeyer, R.C. and E.R. Morris, *Understanding LSTM--a tutorial into long short-term memory recurrent neural networks.* arXiv preprint arXiv:1909.09586, 2019.

241. MATLAB, *Deep Learning Using Bayesian Optimization*. MathWorks/ MATLAB.

242. Ma, Y., et al., *Adaptive Elastic Training for Sparse Deep Learning on Heterogeneous Multi-GPU Servers.* arXiv preprint arXiv:2110.07029, 2021.

243. AEMO, *NEM Engineering Framework*. 2021, Australian Energy Market Operator.

244. Murphy, G., et al., *Real time fault level monitoring.* 2019.

245. Matignon, L., G.J. Laurent, and N. Le Fort-Piat, *Independent reinforcement learners in cooperative markov games: a survey regarding coordination problems.* The Knowledge Engineering Review, 2012. **27**(1): p. 1-31.

246. Gheisarnejad, M., H. Farsizadeh, and M.H. Khooban, *A novel non-linear deep reinforcement learning controller for DC/DC power buck converters.* IEEE Transactions on Industrial Electronics, 2020.

247. Cui, C., N. Yan, and C. Zhang, *An Intelligent Control Strategy for buck DC-DC Converter via Deep Reinforcement Learning.* arXiv preprint arXiv:2008.04542, 2020.

248. Sri, A. *Everything you need to know about Reinforcement Learning in 80 minutes*. 2022.

249. Pan, L., et al., *Reinforcement learning with dynamic boltzmann softmax updates.* arXiv preprint arXiv:1903.05926, 2019.

250. Hong, Z.-W., et al., *A deep policy inference q-network for multi-agent systems.* arXiv preprint arXiv:1712.07893, 2017.

251. Schaul, T., et al., *Prioritized experience replay.* arXiv preprint arXiv:1511.05952, 2015.

252. Dabney, W., et al. *Distributional reinforcement learning with quantile regression*. in *Proceedings of the AAAI Conference on Artificial Intelligence*. 2018.

253. Arulkumaran, K., et al., *A brief survey of deep reinforcement learning.* arXiv preprint arXiv:1708.05866, 2017.

Attachments

Article 1

Shrestha, A., Mohammed A.M. Y., Sharma, B. and Gonzalez-Longatt, F. A narrative review highlighting challenges and opportunities for making 100% renewable grid. [Submitted, Renewable and Sustainable Energy Reviews]

Not available in digital version

Article 2

Review

Frequency Stability Issues and Research Opportunities in Converter Dominated Power System

Ashish Shrestha *◉ and Francisco Gonzalez-Longatt *◉

Department of Electrical Engineering, Information Technology and Cybernetics,
University of South-Eastern Norway, N-3918 Porsgrunn, Norway
* Correspondence: sthashish2010@gmail.com (A.S.); fglongatt@fglongatt.org (F.G.-L.)

Abstract: Stable power supply has become a crucial thing in the current era of technology and automation. Although the power system has multiple stability issues and causes, frequency fluctuation plays a vital role in normal operation, whereby a system with significant frequency deviation can lead to the needless blackouts of the whole power system. With the rapid growth in power electronic converter (PEC)-based technologies and the huge penetration of nonsynchronous generators, the modern power system is becoming more complex by the day. This paper provides a comprehensive study on the stability issues that occur in modern power systems, mainly due to PEC-based technology integration. The in-depth reasons and the impacts of unstable power systems, along with their controlling techniques, are discussed to generate a clear understanding. Furthermore, the importance of frequency stability in a power system is discussed with respect to some important events that occurred in the past. This paper also discusses some potential techniques that could be performed to overcome the existing and/or upcoming challenges in the upgrading power system.

Keywords: low inertia; power electronic converter (PEC)-based technologies; power system stability

1. Introduction

Energy generation from renewable energy sources (RESs) leads to numerous benefits for the environmental, financial, technological, social, health, and other sectors. The penetration of RESs can help to reduce the greenhouse emissions generated from thermal power plants and, hence, most countries have developed policies to enhance the implementation of renewable energy by integrating a new form of RESs into the national/international grid system [1]. However, there are numerous challenges in RESs such as high cost, low reliability, poor power quality, and problems in maintenance and monitoring activities [2]. Because of the periodic nature and dependency on weather and environmental factors, the characteristics of the energy generated from RESs such as solar and wind energy are unreliable and unpredictable, resulting in unstable conditions of the main power system [3]. The disturbances created by the unpredictable generation of power from these resources have become an issue in the current power system, and power system developers are in a transition phase to penetrate a significant portion of RESs into the main grid [4,5]. In addition, these resources contain PECs as the fundamental units, which lead to stability issues in the power system. If the system is not modified, having a significant proportion of RESs and PECs means a vulnerable and unsustainable system, which will significantly affect the operation of the power system [6].

Figure 1 presents a classification of the stability issues that occur in electrical power systems. In conventional definitions, there are three types of stability issues: (a) rotor angle instability, (b) frequency instability, and (c) voltage instability. Among these three stability issues, rotor angle stability plays an essential role in system synchronization, which should be resolved within 3 to 10 s for a transient state and 10–20 s for a steady state, and this is, thus, considered a short-term stability problem [7]. This problem can be adequately solved via the application of power system stabilizers (PSS) or PEC-based exciters, and it can be

prevented through generator tripping. Similarly, frequency stability indicates the power system's ability to maintain its operating frequency within an acceptable range, whereby instability can occur because of supply/demand unbalance. It takes a few seconds to several minutes for restoration, and this is considered a short-term and/or long-term stability problem. On the other hand, the voltage stability of a power system plays a vital role in maintaining the receiving end voltage within an acceptable range; it takes a few seconds to several minutes for restoration, and this is, thus, considered a short-term and/or long-term stability problem [7]. For short-term voltage stability, automatic voltage regulators (AVR), excitation systems, and induction motors can be used, whereas HVDC interconnections, adjustable tap transformers, and generator excitation current limiters can be used for long-term voltage stability restoration. However, modern power systems contain a considerable number of PEC-based technologies, and they have undergone significant transformation in the last decade; hence, new elements have been introduced in terms of power system stability: (a) converter driven stability and (b) resonance stability [8–11]. Converter-driven stability concerns the oscillation within a power system because of the cross-coupling phenomenon between dynamic electromechanical devices and the transient nature of electromagnetic grid networks [11]. On the other hand, resonance stability takes into account periodic and insufficient energy dissipation within a system, resulting in a form of oscillation [10].
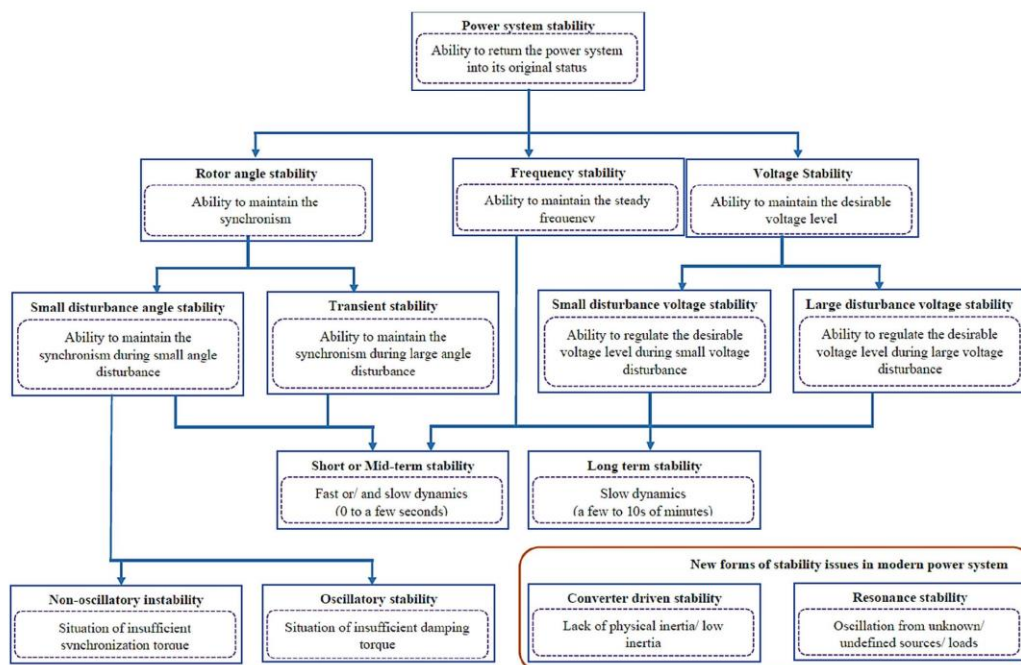

Figure 1. Power system stability classification.

A power system with RES integration can become unstable for two main reasons: (a) the high penetration of PEC-based energy resources such as solar PV and wind turbine reducing the system inertia; (b) RESs being unable to balance the demand/supply chain because of their unpredictable patterns [12–14]. Predicting the time-series value of the demand and generation is very complex and slow; thus, systems can achieve stability by solely focusing on the demand. The high penetration of nonsynchronous generators

with PECs reduces system inertia and increases the potential of unstable frequency in a power system. Frequency fluctuation plays a vital role in normal operation, whereby a system with comparatively low inertia can lead to needless blackouts of the power system [15]. A drop in system inertia leads to a significant rise in RoCoF and increases the value of nadir frequency. However, most power systems contain protection equipment with conventional operation settings, which need to be upgraded following the massive integration of PEC-based technologies [16]. Several research and development activities have been conducted on voltage stability, rotor angle stability, and frequency control methods. However, limited research activities have considered real-time stability control, despite them being the primary reason behind the numerous blackouts recorded in the last few years [17].

With the introduction of new concepts (i.e., PEC-based technologies) and policies, operation is becoming more complex; hence, some technoeconomic approaches and technologies have to be identified that guarantee the secure and reliable operation of the power system. Several research works have tried to address the issues by proposing various concepts. However, a complex framework in which neglects potential uncertainties may lead to impractical results, with problems arising during the real-world implementation of the proposed method [18,19]. Hence, a detailed study on unique and practical methods should be conducted to overcome the existing and/or upcoming challenges in upgrading the power system structure and operation approaches.

The aim of this paper was to present comprehensive information on the stability issues in modern power systems as a result of the high penetration of PEC-based technologies and unpredictable RESs such as solar and wind energy. Furthermore, the objective of this article was to provide a detailed survey on frequency stability issues and their potential solutions via published scientific documents. This paper first introduces the background and a basic overview of the stability problems faced by modern power systems. Section 2 presents an overview of the comprehensive works conducted previously by various researchers and institutions. Section 3 covers the frequency stability concepts in depth, along with their response, regulations, control approaches, and impact on the power system. Some case studies are discussed to analyze the importance of frequency stability in modern power systems. The most important topic of this article (i.e., frequency stability in PEC-based power systems) is discussed in Section 4. The issues of short-term frequency instability and the challenges caused by PEC-based technologies in power systems are discussed in detail. Furthermore, potential solutions are discussed. Lastly, in Section 5, conclusions are drawn and discussed.

2. Previous Studies

Modern power systems are more focused on technoeconomic operation, along with environmental constraints. To improve the operational constraints, the regulatory body can replace the control system with an optimized approach and/or include an optimized supervisory system without modification in the main system [20]. The inclusion of a new control system may become expensive, since the existing system has to be replaced, whereas the second approach is quite popular and practical in rapidly growing systems. However, with the increasing trend of RES integration and PEC-based technologies, existing power systems face new challenges such as unbalanced frequency resilience and low grid inertia [21]; hence, tools need to be introduced that dynamically monitor, analyze, improve, and visualize the system characteristics [22]. It is clear that conventional control technologies are not appropriate for modern power systems; thus, a new way of thinking is necessary [23].

The concept of battery energy storage systems (BESSs) was used to regulate the frequency of a power system in [24,25]. In [26], a self-tuning PID controller was indigested to increase transient stability by using fuzzy logic and thyristor-controlled series compensation (TCSC). Similarly, in [27], a controller was proposed using fuzzy logic and a neural network. Compensators such as static VAR compensators (SVCs) and static compensators

(STATCOMs) have been used to improve the first swing stability of power systems via a discontinuous control strategy [28,29]. A controller was discussed for the improvement of transient stability through the extraction of a synchronous generator in [30]. Teng et al. introduced the concept of EV integration to improve the frequency response of the Great Britain power system [31], while Liu et al. presented the effects on secondary frequency control via EV integration [32]. Integrating EVs as a distributed energy resource (DER) is highly adopted in modern power systems to improve the frequency quality. Similarly, some studies have presented the application of demand-side management (DSM) in power system security [33–35]. Likewise, various techniques have been proposed and investigated to address the stability issues that occur in PEC-based power systems. Figure 2 presents the classification of frequency control techniques.
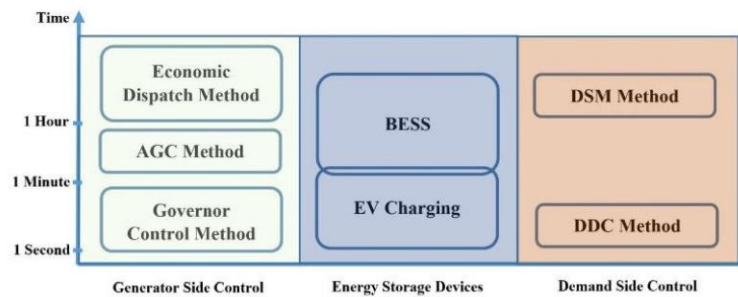

Figure 2. General techniques for regulating frequency in RES-based power systems.

Numerous researches have presented automatic generation control (AGC) as a traditional method to regulate power systems. Usually, the frequency of a system is monitored, whereas the AGC maintains regulation by varying the rate of generation. Behera et al. adopted the harmony search (HS) algorithm as the optimization tool and integral square time square error (ISTSE) as the objective function to identify the best parameters in the controller [36]. AGC was implemented using superconducting magnetic energy storage (SMES) to analyze the performance of both the controller and the power system in [37]. The authors optimized the controller parameters for system stability by using the second law of Lyapunov. In [38], the authors suggested a combined approach using a tilted integral derivative (TID) controller and teaching/learning-based optimization and pattern search (hTLBO-PS) as a new AGC method under a deregulated environment. In [39], an ecological population cooperative control (EPCC) strategy was proposed as an AGC for an islanded smart grid. The authors used the concept of a multiagent system stochastic consensus game (MAS-SCG) to determine the optimal power command for controlling the isolated grid in an optimal cooperative mode. Ramakrishna et al. conducted a detailed transient analysis for individual AGC within a multisource power system [40]. Similarly, an artificial neural network (ANN) was applied to analyze AGC problems in [41]. In [42], the parameter-plane approach was applied to identify the optimal controller parameters, and a sensitivity analysis was carried out to examine stability via AGC. Similarly, in [43], a hybrid technique was proposed for AGC of multiarea power systems by combining the firefly algorithm and pattern search method. As shown in Figure 2, AGC is a general technique that regulates system frequency by controlling the generator-side parameters. Although it works as a secondary response and takes a few minutes, it is considered a fundamental method for the frequency regulation of power systems.

Model predictive control (MPC) is another popular method. Cui et al. proposed a multimodal long short-term memory (M-LSTM) deep learning approach to determine the time-varying variables of composite load modeling (CLM) for a system-wide load study [44]. Similarly, a time-varying model was proposed to identify the parameters for CLM in [45]. A time-varying model was presented to measure the penetration level of

solar PV in a distribution system in [46]. A method based on MPC was developed to enhance the transient stability of a power system using superconducting magnetic energy storage (SMEA) units [47]. In [48], an approach was presented to determine the real-time system's scheme and regulate the voltage within a limit. Ersdal et al. investigated an MPC-based control method to regulate frequency in a wind-energy-integrated power system by considering three different disturbances: positive, negative, and neutral [49]. A hybrid control system consisting of the MPC method and a neural network was studied to improve the stability of a power system in [50]. A combination of feedback linearization and MPC approaches was used to control the firing angle of a thyristor to improve the transient stability of a system through the regulation of TCSC reactance [51]. Furthermore, the concept of transient energy function (TEF) was combined with MPC to obtain multiple unified power flow controllers (UPFCs), thereby improving system stability [52]. In [20], the authors presented a controlling approach by utilizing the secondary frequency of the power system, whereby a hierarchical-based MPC was used to regulate the primary and secondary frequency. Gomez et al. proposed the concept of a distributed MPC, in which the droop and transferred power were taken as the input parameters to control the frequency and voltage of the microgrid system [53]. Similarly, MPC has been implemented in diverse applications such as to control the TCSC for the enhancement of transient stability [54], to damp out the oscillated power in an HVDC system [55], to manage the distributed generated energy [56], and to stabilize the grid after a contingency [23]. As with other techniques, the important feature of MPC is its plug-and-play structure, facilitating redesign and theoretical evaluation of the structure of a controller. In previous research works, the MPC concept was widely used in the regulation of power systems, especially in terms of frequency stability.

Similarly, various researches presented the dynamic demand control (DDC) approach for regulating the grid frequency. Shrot et al. proposed this concept as a new technique for frequency stabilization in 2007 [57]. Shi et al. presented a comprehensive review of DDC along, with an algorithm and a future vision for system frequency regulation [58]. This study also discussed the various technical and practical factors that play an essential role in the implementation of a DDC approach. Since the individual load is stochastic, and the power system contains a massive number of loads, the adopted approach must identify the predictable pattern for all loads, as well as their generation, and it must provide an appropriate control step to maintain the regulation [58]. On the other hand, Zhu et al. investigated robust load frequency control (RLFC) along with DDC for the regulation of power systems via communication networks [59]. The authors used communication networks in load frequency control (LFC) together with DDC in demand-side response (DSR) to aggregate the well-regulated loads. Qingxin et al. proposed a thermostatic load control (TLC) strategy, a form of DDC, in which thermostatic loads were used, i.e., heating, ventilation, and air-conditioning (HVAC) units and electric water heaters (EWHs) [60]. A hybrid DDC concept was introduced to provide a rapid and steady regulation of primary and secondary frequency in [61], by replacing the generator reserves. A D-partition method-based LFC approach was proposed for DGs by implementing a PI controller using the conventional Ziegler–Nichols method [62]. A detailed study on the effects of DDC on the frequency was presented in [63], in which it was observed that DDC can minimize the variance (around 30–40%) of the fluctuation. However, in the DDC method, the randomization of each iteration is necessary to minimize the oscillatory instabilities of the frequency [57,64]. As with other conventional techniques, DDC is adopted for its fast response, flexible operation, and economic efficiency.

3. Frequency Stability in Power Systems

To operate a power system in a reliable and efficient manner, different parameters must be within an acceptable limit. Among the numerous parameters, stable frequency is one that plays an essential role in the proper operation of a power system. Basically, the frequency of a system should be maintained within an acceptable range, thereby preventing

issues such as the total generation capacity trying to balance the total load. However, both generation and demand change dynamically, which may lead to an imbalance between the total generation and total demand within that system for an instant of time. This imbalance creates a frequency deviation. If the deviation is within an acceptable range, there will be no significant impact; however, if it crosses a certain threshold, it will affect the power system's operation, reliability, efficiency, and security, as well as degrade load performance, overload transmission lines, and lead to protection failures [7].

Mathematically, frequency fluctuation occurs when the supply/demand balance within a system deviates from the norm (i.e., $P_M(t) \neq P_L(t)$). Here, $P_M(t)$ is the mechanical power/generated power, and $P_L(t)$ is the electrical load at an instant of time. Basically, the system frequency is directly proportional to the generator's speed; the system's frequency increases with an increase in rotor speed and vice versa. When the system demand increases, the speed of the rotor decreases slowly, and similar results occur in the case of frequency (i.e., $P_M(t) < P_L(t)$). Similarly, the rotor speed and the frequency increase with a decrease in order of the system load (i.e., $P_M(t) > P_L(t)$). Hence, the generated power must be equal to the sum of the demand power and power losses; otherwise, frequency deviation will occur. Mathematically, the relationship between frequency and power deviation within a system can be expressed by the swing equation, as given below.

$$\frac{2H}{\omega_s}\frac{d^2\delta}{dt^2} = P_M - P_L \tag{1}$$

However, in practical cases, the frequency is sensitive to different factors, which are not considered in this study. Nevertheless, the characteristics of the dynamics can be discussed by considering some examples. The authors took two incidents from the Great Britain power system for discussion. Figure 3 shows the dynamic changes in electricity demand and system frequency in the Great Britain power system during the Royal Wedding of Prince William and Catherine on 29 April 2011. Here, significant rises and falls in the electricity demand can be observed, which resulted in drastic frequency fluctuation. Royal Weddings are considered special events in the history of Great Britain, and most British people attended the event whether physically or virtually. Because of the operation of a large number of electronic appliances, the load demand on that day was very high in Great Britain. However, such special events are few in number and should not be missed; hence, as shown in Figure 3, the total electric demand rose significantly during that event, but dropped shortly after its completion. On that day, the British power system observed a demand rise of 2300 MW within a few minutes, followed by a power drop of 3100 MW. This type of sharp rise and fall can cause significant fluctuation in the system frequency, hindering its maintenance within the acceptable range. Similarly, Figure 4 presents the frequency fluctuation in the Great Britain power system during the failure of the Sizewell B nuclear power plant on 28 May 2008. As shown in Figure 4, the power system faced three power system failures and one embedded generation failure (i.e., 1993 MW of total failure) in a cascading manner within just 3.5 min. The capacity of the failed power system was higher than the actual reserve capacity of the power system; thus, balance could not be achieved. As such, the frequency crossed the acceptable limit, and the electrical supply (i.e., 546 MW) of a certain part of the city was cut off for stability maintenance. This accident occurred because of enormous changes on the generation side within a small period. Hence, frequency stability is vital for the proper operation of a power system.

___
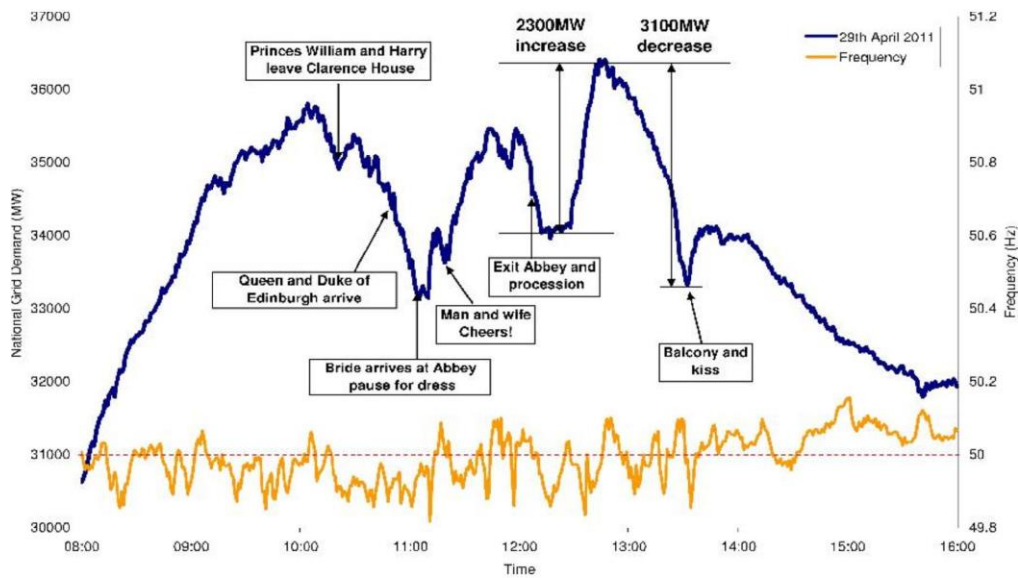
Figure 3. Change in electricity demand and system frequency in the Great Britain power system during the Royal Wedding of Prince William and Catherine on 29 April 2011 [65].
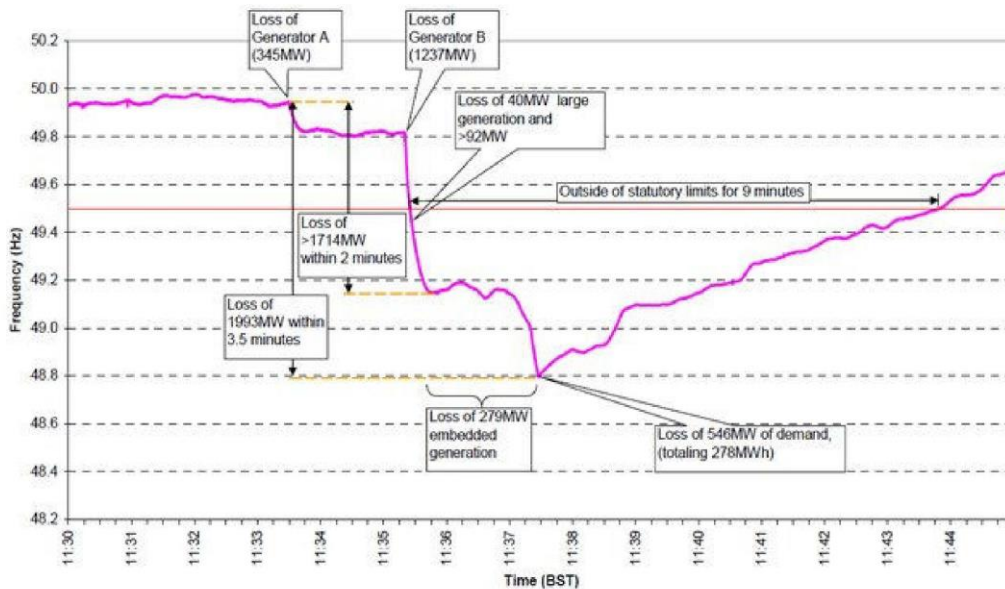

Figure 4. Frequency fluctuation in the Great Britain power system during the failure of the Sizewell B nuclear power plant on 28 May 2008 [65].

3.1. Frequency Response and Regulation Techniques

To maintain an acceptable frequency range, regular injection and/or withdrawal of generated power takes place. This process must quickly respond to dynamic load changes and establish supply/demand (or energy) balance. The power system is flexible in terms of power generation, which can be maintained during load changes so as to regulate the system frequency [66]. This is a continuous process. As shown in Figure 3, significant rises (2300 MW) and drops (3100 MW) in demand could be observed in the Great Britain power system within a short period (the Royal Wedding). However, the frequency of the system was maintained within the range of 49.8 Hz to 50.2 Hz; this process is called frequency regulation. In every power system, there is a predefined normal operating frequency band (NOFB) to maintain the system. Table 1 presents an overview of the nominal frequency interval and the critical frequency interval of different countries.

Table 1. Nominal and critical frequency intervals in the power systems of different countries.

Country	Nominal Frequency (Hz)	Critical Frequency (Hz)	References
Great Britain	49.5–50.5	47–52	[67–69]
Germany	49.5–50.5	47–52	[69–71]
France	49.5–50.5	47–52	[69,70]
Belgium	49.5–50.5	47–52	[69]
Austria	49.5–50.5	47.5–51.5	[69]
Australia	49.75–50.25	47–52	[72–74]
Ireland	49.8–50.2	47–52	[69]
Italy	49.1–50.1	47.5–51.5	[69]
Poland	49.5–50.5	47–52	[69]
Denmark	49.9–50.1	47.5–51	[75–77]
China	49.8–50.2	48–51	[78]

Because of the differences in electric generation and demand, systems can face power deviation, which further results in frequency instability. For proper and effective operation of a power system, it may balance the demand/supply chain by introducing, for example, a significant reservoir for an extensive system or a BESS for a small system [79]. However, this approach may not be sufficient to maintain the equilibrium state on a real-time basis; thus, the generating plant must have the feature of flexible generation. Flexible generation may support the system in providing instant balance and reducing the potential causes of failure [79,80]. In addition, some critical issues may occur following large deviations within a short period, which must be handled for the protection of the whole power system. Hence, control measures are implemented at different levels to maintain the NOFB and to protect the whole power system: (a) primary control, (b) secondary control, (c) tertiary control, and (d) emergency control. Figure 5 shows the frequency control techniques of a conventional power system used to maintain the frequency deviation within an acceptable range in order to operate the system securely and reliably. Similarly, Figure 6 presents the frequency response of a power system under various control actions and their characteristics. As shown in Figure 6, the primary control method is the first action taken by the system for stability, which is fast compared to measures. Similarly, secondary and tertiary control actions are activated more slowly than primary control. The response time for the various control actions is given in the same figure; however, these may vary for different nations and power systems. For a detailed comparison, Table 2 provides a list of control methods and their response periods in various countries.
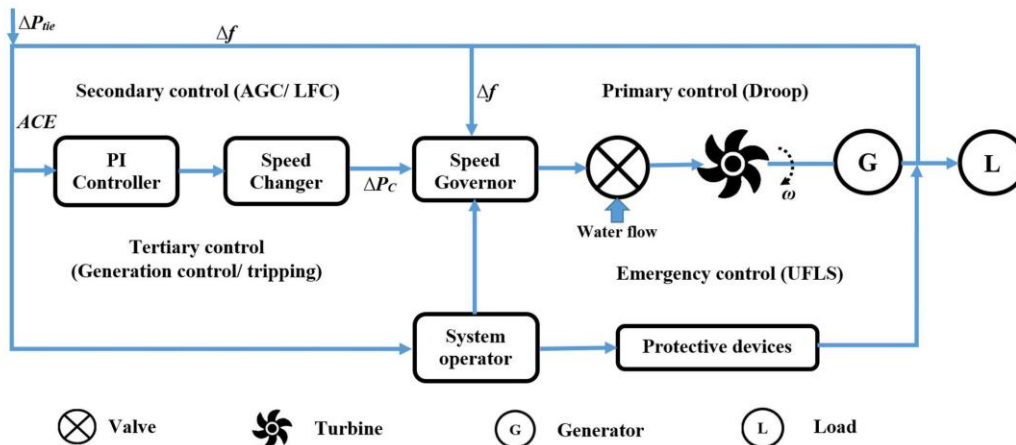
**Figure 5.** Frequency control techniques/loops in a power system.
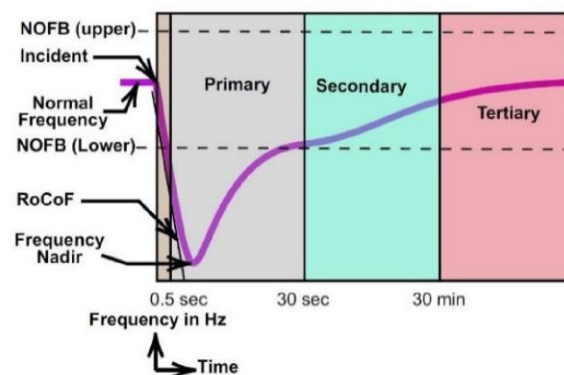
Figure 6. Frequency response of a power system under different control actions.

In a power system, the system frequency is directly related to the angular velocity of the rotor (i.e., $f \propto N_S$); frequency increases with the increase in rotor speed and vice versa. Hence, frequency control in a conventional power system is akin to the control of rotor speed. At the first stage, the aim is to maintain the speed of the turbine/generator set (i.e., rotor) through the application of a governor mechanism, which senses the rotor speed and regulates the flow of water/steam. A small deviation in speed and frequency can be restored by locally changing the mechanical power outputs. This technique is automatic and based on a drop in the generator, which regulates the frequency disturbance within a few seconds. This is the first stage of the frequency control mechanism and works as the first line of defense in a power system, and it is considered the primary frequency control technique. The primary frequency control technique is very critical for the restoration; therefore, it should meet the standards and specifications for deployment start, full availability, deployment end, droop setting, full deployment, frequency characteristics, and controller insensitivity [81].

Table 2. Frequency control responses in different countries.

Country	Primary Control	Secondary Control	Others	References
Great Britain	Active power of the generation unit increases/decreases within 10 to 30 s of the frequency deviation.	Active power of the generation unit increases/decreases within 30 s to 30 min of the frequency deviation.	High-frequency response is in action, which acts within 10 s of the frequency deviation.	[67,68]
Germany	The generation unit can achieve 100% of active power changes within 30 s and maintain frequency for the next 15 min.	The generation unit is able to achieve 100% of active power changes within 5 min.	Minutes reserve is adopted, which responds within 15 min. The power supply must be delivered for at least 7.5 min of the specific quarter hours.	[69–71]
China	Active power of the generation unit increases/decreases within 3 to 15 s of the frequency deviation.	Active power of the generation unit increases/decreases for a maximum of 1 min.	Power plants are capable of setting and enforcing automatic control for the active power and power ramp rate (e.g., an integrated wind power plant contains 1 min and 10 min ramp rates). During the period of severing deviation, power plants can instantly control their generation as instructed by the TSO.	[78,82,83]
France/Italy	50% of active power increases/decreases within 15 s and 100% within 30 s, continued for a maximum of 15 min.	Activated within 30 s and continued for a maximum of 15 min.	Tertiary control is adopted, which activates along with secondary control, and continues for a maximum of 15 min.	[69,70]
Denmark	A droop of 18,000 MW/Hz is maintained.		Reserve control is adopted, where the system is regulated within 2 to 3 min of 0.01 Hz frequency deviation. If the deviation becomes higher than 0.05 Hz, 50% of system reserve is distributed within 5 s, and 100% is distributed within 30 s.	[69,75–77]
India	The generation unit must provide a response to changes of 5% droop (i.e., 40% of active power changes with a frequency change of 1 Hz).	A 30 s delay is provided to activate the secondary reserves, which are entirely activated within 15 min and continued for a maximum of 30 min.	A tertiary control mechanism is available as a supportive method of secondary control. Tertiary control is fully activated within 15 min and continued for a maximum period of 60 min. Moreover, UFLS is implemented with three thresholds (e.g., adopted thresholds in the south of India are 49.5 Hz and 0.2 Hz/s, 49.3 Hz and 0.2 Hz/s, and 49.3 Hz and 0.3 Hz/s).	[84–87]

When the frequency deviation increases and the system enters into non-normal operation, the primary frequency control technique may be unable to restore the system frequency; hence, an additional technique is required for system restoration. The second stage of frequency restoration in a power system is called the secondary frequency control technique. Basically, the primary frequency control technique is used to control the frequency in the short term, whereas the secondary is used to direct the primary one to prevent the system frequency from exceeding the desired limits for a long period [88]. The required power at this stage is delivered by both the spinning and the non-spinning reserve capacities for the balancing of system load and frequency, which is also called the load

170

frequency control (LFC) method [89]. The secondary frequency control technique conducts automatic and centralized control by utilizing the system reserve capacity and restores the system frequency within a few minutes [90]. There are two types of control: (a) unit level and (b) system level. In the unit-level secondary control, the reference value of load–frequency adjustment for the governor is managed by a unit load controller, whereas an automatic generation control (AGC) system is used as the system-level secondary control technique. The unit-level controllers simply supervise the controlling variables that can influence system operation and require primary control actions [90]. On the other hand, the coordination of all power generators within a power system is managed by the AGC, but the AGC is not responsible for direct changes in system frequency; it simply oversees the controllers in initiating primary control actions (as a secondary control method) [91,92]. One of the main objectives of the AGC and/or LFC is to maintain the system frequency by coordinating and exchanging the power (i.e., ΔP_{tie}) with the neighboring control area for a specified period. The area control error (ACE), i.e., a measurement of the actual imbalance of real power in an interconnected power system, is calculated and used to command the controllers with some processed control signals. In the case of stable system frequency, a lower value of ACE (i.e., close to zero) is expected in each power plant area [79]. The deployment time, controller organization, controller cycle time, and controller types should be specified during the secondary control of frequency in a power system [81].

The third stage of the frequency control method is called the tertiary frequency control technique, which is a manual (or automatic) control technique involving a change in the working rate of power generation. It is conducted during situations of serious supply/demand unbalance following sharp frequency deviations, whereby the secondary control is unable to restore the system. It adopts the concepts of adjustment, rescheduling, and deployment of new power generators, and it can take from tens of minutes to hours for the restoration of sufficient secondary control reserve [89]. This technique can be considered the economic dispatch method, and it is implemented in a completely deregulated market setting [93]. Furthermore, tertiary frequency control can be considered a supportive action for secondary control, since it is intended to coordinate the reserves and relieve the secondary control response by lowering the value (near zero) of ACE [94]. Because of disturbances on the generation and/or demand side, if the frequency deviation crosses the acceptable limits and the control techniques fail to restore the system, standby supplies or emergency actions need to be applied to minimize the risk of cascade faults or even system blackouts. A scheme such as under frequency load shedding (UFLS) is used in cases of insufficient generation and/or significant frequency drop. Similarly, generation stations are disconnected in the case of excess generation and/or frequency increases.

3.2. Case Studies

Numerous consequences of frequency instability can occur, with the failure and/or system blackout being the major ones. System blackouts happen when some fault occurs in the power system (i.e., power plant and/or transmission medium), and significant power is lost in a part of or the whole power system. A significant drop in power supply on the consumer side (because of the fault) may create power deviation, which may lead to frequency deviation outside of the acceptable range. At first, the control mechanisms discussed in Section 3.1 try to restore the power system; if these are unsuccessful, the system faces cascading failures and even system blackout can occur. In the past, there have been many such cases of blackouts all over the world. Most events occurred because of system failures in terms of generation and transmission lines. The major causes of these failures were either technical issues or natural hazards. Some of the cases are discussed below.

3.2.1. Power System Blackout in Great Britain on 28 May 2008

Around 0.5 million people and several industries, businesses, and railways across London, Cheshire, Merseyside, and East Anglia were affected by the power loss on 28 May 2008. It started when the Longannet power station went offline because of some technical issues

after maintenance. Within 2 min, the Sizewell B nuclear plant also faced issues and failed to produce power. After another minute, embedded generators also faced problems and were removed from the Great Britain power system. Figure 4 provides a clear picture of the events and the frequency fluctuation as a result of these failures. As shown in Figure 4, the power system lost around 1993 MW of power within 3.5 min, which could not be restored by the reserved capacity of the system; thus, the system failed to operate within an acceptable frequency range. As a result, around 546 MW of load was automatically shut down as per the protection precautions [95,96].

3.2.2. Power System Blackout in Northern and Eastern India on 30 and 31 July 2012

The Indian power system faced a large failure on 30 and 31 July 2012, which affected around 700 million people from 20 states of the country. As per the inquiry committee, the Central Electricity Regulatory Commission (CERA), the major reasons behind these blackouts were system failures due to some technical and seasonal issues. The day before-hand, the Indian power system faced five issues in the transmission lines: (a) unplanned shutdown of 400 kV Bina–Gwalior–Agra II transmission line, (b) trip of 220 kV Kota–Badod transmission line, (c) phase-to-earth fault in 220 kV Binmal–Sirohi transmission line, (d) trip of 400 kV Bhinmal–Kankroli transmission line, and (e) emergency outage of 400 kV Zerda–Kankroli transmission line. The first blackout occurred on 30 July, which affected eight states of the country. Just before this incident, the demand of the Northern Region was calculated to be around 35,669 MW, whereas the generation was only 32,636. At the same time, the system frequency was measured to be 49.68 Hz. The major reasons behind the blackout on 30 July were (a) unplanned shutdown of 400 kV Bina–Gwalior–Agra II trans-mission line, which created electrical stress on other transmission lines, (b) unscheduled importation of power to the Northern Region from the Eastern Region in large amounts, (c) lack of proper monitoring and coordination by the power utilities, since no action was taken to reduce the total transfer capability after the transmission line failures, (d) stoppage of a few power generation plants, and (e) power swing in the Eastern Region because of the unscheduled import/export and transmission line failure. This blackout affected all sectors and was completely restored after 13.5 h. Then, 21 h later, three regions (Northern, Eastern, and Northeastern) faced similar issues, whereby consumers (around 48 GW) were disturbed. However, immediate actions were taken at that instant, and the system was recovered after 8.5 h. During the blackouts, some regions faced issues of overfrequency and high voltages, because of the unscheduled stoppage of power export to other states. Figure 7a,b show the frequency dynamics at different locations of Northern India during the blackouts on 30 and 31 July 2012 [87].

3.2.3. Series of Blackouts in Venezuela in 2019

Venezuela faced a long series of power system failures and blackouts in 2019, which affected millions of people, and many people even lost their life. During these blackouts, the transportation, airport, telecommunication, industrial, hospital, education, water services, food products, and household sectors were affected. The major reasons behind these system outages were considered to be irregular system maintenance, mishandling of the system, and lack of technical human resources. The first series of nationwide outages started on 7 March 2019, when a bush fire occurred near the Malena substation in eastern Venezuela, where around 70–80% of the country's electricity is generated by the Guri dam electricity plant (10,235 MW installed capacity and 47,000 GWh annual generation). The fire affected the 765 kV transmission line between the San Gerónimo B and Malena substations, further resulting in the overload and failure of alternative routes. It took more than 7 days to restore the system and provide electricity. Roughly 1.5 weeks later, the power system failed a second time, which affected 14 states of Venezuela, before recovering after 3 days. A similar problem was recorded after just 24 h of system restoration. System failures were also observed in April and July in numerous states [97–99].
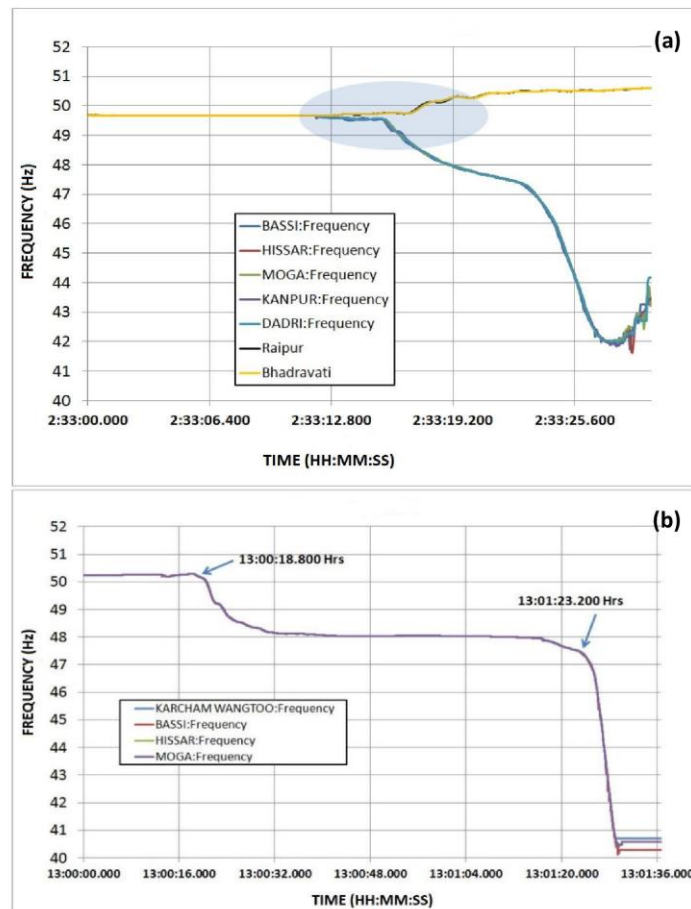
Figure 7. Frequency dynamics at different locations during the blackouts in India (**a**) on 30 July and (**b**) on 31 July [87].

3.2.4. Power System Blackouts in Australia

Australia faced a power system blackout on 28 September 2016, when a 275 kV single-circuit transmission line and 275 kV double-circuit transmission line were damaged by tornadoes. Several failures were observed in a cascading manner just after the shutdown of the transmission lines. Six voltage dips were observed in the South Australian power system after the failures. Nine local wind farms reduced their production as per their protection features, which resulted in 456 MW of power reduction within 7 s (the total demand of the South Australian system was 1826 MW at that instant). There was an attempt to address the reduction in generation by importing power, but this was unsuccessful because of the failure of the Heywood interconnector. Then, the South Australian grid went into isolated mode, and the whole system experienced a blackout in an attempt to maintain the isolated system frequency within acceptable limits. Figure 8 presents the actual dynamics of the South Australian wind farms, along with their generated and reduced power profile, during the system failures. Similarly, Figure 9 shows the frequencies of various sections of the South Australian grid during the system failure. During this

event, the system frequency dropped to 47 Hz from 49.5 Hz in just 0.4 s with an average RoCoF of 6.25 Hz/s. The system was restored in around 4.5 h for 40% of consumers and around 8 h for 80–90% of consumers. Complete restoration was achieved in 12 days via bypassing the transmission lines [73].
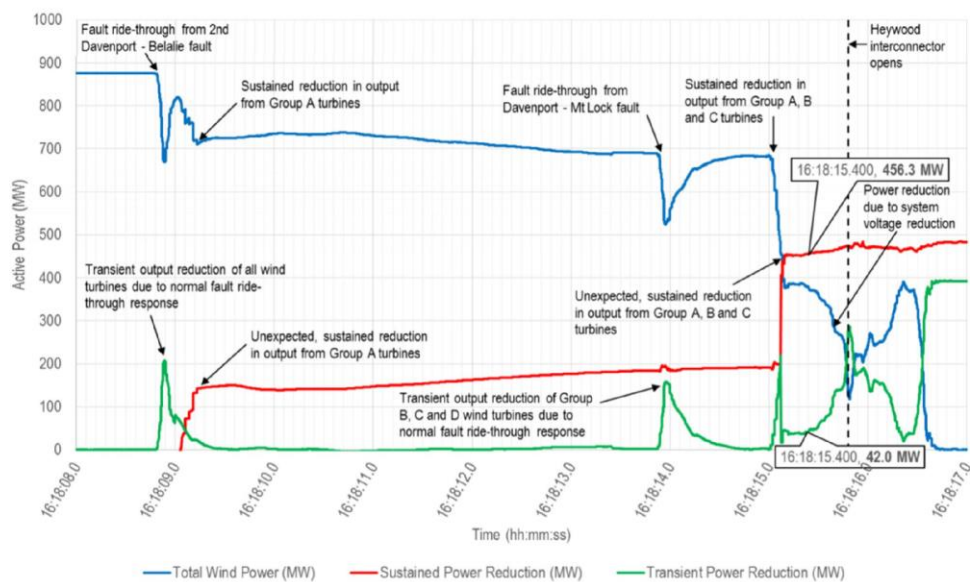

Figure 8. Dynamics of wind farms in South Australian power system during the incident on 28 September 2016 [73].
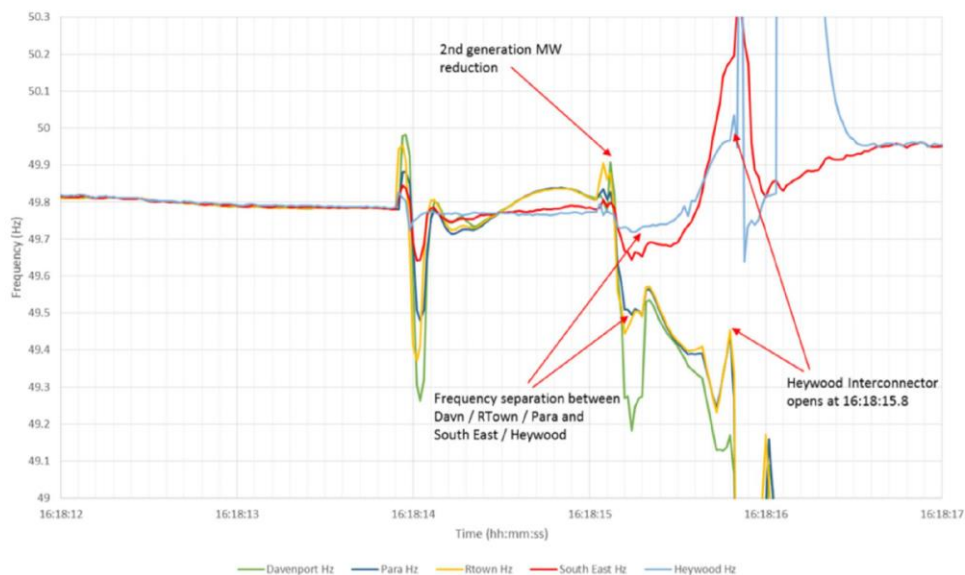

Figure 9. Dynamics of frequency in various nodes of South Australian grid during the failure on 28 September 2016 [73].

Furthermore, similar events were also recorded on 1 November 2015 (110,000 households affected), 1 December 2016 (200,000 households affected and restored after 1 h), 27 December 2016 (125,000 households affected and restored after 4 days), 20 January 2017 (58,000 households affected), 8 February 2017 (90,000 households affected), and 25 August 2018 in the Australian power system. These events highlighted the vulnerability and sensitivity of the Australian power system. The major issues behind these frequent failures are considered to be the high penetration of PEC-based technologies and the unpredictable nature of RESs, as well as the damage of transmission lines from natural disasters [74].

3.2.5. Power System Blackouts in California, USA

California is the state that has faced the greatest number of system failures in the history of the USA. From 2008 to 2017, 4297 power outages were recorded just in California [100]. It is quite challenging to cover all failures; thus, this subsection only discusses the blackout that occurred in California last year. On 14 August 2020, a giant rolling blackout was implemented in California because of the high electrical demand. Because of a huge wildfire, the maximum temperature of California reached up to 130 °C. Because of the COVID-19 pandemic, most people were also staying at their homes and using their electrical appliances. Furthermore, the extreme heatwave forced people to operate their air-conditioning units, which significantly increased the total system demand. According to the data from the California Energy Commission, a large proportion of electricity is generated from RESs, with plans to increase the proportion to 60% by 2030. In 2019, 21.04% of electricity in California was generated by solar and wind energy resources [101]. On 14 August, a 470 MW solar power plant and several wind power plants (1000 MW total production) failed because of the excessive demand [102]. At the same time, so-called reliable power generators unexpectedly went offline [103]. The rolling blackout was implemented at around 6:30 p.m., when the power generation from solar power plants was disappearing, and continued until 9:00 p.m. [104]. According to various statements, it seems that this incident occurred because of the supply deficit compared to the high demand.

Several initial causes can lead to system outages. A previous study [105] presented statistical data from a survey conducted from 2011 to 2019 in some parts of the world, showing that around 50% of system blackouts were initiated due to bad weather and falling of trees, 31.8% were initiated due to equipment and human failures, 10.6% were initiated due to some form of vehicle accidents, 1.5% were initiated due to animal activities, and 6.1% were initiated due to overdemand of electricity. In 2017, the USA faced a total of 3526 outages with a total duration of 284,086 min and an average duration of 81 min [106]. Around 36 million people were affected by these events. In the USA, the power outages were caused by seven significant reasons, with bad weather and falling of trees contributing a significant proportion (i.e., 1159 events). Moreover, 791 outage events were caused by human and equipment errors, 444 were caused by vehicle accidents, 173 were caused by animal activities, seven were caused by overdemand, 244 were planned outages, 15 were caused by theft/vandalism, and 693 events resulted from unknown causes in 2017 [106].

3.2.6. Inferences

As we all know, wind energy is quite unpredictable, and solar power plants only produce energy during the daytime; thus, some form of a reliable power plant must be present as a backup. The power system must maintain frequency within an acceptable range; otherwise, the system may fail. When failure occurs, unbalance is created within that power system, which may lead to system blackouts if not resolved properly. The five cases presented above provide a clear map of the importance of frequency stability for the reliable operation of a power system. Among the five case studies, the blackout of Great Britain was caused by power generation failure; 1993 MW of generation was lost within 3.5 min, which could not be recovered by the system in time. The system blackouts in India were the results of transmission line failures. Similarly, in Venezuela, a large proportion of generation was isolated because of transmission line failure. However, in

the cases of Australia and California, natural disasters were the cause of system failures. In all cases, power systems suffered from instability. Because of the supply/demand unbalance, some parts of or the whole power system faced problems, resulting in forced or rolling blackouts. The British, Indian, and Venezuelan power systems are mainly supplied via conventional power generators (i.e., synchronous generators). However, in Australia and California, a large proportion of electricity is produced through PEC-based RESs. In comparison to conventional power systems, modern power systems with significant PEC-based technologies record a high number of system outages. Numerous statements have been made on the penetration of RESs and their issues. With the increase in PEC-based technologies, systems are becoming more complex; therefore, advanced technologies and appropriate approaches must be introduced into the modern power systems.

4. Open Issues of Frequency Instability and the Way Forward

Modern power systems are adopting a significant transformation in generation, transmission, distribution, and utilization levels with the introduction of rapidly growing PEC-based technologies, due to the massive integration of PEC-based RESs, including solar PV and wind turbines, whereas the appliances and control methods in other sectors are dependent on the PECs. As discussed in Section 1, short-term frequency instability can occur in modern power systems because of two main reasons: (a) the high penetration of PEC-based energy resources such as solar PV and wind turbine reducing the system inertia, and (b) RESs being unable to balance the demand/supply chain because of their unpredictable patterns. Modern power systems are becoming more complex because of these rapid transformations. This section presents the issues caused by these transformations in detail, and some of the potential solutions are thoroughly discussed.

4.1. Issues of PEC-Based Technologies in a Power System

RESs, especially solar and wind energy, are stochastic in nature. The solar and wind resources have variable trends over multiple timescales (daily and seasonal). On the other hand, demand is also stochastic and varies continuously. In modern power systems, both the generation and the load vary over periods of minutes and hours [107]. Numerous studies have been conducted on the forecasting of solar and wind power generation, which have been further implemented to reduce the uncertainty of power systems [108–115]. However, the forecasted results are not accurate for an exact time scale and may create a drastic deviation in the system frequency, especially in a low-inertia power grid [107]. Thus, the increase in PEC penetration increases the stochastic variation of the active power generation in a power system, which may lead to unpredictable situations within that system [116].

In the conventional power system, synchronous generators work as the source of inertia since the rotating mass provides the physical characteristics within that system. The system frequency is directly associated with the rotation of the machine, and the system inertia created by the synchronous machine helps to maintain the system frequency by minimizing the initial frequency deviations. To do this, the total mechanical inertia has some resistive properties (in virtual mode) with respect to changing the rotation of the machine [117]. As given by Equation (1), a small unbalance in power generation and load can create a frequency deviation within a power system. The frequency response of a power system under an unbalanced condition can be seen in Figure 6. An extended form of Equation (1) is given in Equations (2) and (3). Here, H is the inertia constant, f is the system frequency, S is the rated power of machine, E_{kin} is the kinetic energy, H_{sys} is the equivalent inertia of the whole power system, S_{sys} is the system base, and H_i and S_i are the inertia and rated power of the i-th machine.

$$H = \frac{(J\omega_0{}^2)/2}{S} = \frac{E_{kin}}{S} = \frac{H_i\,S_i}{S_{sys}}. \tag{2}$$

$$H_{sys} = \frac{E_{kin,\,sys}}{S_{sys}} = \frac{\sum_{i=1}^{n} H_i S_i}{S_{sys}}. \tag{3}$$

From the above equations, it is clear that the system inertia is directly proportional to the kinetic energy of the machine for a constant rated power; with an increase in the proportion of kinetic energy (i.e., synchronous type generation), the system inertia increases. The conventional power system contains synchronous generators as the source of kinetic energy, as well as the system inertia, but modern power systems have both less kinetic energy and less inertia. On the other hand, most appliances and the equipment control mechanisms adopted in modern power systems are based on PEC technologies, which significantly reduces the inertia. The rate of inclusion of such technologies is increasing day by day, resulting in decreases in system inertia at a drastic rate [118].

In a power system with multiple generators, each machine should run at the same frequency (i.e., synchronism). If a big power deviation takes place, individual power generators within a power system may lose synchronization, followed by dissimilar fluctuating motions around the center of inertia (COI) [119,120]. At this stage, the frequency of each unit may not be the same, instead presenting an oscillating tendency. The rate of oscillation is dependent on the difference between $P_M(t)$ and $P_L(t)$, as given in Equation (1). However, the frequency of each unit is closed to the COI (see Equations (4) and (5)), and the damping and inertial forces among the units try to pull the whole system back into synchronization [120]. If these forces are unable to maintain the system in its original state, some form of control mechanism should be activated to maintain system stability. From Equations (5) and (6), it is clear that the system frequency and its changing rate are directly related to the inertia of the power grid. A lower system inertia leads to a higher fluctuation of frequency. For a better visualization of these issues, Figure 10a,b can be analyzed, which present the frequency dynamics for different inertial constants and power deviations. From Figure 10a, it can be seen that the reduced system inertia creates a higher frequency deviation, which may lead to an unstable power system. Similarly, Figure 10b shows the dynamic characteristics of the frequency with changes in the power deviation. Here, for analysis, the values of the constants in the transfer function were taken from [7].

$$f_{COI} = \frac{\sum_{i=1}^{n} H_i S_i f_i}{\sum_{i=1}^{n} H_i S_i}. \tag{4}$$

$$f_{COI}(t) = 1 + \frac{\Delta P}{2H_{sys}}\, t. \tag{5}$$

$$RoCoF = \frac{\Delta P}{2H_{sys}}. \tag{6}$$

In addition to frequency fluctuation, the huge penetration of PEC technologies creates other stability issues in a power system. The rotor angle stability and the small-signal stability of a power system are directly linked to the synchronous generators connected to the grid [121]. The huge penetration of PEC-based RESs reduces the proportion of synchronous generators in a power system, which may affect the shape, frequency, and damping factor of the rotor oscillation [10]. Furthermore, the power system is unable to use the power system stabilizer connected to the synchronous generator. In the case of large disturbances, transient instability may also occur in the system via changing the power flow in tie-lines [122]. The frequency stability is also linked to the rotor angle stability since the rotor speed of the generators is adjusted on the basis of the system's frequency [123]. Since PEC-based technologies have the ability to control the active and reactive power on both the generation and the load sides, they can be used to maintain rotor angle stability and the frequency stability in the pipeline [116,124]. Furthermore, a low-inertia power system would be capable of maintaining the frequency balance during a significant deviation via rapid generation/load changes [125].
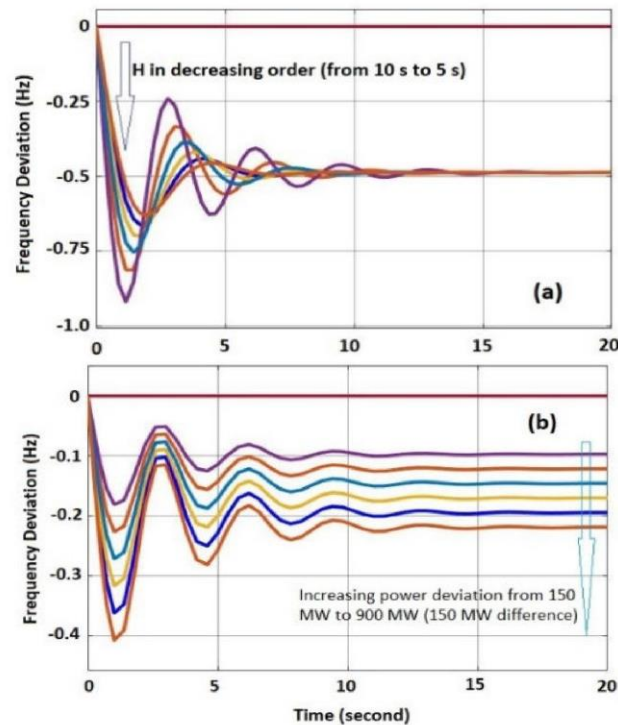
Figure 10. Frequency dynamics for (**a**) different inertial constants and (**b**) different power deviations.

On the other hand, PEC-based technologies introduce two new forms of stability issues: resonance and converter-driven stability. The first (i.e., resonance stability) occurs during the periodic exchange of energy in an oscillatory manner because of the insufficient dissipation of energy while magnifying the magnitude of the parameters (i.e., voltage, current, torque, etc.) [10]. Two types of resonance stability exist: (a) torsional and (b) electrical resonance. Torsional resonance basically occurs in conventional power systems that contain synchronous generators, whereas electrical resonance occurs in systems containing RESs (especially variable-speed induction generators in wind turbines). This resonance can lead to large oscillations in current and voltage, as well as large perturbations in electrical torque, which further impact the electrical and mechanical components [10]. Similarly, the second (i.e., converter-driven stability) is fully associated with PEC control and occurs in the form of oscillation due to the cross-coupling phenomenon between the dynamic electromechanical devices and the transient nature of electromagnetic grid networks [11].

4.2. Future Studies

According to the literature, the adopted approach of system stability involves the control of appropriate mechanisms by taking into consideration some response parameters. However, with respect to the abovementioned issues, the classical methods cannot effectively address the problems because of their slow response, low accuracy, and poor robustness. Generation-side control approaches are mostly focused on the supply/demand balance, whereas frequency fluctuation issues can be effectively addressed by demand-side control methods [126,127]. Response parameters such as RoCoF, nadir frequency, and OD are important indicators of the system's status, allowing intelligent selection of the appropriate control approach. To regulate the system's characteristics and maintain system

stability, the real-time response must be measured within microseconds, for which an efficient and intelligent controller is necessary. The response time is the primary concern during the implementation of a control mechanism in the system. Moreover, the power generation characteristics from RESs are unpredictable and fluctuate drastically; thus, the controller must be robust so that it can handle abnormal situations. The system is required to manage and protect the components from failure. Furthermore, most studies were conducted for the integration of big plants such as solar farms and wind farms; however, in current practice, people are installing distributed energy systems on smaller scales [128,129]. Various trading practices and control mechanisms are being introduced, which further leads to problems in system operation and protection [130,131]. Such problems must be addressed by bottom-up approaches and not only for big power plants. Several studies have been conducted to address the issues of low-inertia power systems, but concrete results were not achieved with practical and efficient validation, and several limitations were identified. Some potential fields of study are discussed in this section to address the current issues of PEC-dominated power systems.

4.2.1. Grid-Forming Power Converters

Conventional inverters were designed to work as current sources concerning the grid parameters, whereby synchronous generators are basically used as the reference system (i.e., slack bus), and the generators connected to the inverter act as the power contributors (i.e., following type). These conventional inverters use PLL to synchronize the connected power generators to the power grid [132]. However, the inverter must be able to handle occasional perturbations such as sudden voltage fluctuations and phase changes so as to re-establish the system synchronization [133]. With the increase in the proportion of nonsynchronous generators, modern power systems are becoming dominated by PEC technologies, and the concept of grid-following inverters is becoming outdated due to the need for a reference system (i.e., synchronous generator) to maintain the parameters [107]. Hence, a form of PEC-based resource must be introduced into modern power systems to set the relevant parameters, instead of following the existing values (as done by grid-following inverters).

A grid-forming power converter is a power electronic unit that helps to control the voltage amplitude and frequency (i.e., magnitude and angle of the voltage) at the point of common coupling (PCC) within a power system [134,135]. Its main function is to regulate the output voltage and/or current so that the system frequency and the voltage remain in an acceptable range. Since a grid-forming converter is capable of injecting instantaneous active and reactive power for frequency and voltage regulation within a system, it can be considered as the slack bus unit in an isolated energy system [134,136]. However, it can be used in both isolated and grid-connected mode, behaving as a synchronous generator in traditional power systems [134]. Basically, the grid-forming inverter adopts four techniques, as shown in Figure 11. The concept of the grid-forming inverter with new adaptations can address the above-discussed issues, but its actual characteristics, response, and impact are unknown [137]. Numerous studies have proposed adaptions, along with a description of their performance, in the past few years. One of the popular methods used with synchronous generators and inverters is droop control, which established a linear relationship between frequency (active power) and voltage (reactive power) [138]. A fractional-order controller for a grid-forming inverter was proposed with the target group of high-energy applications, but the system dynamics were found to be slow and unstable [139,140]. Virtual oscillator control-based strategies were proposed in [141,142] for performance improvement, but these approaches are still in the experimental phase and need genuine validation. A sliding mode control was proposed for an AC voltage loop with an inner current loop in [143], but this concept is quite complicated and suffers from high computational cost. Similarly, state-feedback control techniques for direct AC voltage control within a grid-forming inverter have coupling issues with the active power [144]. From the studies taken from the literature, it can be observed that the adaptation processes of new concepts with grid-forming inverters are in progress, but no practical and reliable

solutions have been obtained to date. Some significant research can be done in this sector for the advancement of this concept in the future. For example, the combination of multiple grid-forming concepts (e.g., a hybrid model of a virtual oscillator and matching control) can be conducted by highlighting the strengths and neglecting the drawbacks of specific methods (i.e., the virtual oscillator control method has the best large-signal behavior, while matching control method is more robust; thus, a better result can be achieved through their combination) [145].
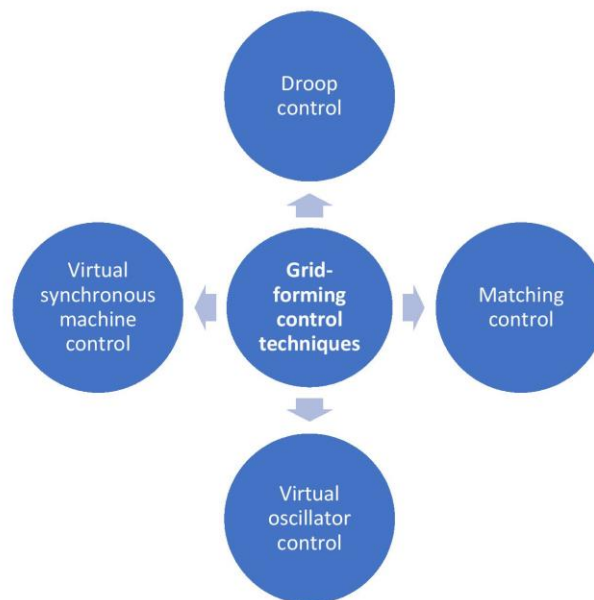
Figure 11. Different techniques used in grid-forming converters.

4.2.2. VPP/VSG with a New Dimension

PEC-based generators use a droop control mechanism to maintain frequency, but most of them adopt the approach of power sharing in a steady-state but not transient mode [146]. In addition, the droop control mechanism lacks technical parameters, including system inertia, which was addressed by the introduction of a concept called virtual power plant (VPP) or virtual synchronous generator (VSG) [147,148]. The VPP produces the required inertia virtually by introducing an appropriate amount of power, and the inertia minimized the variation in frequency (both primary and secondary) caused by various factors and events [16,149]. The ability to introduce appropriate power (both active and reactive) for the stability of frequency and voltage is an essential characteristic of an effective VPP [150]. However, it takes a few minutes to switch RESs (especially wind energy) from one steady state to another state during normal operation. Hence, a BESS is always introduced along with VPPs to maintain balanced energy conditions and provide virtual inertia during the transient stage [150,151]. On the other hand, the complexity may be increased with an increase in the number of VPPs within the system [152,153].

These challenges can be addressed by maintaining efficient coordination among the VPPs that link and share the required inertial proportion [154]. In order to achieve this objective, intelligent architecture can be introduced to monitor, estimate, and control the parameters on a real-time basis. An example of an intelligent architecture is presented in Figure 12. In the proposed system, the distributed VPPs and BESSs provide virtual inertia for their respective RESs, whereby all systems are controlled via the hierarchical control

architecture. A short-term time-series forecasting model can be developed to forecast the electrical parameters within the power system, which can be utilized to identify optimum coordination among the associated technologies (i.e., size and location of the VPPs, PECs, and grid parameters), such that the system can be securely and reliably operated. A deep learning-based hierarchical control mechanism can be developed to coordinate the distributed and central control system, as well as dynamically oversee the whole power system for normal operation. The proposed model is based on a distributed concept, which can manage the allocation of power, thereby controlling the whole power system. Various platforms can be used to develop this real-time tool, which allows interpreting and visualizing the data received from hardware in a user-friendly way. One of the main concerns during the design and implementation of the proposed system is that the central control must work in proactive way, since the communication process (i.e., data sending and receiving) takes some time, which may delay the whole control process. For this, the optimization and forecasting models must be efficient and accurate so that the system can promptly predict the characteristics and introduce actions at the right time.
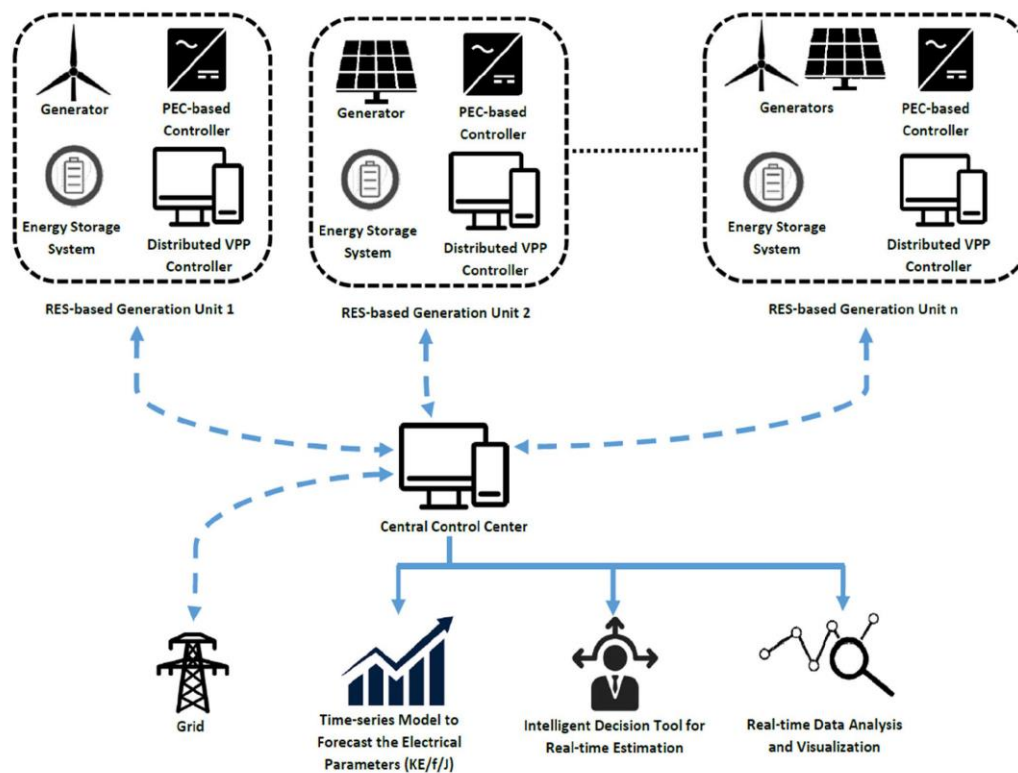

Figure 12. System overview of architecture with intelligent optimization and decision-making model.

4.2.3. Other Solutions

With the identified problem of frequency control in low-inertia power systems, numerous potential solutions have been invented and/or are undergoing investigation. Several research articles have proposed efficient and robust methods to address the frequency control issues of low-inertia systems, as listed in Table 3.

Table 3. List of possible concepts to address the issues occurring in PEC-based power systems.

Concept	Features	References
Inertia emulation via electronic components and BESSs	This concept introduces electronic devices such as supercapacitors or BESSs to provide the inertial response to the power system during a fault or unstable situation (i.e., the condition of frequency deviation). The reduced power during power system unbalance or fault can be compensated for by the introduced components to support the frequency response, similarly to conventional synchronous generators. Additionally, this concept helps in system synchronization by providing virtual control methods.	[155]
Incentivizing synchronous condensers or high-inertia generators	Synchronous condensers can be introduced to provide the inertia and short-circuit power in low-inertia grid systems via voltage recovery concepts during system instability. Generally, this technique considers the emulated generators as conventional generators, which can provide the required inertia and the active and reactive powers. One of the complexities of this technique is the requirement of an optimized technique for the selection of appropriate capacities and the locations of emulated generators.	[156,157]
Curtailment methods and grid code modification	Power production limits, instantaneous combined cycle generation limits, or price signals can be used to increase the inertia contribution. This approach is mostly based on the planning and operation of the existing power system, rather than adopting new technologies. Furthermore, the existing grid code can be changed to maintain the system during acceptable system instability. For example, the operational settings of the existing control equipment can be revised so as to increase the acceptable limit, whereby no automatic shutdown would take place during small levels of deviation.	[137,158]

5. Conclusions

The introduction of PEC-based technologies is drastically reducing system inertia, thereby leading to numerous issues in power system stability. The inclusion of inertial support might be the best option, but this requires robust, secure, reliable, and practical solutions to maintain the system within an acceptable inertia level. Researches have been conducted to address the problems of low-inertia systems due to PEC-based technologies. However, the proposed studies did not yield concrete results with practical and efficient validation, and several limitations were highlighted. Nevertheless, there are many research gaps in this area which can be filled in the future. On the basis of the studies taken from the literature, two major tasks were identified to address the discussed issues: (a) modification of the grid codes as per the current situation, as well as the adaptation of the new operational strategies; (b) introduction of a new device (maybe PEC-based) for this specific purpose. According to a previous study, the following improvements are recommended: (a) intelligent PEC-based technologies to improve the time response, accuracy, and robustness of controllers and their combinations, (b) intelligent techniques to optimize the rating and coordination of integrated RESs, and (c) intelligent models to optimize the size, number, and location of BESSs within the VPP configuration.

References

1. Verzijlbergh, R.; De Vries, L.; Dijkema, G.; Herder, P. Institutional challenges caused by the integration of renewable energy sources in the European electricity sector. *Renew. Sustain. Energy Rev.* **2017**, *75*, 660–667. [CrossRef]
2. Shrestha, A.; Rajbhandari, Y.; Khadka, N.; Bista, A.; Marahatta, A.; Dahal, R.; Mallik, J.K.; Thapa, A.; Hayes, B.P.; Korba, P. Status of Micro/Mini-Grid Systems in a Himalayan Nation: A Comprehensive Review. *IEEE Access* **2020**, *8*, 120983–120998. [CrossRef]
3. Shrestha, A.; Rana, L.B.; Singh, A.; Phuyal, S.; Ghimire, A.; Giri, R.; Kattel, R.; Karki, K.; Jha, S.K. Assessment of electricity excess in an isolated hybrid energy system: A case study of a Dangiwada village in rural Nepal. *Energy Procedia* **2019**, *160*, 76–83. [CrossRef]
4. Hossain, J.; Mahmud, A. *Renewable Energy Integration: Challenges and Solutions*; Springer Singapore Heidelberg: Singapore, 2014. [CrossRef]
5. Energy, U. The Challenge of Sustainability. World Energy Assessment, UNDP-WEC. Available online: https://www.osti.gov/etdeweb/biblio/20228512 (accessed on 2 October 2021).
6. Hou, Q.; Du, E.; Zhang, N.; Kang, C. Impact of High Renewable Penetration on the Power System Operation Mode: A Data-Driven Approach. *IEEE Trans. Power Syst.* **2019**, *35*, 731–741. [CrossRef]
7. Bevrani, H. *Robust Power System Frequency Control*; Springer: Berlin/Heidelberg, Germany, 2009; Volume 85.
8. Hatziargyriou, N.; Milanović, J.; Rahmann, C.; Ajjarapu, V.; Cañizares, C.; Erlich, I.; Hill, D.; Hiskens, I.; Kamwa, I.; Pal, B.; et al. *Stability Definitions and Characterization of Dynamic Behavior in Systems with High Penetration of Power Electronic Interfaced Technologies*; Technical Report PES-TR77, Power System Dynamic Performance Committee; IEEE Power and Energy Society: Piscataway, NJ, USA, 2020.
9. Peng, Q.; Jiang, Q.; Yang, Y.; Liu, T.; Wang, H.; Blaabjerg, F. On the stability of power electronics-dominated systems: Challenges and potential solutions. *IEEE Trans. Ind. Appl.* **2019**, *55*, 7657–7670. [CrossRef]
10. Hatziargyriou, N.; Milanovic, J.; Rahmann, C.; Ajjarapu, V.; Canizares, C.; Erlich, I.; Hill, D.; Hiskens, I.; Kamwa, I.; Pal, B. Definition and Classification of Power System Stability Revisited & Extended. *IEEE Trans. Power Syst.* **2020**, *36*, 3271–3281.
11. Kroposki, B.; Johnson, B.; Zhang, Y.; Gevorgian, V.; Denholm, P.; Hodge, B.-M.; Hannegan, B. Achieving a 100% renewable grid: Operating electric power systems with extremely high levels of variable renewable energy. *IEEE Power Energy Mag.* **2017**, *15*, 61–73. [CrossRef]
12. Wang, Y.; Silva-Saravia, H.; Pulgar-Painemal, H. Actuator placement for enhanced grid dynamic performance: A machine learning approach. *IEEE Trans. Power Syst.* **2019**, *34*, 3119–3128. [CrossRef]
13. Pei, W.; Chen, Y.; Sheng, K.; Deng, W.; Du, Y.; Qi, Z.; Kong, L. Temporal-spatial analysis and improvement measures of Chinese power system for wind power curtailment problem. *Renew. Sustain. Energy Rev.* **2015**, *49*, 148–168. [CrossRef]
14. Khadka, N.; Paudel, R.; Adhikary, B.; Bista, A.; Sharma, S.; Shrestha, A. Transient Stability in Renewable Energy Penetrated Power Systems: A Review. In Proceedings of the RESSD 2020 International Conference on Role of Energy for Sustainable Social Development in 'New Normal' Era, Kathmandu, Nepal, 28–29 December 2020.
15. Ju, W.; Sun, K.; Yao, R. Simulation of cascading outages using a power-flow model considering frequency. *IEEE Access* **2018**, *6*, 37784–37795. [CrossRef]
16. Othman, M.H.; Mokhlis, H.; Mubin, M.; Talpur, S.; Ab Aziz, N.F.; Dradi, M.; Mohamad, H. Progress in control and coordination of energy storage system-based VSG: A review. *IET Renew. Power Gener.* **2019**, *14*, 177–187. [CrossRef]
17. Vandenberghe, F.; Grebe, E.; Klaar, D.; Kleinekorte, K.; Rodriguez, J.; Erven, H.; Tassan, L. FINAL REPORT of the Investigation Committee on the 28 September 2003 Blackout in Italy. *UCTE Tech. Rep.* **2004**. Available online: https://eepublicdownloads.entsoe.eu/clean-documents/pre2015/publications/ce/otherreports/20040427_UCTE_IC_Final_report.pdf (accessed on 8 February 2021).
18. Bevrani, H.; Hiyama, T. *Intelligent Automatic Generation Control*; CRC Press: New York, NY, USA, 2017.
19. Bevrani, H.; Hiyama, T. On load–frequency regulation with time delays: Design and real-time implementation. *IEEE Trans. Energy Convers.* **2009**, *24*, 292–300. [CrossRef]
20. Milla, F.; Duarte-Mermoud, M.A.; Aguila-Camacho, N. Hierarchical mpc secondary control for electric power system. *Math. Probl. Eng.* **2014**, *2014*. [CrossRef]
21. Chamorro, H.R.; Sanchez, A.C.; Pantoja, A.; Zelinka, I.; Gonzalez-Longatt, F.; Sood, V.K. A network control system for hydro plants to counteract the non-synchronous generation integration. *Int. J. Electr. Power Energy Syst.* **2019**, *105*, 404–419. [CrossRef]
22. Hyndman, R.J.; Liu, X.A.; Pinson, P. Visualizing big energy data: Solutions for this crucial component of data analysis. *IEEE Power Energy Mag.* **2018**, *16*, 18–25. [CrossRef]

23. Bonfiglio, A.; Oliveri, A.; Procopio, R.; Delfino, F.; Denegri, G.; Invernizzi, M.; Storace, M. Improving power grids transient stability via model predictive control. In Proceedings of the 2014 Power Systems Computation Conference, Wroclaw, Poland, 18–22 August 2014; pp. 1–7.

24. Cheng, M.; Sami, S.S.; Wu, J. Benefits of using virtual energy storage system for power system frequency response. *Appl. Energy* **2017**, *194*, 376–385. [CrossRef]

25. Lee, S.-J.; Kim, J.-H.; Kim, C.-H.; Kim, S.-K.; Kim, E.-S.; Kim, D.-U.; Mehmood, K.K.; Khan, S.U. Coordinated control algorithm for distributed battery energy storage systems for mitigating voltage and frequency deviations. *IEEE Trans. Smart Grid* **2015**, *7*, 1713–1722. [CrossRef]

26. Kumar, P.S. Transient stability enhancement of power system using TCSC. *Int. J. Electr. Comput. Eng.* **2012**, *2*, 317. [CrossRef]

27. Wang, M.-H.; Chen, H.-C. Transient stability control of multimachine power systems using flywheel energy injection. *IEE Proc. Gener. Transm. Distrib.* **2005**, *152*, 589–596. [CrossRef]

28. Haque, M. Improvement of first swing stability limit by utilizing full benefit of shunt FACTS devices. *IEEE Trans. Power Syst.* **2004**, *19*, 1894–1902. [CrossRef]

29. Murali, D.; Rajaram, M.; Reka, N. Comparison of FACTS devices for power system stability enhancement. *Int. J. Comput. Appl.* **2010**, *8*, 30–35. [CrossRef]

30. Guo, G.; Wang, Y.; Lim, K.-Y.; Gao, L. Robust nonlinear controller for power system transient stability enhancement with voltage regulation. *IEE Proc. Gener. Transm. Distrib.* **1996**, *143*, 407–412. [CrossRef]

31. Teng, F.; Mu, Y.; Jia, H.; Wu, J.; Zeng, P.; Strbac, G. Challenges on primary frequency control and potential solution from EVs in the future GB electricity system. *Appl. Energy* **2017**, *194*, 353–362. [CrossRef]

32. Liu, H.; Huang, K.; Wang, N.; Qi, J.; Wu, Q.; Ma, S.; Li, C. Optimal dispatch for participation of electric vehicles in frequency regulation based on area control error and area regulation requirement. *Appl. Energy* **2019**, *240*, 46–55. [CrossRef]

33. Aghaei, J.; Alizadeh, M.-I.; Siano, P.; Heidari, A. Contribution of emergency demand response programs in power system reliability. *Energy* **2016**, *103*, 688–696. [CrossRef]

34. Babahajiani, P.; Shafiee, Q.; Bevrani, H. Intelligent demand response contribution in frequency control of multi-area power systems. *IEEE Trans. Smart Grid* **2016**, *9*, 1282–1291. [CrossRef]

35. Marahatta, A.; Rajbhandari, Y.; Shrestha, A.; Singh, A.; Gachhadar, A.; Thapa, A. Priority-based low voltage DC microgrid system for rural electrification. *Energy Rep.* **2021**, *7*, 43–51. [CrossRef]

36. Behera, A.; Panigrahi, T.K.; Sahoo, A.K. A FO-PID Controlled Automatic Generation Control of Multi Area Power Systems Tuned by Harmony Search. *Recent Adv. Electr. Electron. Eng.* **2020**, *13*, 101–109. [CrossRef]

37. Tripathy, S.; NAIR, P.C.; Rao, N. Automatic generation control with superconducting magnetic energy storage in power system. *Electr. Mach. Power Syst.* **1994**, *22*, 317–338. [CrossRef]

38. Khamari, D.; Sahu, R.K.; Gorripotu, T.S.; Panda, S. Automatic generation control of power system in deregulated environment using hybrid TLBO and pattern search technique. *Ain Shams Eng. J.* **2019**, *11*, 553–573. [CrossRef]

39. Xi, L.; Li, Y.; Huang, Y.; Lu, L.; Chen, J. A novel automatic generation control method based on the ecological population cooperative control for the islanded smart grid. *Complexity* **2018**, *2018*. [CrossRef]

40. Ramakrishna, K.; Bhatti, T. Automatic generation control of single area power system with multi-source power generation. *Proc. Inst. Mech. Eng. Part A J. Power Energy* **2008**, *222*, 1–11. [CrossRef]

41. Zeynelgil, H.; Demiroren, A.; Sengor, N. The application of ANN technique to automatic generation control for multi-area power system. *Int. J. Electr. Power Energy Syst.* **2002**, *24*, 345–354. [CrossRef]

42. Nanda, J.; Kaul, B. Automatic generation control of an interconnected power system. *Proc. Inst. Electr. Eng.* **1978**, *125*, 385–390. [CrossRef]

43. Sahu, R.K.; Panda, S.; Padhan, S. A hybrid firefly algorithm and pattern search technique for automatic generation control of multi area power systems. *Int. J. Electr. Power Energy Syst.* **2015**, *64*, 9–23. [CrossRef]

44. Cui, M.; Khodayar, M.; Chen, C.; Wang, X.; Zhang, Y.; Khodayar, M.E. Deep Learning-Based Time-Varying Parameter Identification for System-Wide Load Modeling. *IEEE Trans. Smart Grid* **2019**, *10*, 6102–6114. [CrossRef]

45. Wang, C.; Wang, Z.; Wang, J.; Zhao, D. Robust time-varying parameter identification for composite load modeling. *IEEE Trans. Smart Grid* **2017**, *10*, 967–979. [CrossRef]

46. Hung, D.Q.; Mithulananthan, N.; Lee, K.Y. Determining PV penetration for distribution systems with time-varying load models. *IEEE Trans. Power Syst.* **2014**, *29*, 3048–3057. [CrossRef]

47. Kiaei, I.; Lotfifard, S. Tube-based model predictive control of energy storage systems for enhancing transient stability of power systems. *IEEE Trans. Smart Grid* **2017**, *9*, 6438–6447. [CrossRef]

48. Jin, L.; Kumar, R.; Elia, N. Model predictive control-based real-time power system protection schemes. *IEEE Trans. Power Syst.* **2009**, *25*, 988–998. [CrossRef]

49. Ersdal, A.M.; Fabozzi, D.; Imsland, L.; Thornhill, N.F. Model predictive control for power system frequency control taking into account imbalance uncertainty. *IFAC Proc. Vol.* **2014**, *47*, 981–986. [CrossRef]

50. Ball, S. Neural Network Predictive Control Applied to Power System Stability. In *Intelligent Systems Design and Applications*; Springer: Berlin/Heidelberg, Germany, 2003; pp. 43–51.

51. Venkatesh, C.; Deepak, T.; Rajesh, K.; Krishna, K.; Kamath, A. Flatness based TCSC controller for transient stability enhancement of power system. In Proceedings of the 2010 Modern Electric Power Systems, Wroclaw, Poland, 20–22 September 2010; pp. 1–6.

52. Sun, J.; Zheng, H.; DeMarco, C.L.; Chai, Y. Energy function-based model predictive control with UPFCs for relieving power system dynamic current violation. *IEEE Trans. Smart Grid* **2016**, *7*, 2933–2942. [CrossRef]
53. Gómez, J.S.; Sáez, D.; Simpson-Porco, J.W.; Cárdenas, R. Distributed Predictive Control for Frequency and Voltage Regulation in Microgrids. *IEEE Trans. Smart Grid* **2019**, *11*, 1319–1329. [CrossRef]
54. Ngamroo, I.; Vachirasricirikul, S. Coordinated control of optimized SFCL and SMES for improvement of power system transient stability. *IEEE Trans. Appl.* **2011**, *22*, 5600805. [CrossRef]
55. Fuchs, A.; Imhof, M.; Demiray, T.; Morari, M. Stabilization of large power systems using VSC–HVDC and model predictive control. *IEEE Trans. Power Deliv.* **2013**, *29*, 480–488. [CrossRef]
56. Falahi, M.; Lotfifard, S.; Ehsani, M.; Butler-Purry, K. Dynamic model predictive-based energy management of DG integrated distribution systems. *IEEE Trans. Power Deliv.* **2013**, *28*, 2217–2227. [CrossRef]
57. Short, J.A.; Infield, D.G.; Freris, L.L. Stabilization of grid frequency through dynamic demand control. *IEEE Trans. power Syst.* **2007**, *22*, 1284–1293. [CrossRef]
58. Shi, Q.; Li, F.; Hu, Q.; Wang, Z. Dynamic demand control for system frequency regulation: Concept review, algorithm comparison, and future vision. *Electr. Power Syst. Res.* **2018**, *154*, 75–87. [CrossRef]
59. Zhu, Q.; Jiang, L.; Yao, W.; Zhang, C.-K.; Luo, C. Robust load frequency control with dynamic demand response for deregulated power systems considering communication delays. *Electr. Power Compon. Syst.* **2017**, *45*, 75–87. [CrossRef]
60. Shi, Q.; Li, F.; Liu, G.; Shi, D.; Yi, Z.; Wang, Z. Thermostatic load control for system frequency regulation considering daily demand profile and progressive recovery. *IEEE Trans. Smart Grid* **2019**, *10*, 6259–6270. [CrossRef]
61. Shi, Q.; Cui, H.; Li, F.; Liu, Y.; Ju, W.; Sun, Y. A hybrid dynamic demand control strategy for power system frequency regulation. *CSEE J. Power Energy Syst.* **2017**, *3*, 176–185. [CrossRef]
62. Veronica, A.J.; Kumar, N.S.; Gonzalez-Longatt, F. Design of Load Frequency Control for a Microgrid Using D-partition Method. *Int. J. Emerg. Electr. Power Syst.* **2020**, *21*. [CrossRef]
63. Tchuisseu, E.T.; Gomila, D.; Brunner, D.; Colet, P. Effects of dynamic-demand-control appliances on the power grid frequency. *Phys. Rev. E* **2017**, *96*, 022302. [CrossRef] [PubMed]
64. Mohsenian-Rad, A.-H.; Wong, V.W.; Jatskevich, J.; Schober, R.; Leon-Garcia, A. Autonomous demand-side management based on game-theoretic energy consumption scheduling for the future smart grid. *IEEE Trans. Smart Grid* **2010**, *1*, 320–331. [CrossRef]
65. Gonzalez-Longatt, F. *Introduction to Power Systems*, Presentation Slide. 2019. [CrossRef]
66. Hamon, C.; Perninge, M.; Soder, L. Frequency Control: Operation of Frequency Control Schemes in Power Systems with Large Amounts of Wind Power. Dectoral dissertation, KTH Royal Institute of Technology, Stockholm, Sweden, 2016.
67. ESO. *Grid Code (GC)*, Ofgem, Editor, nationalgridESO. Available online: https://www.nationalgrideso.com/industry-information/codes/grid-code#:~{}:text=The%20Grid%20Code%20details%20the,of%20System%20Code%20(CUSC) (accessed on 3 December 2021).
68. Group, N.G. *The Grid Code Issues 5 Revision 21*; National Grid Electricity Transmission: London, UK, 2017.
69. Luo, X.; Wang, J.; Wojcik, J.D.; Wang, J.; Li, D.; Draganescu, M.; Li, Y.; Miao, S. Review of voltage and frequency grid code specifications for electrical energy storage applications. *Energies* **2018**, *11*, 1070. [CrossRef]
70. Cobben, S.; Gaiddon, B.; Laukamp, H. *Impact of Photovoltaic Generation on Power Quality in Urban Areas with High PV Population: Results from Monitoring Campaigns*; Tech. Rep.; Intelligent Energy Europe: Brussels, Belgium, 2008; p. 420208.
71. Hirth, L.; Ziegenhagen, I. Control Power and Variable Renewables: A Glimpse at German Data. 2013. Available online: https://www.feem.it/en/publications/feem-working-papers-note-di-lavoro-series/control-power-and-variable-renewables-a-glimpse-at-german-data/ (accessed on 10 July 2021).
72. Regulator, A.E. (Ed.) *Electricity Transmission*; Australian Government: Canberra, Australia, 2009.
73. Operator, A.E.M. Black system south Australia 28 September 2016. *Rep. Aust. Energy Mark. Oper. Ltd.* **2017**.
74. Warren, M. South Australia's Blackouts: It's Not Black or White. Available online: https://www.energycouncil.com.au/analysis/south-australias-blackouts-not-as-simple-as-it-looks/ (accessed on 16 September 2020).
75. Christiansen, W.; Johnsen, D.T. *Analysis of requirements in selected Grid Codes*; Prepared for Orsted-DTU Section of Electric Power Engineering, Technical University of Denmark (DTU): Copenhagen, Denmark, 2006.
76. Cha, S.-T.; Wu, Q.; Østergaard, J. Frequency Stabilizing Scheme for a Danish Island Grid. In Proceedings of the 3rd IEEE PES Innovative Smart Grid Technologies (ISGT) Europe Conference (IEEE PES ISGT Europe 2012), Berlin, Germany, 14–17 October 2012.
77. Møller Andersen, F.; Grenaa Jensen, S.; Larsen, H.V.; Meibom, P.; Ravn, H.; Skytte, K.; Togeby, M. *Analyses of Demand Response in Denmark*; Risoe National Lab.: Roskilde, Denmark, 2006.
78. *DL T 1040–2007 Grid Operation Guidelines*; DOC88: Beijing, China, 2007.
79. Handbook, U.O. *Appendix 1: Load-Frequency-Control and Performance*; UCTE: Brussels, Belgium, 2004.
80. Lazarev, G.; Hrustalyov, V.; Garievskij, M. *Non-Baseload Operation in Nuclear Power Plants: Load Following and Frequency Control Modes of Flexible Operation*; Nuclear Energy Series; International Atomic Energy Agency: Vienna, Austria, 2018; p. 173.
81. Pandurangan, V.; Zareipour, H.; Malik, O. Frequency Regulation Services: A Comparative Study of Select North American and European Reserve Markets. In Proceedings of the 2012 North American Power Symposium (NAPS), Champaign, IL, USA, 9–11 September 2012; pp. 1–8.
82. Gao, D.W.; Muljadi, E.; Tian, T.; Miller, M.; Wang, W. *Comparison of Standards and Technical Requirements of Grid-Connected Wind Power Plants in China and the United States*; National Renewable Energy Lab. (NREL): Golden, CO, USA, 2016.

83. 19963-G.T. *Technical Rule for Connecting Wind Farm to Power System*; State Electricity Regulatory Commission of People's Republic of China: Beijing, China, 2011.
84. Bakshi, A.S.; Croop, D.; Endress, E.; Staschus, K.; Bose, A. *Report of Expert Group to Review and Suggest Measures for Bringing Power System Operation Closer to National Reference Frequency*; Central Electricity Regulatory Commission: New Delhi, India, 2017.
85. Nath, R.; Bakshi, A.S.; Ravinder, S.; Narasimhan, S.R.; Jain, H.; Shrivastava, S.C. *Report of the Expert Group: Review of Indian Electricity Grid Code*; Community Emergency Response Team: New Delhi, India, 2020.
86. Community Emergency Response Team. *Grid Security Need for Tightening of Frequency Band & Other Measures*; Community Emergency Response Team: New Delhi, India, 2011.
87. Committee, E. *Report of the Enquiry Committee on Grid Disturbance in Northern Region on 30th July 2012 and in Northern, Eastern & North-Eastern Region on 31st July, 2012*; Central Electricity Regulatory Commission: New Delhi, India.
88. Undrill, J. *Notes of Frequency Control for the Australian Energy Market Operator*; Australian Energy Market Commission: Canbera, Australia, 2019.
89. Prepared by NERC RS Committee. *Balancing and Frequency Control: A Technical Document Prepared by the NERC Resources Subcommittee*; NERC Technical Report; NERC RS Committee: Atlanta, GA, USA, 2011.
90. Weckx, S.; D'hulst, R.; Driesen, J. Primary and Secondary Frequency Support by a Multi-Agent Demand Control System. *IEEE Trans. Power Syst.* **2014**, *30*, 1394–1404. [CrossRef]
91. Oshnoei, A.; Khezri, R.; Muyeen, S.; Blaabjerg, F. On the contribution of wind farms in automatic generation control: Review and new control approach. *Appl. Sci.* **2018**, *8*, 1848. [CrossRef]
92. Tarnowski, G.C. Coordinated Frequency Control of Wind Turbines in Power Systems with High Wind Power Penetration. Ph.D. Thesis, Technical University of Denmark (DTU), Copenhagen, Denmark, 2012.
93. Perninge, M.; Eriksson, R. Optimal tertiary frequency control in power systems with market-based regulation. *IFAC-Pap* **2017**, *50*, 4374–4381.
94. Force, S.T. *Primary Frequency Response Stakeholder Education Part 1 of 2*; PJM: Audubon, PA, USA, 2017; Available online: https://www.pjm.com/-/media/committees-groups/task-forces/pfrstf/20170901/20170901-primary-frequency-response-education-part-1-of-2.ashx (accessed on 10 July 2021).
95. Power Returns Following Blackouts. *BBC News Channel*, 28 May 2008.
96. Milner, M.; Wearden, G. Q & A: Blackout Britain. *The Guardian*, 2008.
97. Venezuela Crisis: Fresh Power Cuts Black Out Caracas. *BBC News*, 26 March 2019.
98. No End in Sight to Venezuela's Blackout, Experts Warn. *The New York Times*, 11 March 2019.
99. Dayton, R. Maduro's Revolutionary Guards: The Rise of Paramilitarism in Venezuela. *SunSentinel*, 2019.
100. *Blackout Traker: United States Annual Report 2018*; EATON Powering Business Worldwide: Ohio, OH, USA, 2019.
101. Nyberg, M. *2019 Total System Electric Generation*; California Energy Commission: Sacramento, CA, USA, 2020.
102. Mossburg, C. More than 3 Million California Homes May Lose Power in Record Heat Wave Due to Rolling Blackouts. *CNN*, USA. 17 August 2020.
103. Borunda, A. Why Renewables aren't to Blame for California's Blackouts. *National Geographic*, 2020.
104. Kasler, D.; Heerer, M. California Avoided Rolling Blackouts for Two Decades. What Went Wrong on the Grid? *The Sacramento Bee*, 2020.
105. Haes Alhelou, H.; Hamedani-Golshan, M.E.; Njenda, T.C.; Siano, P. A survey on power system blackout and cascading events: Research motivations and challenges. *Energies* **2019**, *12*, 682. [CrossRef]
106. *Blackout Tracker: United States Annual Report 2017*; EATON Power Business Worldwide: Scottsdale, AZ, USA, 2018.
107. Hodge, B.M.S.; Jain, H.; Brancucci, C.; Seo, G.S.; Korpås, M.; Kiviluoma, J.; Holttinen, H.; Smith, J.C.; Orths, A.; Estanqueiro, A. Addressing technical challenges in 100% variable inverter-based renewable energy power systems. *Wiley Interdiscip. Rev. Energy Environ.* **2020**, *9*, e376. [CrossRef]
108. Alani, A.Y.; Osunmakinde, I.O. Short-term multiple forecasting of electric energy loads for sustainable demand planning in smart grids for smart homes. *Sustainability* **2017**, *9*, 1972. [CrossRef]
109. Remon, D.; Cantarellas, A.M.; Mauricio, J.M.; Rodriguez, P. Power system stability analysis under increasing penetration of photovoltaic power plants with synchronous power controllers. *IET Renew. Power Gener.* **2017**, *11*, 733–741. [CrossRef]
110. Peters, D.; Kilper, T.; Calais, M.; Jamal, T.; von Maydell, K. Solar short-term forecasts for predictive control of battery storage capacities in remote PV diesel networks. In *Transition Towards 100% Renewable Energy*; Springer: Berlin/Heidelberg, Germany, 2018; pp. 325–333.
111. Xu, Y.; Zhang, R.; Zhao, J.; Dong, Z.Y.; Wang, D.; Yang, H.; Wong, K.P. Assessing short-term voltage stability of electric power systems by a hierarchical intelligent system. *IEEE Trans. neural Netw. Learn. Syst.* **2015**, *27*, 1686–1696. [CrossRef]
112. Wang, J.; Li, P.; Ran, R.; Che, Y.; Zhou, Y. A short-term photovoltaic power prediction model based on the gradient boost decision tree. *Appl. Sci.* **2018**, *8*, 689. [CrossRef]
113. Du, P.; Wang, J.; Yang, W.; Niu, T. A novel hybrid model for short-term wind power forecasting. *Appl. Soft Comput.* **2019**, *80*, 93–106. [CrossRef]
114. Barbounis, T.G.; Theocharis, J.B.; Alexiadis, M.C.; Dokopoulos, P.S. Long-term wind speed and power forecasting using local recurrent neural network models. *IEEE Trans. Energy Convers.* **2006**, *21*, 273–284. [CrossRef]
115. Negnevitsky, M.; Nguyen, D.H.; Piekutowski, M. Risk assessment for power system operation planning with high wind power penetration. *IEEE Trans. Power Syst.* **2014**, *30*, 1359–1368. [CrossRef]

116. Mitra, A.; Chatterjee, D. Active power control of DFIG-based wind farm for improvement of transient stability of power systems. *IEEE Trans. Power Syst.* **2015**, *31*, 82–93. [CrossRef]
117. Tielens, P.; Henneaux, P.; Cole, S. Penetration of renewables and reduction of synchronous inertia in the European power system-Analysis and solutions. ASSET project, DG Energy Unit C.2. European Uunion, 2018.
118. Shrestha, A.; Ghimire, B.; Gonzalez-Longatt, F. A Bayesian Model to Forecast the Time Series Kinetic Energy Data for a Power System. *Energies* **2021**, *14*, 3299. [CrossRef]
119. Ulbig, A.; Borsche, T.S.; Andersson, G. Impact of low rotational inertia on power system stability and operation. *IFAC Proc. Vol.* **2014**, *47*, 7290–7297. [CrossRef]
120. Zografos, D. *Power System Inertia Estimation and Frequency Response Assessment*; KTH Royal Institute of Technology: Stockholm, Sweden, 2019.
121. Kundur, P.; Paserba, J.; Ajjarapu, V.; Andersson, G.; Bose, A.; Canizares, C.; Hatziargyriou, N.; Hill, D.; Stankovic, A.; Taylor, C. Definition and classification of power system stability IEEE/CIGRE joint task force on stability terms and definitions. *IEEE Trans. Power Syst.* **2004**, *19*, 1387–1401.
122. Kundur, P.; Balu, N.J.; Lauby, M.G. *Power System Stability and Control*; McGraw-hill: New York, NY, USA, 1994; Volume 7.
123. Meegahapola, L.; Sguarezi, A.; Bryant, J.S.; Gu, M.; Conde D, E.R.; Cunha, R. Power System Stability with Power-Electronic Converter Interfaced Renewable Power Generation: Present Issues and Future Trends. *Energies* **2020**, *13*, 3441. [CrossRef]
124. Munkhchuluun, E.; Meegahapola, L.; Vahidnia, A. The Large Disturbance Rotor Angle Stability with DFIG Wind Farms. In Proceedings of the 2019 9th International Conference on Power and Energy Systems (ICPES), Perth, Australia, 10–12 December 2019; pp. 1–6.
125. Mansouri, N.; Lashab, A.; Sera, D.; Guerrero, J.M.; Cherif, A. Large photovoltaic power plants integration: A review of challenges and solutions. *Energies* **2019**, *12*, 3798. [CrossRef]
126. Qdr, Q. *Benefits of Demand Response in Electricity Markets and Recommendations for Achieving Them*; Tech. Rep; US Dept. Energy: Washington, DC, USA, 2006.
127. Albadi, M.H.; El-Saadany, E.F. A summary of demand response in electricity markets. *Electr. Power Syst. Res.* **2008**, *78*, 1989–1996. [CrossRef]
128. Khadka, N.; Bista, A.; Adhikari, B.; Shrestha, A.; Bista, D.; Adhikary, B. Current Practices of Solar Photovoltaic Panel Cleaning System and Future Prospects of Machine Learning Implementation. *IEEE Access* **2020**, *8*, 135948–135962. [CrossRef]
129. Shrestha, A.; Bishwokarma, R.; Chapagain, A.; Banjara, S.; Aryal, S.; Mali, B.; Thapa, R.; Bista, D.; Hayes, B.P.; Papadakis, A. Peer-to-peer energy trading in micro/mini-grids for local energy communities: A review and case study of Nepal. *IEEE Access* **2019**, *7*, 131911–131928. [CrossRef]
130. Shrestha, A.; Kattel, R.; Dachhepatic, M.; Mali, B.; Thapa, R.; Singh, A.; Bista, D.; Adhikary, B.; Papadakis, A.; Maskey, R.K. Comparative study of different approaches for islanding detection of distributed generation systems. *Appl. Syst. Innov.* **2019**, *2*, 25. [CrossRef]
131. Shrestha, P.; Shrestha, A.; Shrestha, N.T.; Papadakis, A.; Maskey, R.K. Assessment on scaling-up of mini-grid initiative: Case study of mini-grid in rural Nepal. *Int. J. Precis. Eng. Manuf.-Green Technol.* **2021**, *8*, 217–231. [CrossRef]
132. Dong, D.; Wen, B.; Boroyevich, D.; Mattavelli, P.; Xue, Y. Analysis of phase-locked loop low-frequency stability in three-phase grid-connected power converters considering impedance interactions. *IEEE Trans. Ind. Electron.* **2014**, *62*, 310–321. [CrossRef]
133. Anani, N.; Al-Kharji AlAli, O.; Al-Qutayri, M.; Al-Araji, S. Synchronization of a renewable energy inverter with the grid. *J. Renew. Sustain. Energy* **2012**, *4*, 043103. [CrossRef]
134. Rocabert, J.; Luna, A.; Blaabjerg, F.; Rodriguez, P. Control of power converters in AC microgrids. *IEEE Trans. Power Electron.* **2012**, *27*, 4734–4749. [CrossRef]
135. Paquette, A.D.; Reno, M.J.; Harley, R.G.; Divan, D.M. Sharing transient loads: Causes of unequal transient load sharing in islanded microgrid operation. *IEEE Ind. Appl. Mag.* **2013**, *20*, 23–34. [CrossRef]
136. Paolone, M.; Gaunt, T.; Guillaud, X.; Liserre, M.; Meliopoulos, S.; Monti, A.; Van Cutsem, T.; Vittal, V.; Vournas, C. Fundamentals of power systems modelling in the presence of converter-interfaced generation. *Electr. Power Syst. Res.* **2020**, *189*, 106811. [CrossRef]
137. Johnson, S.C.; Rhodes, J.D.; Webber, M.E. Understanding the impact of non-synchronous wind and solar generation on grid stability and identifying mitigation pathways. *Appl. Energy* **2020**, *262*, 114492. [CrossRef]
138. De Brabandere, K.; Bolsens, B.; Van den Keybus, J.; Woyte, A.; Driesen, J.; Belmans, R. A voltage and frequency droop control method for parallel inverters. *IEEE Trans. Power Electron.* **2007**, *22*, 1107–1115. [CrossRef]
139. Qoria, T.; Gruson, F.; Colas, F.; Guillaud, X.; Debry, M.-S.; Prevost, T. Tuning of cascaded controllers for robust grid-forming Voltage Source Converter. In Proceedings of the 2018 Power Systems Computation Conference (PSCC), Dublin, Ireland, 11–15 June 2018; pp. 1–7.
140. D'Arco, S.; Suul, J.A.; Fosso, O.B. Automatic tuning of cascaded controllers for power converters using eigenvalue parametric sensitivities. *IEEE Trans. Ind. Appl.* **2014**, *51*, 1743–1753. [CrossRef]
141. Johnson, B.B.; Sinha, M.; Ainsworth, N.G.; Dörfler, F.; Dhople, S.V. Synthesizing virtual oscillators to control islanded inverters. *IEEE Trans. Power Electron.* **2015**, *31*, 6002–6015. [CrossRef]
142. Seo, G.-S.; Colombino, M.; Subotic, I.; Johnson, B.; Groß, D.; Dörfler, F. Dispatchable virtual oscillator control for decentralized inverter-dominated power systems: Analysis and experiments. In Proceedings of the 2019 IEEE Applied Power Electronics Conference and Exposition (APEC), Anaheim, CA, USA, 17–21 March 2019; pp. 561–566.

143. Li, Z.; Zang, C.; Zeng, P.; Yu, H.; Li, S.; Bian, J. Control of a Grid-Forming Inverter Based on Sliding-Mode and Mixed $H_2/H\infty$ Control. *IEEE Trans. Ind. Electron.* **2016**, *64*, 3862–3872. [CrossRef]

144. Qoria, T.; Li, C.; Oue, K.; Gruson, F.; Colas, F.; Guillaud, X. Direct AC voltage control for grid-forming inverters. *J. Power Electron.* **2020**, *20*, 198–211. [CrossRef]

145. Dörfler, F. Control of Power Converters in Low-Inertia Power Systems. In *KTH Workshop: Emerging Topics in Control of Power Systems*; KTH Campus: Södertälje, Sweden; Available online: https://sites.google.com/view/kth-topics-power-system/home (accessed on 12 December 2020).

146. Liang, X.; Karim, C.A.B. Virtual synchronous machine method in renewable energy integration. In Proceedings of the 2016 IEEE PES Asia-Pacific Power and Energy Engineering Conference (APPEEC), Xi'an, China, 25–28 October 2016; pp. 364–368.

147. Yap, K.Y.; Sarimuthu, C.R.; Lim, J.M.-Y. Virtual Inertia-Based Inverters for Mitigating Frequency Instability in Grid-Connected Renewable Energy System: A Review. *Appl. Sci.* **2019**, *9*, 5300. [CrossRef]

148. Mosca, C.; Arrigo, F.; Mazza, A.; Bompard, E.; Carpaneto, E.; Chicco, G.; Cuccia, P. Mitigation of frequency stability issues in low inertia power systems using synchronous compensators and battery energy storage systems. *IET Gener. Transm. Distrib.* **2019**, *13*, 3951–3959. [CrossRef]

149. Liu, J.; Hossain, M.; Lu, J.; Rafi, F.; Li, H. A hybrid AC/DC microgrid control system based on a virtual synchronous generator for smooth transient performances. *Electr. Power Syst. Res.* **2018**, *162*, 169–182. [CrossRef]

150. Bevrani, H.; Ise, T.; Miura, Y. Virtual synchronous generators: A survey and new perspectives. *Int. J. Electr. Power Energy Syst.* **2014**, *54*, 244–254. [CrossRef]

151. Shintai, T.; Miura, Y.; Ise, T. Oscillation damping of a distributed generator using a virtual synchronous generator. *IEEE Trans. Power Deliv.* **2014**, *29*, 668–676. [CrossRef]

152. Liu, J.; Miura, Y.; Ise, T. Power quality improvement of microgrids by virtual synchronous generator control. In Proceedings of the 2016 Electric Power Quality and Supply Reliability (PQ), Tallinn, Estonia, 29–31 August 2016; pp. 119–124.

153. D'Arco, S.; Suul, J.A. A synchronization controller for grid reconnection of islanded virtual synchronous machines. In Proceedings of the 2015 IEEE 6th International Symposium on Power Electronics for Distributed Generation Systems (PEDG), Aachen, Germany, 22–25 June 2015; pp. 1–8.

154. Poolla, B.K.; Bolognani, S.; Dörfler, F. Optimal placement of virtual inertia in power grids. *IEEE Trans. Autom. Control.* **2017**, *62*, 6209–6220. [CrossRef]

155. Peña Asensio, A.; Gonzalez-Longatt, F.; Arnaltes, S.; Rodríguez-Amenedo, J.L. Analysis of the Converter Synchronizing Method for the Contribution of Battery Energy Storage Systems to Inertia Emulation. *Energies* **2020**, *13*, 1478. [CrossRef]

156. Marrazi, E.; Yang, G.; Weinreich-Jensen, P. Allocation of synchronous condensers for restoration of system short-circuit power. *J. Mod. Power Syst. Clean Energy* **2018**, *6*, 17–26. [CrossRef]

157. ElectraNet. *Economic Life for ElectraNEt Synchronous Condensers*; GHD Advisory: Canbera, Australia, 2019.

158. Energy Sector Management Assistance Program. *Grid Integration Requirements for Variable Renewable Energy*; World Bank eLibrary: Washington, DC, USA, 2019.

Article 3

Shrestha, A. and Gonzalez-Longatt, F., 2021. Parametric sensitivity analysis of rotor angle stability indicators. Energies, vol. 14, issue 16, pp. 5023. doi: 10.3390/en14165023

energies MDPI

Article

Parametric Sensitivity Analysis of Rotor Angle Stability Indicators †

Ashish Shrestha * and Francisco Gonzalez-Longatt *

Department of Electrical Engineering, Information Technology and Cybernetics, University of South-Eastern Norway, N-3918 Porsgrunn, Norway
* Correspondence: sthashish2010@gmail.com (A.S.); fglongatt@fglongatt.org (F.G.-L.)
† This paper is an extended version of a paper that will be presented at the 8th International Conference on Power and Energy Systems Engineering at Fukuoka Institute of Technology, Fukuoka, Japan, 10–12 September 2021.

Abstract: With the increasing penetration rate of Power Electronic Converter (PEC) based technologies, the electrical power systems are facing the problem of transient stability since the PEC based technologies do not contribute to the system inertia, and the proportion of synchronous generators (i.e., the source of inertia) is in decreasing rate. In addition, PEC based technologies' components have poor inherent damping. It is very important to analyze the system characteristics of a power system to minimize the potential instabilities during the contingencies. This paper presents the parametric sensitivity analysis of the rotor angle stability indicators for the 39-bus New England power system. The indicators of rotor angle stability analysis such as critical fault clearing time (CCT), Eigenvalue points, damping ratio, frequency deviation, voltage deviation, and generator's speed deviation are identified and analyzed for three case scenarios; each scenario has six sub-cases with different inertia constants. The results show that the CCTs for each component will be reduced if the inertia reduces at any section of a multi-machine power system. Although the applied three scenarios with six sub-cases are identified to be stable in this analysis, the decreasing inertia constant has significant impact on the power system dynamics.

Keywords: power system dynamics; power system stability; low inertial power system

1. Introduction

Power systems have become more complex than in the past, caused by the integration of numerous Distributed Generation Resources (DGRs) and the rapidly growing power electronic converter (PEC) based technologies. The modern power system faces complex transformation in all levels, such as generation, transmission, distribution, and utilization [1]. With this rapid transformation, the modern power system faces significant changes in the power system dynamics; one of the main reasons behind this is reduction of system inertia because of these PEC-based technologies [2]. In the conventional power system, most of the power generators were of the synchronous type; they are characterized as the source of rotational inertia in a power system, whereas in a modern power system, the proportion of synchronous generators is at a decreasing rate [3]. Moreover, the PEC-based technologies adopted in the generation (e.g., kinetic energy less solar PV and doubly-fed induction generator based wind turbines), transmission line (e.g., HVDC), distribution system (e.g., controllers), and utilization level (e.g., controller based equipment) do not contribute to the system inertia, which results in a drop of system inertia in the modern power system, resulting in drastic changes in the system dynamics [4]. Not only these but the transient stability of the DGR integrated power system is also highly sensitive to the proportion of the penetration level, fault location and its severity [5]. Titlens et al. presented a detailed study on the relevance of inertia in the operation and control of a power system, which shows that the decreasing system inertia results in the high Rate of Change of Frequency (RoCoF) values and frequency deviation, which may increase the system instability [6]. The DGRs are integrated into the distribution lines at a low voltage

level, which increases the amount of fault current [7]. Hence the penetration of DGRs on a considerable scale can lead to problems in overall frequency response, transient stability, fault rid-through capability, voltage response, load-following capability and system regulation [8].

Impact assessment is an important task from the planning and operation prospects since an unidentified proportion of parameters may create system instability and even system blackouts, especially after a fault within that system. Some studies had been conducted to assess system performance and their sensitivity under a different mode of operations. Jorge performed an assessment on the frequency and transient stability of the RESs penetrated grid, in which the author focused on the transient instability in the power system by considering the grid parameters [9]. A study [10], proposed a systematic approach to analyzing the transient stability of the 39-bus New England power system, where the authors considered the generator-based threshold as a limit function. Similarly, Perilla et al. investigated the degree of the transient stability enhancement in the wind turbine integrated power system via parametric sensitivity and sophisticated approaches [11]. Sajadi et al. presented a comprehensive study on established transient stability indicators including rotor angle difference, rate of machine acceleration, and transient potential and kinetic energies [12]. Tamimi et al. investigated the impact of penetration levels of solar PV through small-signal stability for the real data of Ontario power system and its neighboring system, which concluded that the distributed solar systems are more advantageous than the single solar farm considering the stability of a power system [13]. However, the eigenvalue analysis showed that the DGR penetration has no significant impacts on small-signal stability [13]. On the other hand, Pieter Tielens concluded that the eigenvalues move toward the negative of the real part with poor damping with the decreasing inertia, and the system stability becomes sensitive with the generation plant's location [14]. Wang et al. conducted a study on the CCTs for a microgrid system under fault conditions, which concluded that the CCTs are highly sensitive to the DGR penetration level and the wind turbine crowbar protection insertion time [15]. Sadhana et al. conducted the small signal stability analysis for the grid-tied DGR with the effect of uncertain wind turbine penetration by using Lyapunov's stability criteria and concluded that the wind penetration has no effects on the low-frequency oscillation at a remote area [16].

Studies conducted for a variety of case studies present different results and conclusions, which may mislead the audience. The same factors that have been found to be sensitive for a case have not been found to be sensitive for other cases. However, the parametric sensitivity analysis is very important to analyze the power system dynamics, which can help to reduce the potential effects on a specific case system. Hence, this paper is conducted to analyze the parametric sensitivity of the rotor angle stability indicators of a multi-machine power system. The major contributions of this paper are as follows:

a. Transient stability assessment and small-signal stability assessment are conducted to calculate the indicators considering the three scenarios and six sub-cases. The DIgSILENT Programming Language (DPL) is used as the scripting tool for the execution task, and the case study of 39 Bus New England power system is taken for this study. Statistical analysis has been performed to analyze and visualize the characteristics of the indicators in different cases and sub-cases.

b. The assessments have been conducted for both the transmission lines and the bus systems. Different DPL has been implemented to evaluate the indicators for both systems.

c. The area-wise impact of reduced inertia has been discussed within a multi-machine power system. For this, the inertia of an area is reduced, and its impacts on overall system have been observed. From this analysis, it is found that the reduced inertia affects the local area significantly, whereas the neighboring areas have been less affected.

The authors of this paper aim to present the parametric sensitivity analysis of the rotor angle stability indicators with the power system inertia, which may help to analyze the

dynamics of that system under its normal operation as well as in contingency. This paper first discussed the stability problems that occur in the power system by DGR penetration via previously published works. Section 2 presents the adopted methodology and the assumptions made during the analysis. The obtained results are discussed in Section 3, based on which conclusions have been drawn and discussed in Section 4.

2. Method and Assumptions

CCT is the time interval up to which the occurred fault must be cleared so that the system retains its stability, and it is important to analyze the performance evaluation that can be depended on various factors such as inertia constant of a machine, system frequency, critical clearing angle and the initial power angle [17]. CCT has an important role in the power system since the system must restore its original state within that time. A lower value of CCT leads to system instability if the system is unable to retain its original state within that value of time. Similarly, the eigenvalue is the next indicator used in the rotor angle stability analysis. The eigenvalues are the system modes (or value of the system property) that provide the status of a system in a linear invariant system. It must require to be stable of all modes for a stable power system; all of the conjugated eigenvalues ($\alpha \pm j\omega$) must have the negative valued real part. For a stable power system, it is also desired that the oscillations of electromechanical machines must be damped out as soon as possible. For simplicity, the outcomes of the eigenvalue analysis are presented in the form of damped frequency and damping for each system mode. During the analysis, the system is considered as the classic one; hence, there are 2*n modes for n number of generators (e.g., 20 modes for 10 generators). The small-signal stability analysis should be conducted for the obtained modes.

The parametric sensitivity analysis is the study of uncertainty; how a parameter within a function differs from the changes in other values. It has an important role in the system performance assessment from the planning prospects. The main objective of this paper is to present the parametric sensitivity analysis of the rotor angle stability indicators with the power system inertia (i.e., T_{CCT}, λ, ω and ζ). However, the rotor angle stability analysis is highly dimensioned and non-linear from the mathematical point of view, and is presented by a set of differential-algebraic equations as given in Equation (1) [14]:

$$\frac{dX}{dt} = F(X, Y, P) \tag{1}$$

Here, F is the function, X ($X \epsilon \mathbb{R}^{n_x}$) is the vector state variables, Y ($Y \epsilon \mathbb{R}^{n_y}$) is the vector of algebraic variables, and P ($P \epsilon \mathbb{R}^{n_p}$) is the vector of parameters, for the electromechanical dynamics within a power system. Equation (1) presents the dynamics of the power system network, static loads and the generator's stator equation. The dynamics of a synchronous machine can be described by the following differential equation (i.e., swing equation):

$$\frac{2H}{\omega_s} \frac{\partial^2 \delta}{\partial t^2} = \frac{P_m - P_e}{S_{rated}} \tag{2}$$

Here H is the inertia constant in MJ/MVA, S_{rated} is the rating of that machines in MVA, P_m and P_e are the mechanical and electrical power in MW, and ω_s is the angular frequency. The simplified swing equation for a multi-machine system can be written as follows:

$$\frac{2H_{sys}}{\omega_s} \frac{\partial^2 \delta_{sys}}{\partial t^2} = P_m - P_e \text{ [in pu]} \tag{3}$$

However, if the small signal approximation is considered for a multi-machine power system, the dynamic behaviour of an equivalent system can be expressed as Equation (4), where K_D is the damping constant for the equivalent system, and δ_0 is the initial power angle.

$$\frac{2H_{sys}}{\omega_s}\frac{\partial^2\delta_{sys}}{\partial t^2} + K_D\frac{\partial\delta_{sys}}{\partial t} + P_{max}\cos(\delta_0)\delta_{sys} = 0 \tag{4}$$

Equations (5)–(7) present the mathematical expressions for the CCT, overall system frequency and the damping for a power system. From the Equations, the indicators are found to be dependent on the system inertia.

$$T_{CCT} = \sqrt{\frac{4H_{sys}}{\omega_s\,P_{max}}(\delta_{CCT} - \delta_0)}\ [\text{in s}] \tag{5}$$

$$\omega_{sys} = \sqrt{\frac{\omega_s\,P_{max}\cos\delta_0}{2H_{sys}}}\ [\text{in rad/s}] \tag{6}$$

$$\zeta = \frac{1}{2}K_D\sqrt{\frac{\omega_s}{2H_{sys}\,P_{max}\,\cos\delta_0}} \tag{7}$$

In this paper, the parametric sensitivity analysis of such indicators has been conducted with respect to the inertia constants. From these mathematical expressions, it can be concluded that the rotor angle stability indicators are dependent on the system inertia constant, and the stability analysis of such indicators can be conducted concerning system inertia for a specific case, which further helps to analyze the system dynamics under different operating conditions.

This paper takes the IEEE 39 Bus New England power system as the case study that contains ten generators, 39 buses and 33 connecting lines as shown in Figure 1. The total system is divided into three parts (i.e., West, North and South) based on their geographical structure and separated by the blue lines as shown in Figure 1. The West area is considered as a single generator for the aggregated power system containing multi-machines (i.e., G1), whereas the North area contains three generators (i.e., G8, G9, and G10) and the South area contains six generators (i.e., G2, G3, G4, G5, G6, and G7). All of the components of the power system are modelled in a powerful tool called DIgSILENT PowerFactory for the analysis, and the DIgSILENT Programming Language (DPL) is used as the scripting tool for the execution task. The DPL files created to evaluate the CCTs for transmission lines and Bus systems can be found in [18,19]. Similarly, the information of the components is referred to from a paper [20]. After the interfacing of DPLs with the network in DIgSILENT PowerFactory, the transient stability assessment is conducted to evaluate the values of CCTs and the small-signal stability assessment for the eigenvalues, damping, and damped frequency.

For the sensitivity analysis of the inertia constant, three scenarios and six sub-cases for each scenario have been considered in this study. As shown in Table 1, in the first scenario, the inertia level of the West and South areas was taken as normal and that of the North area is considered as low. Similarly, the inertia level of the South area is taken as low in the second scenario, whereas both areas (North and South) are considered with low inertia levels in the third scenario. The nominal values of the inertia constants are considered as the original value taken from the source [20], whereas for low inertia value, five steps (i.e., 50, 60, 70, 80, and 90% of nominal inertia value) have been implemented and analyzed with six sub-cases (i.e., base case H, 0.9H, 0.8H, 0.7H, 0.6H, and 0.5H). The important indicators of the power system stability such as CCTs, eigenvalue points, damping, and damped frequency are identified for these three scenarios and the sub-cases, and the conclusions have been drawn from the observed results.
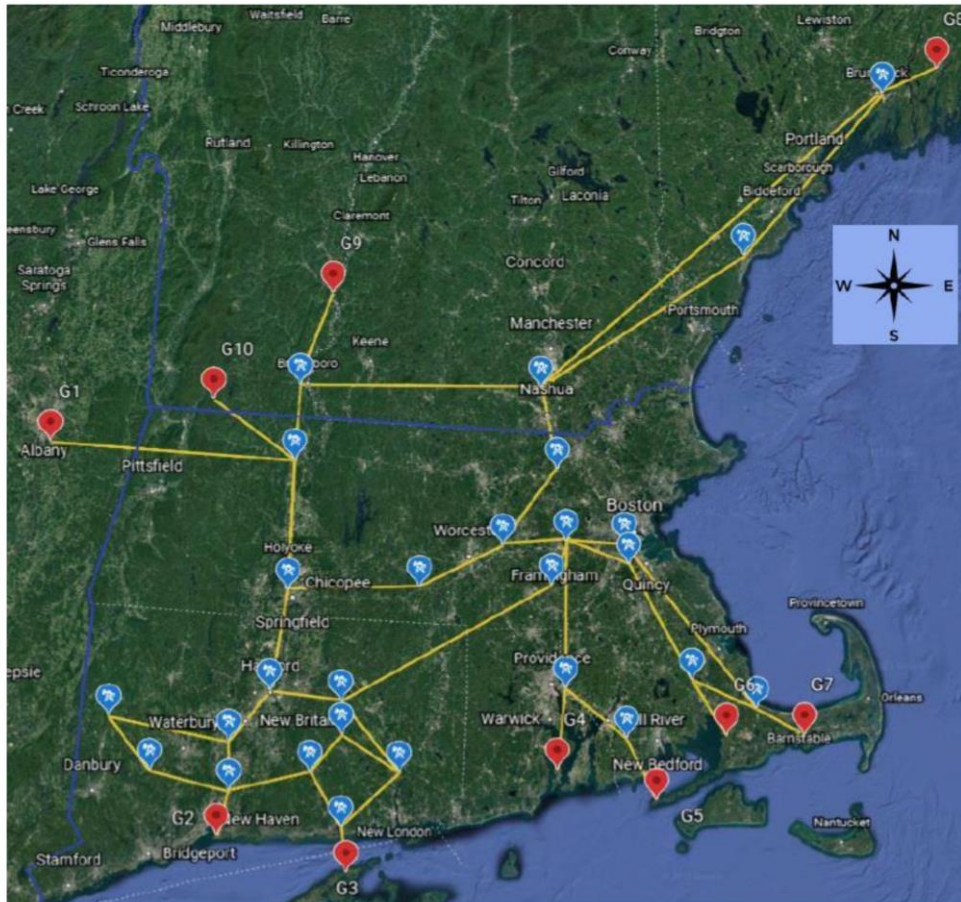
Figure 1. The divided three zones of IEEE 39 Bus New England power system. Here in the Figure, the Generator buses are presented with the red place-marks, PQ buses are with the blue place-marks, and the transmission lines are with yellow lines.

Table 1. Assumed cases for the sensitivity analysis.

Scenarios	West	North	South
a	Normal	Low	Normal
b	Normal	Normal	Low
c	Normal	Low	Low

3. Simulation Outcomes

For the case study of 39 Bus New England power system, the CCTs at each transmission line have been identified by considering the three scenarios and six sub-cases. During the analysis, at first, a fault is created in a line, and the DPL is used to identify the CCTs for each transmission line. The results obtained from the simulation have been visualized and presented in Figure 2. Figure 2a–c presents the CCTs obtained at each transmission line at different values of inertia constant (i.e., H, 0.9H, 0.8H, 0.7H, 0.6H, and 0.5H), and categorized for the three scenarios as given in Table 1. In most of the transmission lines,

the CCTs decrease with the decrease in inertia constant, which can be seen in the figure clearly. In comparison to scenario 'a', scenario 'b' has more difference rate, while scenario 'c' has more difference rate than the other two scenarios since the overall system inertia is decreased in the same way (i.e., $H_a > H_b > H_c$). In Figure 2, the slope of the graph indicates the difference rate of the CCTs for the scenarios, where it is found to be higher in scenario 'c' in comparison to the other two scenarios. In all of the scenarios, the CCTs for the transmission lines near the G1 (i.e., Line 03–04, Line 01–39, Line 09–39, and Line 01–02) are observed to be quite higher than compared to others. To investigate the reason behind this, the CCTs at separate areas of the power system have been identified in different scenarios with all sub-cases. The detailed information on the CCTs is listed in Table 2.

Table 2. CCTs in different areas of 33-bus New England system at different scenarios.

	Scenarios	a (s)	b (s)	c (s)
West	Base case	0.9960	0.9960	0.9960
	0.9H	0.9810	0.9505	0.9090
	0.8H	0.8790	0.8560	0.7575
	0.7H	0.8790	0.7195	0.6740
	0.6H	0.8785	0.6285	0.5905
	0.5H	0.8330	0.5680	0.4995
North	Base case	0.2033	0.2033	0.2033
	0.9H	0.1986	0.1966	0.1901
	0.8H	0.1911	0.1873	0.1741
	0.7H	0.1817	0.1778	0.1608
	0.6H	0.1693	0.1663	0.1446
	0.5H	0.1589	0.1531	0.1276
South	Base case	0.2415	0.2415	0.2415
	0.9H	0.2415	0.2265	0.2255
	0.8H	0.2415	0.2093	0.2083
	0.7H	0.2405	0.1951	0.1941
	0.6H	0.2405	0.1761	0.1701
	0.5H	0.2405	0.1580	0.1549

As given in Table 2, in all of the cases, the values of CCTs are decreasing from top to down and left to right, since the inertia constant is decreasing in the same order. In scenario 'a', only the inertia of the North area is reduced, but Table 2 shows that the decreased inertia affects the CCTs at all the power systems. However, the difference rate is observed to be higher in the North area and lower in the other two scenarios. Similarly, in scenario 'b', the difference rate is higher in the South area, since the inertia of the South area is reduced in this scenario. Significant effects can be observed in scenario 'c', since the decreased inertia in that scenario is higher in comparison to other scenarios (decreased inertia in the North and South area). From this, it is clear that the CCTs depend on the location. Not only that, the CCTs for all of the components are observed to be reduced with a certain difference rate with the change in inertia at a place. From this data, it is clearly shown that the CCTs of all components decrease with the decrease in inertia at any section of the multi-machine power system, although the effect is higher in the local area and less in the neighboring areas.

On the other side, Figure 3 presents the characteristics of the CCTs for the bus system after disturbance. A similar process to transmission line has been applied to analyze the CCTs at the bus system by creating a fault at a specified bus bar. Like Figure 2, Figure 3a–c presents the CCTs obtained at different bus bars at different values of inertia constant (i.e., H, 0.9H, 0.8H, 0.7H, 0.6H, and 0.5H), but in this stage, the authors have selected a sampled number of buses (i.e., Bus 1, Bus 6, Bus 16, Bus 19, and Bus 29). There is no reason behind the selection of the specified buses; it is just a collection of buses from diverse areas for the purpose of analyzing their nature. From this analysis, it is observed that the CCTs for the buses show the same nature as for the transmission lines: decrease with the decreasing

system inertia. The decreasing rate of CCTs in scenario 'a' is lower than that of scenario 'b', and that in scenario 'b' is lower than that of scenario 'c'.
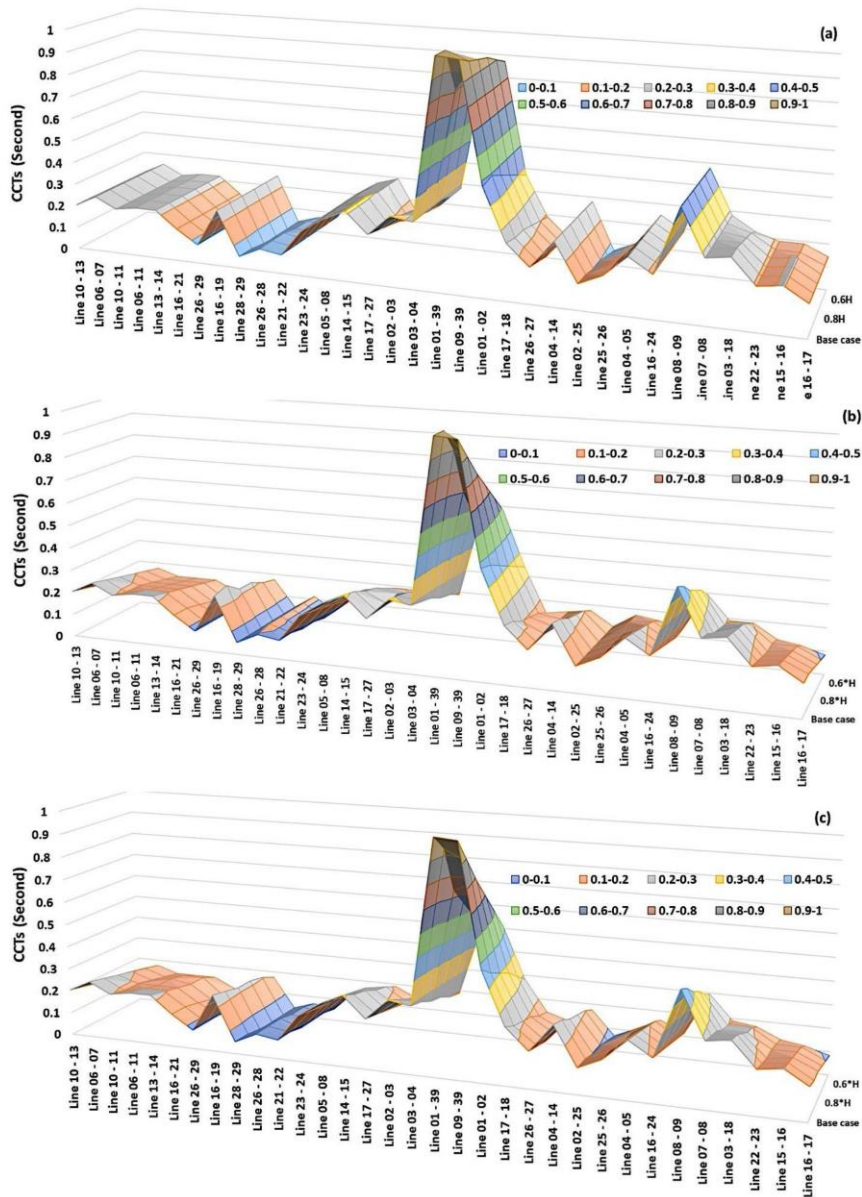

**Figure 2.** Sensitivity analysis of inertia constant with the CCTs at transmission lines for three scenarios (**a**), (**b**) and (**c**).
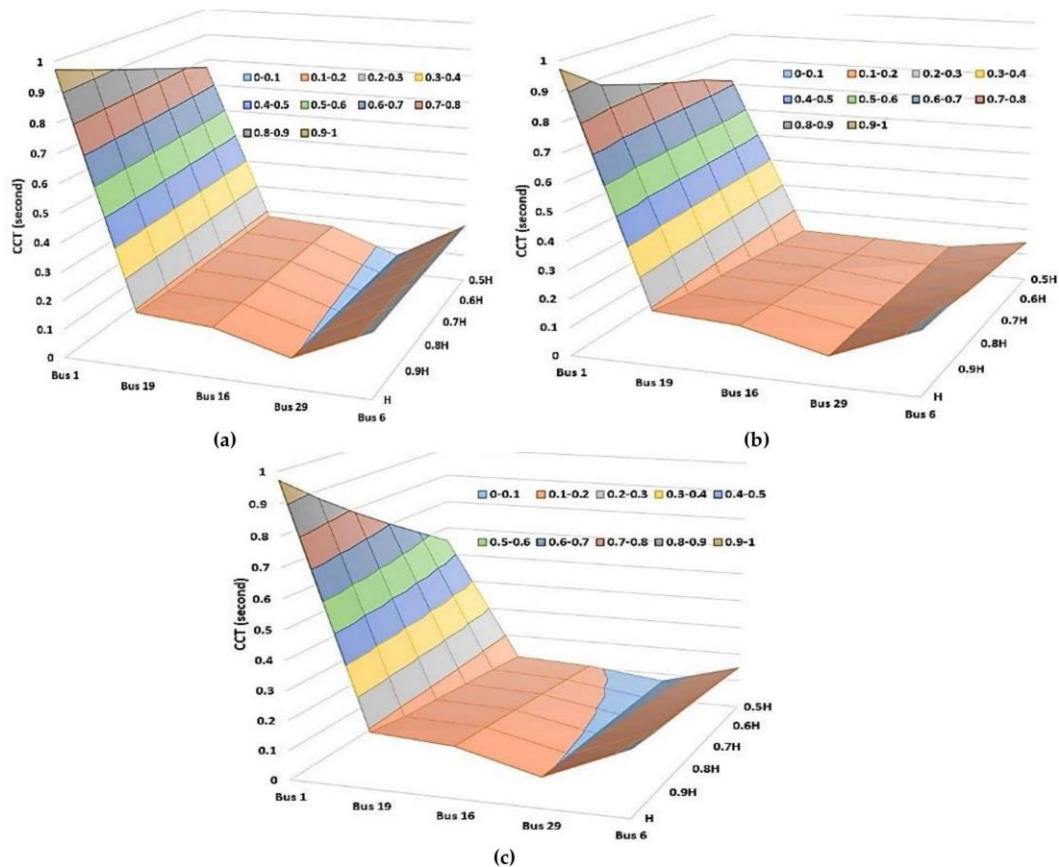
Figure 3. Sensitivity analysis of inertia constant with the CCTs at buses for three scenarios (**a**), (**b**) and (**c**).

Similarly, Figure 4 presents the frequency dynamics at the buses, when the system inertia of all systems differs. At this stage, the inertia of all generators has been changed, and the frequency dynamics are analyzed. As shown in Figure 4, the first spike just after the fault is similar in all cases, but the magnitude of other spikes increases with the decreasing system inertia, although the natures of the spikes are similar. At the original system inertia, the peak frequency is calculated to be 60.68 Hz, whereas the value is calculated to be 61.39 Hz when the system inertia is set to 50%. The number of wave cycle is also increasing for a constant time period of 5 s with the decreasing order of system inertia. A similar effect can be shown in the voltage deviation: higher swing nature with reduced system inertia, as shown in Figure 5. Similarly, the speed deviation of the generators is also affected with the system inertia. As shown in Figure 6, the speed deviation of the generator increases with the decreases in system inertia. The maximum speed deviation is observed in the Generator 7, which is calculated to be 0.8Hz at original system inertia and 1.5 Hz at 0.5H. From all these characteristics, it is observed that the indicators of the power system stability are dependent on the system inertia.
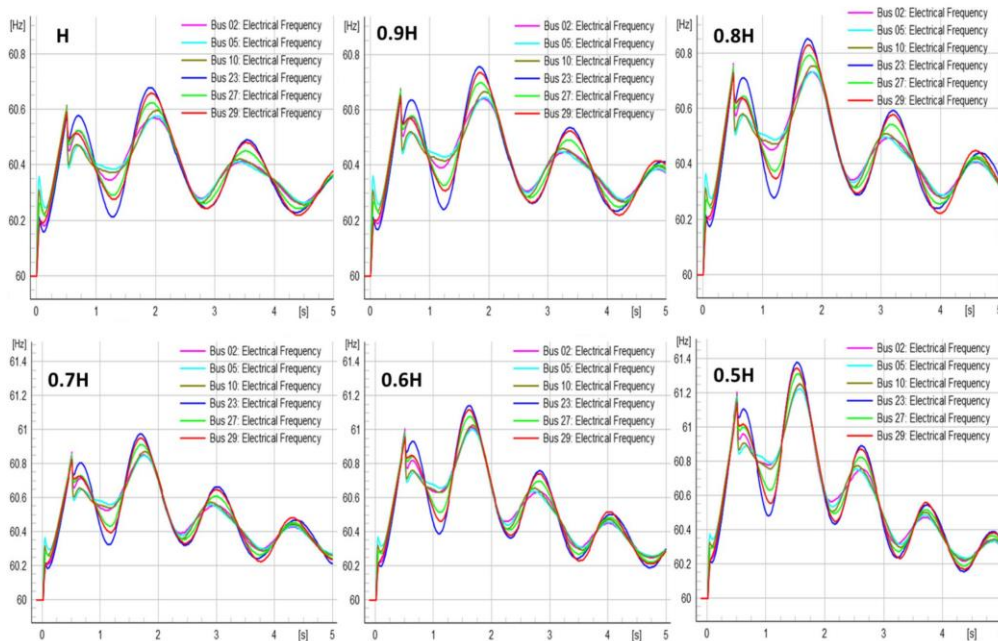
**Figure 4.** Electrical frequency (in Hz) at buses with different generator inertia constants.
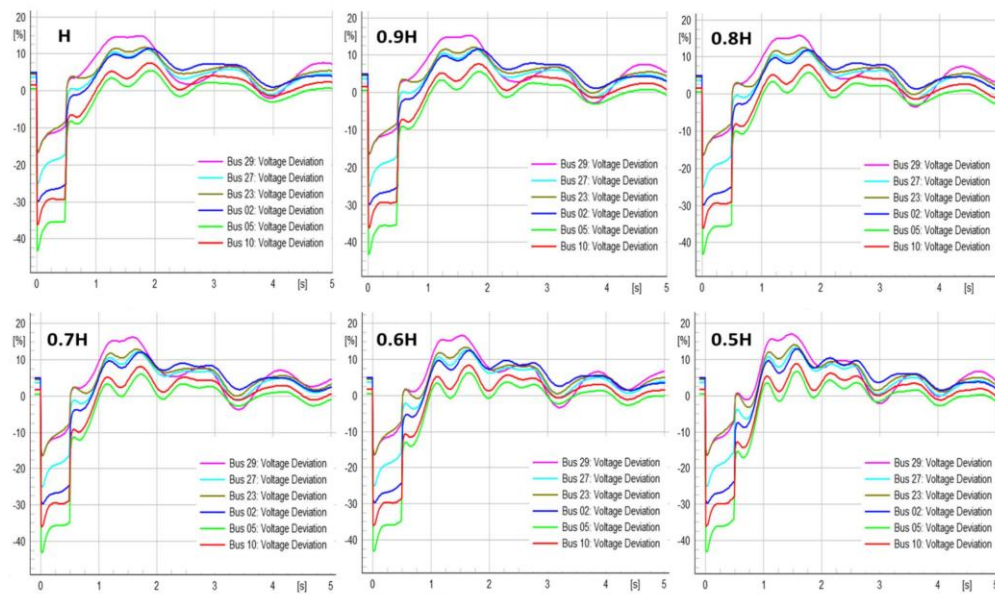
Figure 5. Voltage deviation (in %) at buses with different generator inertia constants.
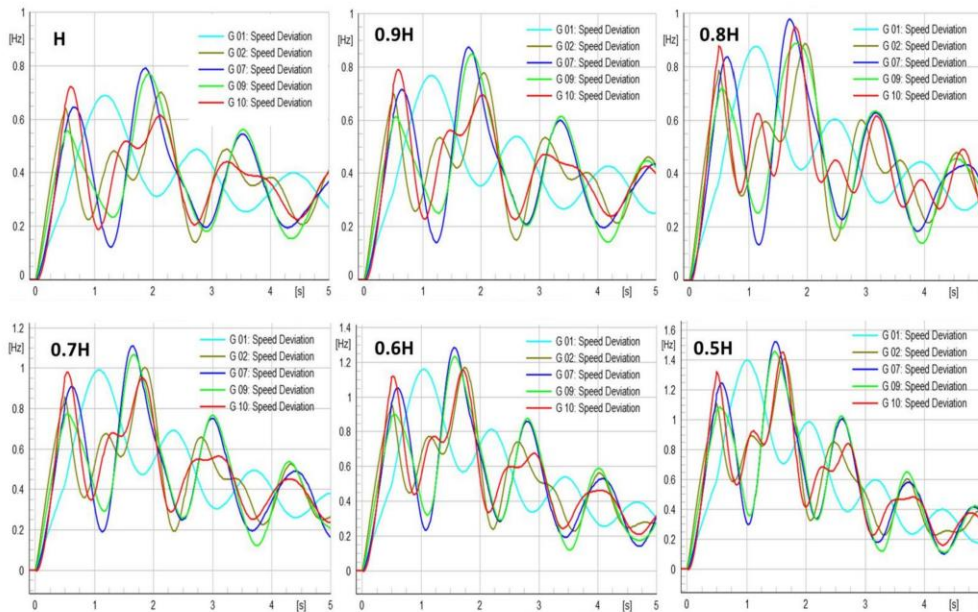
Figure 6. Speed deviation in the generators at different inertia constants.

On the other side, the small-signal stability analysis is conducted to analyze the stability of the case study with the decreasing system inertia constants. The small-signal stability analysis is conducted through the eigenvalue analysis, and the results are shown in Figure 7. Figure 7a–c is the graphs that show the nature of real and imaginary values of eigenvalue points for the three scenarios. It is clearly shown that all of the eigenvalue points lie on negative real parts, which means the system is stable for all of the scenarios. However, the eigenvalue locus can be easily traced for scenario 'a', in comparison to the other two scenarios. From the figures, it is observed that the eigenvalue points scatter more with the decrease in inertia constant.

Similarly, Figure 8 presents the sensitivity of the damping with the inertia constant for the assumed scenarios. The results show that the damping decreases with the increase in the inertia constant. Moreover, it is observed that the slope of the drop is higher in scenario 'b' than that in scenario 'a', and also scenario 'c' has a higher drop than the others. For the first scenario, the peak value of damping for Mode 19 is 0.097143 at 0.5H inertia constant and reached 0.05441 at the base case. In contrast, the peak values for Mode 19 in the second and third scenarios are 0.10565 and 0.108539. From these figures, it is clear that the damping is highly sensitive to the inertia constant.
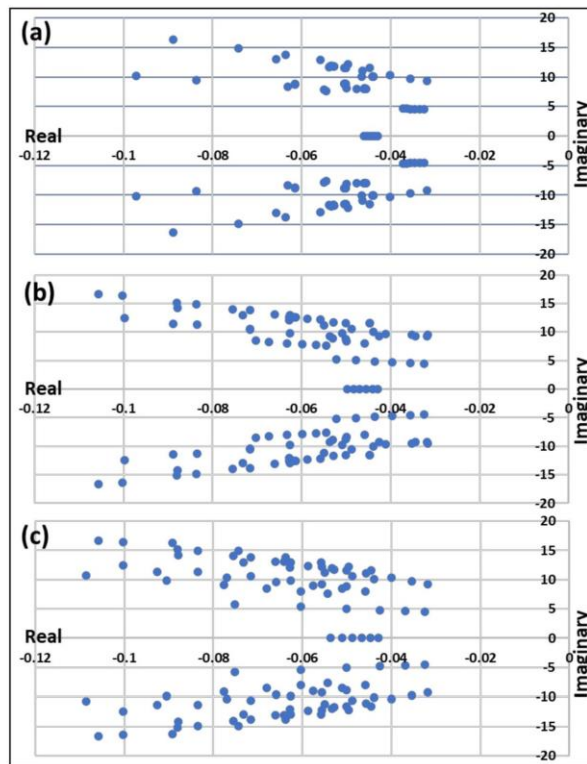
**Figure 7.** Eigenvalue points for three scenarios (**a**), (**b**) and (**c**).
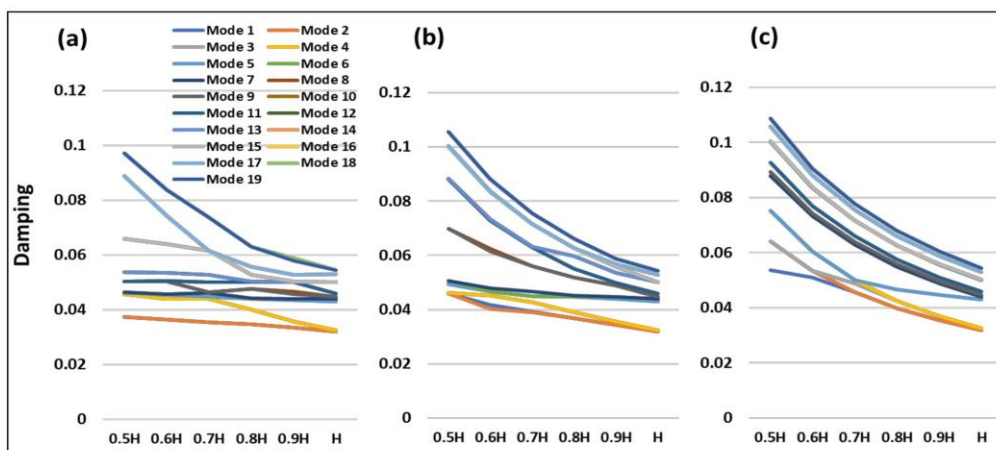
Figure 8. Damping with the increasing order of inertia constant for three scenarios (**a**), (**b**) and (**c**).

4. Discussion and Conclusions

With the increasing concern on renewable energy generation and the rapid development in power electronic converter-based technologies, modern power systems are adopting a new form of architecture and operational strategies. The whole power system is getting into massive transformation including generation, transmission, and distribution as well as in utilization level. Most of the modern power generators are renewable types like solar PV, wind turbine, hydropower, bioenergy, and so on, among which the proportion of solar and wind energy generators are in increasing order. A similar transformation can be observed in the transmission line in the forms of HVDC, in distribution line in the forms of various controllers, and in utilization level in the forms of electronic devices. Overall, the proportion of synchronous generators is at decreasing rate in the modern power system, which is also considered as the source of inertia. Moreover, the PEC based technologies adopted all around the modern power system contain zero or less system inertia. These transformations introduce various issues as the result of distinct changes in the power system dynamics and their characteristics. The unpredictable RESs like solar and wind with low inertia and stochastic demand have a higher potentiality of vulnerability since unpredictable power unbalance can create frequent frequency deviation and lead to system instability. To address the problem, we must understand the dynamics of the system and their dependencies on various parameters.

A number of studies have been conducted to analyze the performance of the modern power system and evaluate the sensitivity under different operational statuses. However, the same factor was found to be sensitive for a case study and not sensitive for others, which creates confusion on the dependency of the system on the system's parameters. Hence, parametric sensitivity analysis is very important to analyze the power system dynamics that can help to minimize the potential impacts.

This paper presents the parametric sensitivity analysis of the rotor angle stability indicators for the case study of the 39-bus New England power system. Two power system analysis studies are used in this assessment: transient and small-signal stability analysis. The studies have been used to identify and analyze the values of indicators (i.e., CCTs, eigenvalue points, damping ratio, frequency deviation, voltage deviation and generator's speed deviation). The sensitivity analysis of the inertia constant with respect to the indicators has been performed by considering three scenarios and six sub-cases. Besides that, the nature of system frequency, speed of the generators, and the voltage profile of the buses are also analyzed as the performance matrixes.

From this study, it is shown that the CCT values are highly dependent on the inertia constant within the power system and decrease significantly with the decreases in the inertia constant. Furthermore, the CCTs of all components decrease with the decrease in inertia at any section of the multi-machine power system, although the effect is higher in the local area and less in the neighboring areas. Among the considered scenarios, the third scenario has significant performance deviations in comparison to the other two scenarios since the third scenario has a significant drop in system inertia. Although all of the scenarios and sub-cases are found to be stable, the decreasing inertia constant affects all of the rotor angle stability indicators significantly. With the decreasing inertia constant, the voltage, frequency, and generator speed are observed to highly deviate. Hence, this study concluded that the power system stability is highly sensitive to the system inertia.

Conflicts of Interest: The authors declare no conflict of interest.

References

1. Shrestha, A.; Gonzalez-Longatt, F. Frequency Stability Issues and Research Opportunities in Converter Dominated Power System. *Energies* **2021**, *14*, 4184. [CrossRef]
2. Shrestha, A.; Ghimire, B.; Gonzalez-Longatt, F. A Bayesian Model to Forecast the Time Series Kinetic Energy Data for a Power System. *Energies* **2021**, *14*, 3299. [CrossRef]
3. Kroposki, B.; Johnson, B.; Zhang, Y.; Gevorgian, V.; Denholm, P.; Hodge, B.-M.; Hannegan, B. Achieving a 100% Renewable Grid: Operating Electric Power Systems with Extremely High Levels of Variable Renewable Energy. *IEEE Power Energy Mag.* **2017**, *15*, 61–73. [CrossRef]
4. Kerdphol, T.; Rahman, F.S.; Mitani, Y. Virtual Inertia Control Application to Enhance Frequency Stability of Interconnected Power Systems with High Renewable Energy Penetration. *Energies* **2018**, *11*, 981. [CrossRef]
5. Khadka, N.; Paudel, R.; Adhikary, B.; Bista, A.; Sharma, S.; Shrestha, A. Transient Stability in Renewable Energy Penetrated Power Systems: A Review. In Proceedings of the RESSD 2020 International Conference on Role of Energy for Sustainable Social Development in 'New Normal'Era, Kathmandu, Nepal, 28–29 December 2020.
6. Tielens, P.; Van Hertem, D. The relevance of inertia in power systems. *Renew. Sustain. Energy Rev.* **2016**, *55*, 999–1009. [CrossRef]
7. Roy, N.K.; Pota, H. Current Status and Issues of Concern for the Integration of Distributed Generation into Electricity Networks. *IEEE Syst. J.* **2014**, *9*, 933–944. [CrossRef]
8. Vittal, V.; McCalley, J.; Ajjarapu, V.; Shanbhag, U.V. *Impact of Increased DFIG Wind Penetration on Power Systems and Markets*; PSERC Publication 09–10; Final Project Report; Power Systems Engineering Research Center: Tempe, AZ, USA, 2009.
9. Mola Jimenez, J. Evaluation of Frequency and Transient Stability Indicators in Future Power Systems with High Levels of Wind Power Generation. Master's Thesis, Faculty of Electrical Engineering Mathematics and Computer Science, Delft University of Technology, Delft, The Netherlands, 2017.
10. Isbeih, Y.J.; El Moursi, M.S.; Xiao, W.; El-Saadany, E.F. Generator-based threshold for transient stability assessment. *IET Smart Grid* **2019**, *2*, 407–419. [CrossRef]
11. Perilla, A.; Papadakis, S.; Torres, J.L.R.; Van Der Meijden, M.; Palensky, P.; Gonzalez-Longatt, F. Transient Stability Performance of Power Systems with High Share of Wind Generators Equipped with Power-Angle Modulation Controllers or Fast Local Voltage Controllers. *Energies* **2020**, *13*, 4205. [CrossRef]
12. Sajadi, A.; Preece, R.; Milanovic, J. Evaluation of suitability of different transient stability indices for identification of critical system states. *arXiv* **2020**, arXiv:2001.03519.
13. Tamimi, B.; Cañizares, C.; Bhattacharya, K. System Stability Impact of Large-Scale and Distributed Solar Photovoltaic Generation: The Case of Ontario, Canada. *IEEE Trans. Sustain. Energy* **2013**, *4*, 680–688. [CrossRef]
14. Tielens, P. Operation and Control of Power Systems with Low Synchronous Inertia. Ph.D. Dissertation, Faculty of Engineering Science, KU Leuven, Leuven, Belgium, 2017.
15. Wang, Y.; Ravishankar, J.; Phung, T. A study on critical clearing time (CCT) of micro-grids under fault conditions. *Renew. Energy* **2016**, *95*, 381–395. [CrossRef]
16. Sadhana, S.G.; Ashok, S.; Kumaravel, S. Small Signal Stability Analysis of Grid Connected Renewable Energy Resources with the Effect of Uncertain Wind Power Penetration. *Energy Procedia* **2017**, *117*, 769–776. [CrossRef]
17. Pavella, M.; Ernst, D.; Ruiz-Vega, D. *Transient Stability of Power Systems: A Unified Approach to Assessment and Control*; Springer: Berlin/Heidelberg, Germany, 2012.
18. Gonzalez-Longatt, F. Ctitical Fault Clearing Transmission Line. 2021. Available online: https://github.com/fglongatt/My_DIgSILENT_PowerFactory/blob/master/Time-Domain-rms/Critical%20Fault%20Clearing%20TL%20FGL.pfd (accessed on 12 June 2021).
19. Gonzalez-Longatt, F. Critical Fault Clearing Bus. 2021. Available online: https://github.com/fglongatt/My_DIgSILENT_PowerFactory/blob/master/Time-Domain-rms/Critical%20Fault%20Clearing%20BUS%20FGL.pfd (accessed on 12 June 2021).
20. Athay, T.; Podmore, R.; Virmani, S. A Practical Method for the Direct Analysis of Transient Stability. *IEEE Trans. Power Appar. Syst.* **1979**, *PAS-98*, 573–584. [CrossRef]

Article 4

Article

A Bayesian Model to Forecast the Time Series Kinetic Energy Data for a Power System

Ashish Shrestha [1,*], Bishal Ghimire [2] and Francisco Gonzalez-Longatt [1]

1   Department of Electrical Engineering, Information Technology and Cybernetics,
     University of South-Eastern Norway, 3918 Porsgrunn, Norway; F.Gonzalez-Longatt@usn.no
2   Department of Electrical and Electronics Engineering, Kathmandu University, Dhulikhel 45200, Nepal;
     bishalghimire1997@gmail.com
*   Correspondence: Ashish.Shrestha@usn.no

Abstract: Withthe massive penetration of electronic power converter (EPC)-based technologies, numerous issues are being noticed in the modern power system that may directly affect system dynamics and operational security. The estimation of system performance parameters is especially important for transmission system operators (TSOs) in order to operate a power system securely. This paper presents a Bayesian model to forecast short-term kinetic energy time series data for a power system, which can thus help TSOs to operate a respective power system securely. A Markov chain Monte Carlo (MCMC) method used as a No-U-Turn sampler and Stan's limited-memory Broyden–Fletcher–Goldfarb–Shanno (LM-BFGS) algorithm is used as the optimization method here. The concept of decomposable time series modeling is adopted to analyze the seasonal characteristics of datasets, and numerous performance measurement matrices are used for model validation. Besides, an autoregressive integrated moving average (ARIMA) model is used to compare the results of the presented model. At last, the optimal size of the training dataset is identified, which is required to forecast the 30-min values of the kinetic energy with a low error. In this study, one-year univariate data (1-min resolution) for the integrated Nordic power system (INPS) are used to forecast the kinetic energy for sequences of 30 min (i.e., short-term sequences). Performance evaluation metrics such as the root-mean-square error (RMSE), mean absolute error (MAE), mean absolute percentage error (MAPE), and mean absolute scaled error (MASE) of the proposed model are calculated here to be 4.67, 3.865, 0.048, and 8.15, respectively. In addition, the performance matrices can be improved by up to 3.28, 2.67, 0.034, and 5.62, respectively, by increasing MCMC sampling. Similarly, 180.5 h of historic data is sufficient to forecast short-term results for the case study here with an accuracy of 1.54504 for the RMSE.

Keywords: time series model; Bayesian model; ARIMA model; performance matrix; power system dynamics

1. Introduction

With the increasing concern over clean and sustainable energy and rapid growth in electronic power converter (EPC)-based technologies, modern power systems are experiencing vast transformation in all sectors, including generation, transmission, distribution, and even utilization. The generation sector is presently integrating EPC-based renewable energy resources (RESs), including photovoltaic panels and wind turbines, whereas the control mechanisms of other sectors are dependent on EPCs. At the same time, the proportion of synchronous generators is reducing in modern power systems, and synchronous generators are considered to be the main source of system inertia. In comparison to the conventional operation mode, the huge penetration of EPC-based technologies presents several changes in the operating dynamics of a modern power system. The major change is a significant drop in system inertia, which may directly affect the frequency quality, and operational security of power supply [1,2]. Frequency quality has an important role

regarding the smooth operation of a power system, where low system inertia can initiate accidental system blackouts [3]. Furthermore, the transient stability of a modern power system is also highly sensitive to the penetration level of EPC-based technologies, along with the given fault location and its severity [4].

Estimating power system performance indicators is an important task that must be conducted for the secure and reliable operation of a power system, especially after disturbance. Numerous studies have been conducted and many are still in the research and development phase to obtain the best solution for estimating system inertia and securing a power system from potential disturbances. Most of studies have focused on frequency quality measurement and monitoring techniques which are further used to estimate the inertia. The work in [5] presented an ambient wide-area measurement technique to estimate power system inertia, in which the authors took the ambient frequency and the active power of the power system by using phasor measurement units (PMU). Similarly, Zhang et al. proposed a synchrophasor measurement-based method to estimate the equivalent inertia of a system containing a wind power plant [6]. Fereidouni et al. proposed an online security assessment tool for the South West Interconnected System in Australia, which monitored and forecasted system inertia on an online basis and estimated parameters such as load damping factors and demand-side inertia [7]. Dynamic regressor extension and mixing procedures have been proposed with the aim to develop an online estimator of power system inertia. In such case, some authors have used a non-linear and aggregated power system model [8]. A swing equation and PMU-based inertia estimation technique for wind power plants has been proposed, where the synchrophasor measurements are taken from a real-time digital simulator using industrial PMUs [9]. Similarly, another study has utilized frequency and voltage response just after disturbance to estimate the inertia by combining two separate approaches (i.e., R for the frequency response and V for the power change due to the load voltage dependency) [10].

The main complication for system inertia estimation methods is that the inertial response between controllers and stabilizers cannot be distinguished, and the system dynamics cannot be analyzed during the normal operation [5]; however, there have been no attempts to estimate system inertia more accurately by forecasting the continuously available data from the power system, such as kinetic energy and power deviations. As such, the discussed issues can be addressed in a more practical way. There are some research articles in which system frequency, nadir frequency, power generation, and load have been used to forecast system performance [11–13]. A number of studies have been conducted to forecast the short-term time series data of load as an indicator for a power system [14–16]. A previous paper from the authors presented a structural time series-based model to forecast the kinetic energy of a power system for a short period, which concluded that the identified value of kinetic energy can be used to estimate the system inertia on a real-time basis [17]. This research article is based on further investigation of that research article and presents a new forecasting method to estimate system performance indicators. Though described in detail further below, the following summarizes the main contributions of this paper:

(a) A Bayesian model used to forecast the univariate time series data of kinetic energy is presented. One year of data for the kinetic energy of the INPS are used to forecast for the next 30 min of data. The results of the presented model are evaluated with other performance metrics and are found to within acceptable limits. Further, the results are cross-checked with the results of the ARIMA model.

(b) The optimum training dataset size required to forecast 30-min values of the kinetic energy via an optimization technique is identified. There may be a considerable number of historical data, and this will result in a greater computational time if all of the data are used in the forecasting process. It is also very important to obtain results as quickly as possible, since decisions (i.e., control actions) must be made at the right time. Hence, determining the optimal training dataset size could be significant in terms of optimizing the required computational time and memory.

The authors of this paper aim to present a method that forecasts the time series data of kinetic energy as an important parameter of a power system. A dataset containing a year of time series data for the INPS (1 sample per minute) is used to forecast short-term results (i.e., the next 30 min) using the Bayesian model presented here. The forecasted time series data of the kinetic energy can be utilized to estimate the system indicators and manage the whole system during normal operation, as well as in case of contingencies. This paper first introduces the background and the problems that arise because of the huge penetration of EPC-based technologies in power grids. The issues regarding a modern power system with massively EPC-based technologies are briefly discussed. In Section 2, the adopted methodologies are described in detail. The models for time series forecasting, their mathematical formulations, and the performance measurement metrics are additionally discussed in detail. Section 3 presents the results of this paper. Finally, the conclusions of this work are presented in Section 4.

2. Methodology

This section is focused on the description of the adopted methodology, which can be seen in Figure 1. A detailed description of the adopted methodology may be seen below.
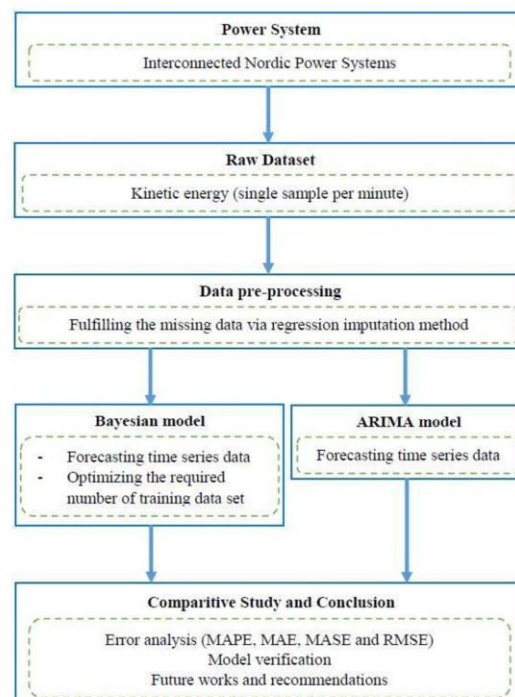

Figure 1. Adopted workflow.

2.1. Data Types and Preparation

The data for the kinetic energy of the INPS for 2019 were taken from the web portal of FINGRID (Finland's transmission system operator). Data were collected each minute, amounting to 525,604 samples in total. The minimum and maximum values of the kinetic energy in 2019 were recorded as 126 GW and 273 GW. Similarly, the mean and median values of the total samples were obtained to be 194.1 GW and 191 GW with a standard deviation of 27.6.

It is important to have reliable and accurate data to correctly analyze performance and visualize results. Incorrect visualization is a result of unreliable data and may mislead viewers. Hence, the raw data here were first processed to minimize possible errors by filtering and fulfilling missing values. In this study, the raw sample sets were passed through a kernel filter to reject errors and a regression impulsion method was used to fulfil the missing values. Overall, 9273 samples were missed among the total set of 525,604 samples (i.e., 1.76%), which were then fulfilled via the regression impulsion method.

2.2. Model Selection

The samples that the authors took were of a univariate type, and the best way to analyze univariate data is with a structural time series model. Various research articles [18,19] have presented structure time series models based on the concept of decomposition for univariate samples. Authors have segregated time series data into different components, like the trend, seasonal, and irregular components. In this research article, the authors adopted the same concept of the structural time series model and decomposed the whole time series model into three components as shown in Equation (1).

$$y(t) = g(t) + s(t) + \epsilon_t \tag{1}$$

where $g(t)$ is the logistic growth (i.e., trend of the data), $s(t)$ is periodic changes, and ϵ_t is the error that provides some random nature of the result. In the presented model, the logistic growth is just a regressor of time with several linear and non-linear fitting and calculated by using Equation (2). In Equation (2), C is the carrying capacity, r is the growth rate, and m is the offset parameter.

$$g(t) = \frac{C}{1 + e^{-r(t-m)}} \tag{2}$$

The carrying capacity and growth rate are not constant values and instead vary with time. Incorrect assumptions may lead to incorrect interpretations. Hence, time-dependent carry capacity (i.e., C_t) and growth rate (i.e., r_t) were considered. Now, the revised relation for the logistic growth is given by Equation (3).

$$g(t) = \frac{C_t}{1 + e^{-(r+a[t]^T \delta)(t-m-a[t]^T Y)}} \tag{3}$$

where δ is the rate of change within the rate adjustment vector ($\delta \in \mathbb{R}^S$) with S_j change points and Y is the adjustment correction vector for offset parameters. Similarly, $a[t]^T$ is a vector which is defined as below:

$$a_j[t] = \begin{cases} 1, & if\ t \geq S_j, \\ 0, & |Otherwise \end{cases} \quad and\ a_j[t] \in (0,1)^S \tag{4}$$

Similarly, the seasonal variation $s(t)$ of the time series parameters can be determined using the Fourier series given in Equation (5). The seasonal variation contains multi-period constraints, such as seasonal changes and human behaviors, which cannot be forecasted by the logistic growth accurately, hence the Fourier series is used to model the periodic functions of time. In the presented model, the parameters (i.e., $a_1, b_1, a_2, b_2, \ldots, a_N, b_N$) with the N Fourier order are used in modeling to identify the seasonal variation for P period.

$$s(t) = \sum_{n=1}^{N} \left(a_n cos\frac{2n\pi t}{P} + b_n sin\frac{2n\pi t}{P} \right) \tag{5}$$

After segregating the time series data into three components, the authors implemented a Bayesian model to forecasting the time series data of kinetic energy. A Bayesian model was selected for this study because it forecasts the future by using a combination of available information and a source of uncertainty in the form of a predictive distribution

with improved accuracy. Later, the ARIMA model was used to compare the results of these two models. The details of these two models are discussed below.

2.2.1. Bayesian Approach

Bayes theorem is widely used in the field of data analysis and is often used to analyze the conditional probability of numerous events, such as forecasting hierarchically structured time series data [20], seasonal time series data [21,22], multi-step-ahead time series prediction [23], general estimation and prediction [24], and statistical analysis [25,26]. A Bayesian approach has been presented to forecast univariate time series data by implementing a technique of sampling the future in [27]. A Bayesian time series forecasting model with the change point and anomaly detection was proposed in [28], where the authors implemented an iterative algorithm with a Kalman filter and smoothing in their analysis, along with a Markov chain Monte Carlo (MCMC) method. Maarten et al. presented that learning Bayesian networks could be used to analyze the time series data of clinical parameters and concluded that the model learning methods could find a good predictive model with a reduced computational time and good interpretation [29]. In [23], the combination of a Kalman filtering model and echoing neural networks was used to predict multi-step-ahead time series data (i.e., a dynamic Bayesian network). Panagiotelis et al. presented a Bayesian density method to forecast intraday electricity prices by using multi-variate skewed t-distributions and a MCMC method [30]. Not only these but there are also the diverse applications of the Bayes theorem.

Theoretically, in Bayes theorem, if X and Y are two events, then the probability of event X with the occurrence of event Y can be calculated using Equation (6). This is the joint probability of two events and does not suggest symmetrical characteristics. In Equation (6), Bayes theorem is defined with the following terms: $P(X|Y)$, posterior probability; $P(X)$, prior; $P(Y|X)$, likelihood; and $P(Y)$, evidence. If the value of the prior, likelihood, and evidence is known, the posterior probability can be calculated mathematically.

$$P(X|Y) = \frac{P(X) \cdot P(Y|X)}{P(Y)}, \text{ for } P(Y) \neq 0 \tag{6}$$

For the specific case of kinetic energy, the relation for the joint distribution over the random inputs is described by Equation (7). Here, P indicates the joint probability distribution function for the conditional probability in the form of $P(KE|pa(KE))$, where KE_i ($KE_i \in KE$) denotes the variables to be analyzed (i.e., kinetic energy) with the influence of their parent variables $pa(KE_i)$. The parent variables include the historical values of the parameter (i.e., historical values of KE), which must be considered during the forecasting of new values.

$$P(KE_1, KE_2, KE_3, \ldots, KE_n) = \prod_{i=1}^{n} P(KE_i | pa(KE_i)) \tag{7}$$

In the conventional manner of estimation via linear regression, Equation (8) is applied with the normally distributed error ($\epsilon_t \sim Normal(0, \sigma^2)$); however, by using Bayes theorem, the estimation can be made more accurate, since, in estimation, Bayesian theory minimizes the posterior expected values of the loss function. In a single sentence, the Bayesian model minimizes the posterior expected loss and maximizes the posterior expectation of a given function. By adopting the Bayes theorem in the linear regression, Equation (9) presents the revised posterior distribution, and Equation (10) gives the likelihood function. In the equations, β is the coefficient and σ^2 is the variance.

$$Y_t = BX_t + \epsilon_t \tag{8}$$

$$H(\beta, \sigma^2 | Y_t) \propto F(Y_t | \beta, \sigma^2) * P(\beta, \sigma^2) \tag{9}$$

$$F(Y_t|\beta,\sigma^2) = (2\pi\sigma^2)^{-T/2} e^{-\frac{(Y_t - \beta X_t)^T (Y_t - \beta X_t)}{2\sigma^2}} \tag{10}$$

As given by Equation (6), the probabilities of conditional events can be identified if the values of the other three parameters are known. In this paper, the authors have calculated the probability of a posterior event and applied it in the forecasting of kinetic energy by using Stan's limited-memory Broyden–Fletcher–Goldfarb–Shanno (LM-BFGS) [31] algorithm as an optimization technique. The LM-BFGS algorithm is very popular in parameter estimation applications and is a quasi-network method, which approximates the BFGS algorithm by utilizing the potential less memory and computational time. The main objective of LF-BFGS is to minimize the unhindered errors within functions. Also, the new value (x_{t+1}) can be obtained using Stan's LM-BFGS algorithm as given in Equation (11) [32], where α_t is the step length that should be satisfy the Wolfe conditions (i.e., sufficient decrease and curvature conditions in line searching method), ∇f_t is the gradient, and H_t is the updated Hessian approximation (n*n symmetric) at the iteration.

$$x_{t+1} = x_t - \alpha_t H_t \nabla f_t \tag{11}$$

In the LM-BFGS algorithm, the estimation of H_t is quite sensitive, which determines the accuracy and efficiency of the model. In comparison to a BFGS algorithm, the LM-BFGS algorithm is capable of computing problems in large iterations with less cost and storage by maintaining simple and compact approximations [32]. The workflow that was followed for the LM-BFGS algorithm in this study is shown in Figure 2. In this approximation, the vector pair in the set of (s_i, y_i) is replaced by the newest set of pairs (s_t, y_t) at each new iteration and is updated accordingly. For example, if the latest iteration is x_t, then the set of vector pair will be (s_i, y_i) at the t-th iteration $(i = t - m, \ldots, t - 1)$. The initial Hessian approximation H_t^0 is considered and continuously identifies updates up to t-th iteration until H_t satisfies the relationship given in Equation (12).

$$
\begin{aligned}
H_t =& \left(V_{t-1}^T \ldots V_{t-m}^T\right) H_t^0 \left(V_{t-m} \ldots V_{t-1}\right) + \rho_{t-m} \left(V_{t-1}^T \ldots V_{t-m+1}^T\right) s_{t-m} s_{t-m}^T \left(V_{t-m+1} \ldots V_{t-1}\right) + \rho_{t-m+1} \\
& \left(V_{t-1}^T \ldots V_{t-m+2}^T\right) s_{t-m+1} s_{t-m+1}^T \left(V_{t-m+2} \ldots V_{t-1}\right) + \ldots + \rho_{t-1} s_{t-1} s_{t-1}^T
\end{aligned} \tag{12}
$$

where, $\rho_t = \frac{1}{y_t^T s_t}$, $V_t = I - \rho_t s_t^T y_t$, $s_t = x_{t+1} - x_t$, and $y_t = \nabla f_{t+1} - \nabla f_t$.
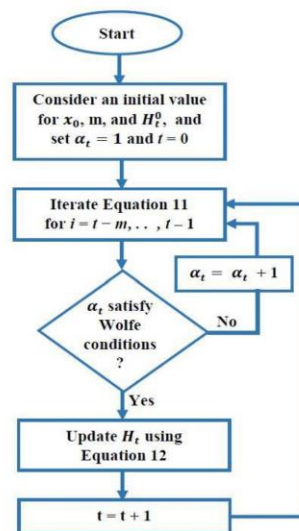

Figure 2. Flow chart of the limited-memory Broyden–Fletcher–Goldfarb–Shanno (LM-BFGS) algorithm.

Further, a MCMC method is used as a No-U-Turn sampler in this study. With an auxiliary variable u and target distribution $f(\theta)$, Equation (13) is used to find the sample θ, and Equation (14) is used to find the marginal distribution of joint distribution $f(u, \theta)$. In these equations, $\pi(\theta)$ is a kernel of the target distribution and z is equal to $\int \pi(\theta)d\theta$. Using these equations, θ can be sampled from the joint distribution and the auxiliary variable can be neglected, which is simply referred to as slice sampling [33]. In this sampling process, the alternative sampling of u and θ is carried out, where θ is fixed initially and sampled for u such that the condition given in Equation (13) will be satisfied (i.e., $0 \leq u \leq \pi(\theta) \rightarrow p(u|\theta) \sim uniform(0, \pi(\theta))$. After that, a horizontal slice region S is formed from the sample θ (S = (θ: u $\leq$ $\pi(\theta)$) [34].

$$f(u, \theta) = \begin{cases} \frac{1}{z} \ if \ 0 \ \leq u \ \leq \ \pi(\theta), \\ 0 \ otherwise \end{cases} \tag{13}$$

$$\int f(u, \theta)du = \int_0^{\pi(\theta)} \frac{1}{z} \ du = \frac{\pi(\theta)}{Z} = f(\theta) \tag{14}$$

After slice sampling, the No-U-Turn sampler initiates with the uniformity as given in Equation (15); however, its efficiency is highly dependent on the probability of the acceptance. The step size will be small for a high acceptance probability that requires many leapfrog steps to generate the subset of candidate $(\theta|p)$ states [34].

$$p(u|\theta) \sim uniform\left(0, e^{(\log f(\theta) - \frac{1}{2} p'M^{-1}p)}\right) \tag{15}$$

2.2.2. ARIMA Approach

An autoregressive integrated moving average (ARIMA) model is a statistical method which is highly used in statistical analysis and the forecasting of time series data. This method uses the concept of a linear combination of past events/values by identifying the dependency of observation and residual errors (ϵ_t). In an ARIMA model, the process ($Z_t = Y_t - Y_{t-d}$) is modeled as $Z_t = \mu + \epsilon_t$, where the residual errors can be described with Equation (16) [25] and the forecasting of the time series predictors (Y_t) can be performed with the autoregressive method as given in Equation (17). In the equations, L is the lag operator, θi is the moving average parameters, p is the order of the lagged observation, d is the degree of difference, and u_t is the white noise defined by ($u_t \sim Normal \ (0, \sigma^2)$). This study uses these concepts and equations to forecast the short-term values of the kinetic energy for validation. A platform called EXPLORATORY has previously been used to perform short-term forecasting with an ARIMA model [35].

$$\epsilon_t = \phi_1 \ \epsilon_{t-1} + \ldots + \phi_p \ \epsilon_{t-p} + u_t - \theta_1 \ u_{t-1} - \ldots - \theta_q \ u_{t-q} \tag{16}$$

where $\phi(L) \ \epsilon_t = \theta(L) \ u_t$ for polynomials with the lag operator ($L^d \ X_t = X_{t-d}$).

$$Y_t = (1 - L)^d X_t \text{ and } (1 - \sum_{i=1}^{p} \varphi_i L^i)Y_t = (1 + \sum_{i=1}^{q} \theta_i L^i)\epsilon_t \tag{17}$$

2.2.3. Optimization

A set of data can most often, but not always, be observed in terms of equally spaced time intervals and can thus be termed as time series data. Unlike other models that account for a temporally dependent structure in the data, the presented model treats the forecasting problem as a curve-fitting exercise. Since these data are a function of time, while modeling, it is assumed that the factors affecting these data are a function of time as well and are not dealt with separately. As this model does not account for temporal dependencies and the output of the model is strictly a function of time, one of the methods to optimize the model is to experiment with the training datasets. This suggests the following question: What training dataset size does the model require for the short-term forecasting of kinetic energy with the least margin error? Hence, an optimization model was created to answer

this question and is shown in Figure 3. At first, the available data (i.e., 525,604 samples) were divided into training and test sets, where the test set contained the last 30 min of data (arranged in minute intervals), and the rest of the data were considered to belong to the training set. Then, with the help of the training dataset, the model predicts the kinetic energy for the next 30 min. The forecasted output and the test dataset are then used to compute the RMSE. The number of training sets was incremented by 15 and the aforementioned process was repeated continuously. The RMSE computed at each step was recorded and plotted against the number of training samples. In the end, the number of the samples with the lowest resulting value for RMSE was considered to be optimal.
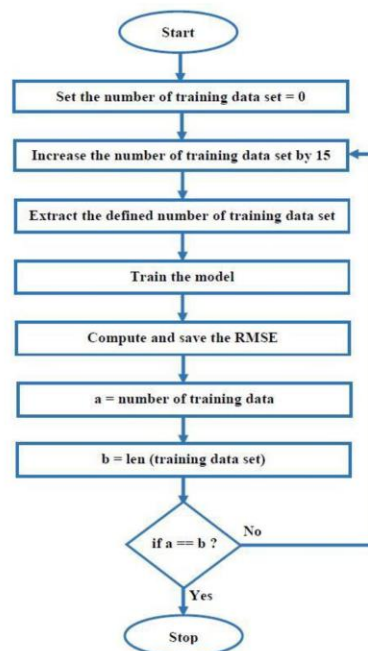

Figure 3. Flow chart of the optimization process.

2.3. Performance Evaluation and Validation

After developing a model, performance evaluation and validation are critical in research and development activities. In this study, a Bayesian model is used to forecast the time series data of kinetic energy within the INPS. The pre-processed data are firstly trained with ideal regression coefficients and an in-sample forecast is produced. In this process, a group of test samples is used for the validation of the results. The size of the test sample was considered to be 30 (i.e., 30 min), since this study is focused on forecasting for a short-term period. Similarly, the proportion of training and validation samples was considered to be 70/30. Figure 4 presents the distributions of the training, testing, and validation samples among the total samples. The forecasting technique used in this study was of an in-sample type. After analyzing the performance of the model and the nature of the kinetic energy, model validation was computed using popular measures like the mean absolute percentage error (MAPE), mean absolute error (MAE), root-mean-square error (RMSE), and mean absolute scaled error (MASE) as given in Equation (18). In Equation (18), y_i and $\hat{y}_i$ indicate the actual and forecasted values, e_j is the error (i.e $y_i - \hat{y}_i$) at the j-th iteration, and the training set is considered for time t ($t = 1, 2, \ldots T$). A platform called EXPLORATORY is used for the performance evaluation and validation of the datasets [35]. EXPLORATORY

uses R as the programming platform and provides the facility of data extraction, data wrangling, data analysis, data visualization, and so on via machine learning algorithms.

$$\text{MAPE} = \frac{1}{n}\sum_{i=1}^{n}\left|\frac{y_i - \hat{y}_i}{y_i}\right|, \ \text{MAE} = \frac{1}{n}\sum_{i=1}^{n}|y_i - \hat{y}_i|, \ \text{RMSE}$$
$$= \sqrt{\frac{1}{n}\sum_{i=1}^{n}(y_i - \hat{y}_i)^2} \ \text{and} \ \text{MASE} = \frac{\frac{1}{J}\sum_{0}^{j}|e_j|}{\frac{1}{T-1}\sum_{t=2}^{T}|y_i - y_{i-1}|} \tag{18}$$
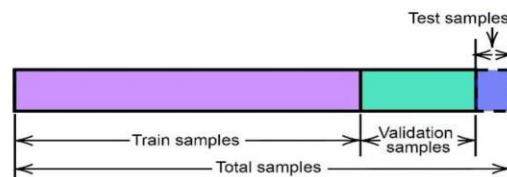
Figure 4. Method of performance evaluation and validation.

3. Results

The main objective of this research paper was to analyze the time series data of kinetic energy and forecast short-term results that could be used for the estimation of power system performance indicators to ensure the secure operation of that system. To achieve this objective, the authors selected the case of the INPS, which interconnects the transmission systems of Norway, Sweden, and eastern Denmark. The respective TSOs have time series data of kinetic energy since 2015, which presents a great opportunity for performance estimation. Hence, the authors took the time series data (one sample per minute) of kinetic energy within the INPS for the whole year of 2019 and utilized the data for further investigation. The characteristics of the data can be visualized as per the box plots given in Figure 5. As shown in Figure 5a, the kinetic energy of the case study was found to be dependent on the weather, where it was comparatively high in winter and low in summer. Figure 5b,c present the weekly and daily characteristics of the kinetic energy, from which it may be observed that the amount of kinetic energy is above average during working hours and below average during non-working hours and holiday periods. Figure 6a,b gives the actual trend of the kinetic energy for the daily and annual period of 2019. A trend with the recorded maximum and minimum values of the kinetic energy can be observed. Overall, for the specific case study of the INPS, the nature of kinetic energy was found to be dependent and the weather.

Figure 7 is focused on the characteristics of the forecasted data, along with the training and testing samples of kinetic energy. In this study, the kinetic energy was forecasted for 30 min. Figure 7a presents the nature of the training, testing, and the forecasted data obtained using the Bayesian model, whereas Figure 7c present the present trend of the kinetic energy and the changing patterns for the datasets. No changing trend points were identified that contributed to the trend variation of the kinetic energy when the Bayesian model is implemented. On the other hand, Figure 7b presents the nature of the training, testing, and the forecasted data for the ARIMA model, and Figure 7d presents the trend for the samples. The changing trend point was observed when the ARIMA model was implemented to forecast the data of kinetic energy within the INPS. Figure 8 shows a zoomed window for the last five hours that presents a clear comparison of the results for the proposed Bayesian model and the ARIMA model. After the short-term forecasting of the collected datasets, the results were used to validate accuracy and for future analysis. The values of RMSE, MAE, MAPE and MASE for the presented Bayesian model were calculated to be 4.67, 3.865, 0.048 and 8.15, which could be further improved by increasing the MCMC sampling. Figure 9 presents the performance metrics of the Bayesian model with different MCMC sampling values, and it is clearly shown that the optimum value is achieved with 200 MCMC samples. At this instant, the values of RMSE, MAE, MAPE, and MASE were identified to be 3.28, 2.67, 0.034, and 5.62. On the other hand, the values of the performance metrics for the ARIMA model were calculated to be 6.15, 4.680, 0.069, and

12.34. From the comparison of both models, the presented Bayesian model was found to be more accurate than the ARIMA model.
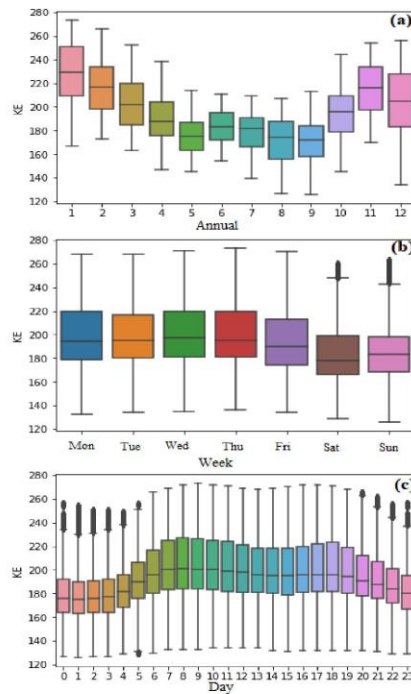
Figure 5. Seasonal variations of KE: (**a**) annual, (**b**) weekly, and (**c**) daily.
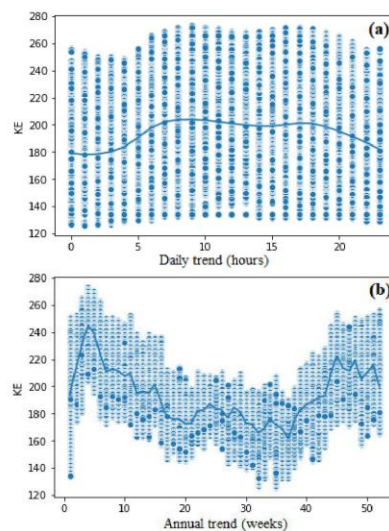
Figure 6. Seasonal trend kinetic energy: (**a**) daily and (**b**) annual.
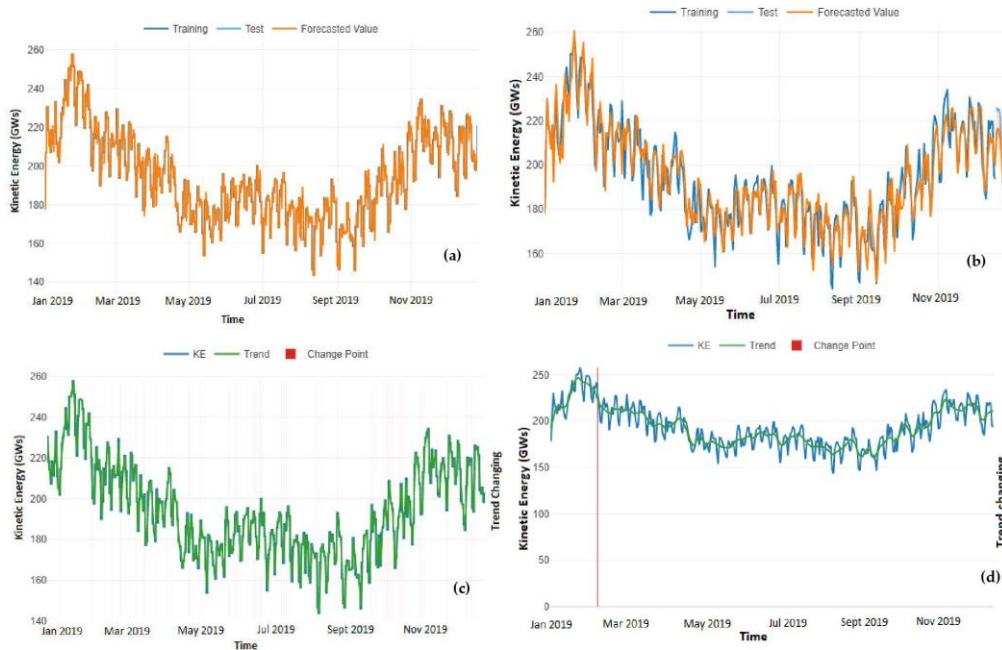
Figure 7. Results showing the nature of training, testing, and forecasted values by using (**a**) the Bayesian model and (**b**) ARIMA model. Similarly, (**c**,**d**) the trend and changing trend patterns for the Bayesian and ARIMA models are shown.
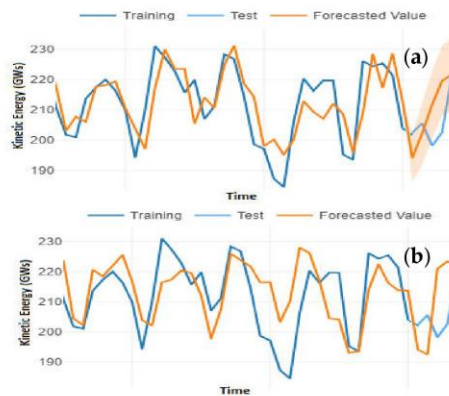

Figure 8. Zoomed window for the last five hours (**a**) for the Bayesian and (**b**) ARIMA models.

Similarly, Figure 10 presents the RMSE for a different number of training sets at which forecasting was computed for the next 30 min. The minimum RMSE (i.e., 1.54504) was obtained when 10,830 min of training samples was used. From this result, it is clear that a training data set of 10,830 min (or 180.5 h) is optimal to forecast the kinetic energy (for the specific case of INPS) for a short-term result (i.e., 30 min) with a value of 1.54504 for the RMSE.
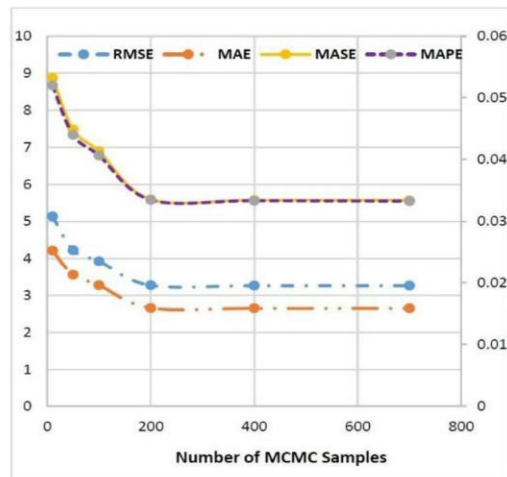
Figure 9. Effect of the Bayesian inference on the performance metrics.

Figure 10. RMSE values for different training sample number values for short-term forecasting.

4. Discussion and Conclusions

With the rapid development of new RESs, most countries are promoting these sources and interconnecting them into their power systems, since conventional power production necessitates the production greenhouse emissions and thus is not sustainable. At the current stage, most power systems are adopting such changes not only in the generation, but also regarding the transformation that occurs in transmission, distribution, and utilization because of the flexibility of EPC-based technologies. Because of this transformation, modern power systems are facing numerous issues. The major issues include maintaining proper frequency quality and an insufficient system rotational inertia within the power system to ensure operational security. In a conventional power system, the large proportion of synchronous generators acts as the source of inertia, which helps the overall system to maintain system frequency by providing inertial support during contingencies; however, unpredictable power sources with low inertia and flexible demand increase vulnerability to system instability in modern power systems since frequent power unbalance can create frequency deviations and this lead to system instability.

There are several power generators within a power system which must be synchronized and operated with the same frequency. During a power deviation event, if the deviation is comparatively high, then each individual machine tends to fluctuate around the centre of inertia (COI) and operate with a dissimilar frequency to other machines, which

may result in system oscillation; however, the frequency of an individual machine close to the COI and some forms of inertial and damping forces attempt to maintain the synchronicity by pulling their frequencies toward the COI. If these forces become insufficient to recover synchronicity, a control mechanism must be applied to recover them, otherwise, the whole power system may undergo an unstable situation and system blackouts may even occur. The stability of a power system is directly dependent on the rate of change of frequency (RoCoF) and the nadir frequency, which are closely associated with system inertia. With an increasing frequency deviation and nadir frequency, an additional control mechanism must be introduced at the right time such that the system operates securely. Also, low system inertia decreases the critical fault clearing time (CCT), which means the minimum time to restore the system to an original stage is drastically decreasing in modern power systems. Hence, the estimation of system inertia, frequency, and/or nadir frequency is especially important for modern power systems.

Several research works have been conducted to estimate performance indicators such that power systems can be operated securely; however, most of them are focused on the measurement and estimation of frequency and nadir frequency. Some researchers have tried to estimate system inertia by taking the parameters from a power system during contingencies; however, one of the most complicated parts of estimation is that an inertial response cannot be distinguished by controlling units, and it is quite difficult to analyze dynamic performance in normal conditions. Forecasting system parameters such as frequency, nadir frequency, power generation, power consumption, and system inertia can be a good option, but this requires additional computational work with complex models and high response times for computation. A practical method that uses available resources is necessary to provide accurate and fast results to estimate system indicators.

This paper presents a practical method to estimate the dynamic characteristics of a power system by forecasting univariate time series data of kinetic energy. A Bayesian model is used to forecast the time series data of the kinetic energy, and a decomposable approach is used to analyze the characteristics of the dataset. From this study, it is found that the kinetic energy can be forecasted and analyzed using the Bayesian model with an acceptable accuracy limit and can be utilized in the estimation of the system inertia and the dynamic characteristics of a power system. Furthermore, the accuracy of the model can be improved by increasing the number of MCMC samples. In the considered case study, the optimized number of MCMC samples was found to be 200. A comparison of the results shows that the presented model is more accurate than an ARIMA model. For the specific data type in this study, a historic data quantity of 180.5 h was sufficient to forecast short-term results (i.e., 30 min) with a value of 1.54504 for the RMSE.

References

1. Kerdphol, T.; Rahman, F.S.; Mitani, Y. Virtual inertia control application to enhance frequency stability of interconnected power systems with high renewable energy penetration. *Energies* **2018**, *11*, 981. [CrossRef]
2. Kroposki, B.; Johnson, B.; Zhang, Y.; Gevorgian, V.; Denholm, P.; Hodge, B.-M.; Hannegan, B. Achieving a 100% renewable grid: Operating electric power systems with extremely high levels of variable renewable energy. *IEEE Power Energy Mag.* **2017**, *15*, 61–73. [CrossRef]
3. Perez-Arriaga, I.J. Managing large scale penetration of intermittent renewables. In Proceedings of the MITEI Symposium on Managing Large-Scale Penetration of Intermittent Renewables, Cambridge, MA, USA, 20 April 2011; p. 2011.
4. Khadka, N.; Paudel, R.; Adhikary, B.; Bista, A.; Sharma, S.; Shrestha, A. Transient Stability in Renewable Energy Penetrated Power Systems: A Review. In Proceedings of the RESSD 2020 International Conference on Role of Energy for Sustainable Social Development in 'New Normal' Era, Kathmandu, Nepal, 28–29 December 2020.
5. Tuttelberg, K.; Kilter, J.; Wilson, D.; Uhlen, K. Estimation of power system inertia from ambient wide area measurements. *IEEE Trans. Power Syst.* **2018**, *33*, 7249–7257. [CrossRef]
6. Zhang, Y.; Bank, J.; Wan, Y.-H.; Muljadi, E.; Corbus, D. Synchrophasor measurement-based wind plant inertia estimation. In Proceedings of the 2013 IEEE Green Technologies Conference (GreenTech), Denver, CO, USA, 4–5 April 2013; pp. 494–499.
7. Fereidouni, A.; Susanto, J.; Mancarella, P.; Hong, N.; Smit, T.; Sharafi, D. Online Security Assessment of Low-Inertia Power Systems: A Real-Time Frequency Stability Tool for the Australian South-West Interconnected System. *arXiv* **2020**, arXiv:2010.14016.
8. Schiffer, J.; Aristidou, P.; Ortega, R. Online estimation of power system inertia using dynamic regressor extension and mixing. *IEEE Trans. Power Syst.* **2019**, *34*, 4993–5001. [CrossRef]
9. Beltran, O.; Peña, R.; Segundo, J.; Esparza, A.; Muljadi, E.; Wenzhong, D. Inertia estimation of wind power plants based on the swing equation and phasor measurement units. *Appl. Sci.* **2018**, *8*, 2413. [CrossRef]
10. Zografos, D.; Ghandhari, M.; Eriksson, R. Power system inertia estimation: Utilization of frequency and voltage response after a disturbance. *Electr. Power Syst. Res.* **2018**, *161*, 52–60. [CrossRef]
11. Zografos, D. *Power System Inertia Estimation and Frequency Response Assessment*; KTH Royal Institute of Technology: Stockholm, Sweden, 2019.
12. Heylen, E.; Strbac, G.; Teng, F. Challenges and opportunities of inertia estimation and forecasting in low-inertia power systems. *arXiv* **2020**, arXiv:2008.12692.
13. Allella, F.; Chiodo, E.; Giannuzzi, G.M.; Lauria, D.; Mottola, F. On-line estimation assessment of power systems inertia with high penetration of renewable generation. *IEEE Access* **2020**, *8*, 62689–62697. [CrossRef]
14. Cancelo, J.R.; Espasa, A.; Grafe, R. Forecasting the electricity load from one day to one week ahead for the Spanish system operator. *Int. J. Forecast.* **2008**, *24*, 588–602. [CrossRef]
15. Amaral, L.F.; Souza, R.C.; Stevenson, M. A smooth transition periodic autoregressive (STPAR) model for short-term load forecasting. *Int. J. Forecast.* **2008**, *24*, 603–615. [CrossRef]
16. Taylor, J.W. An evaluation of methods for very short-term load forecasting using minute-by-minute British data. *Int. J. Forecast.* **2008**, *24*, 645–658. [CrossRef]
17. Gonzalez-Longatt, F.; Acosta, M.; Chamorro, H.; Topic, D. Short-Term Kinetic Energy Forecast using a Structural Time Series Model: Study Case of Nordic Power System. In Proceedings of the 2020 International Conference on Smart Systems and Technologies (SST), Osijek, Croatia, 14–16 October 2020; pp. 173–178.
18. Harvey, A.C.; Peters, S. Estimation procedures for structural time series models. *J. Forecast.* **1990**, *9*, 89–108. [CrossRef]
19. Taylor, S.J.; Letham, B. Forecasting at scale. *Am. Stat.* **2018**, *72*, 37–45. [CrossRef]
20. Novak, J.; McGarvie, S.; Garcia, B.E. A Bayesian model for forecasting hierarchically structured time series. *arXiv* **2017**, arXiv:1711.04738.
21. Vosseler, A.; Weber, E. Forecasting seasonal time series data: A Bayesian model averaging approach. *Comput. Stat.* **2018**, *33*, 1733–1765. [CrossRef]
22. Zeng, Z.; Li, M. Bayesian median autoregression for robust time series forecasting. *Int. J. Forecast.* **2021**, *37*, 1000–1010. [CrossRef]
23. Xiao, Q.; Chaoqin, C.; Li, Z. Time series prediction using dynamic Bayesian network. *Optik* **2017**, *135*, 98–103. [CrossRef]
24. Rodriguez, A.; Puggioni, G. Mixed frequency models: Bayesian approaches to estimation and prediction. *Int. J. Forecast.* **2010**, *26*, 293–311. [CrossRef]
25. Steel, M.F. Bayesian time series analysis. In *Macroeconometrics and Time Series Analysis*; Springer: Berlin, Germany, 2010; pp. 35–45.
26. Ganics, G.; Odendahl, F. Bayesian VAR forecasts, survey information, and structural change in the euro area. *Int. J. Forecast.* **2021**, *37*, 971–999. [CrossRef]
27. Thompson, P.A.; Miller, R.B. Sampling the future: A Bayesian approach to forecasting from univariate time series models. *J. Bus. Econ. Stat.* **1986**, *4*, 427–436.
28. Zhang, A.Y.; Lu, M.; Kong, D.; Yang, J. Bayesian Time Series Forecasting with Change Point and Anomaly Detection. In Proceedings of the Sixth International Conference on Learning Representations, Vancouver, BC, Canada, 30 April–3 May 2018.
29. Van der Heijden, M.; Velikova, M.; Lucas, P.J. Learning Bayesian networks for clinical time series analysis. *J. Biomed. Inform.* **2014**, *48*, 94–105. [CrossRef] [PubMed]
30. Panagiotelis, A.; Smith, M. Bayesian density forecasting of intraday electricity prices using multivariate skew t distributions. *Int. J. Forecast.* **2008**, *24*, 710–727. [CrossRef]

31. Carpenter, B.; Gelman, A.; Hoffman, M.D.; Lee, D.; Goodrich, B.; Betancourt, M.; Brubaker, M.A.; Guo, J.; Li, P.; Riddell, A. Stan: A probabilistic programming language. *Grantee Submiss.* **2017**, *76*, 1–32. [CrossRef]
32. Nocedal, J.; Wright, S. *Numerical Optimization*; Springer Science & Business Media: Berlin, Germany, 2006.
33. Neal, R.M. Slice sampling. *Ann. Stat.* **2003**, *31*, 705–741. [CrossRef]
34. Nishio, M.; Arakawa, A. Performance of Hamiltonian Monte Carlo and No-U-Turn Sampler for estimating genetic parameters and breeding values. *Genet. Sel. Evol.* **2019**, *51*, 73. [CrossRef]
35. Nishida, K. Introduction to Exploratory v6.0. Available online: https://exploratory.io/note/kanaugust/Online-Seminar-28 -Introduction-to-Exploratory-v6-0-EdY3YOC2HC (accessed on 11 June 2020).

Article 5

Day-ahead energy-mix proportion for the secure operation of renewable energy-dominated power system

Ashish Shrestha [a,*], Yaju Rajbhandari [b], Francisco Gonzalez-Longatt [a,**]

[a] Department of Electrical Engineering, Information Technology and Cybernetics, University of South-Eastern Norway, Porsgrunn N-3918, Norway
[b] Department of Electrical and Electronics Engineering, Kathmandu University, Dhulikhel 45200, Nepal

ABSTRACT

Advancements in various scientific fields have encouraged the development of novel tools, techniques, components, methodologies, and innovations aimed at addressing the challenges encountered in modern power systems dominated by inverter-based resources (IBRs). This paper focuses on a concept that leverages historical time-series data obtained from transmission system operators (TSOs) to enhance the secure management and operation of power systems. By employing a data-driven model, the day-ahead values of power generation and load consumption are estimated and integrated with a dynamic model of the power system for further analysis. To optimize energy generation and ensure grid stability, an energy-mix operation and reserve scheduling model is utilized. This model optimally combines different power-generating technologies, including synchronous generators (SGs), grid-following converters (GFLs), and grid-forming converters (GFMs), to meet the energy demands of the day while enhancing the overall system strength. The findings are supported by quantitative analysis utilizing variables such as frequency, power production, terminal voltages, and system non-synchronous penetration (SNSP). Simulation results demonstrate that implementing the proposed concept enables the power system under consideration to operate securely, even in the face of a 38% increase in immediate load, with a maximum SNSP ratio of 59%. These findings highlight the effectiveness of the proposed approach in addressing the reliability, system dynamics, stability, control efficiency, and security challenges posed by IBR-dominated power systems. Furthermore, it is believed that this research contributes to the ongoing efforts in decarbonization, renewable energy integration, and combating global warming by facilitating the secure and optimized operation of renewable energy-dominated power systems.

1. Introduction

As people's knowledge of environmental issues and concerns about sustainability, renewable energy sources (RESs) have witnessed a rise in popularity in recent years. Due to environmental concerns and technological advancement, most countries are incorporating RESs into their grid and planning to make them 100% renewable [1]. The 26th United Nations Climate Change Conference (COP26) was kicked off on 1st November 2021 and mentioned different actions that should be conducted as soon as possible [2]. The major objectives of that conference were: (a) secure global net-zero emissions by mid-century, (b) keep 1.5 °C of global warming compared with pre-industrial levels within reach, (c) commit to mobilizing USD 100 billion per year by 2025 to help developing countries deal with the adverse effects of climate change,

and (d) finalize the set of rules guiding the implementation of the Paris Agreement [2]. These objectives show the interest in renewable energy and RES-based power systems in the current era.

However, there are a lot of issues that should be discussed while talking about the RES-based power system. Reliability, system dynamics, stability, control efficiency, security, and other associated concerns [3], are among the most significant technical challenges faced by the RES industry. Studies [4,5], discussed that the increased usage of power electronic converter (PEC)-based RES complicates the power grid, and may affect the overall performance. The high penetration of PEC-based energy resources, such as wind turbines and solar PV, reduces the system's inertia. As a result of the low inertia of PEC-based technologies, the crucial fault clearance time is drastically shortened [6,7]. These complexities can also contribute to the instability of the power

* Corresponding author.
** Corresponding author.
 E-mail addresses: Ashish.Shrestha@usn.no (A. Shrestha), fglongatt@fglongatt.org (F. Gonzalez-Longatt).
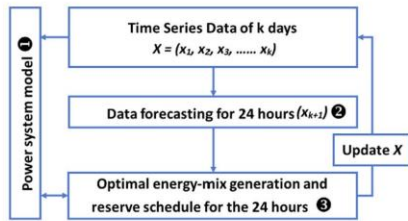
Fig. 1. An overview of the proposed methodology.

system [2]. Also, these RESs are of a stochastic nature, which may introduce complexities in the demand/supply chain within a power system. Introducing an efficient and sufficient reserve to the power system can be a good option to address the challenges of short-term demand/ supply unbalance because of the stochastic nature of RESs [8,9].

Research has been carried out in a variety of dimensions to address the issues of modern power systems caused by the growing penetration of RESs. Technological developments in components such as inverters, converters, controllers, and so on are the essential sectors that can contribute to the secure operation of the power system. In a similar vein, the operating principle and management features of revolving power systems can play major roles in addressing the issues. Researchers are developing a wide variety of ideas and strategies to address the issues that have been identified as being caused by the rapidly shifting topologies of grids and the incorporation of new technology. For example, research papers [9–12] looked at the management of power system security by using economic measurements and the look-ahead dispatch approach. A detailed recovery plan is considered in these papers that guarantees the security of the power system with a possible minimum cost. On the other hand, a method of dynamic rescheduling has been proposed by Zhao et al. [13] for the large roll-out of connected power infrastructure for plug-in electric vehicles operating in extreme conditions. During the rescheduling process, the authors examined the stochastic nature of wind energy and used a real-value and binary particle swarm optimization technique to design the outputs of the project. Ardakani et al. [14], presented a linear chance-constrained optimization-based approach that dispatches and reserves the energy/ power for a day-ahead electricity market so that the RES integrated grid achieves reliable and secure operating points against the contingencies. Differently, Tang et al. [15], presented a stochastic unit commitment model that explores the ability of battery energy storage systems (BESS) to provide grid services by combining energy and reserve markets. It is shown that this model solves the uncertainty of RESs and demand by analyzing BESSs and generators' reserves. Similarly, Zuo et al. [16], studied the performance of a low-inertial power system with grid-following (GFL) and grid-forming (GFM) power converters and a BESS. The authors of this study provided a model with a day-ahead scheduling layer to analyze daily system frequency containment using a day-long time-domain simulation.

While much of the existing literature has explored various dimensions of RES-integrated power systems, there's still a marked lack of focus on optimizing the day-ahead energy portfolio in grids largely dependent on converters, especially those that take advantage of real-time data from transmission system operators (TSOs). Previous studies often simplify the complexities of the grid, overlooking the subtleties of time-series data or failing to examine the coordinated interaction among diverse power-generating technologies in day-ahead planning. Additionally, there has been insufficient emphasis on the nuanced balance between cost factors—from energy production to system integrity—and grid stability. This paper seeks to address these gaps by harnessing detailed time-series data from the TSOs of the Nordic grid. It is aimed at a more dynamic, cost-

effective, and reliable energy configuration that can serve as a practical guide for TSOs. It promotes the optimized use of renewables, contributing to climate mitigation through emission reduction. Concurrently, it is assumed to strengthen grid resilience, offering more dependable solutions for managing the fluctuating nature of renewable energy, a key consideration for climate adaptation. By spotlighting a grid with a high share of RES, this research sets the stage for designing power systems that are sustainable, resilient, and economically sound in a world increasingly faced with climate-induced challenges.

This paper deals with the estimation of the optimal day-ahead energy-mix proportion that would ensure the secure functioning of a power system dominated by converters. To accomplish this goal, this paper uses the time-series data that is accessible on a time-series basis from the TSOs of the Nordic countries. The time-series data is used to estimate the day-ahead values using a data-driven model, which is then utilized to determine the optimal scheduling of the power producers using a model of energy generation and reserve scheduling. Required constraints are taken into consideration during the process of determining the optimal mix of energy from different power-generating technologies (i.e., synchronous generator (SG), GFL, and GFM). The cost of the energy generated from different generators, including charging and discharging of the BESS, generator start-up and shut-down cost, energy reserve cost, and service cost toward system strength are the terms of the objective function. This is done in order to ensure that the secure operation of the power system can be guaranteed in accordance with the regulations of the Nordic TSOs. Throughout the contents, the major contributions of this paper are as follows:

(a) Propose a concept that takes the historical time-series data from the TSOs, estimates a day-long operation stage, and evaluates how securely the power system is operating on a daily basis. This study estimates the best energy-mix proportions for every 24 h utilizing time-series data of generation and consumption of the Nordic grid with a resolution of three minutes.

(b) Data-driven model has been used to forecast the day-ahead values of the parameters that should be required to identify the optimal energy-mix proportion. A long short-term memory (LSTM) network as the forecasting model has been used to achieve state-of-the-art results.

(c) In order to ensure the secure functioning of the system, a model for energy-mix operation and reserve scheduling is utilized. The terms of the objective function include the costs related to generation, operation, maintenance, and system strength.

The presented paper is organized with the following structure. It begins by providing a historical context and an overview of the issues that have surfaced as a result of the widespread adoption of PEC-based technologies in the power grid. The challenges faced by today's power systems, which are reliant on huge amounts of PEC technology, are briefly highlighted. The approaches and presumptions that are used are laid out in Section 2. The datasets and systems that are taken into consideration are also described in detail. In Section 3, the data-driven model has been described that is used for forecasting purposes. In Section 4, the results of the investigation are presented and then thoroughly examined. Finally, the conclusions have been discussed in Section 5.

2. Methodology and assumptions

This section's primary focus is on describing the approaches that are ultimately chosen, as well as the assumptions that are made. Fig. 1 provides a summary of the approaches that are taken into consideration. The approach contains a power system model 1, a data-driven forecasting model 2, and the optimal energy-mix generation and reserve schedule model 3. First, it comes with a model of the power system 1, all of the components of which have been detailed according to the grid standard. The real-world power system provided the source for the
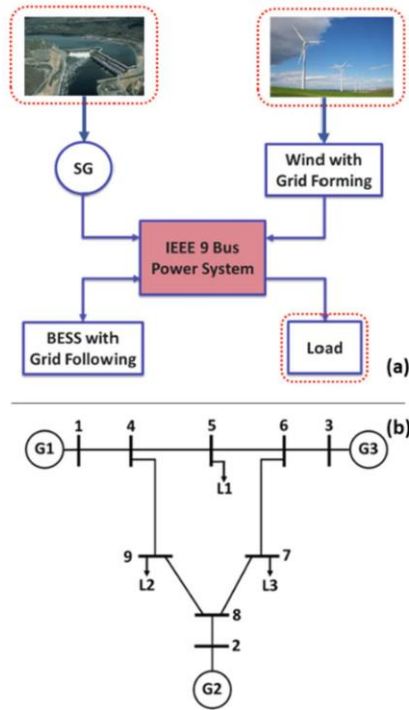
Fig. 2. (a) Overview of the considered system, and (b) Single line diagram of IEEE 9 bus system.

Table 1
Rating of the generators and the loads in the considered power system.

Parameters	Values
Generator 1	163 MW (1.025 pu) at 18 kV
Generator 2	72.19 MW (1.04 pu) at 16.5 kV
Generator 3	85 MW (1.025 pu) at 13.8 kV
Load 1	100 MW/ 35 MVAR
Load 2	125 MW/ 50 MVAR
Load 3	90 MW/ 30 MVAR

independent and variable time series data, which included parameters like power production and consumption. To begin, the time series data has been utilized to make an estimate of the values for the day ahead. The forecasting of the time series data for a day is done with the help of a data-driven forecasting model 2. The optimal scheduling of the power-generating technologies has been determined with an energy generation and reserve schedule model 3 after taking into account the constraints imposed by the power system as well as the time series data that is anticipated for the generation and consumption of power. The response of power-generating technologies such as SG, GFL, and GFM have been analyzed during optimal scheduling. An evaluation of the techno-economic impact is carried out while the appropriate distribution of the components is determined. It is also believed that the reserve schedule ensures the secure operation of the power system. All of these investigations have been conducted with MATLAB software, which contains both the simulation tools as well as the ANN features. The following sub-sections will provide a more in-depth discussion of each component and technique, including all of their particulars.

2.1. Power system components

As discussed in the previous section with Fig. 1, a standard power system model 1 is used to explore day-ahead scheduling with optimal energy-mix for the secure operation of a converter-dominated power system. This is conducted in order to find the best possible solution. The considered system's overview is depicted in Fig. 2(a). The IEEE 9 bus power system as shown in Fig. 2(b) is taken into consideration as the primary network. The rating of the generators and the load centers in the considered IEEE 9 bus power system are given in Table 1. It is also considered that the primary network operates at 230 kV and 50 Hz. Book by P.M. Anderson et al. [17] contains all of the information that is necessary to understand the power system model in further depth. During the course of the investigation, the authors made several assumptions, which can be shown in Fig. 2(a). It is assumed that the first generator is a SG, the second one is a BESS with a GFL, and the third generator contains a wind turbine with a GFM. In this particular investigation, both the dynamic properties of the generations and the load consumption are taken into consideration. The entirety of the system is created using MATLAB Simulink and the time domain is the simulation framework.

The model of the SG used in this study can be defined with Equations (1) and (2). Here in Equations (1) and (2), δ_i is the rotor angle in rad, ω_i is the shaft speed and ω_0 is the nominal speed in pu, H_i is the inertia constant in MJ/MVA, $P_{m,i}$ is the mechanical power, and D_i is the damping torque coefficient of ith generator. The ( ) sign indicates the derivative with respect to time. Similarly, r_a is the armature resistance, $v_{q,i}$ and $v_{d,i}$ represent the q-axis and d-axis components of the voltage, and $i_{q,i}$ and $i_{d,i}$ represent the q- and d-axis components of stator current [18].

$$\dot{\delta}_i = \omega_0(\omega_i - 1) \tag{1}$$

$$2H_i\omega_i\dot{\omega}_i = -D_i\omega_0(\omega_i - 1) + P_{m,i} - \left(v_{q,i}i_{q,i} + v_{d,i}i_{d,i} + r_a i_{d,i}{}^2 + r_a i_{q,i}{}^2\right) \tag{2}$$

Similarly, the grid-forming virtual emulator given in [19], is used as the GFM. A power electronic equipment called a GFM can vary the amplitude (i.e. magnitude and angle) of voltage and frequency at the Point of Common Coupling (PCC) [20,21]. GFM's major duty is to adjust the output voltage and/or current to keep the system frequency and voltage steady. A GFM can be considered as the slack-bus unit in an isolated energy system since it can inject instantaneous active and reactive power for frequency and voltage management [20,22]. It can be mathematically presented as (3) and (4) [19]. Here, ω_i and θ_i are the frequency and angle of voltage, and P_i is the active power generated by the ith generator. Similarly, $\tilde{m_i}$ and $\tilde{d}_i$ are the positive values, known as virtual inertia constant and virtual damping constant.

$$\dot{\theta}_i = \omega_i \tag{3}$$

$$\dot{\omega}_i = -\tilde{d}_i\omega_i - P_i \tag{4}$$

On the other side, GFLs operate as regulated current sources and use a phase-locked loop (PLL) to track the grid phase angle to keep the converters synced with the power grid [23]. In order to regulate the flow of current, one uses the observed phase angle. It regulates the active and reactive currents injected into the electrical grid to accomplish the desired power injection [24]. In the event of a power outage, the grid-following converter simply maintains the output current at the same level as before. However, it is unable to regulate the grid's frequency and voltage directly and must rely on either an additional voltage source or the grid itself [25]. The mathematical representation of the GFL can be presented as (5) and (6) [19].

$$\dot{\hat{\theta}}_i = \hat{\omega}_i \tag{5}$$
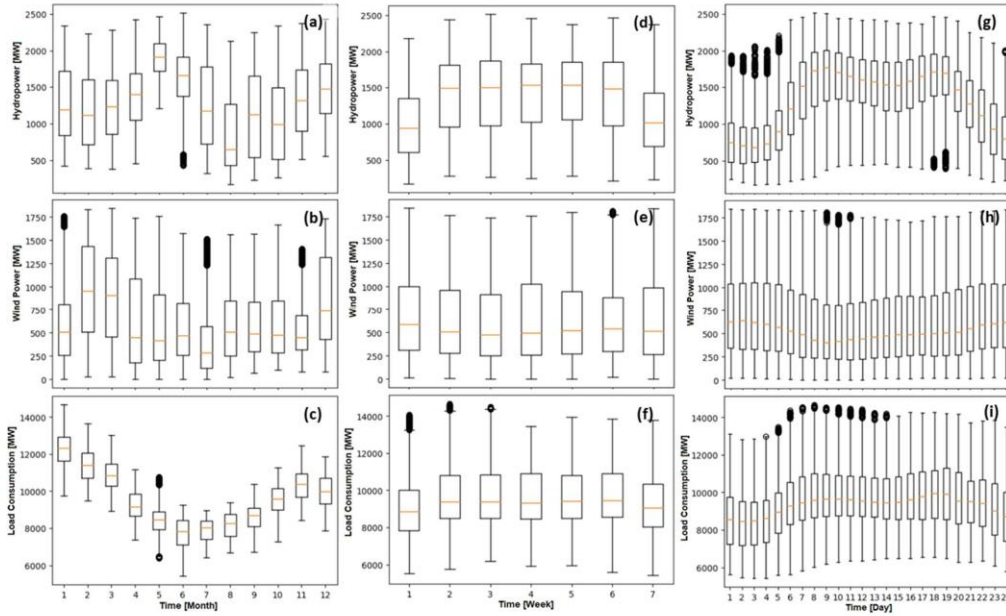
Fig. 3. Seasonal characteristics of the datasets for (a) monthly trend of hydropower, (b) monthly trend of wind power, (c) monthly trend of load consumption, (d) weekly trend of hydropower, (e) weekly trend of wind power, (f) weekly trend of load consumption, (g) daily trend of hydropower, (h) daily trend of wind power, and (i) daily trend of load consumption.

$$\tau_i \dot{\hat{\omega}}_i = -\widehat{\omega}_i - K_{P,i} v_{q,i} - K_{I,i} \int v_{q,i} dt \qquad (6)$$

Here, τ_i is the filter time constant, and $K_{P,i}$ and $K_{I,i}$ are proportional and integral gain constants of the component. Here in these Equations, the sign () indicates the estimated one.

2.2. Datasets

This analysis made use of real data for hydropower production, wind power production, and load consumption. The data are collected for the Nordic grid, and then they are scaled down in order to make them compatible with the IEEE 9 bus standard. Firstly, the data related to power generation and load consumption for the Nordic grid have been taken from the FINGRID TSO [26]. The data on hydropower production is taken from Finland and assumed that it is valid for all Nordic countries since the seasonal streamflow for different rivers from these countries seems to be in similar trends [27,28]. The data is collected throughout the year 2021, and their resolution is three minutes. After observing the raw datasets, it is identified that some of the datasets are not a number (NaN) type, and some seem to be coming from the wrong column. These observations provide a preliminary idea about the outliers within the collected datasets. For detailed investigation, the distribution of datasets is analyzed with the help of normal distribution (i.e., histogram). From the histogram, it is identified that the normal distribution of hydropower lies from minimum zero to a maximum of 3,688.96 MW. Similarly, the minimum and maximum values for wind power may vary from zero to 2,915.54 MW, and those values for load consumption may vary from 4,245.98 to 15,006.4 MW. The datasets that are outside of these limits are considered to be outliers. During the analysis, it is identified that, out of 174,988 samples, 763 outliers have been identified in the hydropower dataset, one in wind power, and 768 in the load consumption datasets.

The identified outliers are then replaced with the mean values of the specific column (i.e., 944.27 for wind power, 1,609.8 for hydropower, and 9,668.44 for load consumption). It is believed that the new dataset reflects all of the qualities of the parameters, despite the fact that the data quality has been enhanced.

The seasonal pattern of the power generators from hydropower and wind power, as well as the load consumption, are evaluated for the purpose of providing a more in-depth understanding of the raw datasets. The box plots that display the monthly, weekly, and daily trend of the power-related parameters are shown in Fig. 3(a-i). It is clear from looking at Fig. 3(a-i) that the power production from wind and hydropower and the load consumption are subject to large amounts of variation. The wind profile is subject to random variation, and the load consumption is contingent on the nature of the consumer, which also exhibits a random nature. Hence, wind power generation and load consumption cannot be controlled, and it is independent. The trend of hydropower output, on the other hand, can be controlled to balance the supply–demand chain, and is considered to be dependent.

After the data have been preprocessed to get rid of any outliers, the data are next scaled down to comply with the requirements of the IEEE 9-bus standard. Normalization technique, as given in Equation (7) [29], is used to scale down the datasets so that the data can be achieved in the required form.

$$Z_i = \frac{X_i - \min(X)}{\max(X) - \min(X)} * Q \qquad (7)$$

Here in Equation (7), X_i is the ith value, $\max(X)$ is the maximum value and $\min(X)$ is the minimum value within the specific datasets. When performing the work of scaling down the data, the power rating of the power-generating technologies and the load consumption, as shown in Table 1, are used as maximum values Q that are needed for normalization. Also, the ratings of the power generators vary from zero to their

4
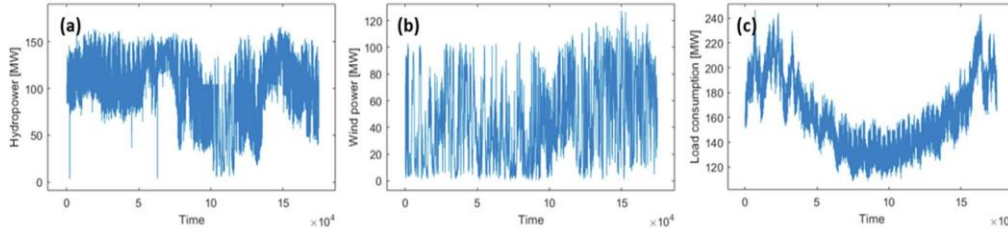
Fig. 4. Down-scaled profile of (a) hydropower, (b) wind power, and (c) load consumption (samples per unit of time).
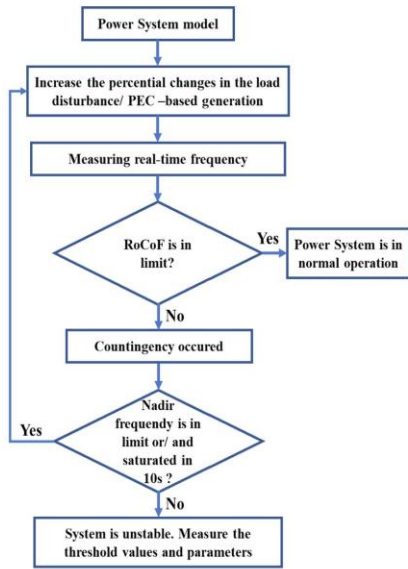

Fig. 5. Processes to determine the threshold values and secure function conditions for the considered power system model.

maximum values (as recorded in the datasets); $\max(X)$ is considered to be the maximum recorded value, whereas the $\min(X)$ is considered to be zero. Fig. 4 presents the characteristics of the scaled datasets, which are employed in this inquiry alongside the forecasting model 2 that provides the values for the parameters one day in advance (especially wind power and load consumption). A detailed description of the forecasting model 2 used in this study is presented in Section 3.

It is possible to consider the discharge of the water as a constant value for the entire day when analyzing the day-ahead estimation because hydropower production is entirely dependent on the flow of the water, and the flow of the water does not change significantly over short periods of time (assuming there are no significant changes in the weather, including rain). However, it is necessary to make frequent forecasts; monthly forecasting can be used for hydropower production. Whereas the nature of wind and the load consumption is stochastic; possibly perfect prediction is required while analyzing it. Hence, this paper highlighted the importance and mainly focused on the day-ahead forecasting of the two parameters: wind power production and load demand.

2.3. Energy-mix operation and reserve scheduling model for secure operation

As described in the introduction section, the main objective of this paper is to identify the optimal energy-mix proportion for the day-ahead operation of a RES-based power grid in a secure way. To identify the optimal proportion of the energy-generating technologies, the authors considered the cost as the objective function, which can be described by Equation (8). In this paper, four terms have been considered as the objective functions: (a) cost of the energy generated through different generators including charging and discharging of the BESS, (b) service charge provided by different power generators to maximize the power system strength, (c) generator start-up and shut-down cost, and (d) energy reserve cost.

$$\min \sum_{t \in \mathcal{T}} \left[\begin{array}{c} \sum_{g \in \mathcal{G}} \left(C_{g,t}^{p} \cdot p_{g,t} + C_{g,t}^{Up} \cdot u_{g,t}^{Up} + C_{g,t}^{Down} \cdot u_{g,t}^{Down} + C_{g,t}^{reserve} \cdot p_{g,t}^{reserve} \right) \\ + \sum_{e \in \mathcal{E}} \left(C_{e,t}^{Dis} \cdot p_{e,t}^{Dis} - C_{e,t}^{Charge} \cdot p_{e,t}^{Charge} \right) \end{array} \right] \tag{8}$$

Here in Equation, $C_{g,t}^{p}$, $C_{g,t}^{Up}$, $C_{g,t}^{Down}$, and $C_{g,t}^{reserve}$ are the cost parameters of the energy, generator start-up, generator shutdown, and reserve, respectively. Similarly, $C_{e,t}^{Dis}$ and $C_{e,t}^{Charge}$ are the cost parameters, whereas $p_{e,t}^{Dis}$ and $p_{e,t}^{Charge}$ are the energy supplied/ consumed while discharging and charging the BESS. $p_{g,t}$ and $p_{g,t}^{reserve}$ are generated energy by the generators at t time and the reserved energy. On the other hand, $u_{g,t}^{Up}$ and $u_{g,t}^{Down}$ are the unit variables that define the startup and shutdown of the generating units. Similarly, the $C_{g,t}^{p}$ is the cost parameters of the energy from different power producers, which are different for different power generators as per their resources and characteristics. For example, the cost of energy/ power generated through RESs is comparatively higher than that from non-renewable energy, since the community has allocated some incentive toward the RESs [30]. When we are talking about RESs, the SG comes as the first choice, since it is flexible to start and shut down, and also it can provide reliable supply and security toward the power system operation. On the other hand, introducing GFM/ virtual inertia is one of the best solutions that can support improving the system strength as well as power system stability. Similarly, BESS can be considered as a form of service provider for additional frequency service [31]. Hence, different energy/ power producer has different characteristics and their own role in the power system's quality, hence, it is most important to analyze the service cost for different generators carefully, while analyzing the cost functions. Equation (9) gives the distribution of the cost parameters for the generated energy, where $C_{g,t}^{sp}$ is the actual cost parameter for the generated energy from different generators, and C_{g}^{ss} is a cost parameter for the service provided by different generators to improve the system strength.

$$C_{g,t}^{p} = C_{g,t}^{sp} + C_{g}^{ss} \tag{9}$$

The idea of system strength is highly complicated and is still in the process of development; it is connected to the benefits of security,
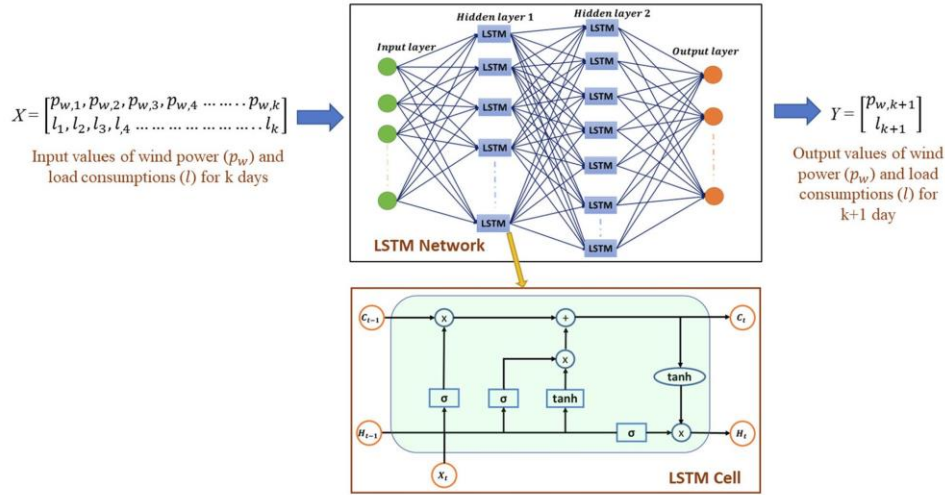
Fig. 6. Overview of the proposed model.

Parameters	Value/ types
Number of hidden layers	$\mathbb{Z}[1,5]$
Number of units in hidden layer	$\mathbb{Z}[10, 200]$
Activation function	[tanh, relu, sigmoid]
Learning rate	$\mathbb{R}[0.00001, 1]$
Dropout value	$\mathbb{R}[0.1, 0.7]$
L2 Regularization	$\mathbb{R}[1e\text{-}10, 1e\text{-}2]$

efficiency, and resiliency that the power system offers to consumers, participants, and investors [32]. In a simple sentence, the displacement of a SG within a power system decreases the system strength, but the increasing penetration should have a higher system strength level to operate the power system in a secure way. Even if the idea of system strength is not popular in the Nordic grid at the present time, this study makes an attempt to incorporate the cost associated with system strength into the calculation of the cost parameters. The idea of system strength is fairly common in Australia, and the Australian Energy Market Operator (AEMO) is responsible for determining the limit of system strength needs for the whole Australian electricity grid every five years [33]. After that, the local transmission network service providers (TNSP)

are accountable for making and acquiring services to solve the system strength deficit in accordance with AEMO's directives. If the connection of generators that need system strength is the source of part of these costs being spent, then the generation in question should also share some of the costs associated with these services, as represented in the system strength mitigation requirement [34]. Hence, the cost related to system strength (i.e., C_g^{ss}) is also included in this study, which can be calculated by using Equation (10).

$$C_g^{ss} = C_{price}^{ss} \left(\frac{\$}{MVA} \right) \times LF^{ss} \times p_g^{ss} (MVA) \qquad (10)$$

Here in Equation (10), C_{price}^{ss} is the system strength unit price, and the LF^{ss} is the system strength location factor; both factors are fixed by the authority every five years (especially for the Australian grid). Similarly, p_g^{ss} is the specified amount of system strength service, which is fixed at the stage of integration with the national grid. The cost parameters used in this paper are taken from regulations established by authorities from Australia, and the USA [35–37].

In order to optimize the cost function for the task at hand, certain constraints are taken into consideration. Equation (11) gives the relationship between the variables that are relevant to the in-operation, startup, and shutdown, while Equation (12) places constraints on the variables that are associated with the startup and the shutdown [16]. It is most important to be under a suitable range for the startup and
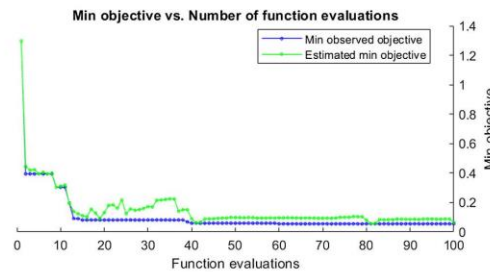

Fig. 7. Minimum objective vs. number of function evaluation.

6

Table 3
Hyperparameters for the presented LSTM model.

| Parameters	Value/ types
Optimizer	Adam
Loss	MSE
Maximum Epoch	100
Mini batch size	32
Dropout value	0.5
Number of hidden layers	2
1st hidden layer	197 hidden units, tanh activation function, uniform initializer
2nd hidden layer	197 hidden units, sigmoid activation function, uniform initializer
Initial learning rate	0.001
Learn rate schedule	piecewise
L2 Regularization	0.00518
Input weight initializer	Glorot, with LR 1 and L2 factor 1
Recurrent weight initializer	Orthogonal, with LR 1 and L2 factor 1
Bias Initializer	Unit-forget-gate, with LR 1 and L2 factor 0

Fig. 8. Loss function with epochs/ iterations.

shutdown of the generators; the generators should follow the grid standards.

$$u_{g,t}^{on} - u_{g,t-1}^{on} = u_{g,t}^{Up} - u_{g,t}^{Down} \tag{11}$$

$$u_{g,t}^{Up} + u_{g,t}^{Down} \leq 1 \tag{12}$$

In a similar manner, Equation (13) [16], describes the link between the amount of energy generated by the generator and the maximum and minimum ramp rates at which the generators may operate, where $RP_{G,t}^{Up}$ and $RP_{G,t}^{Down}$ are the upper and lower bounds of the ramp rates, and $P_{G,t}$ is the power generated for the individual power-generating technologies at t. Ramp rate, also known as the maximum technical capability of a generating plant, is essentially the rating of power that can be changed each minute, and every country defines its values to manage its power

systems. As an illustration, the Nordic TSOs' maximum ramping speed for flow changes is 30 MW/minute, while their maximum ramp changing rates for trading plans from one hour to the next are 600 MW.

$$u_{g,t}^{on}RP_{g,t}^{Down} \leq p_{g,t} - p_{g,t-1} \leq u_{g,t}^{on}RP_{g,t}^{Up} \tag{13}$$

Similarly, the constraint of the bound for the energy that should be reserved to give a sufficient supply is given in Equation (14) [16], where P_G^{min}, P_G^{max}, and $P_{G,t}^{reserve}$ are the minimum, maximum and available reserve bounds. The constraint for the phase angle stability is given in (15), where θ_G^{min} and θ_G^{max} are the minimum and maximum limits of the phase angle, and $(\theta_G - \theta_{SG})$ indicates the differences in the phase angles.

$$p_g^{min} \leq p_{g,t} + p_{g,t}^{reserve} \leq p_g^{max} \tag{14}$$

$$\theta_g^{min} \leq \theta_g - \theta_{sg} \leq \theta_g^{max} \tag{15}$$

Finally, the conditions for active power generation by all of the generators are given in Equation (16) [16]. In addition to this, it is considered that the BESS has not been discharged when the state of charge (SoC) becomes 30% or below, and no charging after the SoC becomes 99%.

$$u_{g,t}^{on}p_g^{min} \leq p_{g,t} \leq u_{g,t}^{on}p_g^{max} \tag{16}$$

One of the important factors used in this paper is system strength or system service cost, for which the system non-synchronous penetration (SNSP) ratio is considered as the metric. SNSP is the ratio of the real-time power generated through the non-SG and net HVDC interconnector import to total demand and HVDC interconnector export. It is mathematically expressed by Equation (17), and it provides a single constraint that encapsulates the issues of transient, voltage and frequency stabilities, and the consequences of transmission faults. Despite being an estimate, the measure has a reasonable real-time indication and can be used for operational as well as planning purposes [38].

$$SNSP\,(\%) = \frac{Non-Synchronous\,Generation + Net\,Interconnector\,Imports}{Demand + Net\,Interconnector\,Exports}$$
$$\times 100 \tag{17}$$

However, the next objective of this paper is to identify the secure operating level of the power system; the authors simulated the power system model with a variety of plausible contingencies by increasing disturbances in load and PEC-based generation. In the worst credible scenario, generation dispatch is changed until the power system model is satisfied. From this condition, the SNSP ratio value is derived, indicating the power system's maximum SNSP ratio limit. Both the maximum threshold and secure functioning SNSP ratios are stated in percentage. Maximum threshold SNSP ratio and secure operational SNSP ratio are related by whichever credible contingency event has the largest influence on the rate of change of frequency (RoCoF) and frequency control. The detailed processes of getting these limits are given in Fig. 5.

3. Data-driven forecasting model

Data-driven model has been shown to be effective and is achieving a high level of accuracy in a variety of application fields, including medicine [39,40], agriculture [41,42], weather [43], power/energy systems [44–49], space [50,51], finance [52,53], and so on. Many ideas have gained widespread recognition, including feedforward networks, recurrent neural networks (RNNs), convolution neural networks (CNNs), and many others. Research articles [45–47,50,54–57] give a comparative review of artificial neural networks (ANNs) applicable to a variety of domains. Each one of them comes with a unique set of benefits and downsides. In this study, the authors adopted the Long Short-Term Memory (LSTM) network because of the following reasons: (a) handling long-term dependencies, (b) dealing with non-linear patterns, and (c)
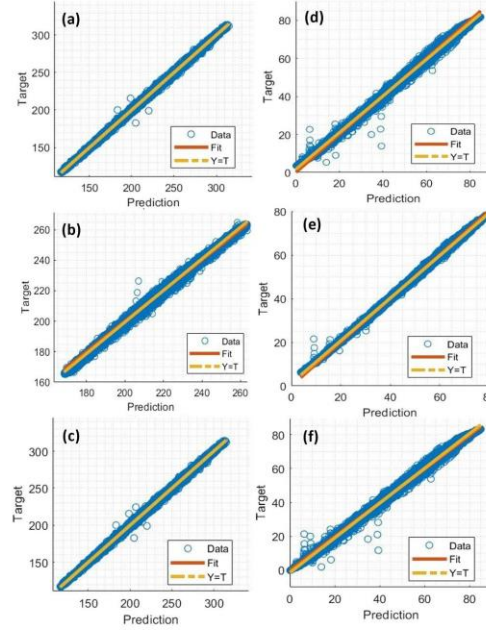
7

Fig. 9. Normalized regression of LSTM model for (a) load training data, (b) load testing data, (c) load all data, (d) wind training data, (e) wind testing data, and (f) wind all data.

robust to noise [58,59]. Because of the discussed characteristics, LSTMs are well-suited for time series forecasting, and they have been effectively employed in a wide variety of real-world problems including time series forecasting. As discussed in the introduction and methodology sections, the main objective of this paper is to estimate the day-ahead energy-mix proportions within a power system so that the power system can operate in a secure way. To obtain this objective, the power generations and load consumptions must be forecasted for the next 24 h, for which LSTMs could be a good option since it has all of the features that need to handle considered datasets and patterns of the outputs that are needed for further investigation.

LSTM is an expanded version of the RNN, which addresses the fundamental problem of having difficulties in learning long-term dependencies. In contrast to RNN, LSTM is equipped with a feature known as extended memory, which gives it the capacity to remember information for a longer time. The most significant improvement that has been made to the LSTM model is the inclusion of four gates, which are as follows: (a) input, (b) forget, (c) update, and (d) output. The forget gate determines whether the memory cell will be updated and controls how much information the current memory cell will receive from a potential new memory cell (19). On the other hand, the update gate determines whether the memory cell will be updated and determines how much information the current memory cell will receive from a memory cell from the previous step (20). Finally, the output gate is responsible for determining the values of the following hidden layer (21). [60]

$$\Gamma_i = \sigma\left(W_i\left[a^{\langle t-1 \rangle}, X^{\langle t \rangle}\right] + b_i\right) \tag{18}$$

$$\Gamma_f = \sigma\left(W_f\left[a^{\langle t-1 \rangle}, X^{\langle t \rangle}\right] + b_f\right) \tag{19}$$

$$\Gamma u = \tanh\left(W_u\left[a^{\langle t-1 \rangle}, X^{\langle t \rangle}\right] + b_u\right) \tag{20}$$

$$\Gamma_0 = \sigma\left(W_0\left[a^{\langle t-1 \rangle}, X^{\langle t \rangle}\right] + b_0\right) \tag{21}$$

Here in these Equations, W and b are the weight matrices and bias vectors of the recurrent network, a and X are the states of the neurons, and σ is the activation function. Using these four gates, the current state of the time-series model can be determined by using Equation (22), and the output can be calculated by using Equation (23). [60]

$$h_t = \tanh\left(W_{hh}h_{t-1} + W_{xh}x_t\right) \tag{22}$$

$$y_t = W_{hy}h_t \tag{23}$$

Going through detail, $h_t \in (-1,1)^h$ is the current state, h_{t-1} is the previous state, $y_t \in R^t$ is the output, $x_t \in R^t$ is the input, $W_{hh} \in R^{h \times t}$ is the weight of the recurrent neuron, W_{xh} is the weight of the input neuron, W_{hy} is the weight of the output neuron, $b \in R^h$ is the bias vector parameters that need to be learned while model training. Fig. 6 presents the basic overview of the architecture of the LSTM model for the case of this study, where the main target is to forecast the day-ahead values of two variables; wind power and load consumption.

When performing analysis with a neural network, it is essential to have suitable values for several hyperparameters. The models' potential for performance-impacting learning behavior can be somewhat regulated by the hyperparameters, which play a role in this process. One of the most challenging aspects of utilizing data-driven models is determining which hyperparameters are appropriate to use. The selection of these hyperparameters can be difficult, and tuning them can take a significant amount of effort. As a consequence of this, the authors decided to utilize Bayesian optimization in order to locate the optimal values for the network hyperparameters. This methodology makes use of objective function evaluations in order to educate a Gaussian process model on the objective function that it keeps internally. For this optimization, the authors used the deep learning application provided by

8
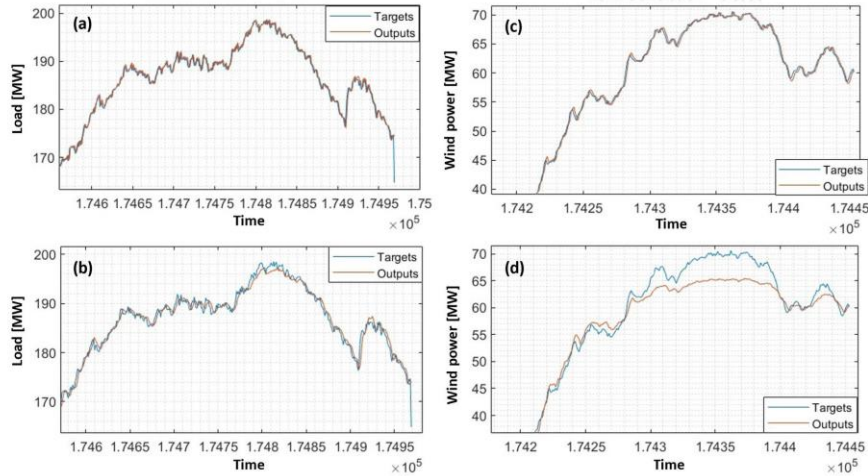
Fig. 10. Outputs (zoomed) for (a) load consumption with LSTM model, (b) load consumption with MLP model, (c) wind power with LSTM model, and (d) wind power with MLP model (samples per unit of time).

Table 4
Error indexes of the presented LSTM and MLP models.

Indexes	LSTM	MLP
MSE	0.0183	0.2125
RMSE	0.1352	0.4609
NRMSE	0.0046	0.0090

MATLAB software [61]. When tuning hyperparameters, a function known as *valErrorFun(optVars)*, which is an optimization function, is taken into consideration. Different ranges for the other parameters have also been provided, which are listed in Table 2. Some of the most important characteristics to consider while designing the architecture of the model are the number of hidden layers and the number of neurons in each layer. On the other hand, the activation function plays an essential role in adding non-linearity and deciding which neuron should be engaged by computing the weighted sum and bias. In a manner comparable to this, the optimal learning rate might change based on the data provided and the network that is being trained. Similarly, the importance of regularization cannot be overstated when it comes to preventing both underfitting and overfitting. In order to facilitate the optimization processes, different potential values have been proposed, each of which takes into account the weight that each of these hyperparameters carries. Fig. 7 illustrates the relationship that exists between the minimal values of the objective function and the evaluation of the function whenever Bayesian optimization is used to determine the optimal values for the hyperparameters. When the simulation is run for a total of 100 epochs, as shown in Fig. 7, the observed and estimated values of the objective function come out to be 0.055348 and 0.0892, respectively. Based on the results provided by the Bayesian optimization, the important hyperparameters have been identified. The full list of the hyperparameters that are utilized for the presented LSTM model is given in Table 3.

Fig. 8 illustrates the errors of the model with epochs, which shows that the training performance of the model improves with the increase in the epoch or/ and iterations. The root mean square error (RMSE) is identified to be 0.1352 at the 100 epochs, whereas the loss function is calculated to be 0.0183. Both of the indicators seem to have decreased at starting in a significant amount, but the rate of change in the remaining parts is quite low, although the values are continuously decreasing. The authors decided to analyze the model for 100 epochs since the rate of change after that point is not significant; it changes at small rates. During the investigation of the performance of the presented model, the regressions of the model have been plotted for the training, testing, and all data sets for both wind power production and load consumption. All of these plots are given in Fig. 9. During the performance analysis of the presented model, the whole dataset has been divided into two sections: training (80%) and testing (20%). The data partitioning approach '*dataPartitioning(opt, data)*' is used to divide the datasets, which implements the gradient aggregation [62]. This is the case where the data on load consumption and wind power are utilized to make forecasts by utilizing the proposed model. The train-test split procedure is used to estimate the performance of algorithms when they are used to make predictions on data that was not used to train the model. The rank correlation values for all of the cases are identified as being higher than 0.980, which indicates the strength of the presented model.

For comparison, the authors also analyzed the datasets with next data-driven model namely, multilayer perceptron (MLP). Similar to LSTM, Bayesian optimization (i.e., trainbr) is used to find the hyperparameters for MLP. For MLP, it is identified that there are two feed-forward levels, with the layers consisting of eighty-nine neuron units. Other hyperparameters include the dropout value '0.2', the starting learning rate '0.005', learn rate schedule 'piecewise', linear regularization '0.00012', activation function 'sigmoid', optimizer 'adam', and so on. The results for power consumption by utilizing LSTM and MLP models are shown in Fig. 10 (a and b), while the outputs for wind power production within the power system are shown in Fig. 10 (c and d). The error indexes such as Mean Square Error (MSE), Root Mean Square Error (RMSE), and Normalized Root Mean Square Error (NRMSE) have been determined for both models and listed in Table 4. From these figures, the presented LSTM model appears to be a good fit for the datasets and the hyperparameters of the models that are being considered.

4. Result and discussion

Section 3 provides a comprehensive breakdown of the forecasting model and the values, whereas Section 2.1 looks into the specifics of the power system that is taken into consideration. Detailed descriptions of

9
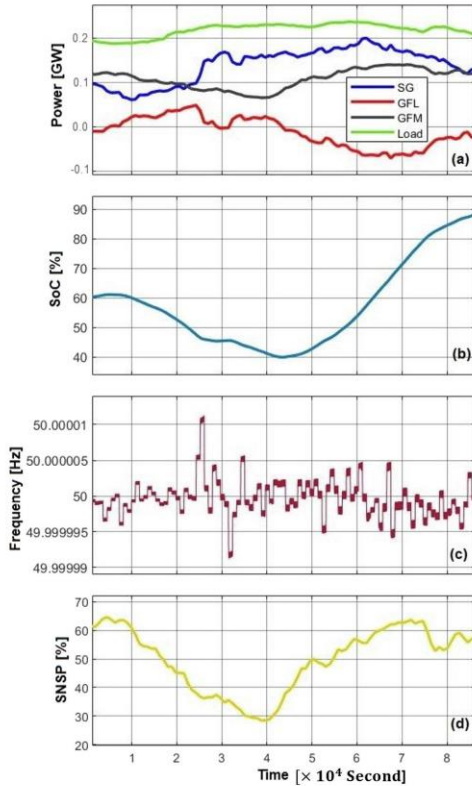
Fig. 11. (a) Power generated through generators, (b) SoC of BESS, (c) system frequency, and (d) SNSP values, for 24 h-time spans (samples per unit of time).

the data-driven model and the considered hyperparameters are discussed in Section 3. Whereas this section primarily centers around the results obtained from incorporating the day-ahead generation and consumption data into the dynamic model of the power system.

To begin with, the data-driven model estimates the variables of power generation and consumption for the next day. After that, these values are inputted into a dynamic model of the power system that

includes an optimization model in order to arrive at a day-ahead optimal energy-mix proportion. It is assumed that the power system is supplied by a SG, wind turbines equipped with GFL, and BESS equipped with GFM in the condition that is being studied here. The optimal amounts of power that are supplied by and consumed by these components are shown in Fig. 11 (a). Here in Fig. 11 (a), when the value of the GFL is positive, the BESS is being discharged. When the value of the GFL is negative, the BESS is charged from the grid with the electricity generated by other generators. The SoC level of the BESS is presented in Fig. 11 (b) for the day ahead simulation scenario. It can be seen from looking at this figure that the minimum SoC that is recorded in this particular one-day simulation is 40 percent, which is well within the acceptable range of values. Similarly, Fig. 11 (c) illustrates the overall system frequency of the power system that is taken into consideration for this simulation model. Under these normal operating conditions, the frequency appears to be fluctuating with less variation, and it falls within the standard frequency limitations allocated by Nordic TSOs.

As discussed in subsection 2.3, the SNSP ratio is computed as the metric to use for the power system in the day-ahead scenario that is taken into consideration. Since the examined power system does not feature an HVDC exchange network, both the import and export values of the interconnector are taken to be zero for the sake of this paper's usual formulation, which is slightly different than Equation (17). It is identified that the SNSP ratio for the investigated situation ranges anywhere from 28% all the way up to 64%, as shown in Fig. 11 (d). These findings pertain to the normal functioning of the power system, where the maximum SNSP ratio is recognized as being 64%. Because of this, it can be assumed that the SNSP value of 64% is within a secure limit for running the power system that is being investigated.

There are certain ratings that apply to power-producing technologies while they are functioning under normal operating conditions. These ratings were taken into consideration when choosing the sizes for those technologies. Fig. 12 (a) illustrates the proportion of total installed capacity that is contributed by each of these three forms of power-generating technologies. In light of this consideration, the proposed model optimizes the power ratings of the technologies dynamically for the day-ahead scenario and allocates resources in accordance with these changes. Fig. 12 (b) depicts the hourly amount of energy supplied by each of these power-generating technologies for the analyzed day-ahead scenario.

However, the operation of the electrical system can be disturbed at any moment in time, and the power grid must be able to withstand that. A power system is susceptible to a wide variety of disturbances, each of which manifests itself in its own distinctive way. There are different types of faults, but some of the more prevalent ones are line-to-line faults, line-to-ground faults, multiple-line-to-ground faults, and so on [17]. Similarly, the sudden addition or subtraction of a large load or/and
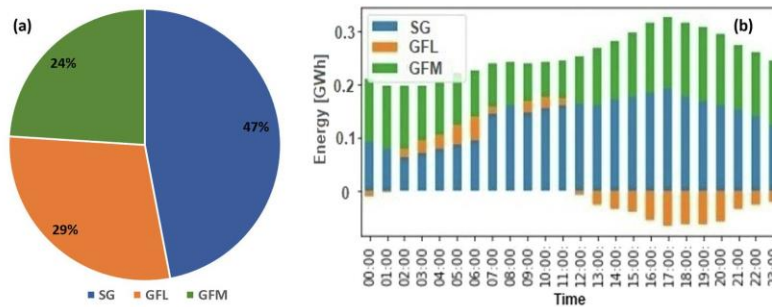

Fig. 12. Figure showing the (a) proportion of installed capacity, and (b) hourly generated electricity at the day-ahead scenario, for the power-generating technologies.

10
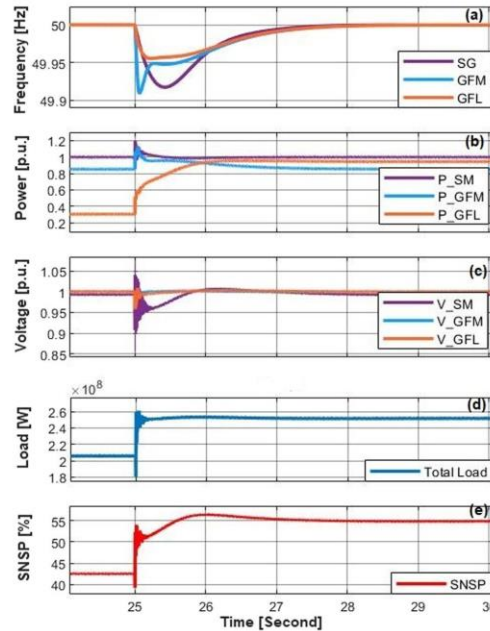
Fig. 13. System's responses (i.e., frequency, generation, voltage, load, and SNSP) at $\Delta P_L = 0.30$ pu.

power generation is considered a common disturbance in a power system, which can affect the performance of the overall power system. Therefore, it is essential to conduct a contingency analysis to evaluate the performance of the power system and ensure its security. Here in this paper, a disturbance is introduced into the model, and the responses to this disturbance have been evaluated using time-domain simulation. Fig. 13 provides a visual representation of the power system's parameters as they change in response to an increase in load of 30% (i.e., $\Delta P_L = 0.30$ pu). As can be seen in Fig. 13, when a load is raised at the 25-second mark, the terminal voltages and frequencies of all generating units begin to decrease, albeit with some degree of variation. At the same time, they boosted their generation in order to fulfill the demand in a secure manner. This allowed for the demand to be met in a manner that was modified within a few seconds and maintained the system's stability. Because a 30% increase in load is significant, it takes a few seconds to maintain the saturation level. Similarly, the voltage level drops quite a bit farther at that precise moment. Nevertheless, within three seconds, most of the parameters achieve/ tend to achieve saturation, and they continue to supply the grid in a secure manner. In addition to that, before disturbance, the SNSP ratio for the considered power system seems to be 43%, whereas the value reached 57% when $\Delta P_L = 0.30$ pu is applied.

In order to conduct a comprehensive study, the level of load disturbance has been adjusted, and the maximum values of the SNSP ratio have been determined. The model of the power system is initially run under normal conditions, and then load disturbances are incorporated into the process. For analysis, different load disturbances are introduced, and the post-disturbance responses are observed. However, as soon as the disturbance reaches 38% of the total load, the system goes into an unstable state. This percentage is determined to be the technical limit of the load disturbance for the scenario that is being studied. The detailed processes of identifying this limit are given in Fig. 5. Fig. 14 displays the maximum SNSP ratio values that have been determined for each of these

load disturbances. As shown in the figure, the SNSP ratio is observed to be 43% while operating under normal conditions, and it grows larger with each rise in the disturbance load ratings. The highest load disturbance that can happen while the power system is running in the mode being looked at is 38%, and this limit must be kept in order to keep things stable. It has been determined that the maximum SNSP ratio value for this stage is 59%, which can be considered the critical limit for power-generating technologies.

5. Conclusion

This paper presents a concept that utilizes historical time-series data from TSOs to estimate the day-long operation and evaluate the secure functioning of a power system on a daily basis. By leveraging the available datasets for the Nordic grid, the paper employs a data-driven model to forecast power generation and load consumption. Through the establishment of an energy-mix operation and reserve schedule model, this paper optimizes the selection of power-generating technologies and ensures sufficient reserves for secure system operation. Dynamic simulations, encompassing a 24-hour period and considering dynamic data on power generation and load consumption, are conducted to determine the optimal energy mix for the day ahead. Furthermore, contingency conditions are analyzed to assess the robustness of the power system model. Quantitative analysis, incorporating factors such as frequency, power generation, terminal voltages, and SNSP value, confirms the effectiveness of the proposed concept. Simulation results demonstrate that the considered power system can continue to operate securely even with an immediate 38% increase in total load, with a maximum SNSP value of 59%. While the highest SNSP value observed during normal operation is 64%, it exceeds 59% only for a brief period. Based on the low probability of encountering an immediate load increase of 38% together with an SNSP value exceeding 59%, it can be concluded that the power system is expected to function
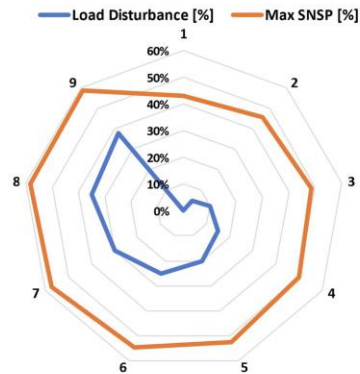
Fig. 14. Maximum SNSP ratio values at different load disturbance.

securely under various circumstances. This research contributes to climate change mitigation and decarbonization strategies by providing a reliable and sustainable approach to power system operation and management.

CRediT authorship contribution statement

Ashish Shrestha: Conceptualization, Formal analysis, Investigation, Methodology, Software, Visualization, Writing – original draft, Writing – review & editing. **Yaju Rajbhandari:** Formal analysis, Software, Visualization, Writing – original draft. **Francisco Gonzalez-Longatt:** Conceptualization, Supervision, Resources, Validation, Writing – original draft, Writing – review & editing.

Declaration of Competing Interest

The authors declare that they have no known competing financial interests or personal relationships that could have appeared to influence the work reported in this paper.

Data availability

Data will be made available on request.

Acknowledgment

Mr. Ashish Shrestha is thankful to the Department of Electrical Engineering, Information Technology and Cybernetics, University of South-Eastern Norway, Porsgrunn, Norway for the support that he receives during his PhD. Also, the authors are thankful to Prof. Nils-Olav Skeie, Assoc. Prof. Ru Yan, Assoc. Prof. Håkon Viumdal, Prof. Ola Marius Lysaker, Assoc. Prof. Ole Magnus Hamre Brastein, Assoc. Prof. Thomos Øyvang, Assoc. Prof. Nurilla Avozov, and Bishal Acharya for their support, suggestions, and motivation during the research period. This research work utilized the real data of Nordic grid for 2021 from FINGRID TSO; the authors would like to thank FINGRID for the datasets.

References

[1] Zappa W, Junginger M, van den Broek M. Is a 100% renewable European power system feasible by 2050? Appl Energy 2019;233:1027–50.
[2] Union, E.C.C.o.t.E. UN climate change conference (COP 26), World Leaders Summit, Glasgow, UK, 1 November 2021. 2021 11/11/2021]; Available from: https://www.consilium.europa.eu/en/meetings/international-summit/2021/11/01/#.
[3] Shrestha A, Ghimire B, Gonzalez-Longatt F. A Bayesian model to forecast the time series kinetic energy data for a power system. Energies 2021;14(11):3299.
[4] Shrestha A, Gonzalez-Longatt F. Frequency stability issues and research opportunities in converter dominated power system. Energies 2021;14(14):4184.
[5] Ju W, Sun K, Yao R. Simulation of cascading outages using a power-flow model considering frequency. IEEE Access 2018;6:37784–95.
[6] Shrestha A, Gonzalez-Longatt F. Parametric Sensitivity Analysis of Rotor Angle Stability Indicators. Energies 2021;14(16):5023.
[7] Shrestha A, Gonzalez-Longatt F. Parametric sensitivity analysis of rotor angle stability indicators: Simulation case. Energy Rep 2022;8:727–35.
[8] Khan S, Gawlik W, Palensky P. Reserve capability assessment considering correlated uncertainty in microgrid. IEEE Trans Sustainable Energy 2015;7(2):637–46.
[9] Gu Y, Xie L. Early detection and optimal corrective measures of power system insecurity in enhanced look-ahead dispatch. IEEE Trans Power Syst 2012;28(2):1297–307.
[10] Gu Y, Xie L. Stochastic look-ahead economic dispatch with variable generation resources. IEEE Trans Power Syst 2016;32(1):17–29.
[11] Tang C, et al. Look-ahead economic dispatch with adjustable confidence interval based on a truncated versatile distribution model for wind power. IEEE Trans Power Syst 2017;33(2):1755–67.
[12] Xie L, et al. Short-term spatio-temporal wind power forecast in robust look-ahead power system dispatch. IEEE Trans Smart Grid 2013;5(1):511–20.
[13] Zhao S, et al. A new power system active rescheduling method considering the dispatchable plug-in electric vehicles and intermittent renewable energies. Appl Energy 2022;314:118715.
[14] Ardakani FF, Mozafari SB, Soleymani S. Scheduling energy and spinning reserve based on linear chance constrained optimization for a wind integrated power system. Ain Shams Eng J 2022;13(3):101582.
[15] Tang Z, et al. Reserve model of energy storage in day-ahead joint energy and reserve markets: A stochastic UC solution. IEEE Trans Smart Grid 2020;12(1):372–82.
[16] Zuo Y, et al. Performance assessment of grid-forming and grid-following converter-interfaced battery energy storage systems on frequency regulation in low-inertia power grids. Sustainable Energy Grids Networks 2021;27:100496.
[17] Anderson PM, Fouad AA. Power system control and stability. John Wiley & Sons; 2008.
[18] Gibbard M, Vowles D. IEEE PES task force on benchmark systems for stability controls simplified 14-generator model of the south east Australian power system. South Australia: The University of Adelaide; 2014.
[19] Poolla BK, Groß D, Dörfler F. Placement and implementation of grid-forming and grid-following virtual inertia and fast frequency response. IEEE Trans Power Syst 2019;34(4):3035–46.
[20] Rocabert J, et al. Control of power converters in AC microgrids. IEEE Trans Power Electron 2012;27(11):4734–49.
[21] Paquette AD, et al. Sharing transient loads: Causes of unequal transient load sharing in islanded microgrid operation. IEEE Ind Appl Mag 2013;20(2):23–34.
[22] Paolone M, et al. Fundamentals of power systems modelling in the presence of converter-interfaced generation. Electr Pow Syst Res 2020;189:106811.
[23] Wang X, et al. Grid-synchronization stability of converter-based resources—An overview. IEEE Open J Industry Appl 2020;1:115–34.
[24] Gao X., et al. Grid-following and grid-forming control in power electronic based power systems: a comparative study. in IECON 2021–47th Annual Conference of the IEEE Industrial Electronics Society. 2021. IEEE.
[25] Du W, et al. Modeling of grid-forming and grid-following inverters for dynamic simulation of large-scale distribution systems. IEEE Trans Power Delivery 2020;36(4):2035–45.
[26] FINGRID, Kinetic energy of the Nordic power system- real time data. 2019.
[27] Ånund K. European hydropower capacity – a study of the correlation between the scandinavian and the alps hydropower system. Hydropower'05 - The Backbone of sustainable Energy Supply. Norway: Stavanger; 2005.
[28] EU, E., River Flow- Projected change in seasonal streamflow for twelve rivers, E.E. Agency, Editor.
[29] ZACH. How to Normalize Data Between 0 and 100. 2020; Available from: https://www.statology.org/normalize-data-between-0-and-100/.
[30] Gielen D, et al. The role of renewable energy in the global energy transformation. Energ Strat Rev 2019;24:38–50.
[31] Impram S, Nese SV, Oral B. Challenges of renewable energy penetration on power system flexibility: A survey. Energ Strat Rev 2020;31:100539.
[32] AEMO, NEM Engineering Framework. 2021, Australian Energy Market Operator.
[33] TransGrid, National Electricity Rules change proposal: Efficient management of system strength on the power system. 2020, Australian Energy Market Operator (AEMO): Australia.
[34] Yu L, et al. An overview of system strength challenges in Australia's National electricity market grid. Electronics 2022;11(2):224.
[35] Baringa; and DigSILENT, Development of Renewable Energy Zones in the NEM. 2020, Australian Renewable Energy Agency: Australia.
[36] Association, U.E.I., Levelized Costs of New Generation Resources in the Annual Energy Outlook 2022. 2022, US Energy Information Administration.
[37] (AER), A.E.R., Quarterly global FCAS prices by services. 2022: Australia.
[38] EirGrid S. System non-synchronous penetration definition and formulation. Ireland: Transmission System Operator; 2018.
[39] Shastri S, et al. Time series forecasting of Covid-19 using deep learning models: India-USA comparative case study. Chaos Solitons Fractals 2020;140:110227.
[40] Kaushik S, et al. AI in healthcare: time-series forecasting using statistical, neural, and ensemble architectures. Front Big Data 2020;3:4.
[41] Kurumatani K. Time series forecasting of agricultural product prices based on recurrent neural networks and its evaluation method. SN Appl Sci 2020;2(8):1–17.

12

[42] Guillén-Navarro MA, et al. A deep learning model to predict lower temperatures in agriculture. J Ambient Intell Smart Environ 2020;12(1):21–34.

[43] Gao Z., et al., Deep learning and the weather forecasting problem: Precipitation nowcasting. Deep Learning for the Earth Sciences: A Comprehensive Approach to Remote Sensing, Climate Science, and Geosciences, 2021: p. 218-239.

[44] Gasparin A, Lukovic S, Alippi C. Deep learning for time series forecasting: The electric load case. CAAI Trans Intelligence Technol 2022;7(1):1–25.

[45] Khodayar M, et al. Deep learning in power systems research: A review. CSEE J Power Energy Syst 2020;7(2):209–20.

[46] Ozcanli AK, Yaprakdal F, Baysal M. Deep learning methods and applications for electrical power systems: A comprehensive review. Int J Energy Res 2020;44(9):7136–57.

[47] Zhang Z, Zhang D, Qiu RC. Deep reinforcement learning for power system applications: An overview. CSEE J Power Energy Syst 2019;6(1):213–25.

[48] Rajbhandari Y, et al. Impact study of temperature on the time series electricity demand of urban nepal for short-term load forecasting. Appl Syst Innovat 2021;4(3):43.

[49] Gorostiza FS, Gonzalez-Longatt FM. Deep reinforcement learning-based controller for SOC management of multi-electrical energy storage system. IEEE Trans Smart Grid 2020;11(6):5039–50.

[50] Wang H, Raj B. A survey: Time travel in deep learning space: An introduction to deep learning models and how deep learning models evolved from the initial ideas. arXiv preprint arXiv:1510.04781, 2015.

[51] Saha S. et al., Deep learning for detecting multiple space-time action tubes in videos. arXiv preprint arXiv:1608.01529, 2016.

[52] Dingli A, Fournier KS. Financial time series forecasting-a deep learning approach. Int J Mach Learn Comput 2017;7(5):118–22.

[53] Lee SI, Yoo SJ. Multimodal deep learning for finance: integrating and forecasting international stock markets. J Supercomput 2020;76(10):8294–312.

[54] Torres JF, et al. Deep learning for time series forecasting: a survey. Big Data 2021;9(1):3–21.

[55] Brownlee J. Deep learning for time series forecasting: predict the future with MLPs, CNNs and LSTMs in Python. 2018: Machine Learning Mastery.

[56] Lim B, Zohren S. Time-series forecasting with deep learning: a survey. Phil Trans R Soc A 2021;379(2194):20200209.

[57] Lara-Benítez P, Carranza-García M, Riquelme JC. An experimental review on deep learning architectures for time series forecasting. Int J Neural Syst 2021;31(03):2130001.

[58] Wu Z, et al. A comprehensive review on deep learning approaches in wind forecasting applications. CAAI Trans Intelligence Technol 2022;7(2):129–43.

[59] Géron A. Hands-on machine learning with scikit-learn and tensorflow: Concepts. Tools, and Techniques to build intelligent systems; 2017.

[60] Staudemeyer RC, Morris ER. Understanding LSTM–a tutorial into long short-term memory recurrent neural networks. arXiv preprint arXiv:1909.09586, 2019.

[61] MATLAB. Deep Learning Using Bayesian Optimization. MathWorks/ MATLAB.

[62] Ma Y. et al., Adaptive Elastic Training for Sparse Deep Learning on Heterogeneous Multi-GPU Servers. arXiv preprint arXiv:2110.07029, 2021.

13

Article 6

Shrestha, A., Marahatta, A., Rajbhandari, Y. and Gonzalez-Longatt, F., 2023. Deep reinforcement learning method in estimation of electricity-mix proportion for the secure operation of converter dominated power system. [Revised, Energy Reports]

1

Deep Reinforcement Learning Approach to Estimate the Energy-mix proportion for Secure Operation of Converter-dominated Power System

Ashish Shrestha[1,*], Anup Marahatta[2], Yaju Rajbhandari[2], Francisco Gonzalez-Longatt[1]
[1]Department of Electrical Engineering, Information Technology and Cybernetics, University of South-Eastern Norway,
Porsgrunn N-3918, Norway
[2]Department of Electrical and Electronics Engineering, Kathmandu University, Dhulikhel 45200, Nepal
Corresponding Email: Ashish.Shrestha@usn.no

Abstract: The dynamic evolution of the modern energy landscape has forced the integration of renewable energy sources (RESs) into power generation, catalyzing a paradigm shift towards converter-dominated power systems. This paper addresses the imperative challenge of optimizing power-generating technologies within these complex systems to ensure both stability and sustainability. The underlying issue lies in effectively managing the energy-mix proportion—balancing the total electricity generated with the overall system load—while accounting for the intermittent nature of RESs. Motivated by the insistent need for adaptive and efficient power system management, this paper presents a pioneering deep reinforcement learning (DRL) approach within modern power system applications. Leveraging the Deep Q-Network (DQN) paradigm, the proposed methodology estimates the energy-mix proportion through a data-driven lens. By integrating MATLAB/Simulink and Python libraries, offline training and online testing validate the approach's applicability in real-world scenarios. Results from comprehensive experiments on an IEEE-9 bus system underscore the efficacy of the DRL-based framework. Notably, the online short circuit level (SCL) emerges as a robust indicator of power system security, a significant innovation in stability assessment. The model demonstrates remarkable responsiveness to load fluctuations, optimizing energy generation and respecting operational constraints. Furthermore, the adaptability of grid-forming (GFM) and grid-following (GFL) converters is showcased, highlighting their resilience in converter-dominated power systems. The study offers a promising avenue for future research and underscores the potential of DRL in power system optimization and operation for a sustainable energy future.

Keywords: Inverter Based Resources; Machine Learning; Power Electronic Converter; Power System Dynamics.

1. INTRODUCTION

As a result of the massive changes that are taking place across a variety of industries, including manufacturing, robotics, information and technology, transportation, and many others, the use of electricity has emerged as one of the most essential building blocks in the modern world. On the other hand, the modern world is concerned with the difficulties surrounding the environment; as a result, there is an increased interest in renewable energy sources (RESs). It has been discovered that the proportion of RESs used in the generation of total electricity around the globe has been rapidly increasing over the last decade (the proportion of RES used globally was 17.68% in 2007 and 27.68% in 2021) [1]. In the effort to reduce the amount of carbon dioxide emitted by power grids around the world, the increasing penetration of RESs (especially inverter-based RESs) has resulted in profound and widespread impacts on the operation, planning, and economics of power systems. The dynamics of the power system are getting more complicated, and additional challenges have been introduced in both its operation and its security [2, 3]. This is especially the case because of the different characteristics of RES technologies. Frequency control, voltage control, fault level control, reactive power management, electromagnetic transient control, dependability, and power quality are some parts of it [4]. However, these are not the only aspects covered. A power system that is dominated by inverter-based resources (IBRs) cannot necessarily supply all of the essential capabilities, and the additional cost to secure these services for the grid needs to be accounted for [5]. As a result, traditional methods are no longer adequate to plan and operate modern power systems.

1.1. Literature review

In order to address the issues that have been identified as being brought on by the rapidly changing topologies of grids and the incorporation of new technologies, researchers are developing a wide range of ideas and strategies. A large number of research and developments have been directed toward methods for maintaining stable voltage, stable rotor angle, and stable frequency [6-8]. A critical technique deserving significant attention is the effective management of instability, whether it occurs in online or real-time scenarios. This is of vital importance due to the fact that instability has consistently emerged as the primary cause behind the countless blackouts documented over the past several decades [9, 10]. Through several research experiments, the researchers discovered techniques for resolving problems with a low-inertia system's frequency management that were both effective and dependable. Many of them participated in the discussion regarding the low inertia system, offering their opinions and suggestions for more enhancements. It seems likely that implementing some kind of inertial support would be the best course of action; nevertheless, in order to keep the system's inertia at an appropriate level, this would need solutions that are long-lasting, secure, dependable, and practically applicable [11]. Similarly, the management features and operating principles of revolving power systems have the potential to play significant roles in the process of finding solutions to problems. From these statements, it's clear that there are different technologies and ways to solve problems that can help with RES-related problems in modern power systems. The authors of this paper believe that the two best options are: (a) the development of new technologies, components, or devices

that have flexible properties that can operate with system dynamics, and (b) proper planning, management, and implementation of operational strategies.

The recent advancements in regulating power electronic converters (PEC), such as grid-following (GFL) and grid-forming (GFM) converters, are prime examples of the significance of the components and the progression of technology. GFM is a kind of PEC that helps in adjusting the frequency and voltage amplitude (i.e., magnitude and angle of the voltage) at the Point of Common Coupling (PCC) [12, 13]. The fundamental function of the GFM is to regulate the output voltage and/or current in such a way that the frequency and voltage of the system remain within acceptable parameters. One of the main advantages of GFM over GFL is that it can set its frequency and synchronize with the grid; it is highly useful in weak power systems [14]. However, because the current in the GFM is limited, it shows complicated transient properties when it is studied with large disturbances [15]. The idea of a GFM that can be changed in different ways might be able to solve the problems that have been brought up, but researchers are still looking into its real features, reactions, and effects [16]. On the other side, GFL has flaws as well; because of its reliance on the grid for synchronization, it is unable to handle the large- integration of converters. At this stage, its successful execution in conjunction with the planning approach has the potential to be a crucial player in the process of resolving the challenges.

In the rapidly evolving realm of converter-dominated systems, there is a pronounced focus on forecasting future challenges and potential opportunities, as highlighted by a study [16]. Ardakani et al. [17], propose a linear chance-constrained optimization methodology for the day-ahead electricity market, ensuring that grids integrated with RES maintain security and reliability against potential disruptions. In contrast, Tang et al. [18], put forward a stochastic unit commitment model which underscores the potential of battery energy storage systems (BESS) to render grid services by merging energy and reserve markets. Their model specifically addresses the uncertainties tied to RESs and demand, shedding light on the reserves of BESSs and generators. Confirming this sentiment, Zuo et al. [19], analyzed the efficacy of a low-inertial power system equipped with GFL and GFM, alongside a BESS. A doctoral research project [20], aspires to devise innovative control strategies, targeting challenges spawned by diminished rotational inertia in modern power systems. The core emphasis of this research splits into two dominant themes: frequency control anchored in Fast Frequency Response (FFR) strategies and frequency control during urgent scenarios with a focus on the Under Frequency Load Shedding (UFLS) scheme. Concurrently, several research papers [21-24] investigate into the strategic management of power system security, leveraging economic indicators and forward-thinking dispatch strategies. Collectively, these works defend operational strategies with an overarching aim to reinforce the reliability and security of power systems.

Similarly, there has been a notable increase in the adoption of cutting-edge tools and methodologies with the intent to strengthen efficiency, reliability, and safety. For example, blockchain technology is paving the way for a new era in energy trade by fostering transparent and impenetrable direct energy transactions, which is leveling the playing field in the energy sector [25, 26]. Digital twins, serving as digital mirrors of tangible energy infrastructure, are enhancing the capacity for real-time tracking and simulation-driven evaluations, empowering system operators to predict grid reactions and refine their decision-making [27]. The blending of digital and physical realms, known as the cyber-physical framework, merges algorithmic and tangible components within power systems, providing a comprehensive solution to grid operations while fortifying defenses against approaching challenges [28, 29]. With the expanding influence of the Internet of Things (IoT), devices like intelligent meters and detectors are contributing a deluge of data, fortifying network links, and hastening the shift to intelligent power grids [30]. Additionally, Machine Learning (ML) and data-driven approaches are emerging as a keystone for activities such as preventative maintenance, demand projection, and spotting irregularities, leading to a more agile and anticipative grid management approach [31-33]. Collectively, these advancements are propelling the power system sector into a phase marked by enhanced connectivity, intelligence, and sustainability.

In discussing the various methodologies, tools, and techniques, it's vital to consideration in the benchmarks for evaluating grid performance and metrics for evaluating the robustness of power systems [34]. The performance of power systems can be assessed using several criteria, including: (a) system strength (SS), (b) metrics related to power quality, (c) reliability measures, (d) stability benchmarks, (e) metrics of operational efficiency, (f) resilience and security measures, and (g) environmental and sustainability standards, among others [35-37]. Each criterion offers a distinctive perspective to review and examine the efficacy of the power system. Within the framework of an IBR-dominated power system, robustness becomes especially crucial [34]. For instance, SS, often assessed by the short-circuit capacity, reveals the grid's resilience to external disturbances [38]. A grid with higher strength is more adept at sustaining consistent voltage levels when confronted with disturbances, thus ensuring a smooth operational experience for all grid-connected devices and machinery. While guidelines do acknowledge the strength services that transmission network service providers (TNSPs) must deliver, they don't cover the strength rectification mandated for new or evolving power-generating connections. This perspective is fundamentally tied to the advantages of efficiency, security, and resilience that the grid supplies [39]. Notably, as the share of PEC-dominated solutions expands within a power grid, a more enhanced strength threshold becomes indispensable for secure system operations.

1.2. Research gap and motivation

Modern power systems have evolved considerably with the integration of IBRs and the increasing dominance of RESs. While there is extensive literature that underscores various methods of maintaining equilibrium within power systems dominated by these resources, a comprehensive solution remains ambiguous. Many of the existing studies have explored diverse possibilities, tackling frequency control issues and offering scientific approaches to address the challenges brought on by IBRs. However, recurring themes such as communication complications, processing delays, high computational power demands, and accuracy concerns

remain prevalent [40-42]. This landscape presents a pronounced research gap: the absence of a real-time approach tailored to the unique requirements of an IBR-dominated system [43]. A holistic solution must facilitate the accurate estimation of the real-time electricity-mix proportion, ensuring the secure operation of the system in both routine and emergency scenarios.

The necessity for computational efficiency further compounds the challenge. While data-driven methods offer time efficiency, they often overlook the sophisticated physical topology of power systems, thereby missing out on mining complete information [44]. On the other hand, model-based simulation, though potentially effective, comes with the baggage of computational intensity and prolonged response time [45, 46]. The dynamic evolution towards converter-dominated power systems, punctuated by the intermittent nature of RESs, amplifies the urgency of this research gap. A key challenge emerges optimizing the energy-mix proportion to ensure both system stability and sustainability, while simultaneously managing the unpredictability introduced by RESs. The motivation behind this research stems from this gap, driving the quest for an adaptive, efficient, and data-driven methodology that seamlessly integrates with the modern energy landscape, prioritizing both stability and sustainability.

1.3. Contribution

Given these identified research gaps, this paper aims to introduce a novel deep learning framework. This approach focuses on estimating the energy-mix proportion within converter-dominated power systems, ensuring secure operation under normal and unforeseen conditions. Notably, the presented deep reinforcement learning (DRL) method adopts a data-driven paradigm, enabling efficient estimation of power-generating technology proportions with reduced computational demands and desired time frames. The estimation process accounts for percentile changes in both load and generation, facilitating the identification of values critical for ensuring the secure operation of the examined power system. The paper's major contributions encompass:

a. This research paper introduces a DRL-based approach for managing the operation of power-generating technologies in converter-dominated power systems, addressing a critical gap in existing research. The Deep Q-Network (DQN) approach effectively manages synchronous generators (SG), GFM, and GFL, crucial elements in systems.

b. This research paper demonstrates the successful integration of MATLAB/Simulink and Python libraries for both offline training and online testing. Such a hybrid approach stands as a testament to the paper's commitment to robust, practical solutions, ensuring that model training and validation reflect genuine, on-ground scenarios.

c. Utilization of the online short circuit level (SCL) as an indicator of power system robustness, offering a reliable metric for system analysis and evaluation. Beyond its traditional applications, SCL is introduced here as an intelligent indicator of power system robustness. This step provides a reliable metric for system analysis and evaluation, allowing for a deeper understanding of power system security.

1.4. Organization of paper

The following outlines provide an overview of the paper that has been delivered. In Section 2, the basics of the relevant terminology and the problem formulations have been presented. Following that, Section 3 provides a detailed explanation of the approach that is used when carrying out this research work. Given that it contains a detailed discussion of the proposed ideas for both the DRL model and the architecture, Section 4 is a very important part of this research paper. After that, the simulation work and the results are shown in Section 5, and Sections 6 and 7 present the discussion and conclusions that have been drawn from the results.

2. ENERGY MIX IN CONVERTER-DOMINATED POWER SYSTEM

The combination of the different fuels/ resources/ technologies utilized to produce energy in a certain geographic area is referred to as the energy mix (also known as the power-generating mix). The authors, however, are concerned with the energy-mix notion in a power system that is assumed to be based entirely on RESs. The energy-mix in this case provides a solution to the question of which RES and how much power must be produced to meet the electrical demand. Basically, hydroelectric projects which feature SG, and IBRs will make up the majority of the system's contribution if 100% RESs are assumed to be the source. PECs may be broadly divided into two categories: GFM and GFL. Fig. 1 provides an overview of the power system with power-generating technologies that are expected to be in charge of meeting demand and supplying it. Equation (1) gives the actual relation of the generated power (P_t^T), demand (L_t^T), and the total losses ($P_{loss,t}^T$) within a power system. The overall amount of power produced using these technologies ought to be equal to the total demand if it is assumed that there are no losses in the transmission and distribution lines, as given in Equation (2). The symbols $P_{SG,t}$, $P_{GFL,t}$, and $P_{GFM,t}$ represent the power produced at t by the SG, GFL, and GFM, which are expected to meet the total electrical demand with the desired power quality.

4
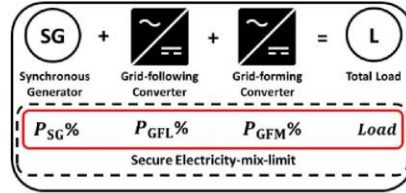
Fig. 1. Power generating technologies available in 100% RES-based power systems.

$$L_t^T + P_{loss,t}^T = P_t^T \tag{1}$$

$$P_{SG,t} + P_{GFL,t} + P_{GFM,t} = P_t^T = L_t^T \tag{2}$$

However, in order to operate the power system securely, both the demand and the electricity generated by RESs like solar and wind must be regulated simultaneously, necessitating the analysis of simultaneous equations with several variables. Some of the things that must be considered are: how reliable and robust the energy sources and power generation technologies are; how the generators react in an emergency; and how strong the power grid is. In this stage, the main challenge is to identify the suitable proportion of the power-generating technologies that can deal with the discussed factors efficiently while operating the power system and guarantee secure operation. SG is regarded as the best generator source since it has most of the necessary features to keep the power system running safely even in contingencies. Basically, the characteristics of SG can be described by Equation (3), popularly known as the swing equation.

$$J \frac{d(\omega_{ref} - \omega_0)}{dt} = P_{SG,ref} - P_{SG} - D(\omega_{ref} - \omega_0) \tag{3}$$

Here in Equation (3), $P_{SG,ref}$ indicates the reference active power (i.e., mechanical power of the SG), P_{SG} indicates the output power (i.e., electromagnetic power), J indicates the inertia coefficient, D indicates the damping factor, ω_{ref} indicates the reference of the angular frequency, and ω_0 indicates the nominal angular frequency of the grid.

Let us consider, a change in load (ΔL_t) has occurred at t, and the intention is to calculate the power at ($t + 1$), then Equation (3) can be written in the form of Equation (4), where $P_{SG,t+1}$ gives the output power for SG after the disturbance, $P_{SG,t}$ gives the reference active power, and $\omega_{SG,t}$ gives the reference of the angular frequency.

$$P_{SG,t+1} = P_{SG,t} + J \frac{d(\omega_0 - \omega_{SG,t})}{dt} + D(\omega_0 - \omega_{SG,t}) \tag{4}$$

However, the PECs, which added complexity to the dynamics of the power system, are replacing conventional SG-based generation resources (especially non-renewable) in increasing order. In this condition, a good source of power for a secure power system could be GFM. It is the main responsibility of GFM in a power system to adjust the output voltage and/or current in order to maintain the system's frequency and voltage steady. The amount of power that should be provided by the GFM under certain changes in load (ΔL_t) can be calculated by using Equation (5), where $\omega_{PCC,t}$ is the reference frequency to be imposed at the PCC, ω_0 is the reference frequency when the GFM injects the reference power $P_{GFM,t}$, and m indicates the droop coefficient factor.

$$P_{GFM,t+1} = P_{GFM,t} + \frac{\omega_0 - \omega_{PCC,t}}{m} \tag{5}$$

Similarly, here in this study, the GFL is used, which implemented the droop controller to adjust the active power that should be injected/ejected by the battery energy storage system (BESS). This GFL is considered to be operated under the grid-supporting mode. In this paper, the main objective of this GFL is to pass the energy from/to BESS by measuring the frequency at the phase-locked loop (PLL), so that the system tries to restore the nominal frequency. Equation (6) gives the suitable active power value supplied/ absorbed by the GFL under load changes ΔL_t, where $\omega_{PLL,t}$ is frequency measured at PLL.

$$P_{GFL,t+1} = P_{GFL,t} + \frac{\omega_0 - \omega_{PLL,t}}{m} \tag{6}$$

While injecting/ ejecting the energy from BESS, some constraints should be followed. First of all, the BESS should have the energy at an acceptable limit (i.e., $SoC_{max} \geq SoC_t \geq SoC_{min}$); BESS will not respond when the state of charge at t (SoC_t) is out of its limits. The maximum amount of power that the BESS can supply/ absorb is given by Equation (7), where E_{BESS}^{max} is the maximum capacity of BESS to store the energy and directly depend on the BESS's size.

$$P_{BESS}^{max} = \frac{E_{BESS}^{max}}{\Delta t} \tag{7}$$

5

Similarly, in Equation (8), the relationship between the variables that are pertinent to the in-operation, start-up, and shutdown of the power-generating technologies is given. For the start-up and shutdown of the generators, it is of the utmost importance to remain within a reasonable range; the generators should adhere to the requirements set by the grid. Hence, constraints are placed on the variables that are associated with the start-up and the shutdown of the power-generating technologies and are given in Equation (9), where $U_{G,t}^{on}$, $U_{G,t}^{Up}$ and $U_{G,t}^{Down}$ are the variables related to unit commitment, start-up and shut-down of the power-generating technologies at t.

$$U_{G,t}^{on} - U_{G,t-1}^{on} = U_{G,t}^{Up} - U_{G,t}^{Down} \tag{8}$$

$$U_{G,t}^{Up} + U_{G,t}^{Down} \leq 1 \tag{9}$$

On the other hand, Equation (10) describes the connection that exists between the quantity of power that can be produced by the generators and the highest and lowest ramp rates that the generators are capable of functioning, where $RP_{G,t}^{Up}$ and $RP_{G,t}^{Down}$ are the upper and lower bounds of the ramp rates, and $P_{G,t}$ is the power generated for the power generators at t. In the same way, Equation (11) shows the conditions for active power generation by all of the generators, where P_G^{min}, P_G^{max}, and $P_{G,t}^{reserve}$ are the minimum, maximum, and available reserve limits. Equation (12) presents the constraints for the phase angle stability, where θ_G^{min} and θ_G^{max} are the minimum and maximum limits of the phase angle, and ($\theta_G - \theta_{SG}$) indicates the differences in the phase angles. Finally, Equation (13) shows the constraints for the amount of energy that should be saved to make sure there is enough power.

$$U_{G,t}^{on} RP_{G,t}^{Down} \leq P_{G,t} - P_{G,t-1} \leq U_{G,t}^{on} RP_{G,t}^{Up} \tag{10}$$

$$P_G^{min} \leq P_{G,t} + P_{G,t}^{reserve} \leq P_G^{max} \tag{11}$$

$$\theta_G^{min} \leq \theta_G - \theta_{SG} \leq \theta_G^{max} \tag{12}$$

$$U_{G,t}^{on} P_G^{min} \leq P_{G,t} \leq U_{G,t}^{on} P_G^{max} \tag{13}$$

The Equations (7-13) [19, 47], provide the constraints to be followed while estimating the generations from the power-generating technologies for continuously operating power systems.

3. ADOPTED METHODOLOGY AND ASSUMPTIONS

3.1. Power system case study

Fig. 2 shows a benchmark system used to assess system performance under the proposed framework. The IEEE 9 bus is taken as the primary network, which is detailed in P.M. Anderson's book [48]. During the analysis, the authors assumed the first generator is a SG, the second is a wind turbine with a GFM, and the third is a BESS with a GFL. The power system model is taken from the author's previous work [47]. As it is known, the total generation P_t^T must be equal (or near equal within an acceptable range) to the total load L_t^T of the power system to operate securely. Similarly, the next energy-mix total P_{t+1}^T must equal (or nearly equal under substantial constraints) the upcoming total load L_{t+1}^T, so no demand/supply unbalance issues will be developed during power system operation. However, wind power and load consumption are stochastic and are independent, the SG and battery energy storage system (BESS) power should be managed based on constraints; the online proportions of SG and GFL power must be recognized based on load consumption and GFM power stochasticity.
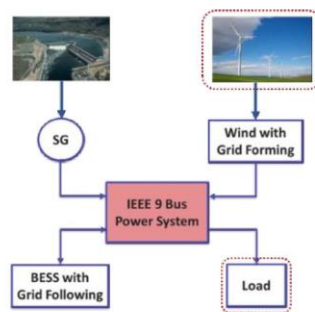

Fig. 2. Overview of the considered power system.

3.2. Estimation framework and datasets

The main concerns that must be considered are the power quality and the security of the system during normal as well as in contingencies; the SS must be sufficient during selecting the constraints and performance assessment. The authors simulate the power system model in MATLAB/ Simulink 2021a in the time domain framework with changes in power productions and connected load in order to analyze the performance of the proposed concept in the considered scenarios. To evaluate the suggested model's performance and the safe functioning during disturbances, several data patterns of load and power generation variations have been gathered, so that the characteristics of the power system components can be analyzed. The whole conception and operation of the considered benchmark adhere to the Nordic TSO's grid code [49]. The most significant constraints taken into account during power system operation are (a) variables related to the running, starting, and shutting down of the generators; (b) the maximum and minimum ramp rates at which the generators may operate; (c) the bound for the amount of energy that should be set aside to provide a sufficient supply; (d) phase angle stability; (e) charging and discharging modes with SoC of the BESS; and (f) values of SCL. In this case, the values of the components that need to be recognized make up Y_t (i.e., power from SG and GFL), when the generator's reserve power capacity is enough at time step t, $Y_t^i = 1$; otherwise, 0 is returned. The appropriate features for the stochastic variables are represented by the second set of feature planes called X_t.
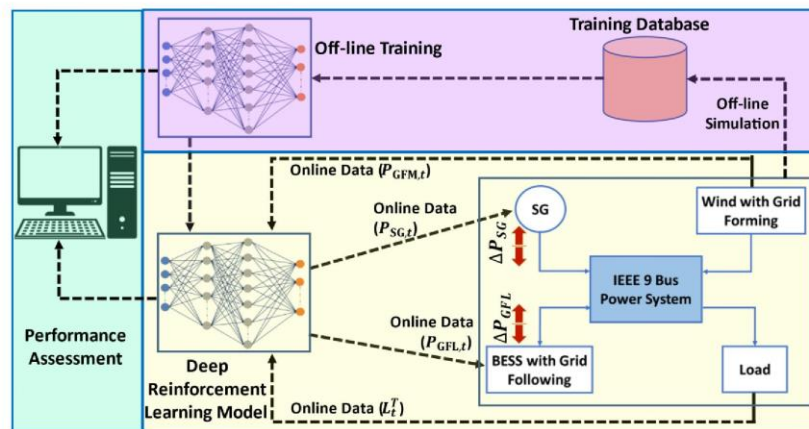

Fig. 3. Overview of the methodology for online energy-mix estimation.

An overview of the proposed methodology is shown in Fig. 3. The authors linked a benchmark power system, which includes several power-generating technologies, to the IEEE 9 bus system as the main network, as illustrated in Fig. 2. First, a power system model in MATLAB/Simulink is simulated in off-line mode with varying system loads and generations for contingency scenarios, and data on different component-related parameters is gathered that can be utilized as a training set for the estimation model. The patterns of variations in the parameters are taken into consideration; sudden load changes have been applied from 1.00 pu to 1.25 pu, while generation from GFM has been varied from 0.75 pu to 1.0 pu, and generation from SG has been varied from 0.75 pu to 1.0 pu. While generating the dataset, the disturbance is introduced and removed (i.e., switching the disturbance/ contingency) every 5 seconds so that the required diverse dataset can be achieved in a sufficient amount. All of the considered set points are given in Table 1. The sampling time and sampling frame of the measurements can be defined during the collection of scope values for the parameters. However, the authors took the samples at 10-millisecond resolutions from 20 to 50-second time scales. Considering the given sampling time and frame, a total of 792,000 samples have been collected as the data sets. While collecting the data sets, white Gaussian noise of 5e-6 noise power with a sample time of 0.01 is used so that practical results can be experienced. The data are gathered through the excitation signals for different load disturbances; a sample of the generated data for $\Delta P_L = 0.25$ pu at 0.85 pu of SG and 1.0 pu of GFM is shown in Fig. 4. In addition, Fig. 5 illustrates the characteristics of the collected datasets. As shown in Fig. 5, the authors collected a diverse dataset, so that most of the scenarios will be covered under consideration.

TABLE 1: Considered variations on generations and load to collect datasets

| Parameters	Values
Load applied	[1.0, 1.05, 1.10, 1.15, 1.20, 1.25] pu
GFM generation	[0.75, 0.80, 0.85, 0.90, 0.95, 1.0] pu
SG generation	[0.75, 0.80, 0.85, 0.90, 0.95, 1.0] pu
Switching close	[25, 35, 45] second marks
Switching open	[30, 40, 50] second marks
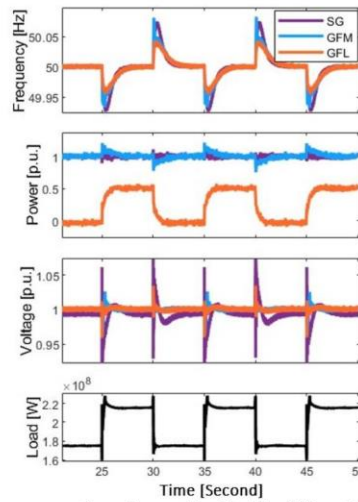
Fig. 4. Sample of frequency, power generation, voltage, and load for $\Delta P_L = 0.25$ pu at 0.85 pu of SG and 1.0 pu of GFM.
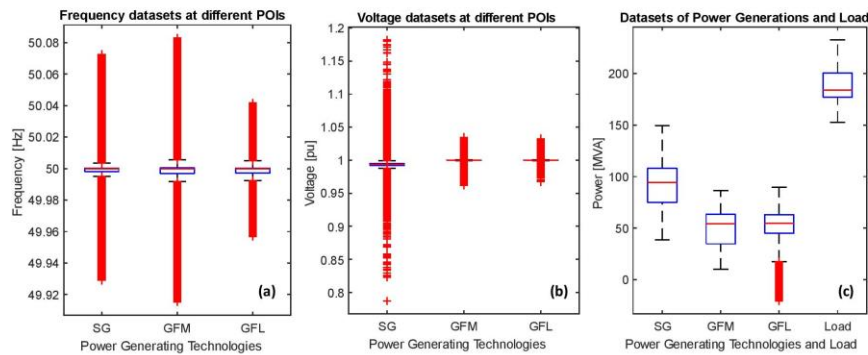

Fig. 5. Box plots of the collected datasets (a) frequency, (b) voltage, and (c) power generations and load

This research work employs a hybrid approach in applying DRL to power system operations, integrating offline training to enhance online decision-making efficiency. The offline training phase involves a detailed analysis of power system component characteristics and the establishment of operational limits. A neural network is trained using previously available data on the power system and the same neural network is transferred to reinforcement learning model to be used and further optimized by the reinforcement learning model. As a result, the DRL algorithm is pre-equipped with substantial knowledge about typical system behaviors, significantly reducing the computational demands during online application and leading to immediate solution generation. However, challenges arise when the system faces conditions beyond the trained operational limits. In these instances, the DRL algorithm, operating on a self-learning mechanism, must adapt online, processing new information and learning to handle these unique conditions. This shift can introduce delays in optimal decision-making, but these delays are relatively minimal compared to the overall enhanced efficiency. The offline training ensures that the DRL algorithm is well-prepared for most scenarios, facilitating immediate responses and reducing computational load under standard operational conditions, thus maintaining a balance between efficiency and adaptability.

A more detailed discussion of the DRL model can be found in Section 4 of the document. In the presented concept, the online data of GFM power and load consumption serve as the inputs (X_t) for the DRL model, while the signals that govern the actual generation from the SG and GFL serve as the outputs (Y_t). Based on the options made by the presented model, the signals manage the SG and GFL generations. There are two options available for each of the two controllable generators (SG and GFL): either raise or reduce generation. The signal to control via these two possibilities with precise quantities (ΔP_{SG} and ΔP_{GFL}) is provided by the presented model. It is a theory of how the power system can manage itself under various circumstances and preserve power

quality while running securely. The model's effectiveness is continually evaluated through performance indexes. In this technique, the power system operates in a time-domain framework in a MATLAB Simulink environment, while the DRL model is computed in a Python environment that is equipped with various libraries like TensorFlow, Keras, SciPy, Scikit-learn, and so on. To operate these two environments, MATLAB interacts with the Python interpreter via the pyrunfile function. The integration between these two environments provides the facilities to evaluate and analyze the online testing results.

3.3. Indicator to assess the power system robustness

In light of the transformative changes displayed within modern power systems, SS has emerged as a pivotal security service that warrants thorough proper planning. The Australian Energy Market Commission (AEMC) defines SS as "a property of an electrical power system, indicative of the magnitude of voltage changes resulting from disturbances or malfunctions within the system" [50]. Essentially, a grid boasting a high SS is considered strong, whereas one with reduced SS is classified as weak. This strength, a testament to a grid's robustness, can be evaluated through metrics such as the short circuit ratio (SCR), X/R ratio, and notably, the short circuit level (SCL) [51].

Central to this discuss is the point of interconnection (POI), where different power-generating technologies integrate with the grid. Here, fault levels are continuously measured, categorizing power systems based on their inherent SS. Systems with elevated fault levels generally possess a remarkable SS, contrasting those with depressed fault levels which are consistently weak. The dynamic behavior of these weak systems renders them highly sensitive to reactive power fluctuations, a feature impaired when IBR-based generators, responsive to voltage variations, produce instantaneous reactive and active power injections at the POI [51]. It is this very fact that leads systems dominated by IBR and distanced from synchronous machines to invariably have reduced SS [52]. This is attributable to IBR's mean contribution to fault level, in plain distinction to the substantial contributions from SGs. A critical consideration centers on the interaction between SGs and IBRs. The displacement of SGs reduces the SS of a power system. Conversely, as IBR-based technology penetration multiplies, there's an essential surge in SS to ensure power system operations [39]. Operational guidelines highlight the obligatory SS services provided by TNSPs [53]. These guidelines, however, do not condense the SS remediation mandatory for power-generating connections. The implications of this oversight are profound. The multiple benefits the electrical system extends - spanning safety, efficiency, and resilience - to its stakeholders, including consumers and investors, hinge on this concept [53].

In this paper, the authors adopted the SCLs as the indicator of the SS, which is identified at the POI of each power-generating technology. Typically, the SCL is derived from Ohm's law and system parameters. While the actual mathematical representation can vary based on the specific configuration and details of the power system, a general expression for SCL at i^{th} POI is shown in Equation (14), where $V_{pre-fault}$ is the voltage at the POI just before the fault occurred, Z_{total} is the total impedance seen from the fault point back to the source. For different types of faults Z_{total} would change, leading to different SCL values.

$$SCL_i = \frac{V_{pre-fault}}{Z_{total}} \tag{14}$$

However, for the online test, online values of SCL are required, which is about continuous or periodic monitoring in online-time during the actual operation of the power system. The purpose of these measurements is to provide up-to-date information about the current system conditions, especially in today's power systems where dynamic changes due to renewable integrations, grid operations, and load variations can rapidly change the system's fault response. To obtain the online values of SCL_i at t^{th} time, Equation (15) is used in this paper, where I_t and V_t are the value of current and voltage through the POI at t^{th} time, and I_{t-1} and V_{t-1} are the value of current and voltage through the POI at $(t-1)^{th}$ time.

$$Online\ SCL_{t,i} = \sqrt{3} \left(\frac{I_t - I_{t-1}}{V_t - V_{t-1}} \right) I_t\ V_t \tag{15}$$

The online-SCL can be monitored by using natural as well as artificial disturbances [54]. While obtaining the values, the SCL is measured by using both disturbances (i.e., hybrid); a signal of white noise is used as the artificial disturbance, and the frequent load and generation changes are responsible for the natural disturbances. After measuring the values of SCL, the minimum SCL value required to be a strong grid is considered while performing the online testing; based on which the energy-mix proportion has been identified for system security.

4. PROPOSED DRL APPROACH AND ARCHITECTURE

Fig. 3 already provides an overview of the methodology used in this paper, and it is clear from this that the DRL technique plays a critical role in this research work. As covered in Section 3, the presented DRL model functions as a decision-making tool that optimizes processes and produces the best possible outcomes, through the application of the data-driven approach. In this paper, the DQN algorithm, a pioneer in deep Q-learning methods, is employed as the chosen DRL approach. This decision is underpinned by five critical considerations. First and foremost, the inherent attributes of the problem domain fit together with the DQN algorithm's strengths, particularly its adeptness at managing high-dimensional state spaces and discrete action spaces. Even when

opposed to the challenges of continuous action spaces identified earlier, it can be navigated using discrete approximations. Secondly, for the broader research community to benchmark progress in DRL, it's pivotal to reference foundational methods. As such, DQN offers a robust baseline, facilitating comparative analyses with more advanced or specialized algorithms. Thirdly, while methods like distributed PPO might confer certain benefits, they also introduce considerable computational demands. Within the confines of the computational resources and research scope, DQN emerges as both practical and convincing. Building on this, the fourth consideration is the prospective extensibility of the presented research work. By initiating with DQN, a robust groundwork for subsequent exploration of advanced methodologies can be laid. Finally, the transparent nature of DQN's architecture and approach ensures interpretability. Such clarity is vital for the objectives of this paper, as to interpret not just the outcomes but the agent's decision-making trajectory as well.

The DQN model presented in this study is developed using collected datasets, with an emphasis on addressing the challenges of a continuous action space. To manage this, the study adopts an action discretization strategy, setting practical limits for generator set points to convert the continuous action space into a series of discrete, manageable actions. This approach allows the DQN model to function effectively, with modifications that retain the critical aspects of the continuous nature of the problem. It is important to note that while action discretization may lead to some level of approximation, the granularity chosen is informed by a balance between operational accuracy and computational feasibility. This enables the model to meet system objectives efficiently without compromising the system's safety or stability, even when encountering conditions outside the trained operational limits.

4.1. DQN Reinforcement learning

The goal of a DRL technique is to continuously interact with the environment while training an agent to learn an optimal policy that maximizes the expected reward return. In comparison to other cutting-edge policy gradient techniques, the Q-learning technique is one of the most straightforward types of model-free reinforcement learning. It is also possible to think of it as an approach to asynchronous dynamic programming that allows agents to learn how to behave best in Markovian domains by experiencing the outcomes of their choices rather than requiring them to create domain maps [55]. Through the experience of learning how to conduct themselves optimally in other domains, the agents are able to learn how to act optimally in Markovian domains [56]. The decision-making procedure is represented by five tuples (S, A, P, R, Y), where S stands for space, A for action space, P for state transition probability, R for reward function, and Y for discount function. The goal of engaging with one's environment should be to maximize the overall reward earned during the training period [57, 58]. Equation (16) can be used to get the best projected action-value function where every state can be reached by the destination in a single step. $R_{t_{k+1}}$ here signifies the reward for executing the action A to move from the state S to the state S' and denotes the discount factor $\gamma \in [0, 1]$ [57].

$$G_t = \sum_{k=0}^{n} \gamma^k * R_{t_{k+1}} \tag{16}$$

However, a DRL's primary goal is to map the appropriate state-action pairings, and in this paper, it is accomplished by creating a Q value "optimal action-value", and changing its value as the algorithm investigates the surrounding environment. The state S' in each of the following sets of potential state-action pairings, given by the notation (S', A'), would have the maximum possible value for that state's action (S, A). There is a need for a component that shows how many current advantages should be kept and how many future rewards should affect the current decision since Equation (17) only considers the present and future rewards [59]. Here, the learning rate (α) is provided to shed some light on the matter. Similarly, any gains are downplayed in importance by using the discount rate (γ). After accounting for these variables, the action-value function is updated and shown in Equation (18).

$$Q_\pi(S, A) = E[R_{t+1} + \gamma \times max_\pi Q(S' + A')] \tag{17}$$

$$Q_\pi(S, A) = (1 - \alpha) + \alpha[R_{t+1} + \gamma \times max_\pi Q(S' + A')] \tag{18}$$

Normally, Q-learning uses the hard max operator to update the value function. However, in this paper, the Dynamic Boltzmann softmax operator (DBSO), $\forall_S \in S$ as given in Equation (19) [60], is used to optimize and update the value function (V_t).

$$\text{boltz}_{\beta_t}(Q(S, \cdot)) = \frac{\sum_{A \in \mathcal{A}} e^{\beta_t Q(S, A)} Q(S, A)}{\sum_{A \in \mathcal{A}} e^{\beta_t Q(S, A)}} \tag{19}$$

Here in Equation (17), β_t is the state-independent sequence, which is a non-negative value and needs to be updated regularly. Processes as given in Equations (20) and (21) [60], are used to update the DBSO in a dynamic way.

$$\forall S, A, Q_{t+1}(S, A) \leftarrow \sum_{s'} p(S' \mid S, A)[R(S, A) + \gamma V_t(S')] \tag{20}$$

$$\forall S, V_{t+1}(S) \leftarrow \text{boltz}_{\beta_t}(Q_{t+1}(S, \cdot)) \tag{21}$$

An agent in a DRL communicates with their environment via the use of actions, and when they complete a state-action pair, they are rewarded for their accomplishment. In order for the DRL to be able to take appropriate action for a state that it has encountered, it should have interacted with the environment for that specific situation and trained itself on it. A policy (π) is required because the model cannot work in an environment in which there is the potential for an infinite number of states; as a result, there is a requirement for the policy. The authors of this paper arrived at a suitable policy by using a neural network in combination with the optimal values obtained from the Q policy, which forms DQN. The overview of the adopted concept is shown in Fig. 6, which depicts the cognitive process that supports the paradigm.
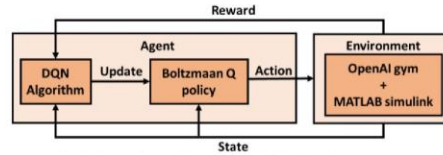

Fig. 6. Overview of the adopted DQN-learning approach.

In the next word, the DQN method expands on the Q learning technique by employing a neural network to make an approximation of the action-value function $Q_\pi(S, A)$. Using Q learning, an agent may learn to behave in a manner that maximizes the projected cumulative reward, $R_{t_0} = \sum_{t=t_0}^{\infty} \gamma^{t-t_0} R_t$, and then put that knowledge to use [61]. The action with the highest value is chosen after an evaluation of the value of each action in each state using a function referred to as the action-value function $Q_\pi(S, A)$. The Bellman equation (17) is an iterative update technique that takes into consideration both the reward that was earned after completing an action as well as the predicted future reward that will come from the following state. One of the most important developments that the DQN algorithm has made is the implementation of experience replay [62]. This gives the agent the ability to learn from their mistakes in the past. The agent remembers its prior experiences in the form of a buffer, which is composed of four tuples (S, A, R, S'). After then, a haphazard selection of events is picked from this buffer and used as input to the neural network while it is being trained. As a direct consequence of this, the learning is more consistent, and the correlation between the events is reduced. The error across batch transitions, B, sampled from the reply memory, can be minimized with the help of Huber loss (22) [63].

$$\mathcal{L} = \frac{1}{|B|} \sum_{(S,A,R,S') \in B} \mathcal{L}(\delta) \tag{22}$$

$$\text{where, } \mathcal{L}(\delta) = \begin{cases} \frac{1}{2}\delta^2 & \text{for } |\delta| \leq 1 \\ |\delta| - \frac{1}{2} & \text{otherwise} \end{cases}$$

Here in Equation (22), δ is the temporal difference error and can be calculated by Equation (23).

$$\delta = Q_\pi(S, A) - \left(R_{t+1} + \gamma \times max_\pi Q(S' + A')\right) \tag{23}$$

Another improvement is the utilization of a target network, which is a different neural network with predetermined parameters that are used to compute the target values [64]. The present condition of the environment is taken into consideration as input by the neural network, which then generates estimated action-values for all possible courses of action. The loss is calculated as the difference between the action-values that are predicted and the target values, which are established with the help of the Bellman equation. Through the use of a neural network and the optimum values derived from the DBSO, the authors have implemented the most effective policy, denoting it as DQN.

4.2. State, reward, and action spaces

The variables used as inputs for the DRL agent are the state spaces. The key components of the power system under consideration that need to be watched over to make sure they are running securely are the frequencies (f_{SG}, f_{GFL}, and f_{GFM}), voltages (V_{SG}, V_{GFL}, and V_{GFM}) and SCLs (SCL_{SG}, SCL_{GFL}, and SCL_{GFM}) at the POIs, total active load (L_t^T), and active power generated through GFM (P_{GFM}). These elements are regarded as inputs while also taking into account the reward spaces that they provide. According to the framework of the presented method, the reward ($R_t = r_f + r_V + r_{SCL}$) is calculated, on the basis of which the DRL proposes a control action over the power system. It is well known that the frequency should be near 50 Hz; if the frequency makes an attempt to be close to 50 Hz, a reward (r_f) will be awarded, and a deduction will be applied if the frequency deviates farther from 50 Hz, as shown in Equation (24).

11

$$r_f = \begin{cases} 1 & \text{for } |df| \leq 0.1\text{Hz} \\ 0 & \text{for } 0.1 \leq |df| \leq 0.2\text{ Hz} \\ -e^{-|df|t} & \text{otherwise} \end{cases} \tag{24}$$

Similar to this, set points for voltages are thought to be represented by values of 1 pu, and the reward (r_V) of 1 will be provided for $|dV| \leq 0.02$ pu, 0 for $0.02 \leq |dV| \leq 0.05$, and exponential deduction will be applied for $0.05 \leq |dV|$. The SCLs at each POI are considered for calculating the reward (r_{SCL}) in the very last, but most important phase. SCLs are believed to be able to recognize the secure functioning of the power system within these reward areas. This is because, in order to estimate the absolute minimum degree of security that must be satisfied, the authors employed SS as an indicator for the power system. As a result, a SCL_{min} value is considered as the standard, and situations that fall within the bounds are considered secure while those that go over the limits are not. Since SCL is one of the important factors that used in this study, the reward allocated for this constraint is considered to be twice of others; when the generator is in secure condition (i.e., under SCL_{min} limit), r_{SCL} =2; otherwise, -2 is rewarded. These rewards apply to all three power-generating technologies.

In contrast, the action spaces represent incremental changes that are made to the generating set points for SG (ΔP_{SG}) and GFL (ΔP_{GFL}) as a consequence of training interactions between the DRL agent and its environment, rather than the ideal generator set points. Although the training objective is to acquire the secure status in a single step, a well-trained DRL agent would be able to obtain the secure status adaptively during the online testing procedure with several adjustment phases.

5. EVALUATION AND OUTCOMES

The IEEE 9 bus system with SG, GFL, and GFM, as shown in Fig. 2, is utilized as the experimental model to gather the dataset as well as to conduct the online test. On the other hand, the DRL technique equipped with data-driven features is used here as the decision-making tool for this investigation. The DRL runs on Python where OpenAI gym is used to create a reinforcement learning environment, whereas the power system operates within a time-domain framework that is provided by the MATLAB Simulink environment. Integrating the operation of these two frameworks is accomplished via the usage of the Python interpreter. The main objective of this integration is to conduct the online test and analyze the performance of the presented methodology with proper validation. The HP ZBook Fury 15 G7 Mobile Workstation, with a processor specification of Intel® Core™ i7-10750 CPU @ 2.60GHz 2.59GHz, 64-bit operating system, and 32 GB of internal RAM, is used for the whole experiment. The processes that are used to run the model in this paper are outlined in Algorithm 1. The outcomes of this analysis are described in sub-sections 5.1 and 5.2.

Algorithm 1	
1	Initialize the neural network
2	Tune the hyperparameters and train the neural network using previously available data.
3	Create a reinforcement learning environment in an OpenAI gym for reinforcement learning.
	A. Initialize action discretization strategy and observation space using gym.
	B. Define a method for dynamic exploration and exploitation rate.
	C. Initialize the communication between reinforcement learning agents in Python and MATLAB Simulink environment.
4	Control the Simulink environment using a reinforcement learning agent and collect the feedback as a reward from the environment.
	A. Give a reward to the associated action based on equation 21.
	B. Optimize the neural network using the Boltzmann optimization method.
5	Repeat step 4 until the training is complete.

5.1. Offline training

Before running the neural network with a reinforcement learning-based environment, the network is first trained offline using collected datasets under considered scenarios. The authors have amassed 792,000 samples, each of which has a resolution of 10 milliseconds and is collected across time intervals ranging from 20 to 50 seconds. After the samples have been collected, the dataset is then used to train and validate the presented data-driven model first. The semi-trained network is then imported into the reinforcement learning environment for further online training. In this process, 95% of the dataset is considered for training purposes and the remaining 5% for validation. The random data splitting method is used to separate the original dataset into training and validation. After that, the epsilon greedy as exploration strategy is used to ensure that the DQN is able to explore the environment and learn a good policy. The adopted DQN's performance indexes and hyperparameters used in this paper are listed in Table 2. For the hyperparameter tuning, the authors used the deep learning application provided by MATLAB software, and value error as the optimization function. The value limits used for hyperparameter tuning are listed in Table 3.

TABLE 2: Performance index and hyperparameters for the DQN agent

Parameters	Value/ types
Optimizer	Adam
Epochs	2000
Batch size	200
Discount factor	0.99
Number of hidden layers	2
1st hidden layer	20 hidden units, tanh activation function, input dimension =3, uniform initializer
2nd hidden layer	20 hidden units, relu activation function, uniform initializer
output layer	1-unit, linear activation function, uniform initializer
Exploration rate	0.99
Learning rate	0.001

TABLE 3: Hyperparameters ranges/ types for tuning

Parameters	Value/ types
Batch size	[100, 200, 300, 400, 500]
Discount factor	[0.95, 0.96, 0.97, 0.98, 0.99]
Number of hidden layers	[1, 2, 3, 4, 5, 6]
Number of units in 1st hidden layer	[10, 20, 30, 40, 50, 60, 70, 80, 90, 100]
Number of units in 2nd hidden layer	[10, 20, 30, 40, 50, 60, 70, 80, 90, 100]
Activation function	[tanh, relu]
Learning rate	[0.0001, 0.001, 0.01, 0.1]

A graphical representation of the datasets is shown in Fig. 7, where the load is thought to be a function of P_{SG}, P_{GFL}, and P_{GFM}. This figure makes it abundantly evident that, when the load is modest, SG and GFM provide the power. As the demand grows, so does the output from all power-generating technologies. However, the GFL provides the supply for heavy loads or in the event that the GFM supply is insufficient. According to this pattern, the SG seems to be the fundamental source of power for all levels of loads, while the GFL provides power for higher levels of loads.
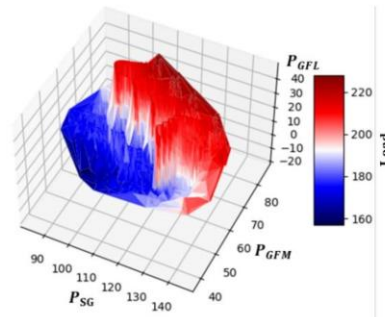

Fig. 7. Graphical representation of pre-trained datasets as the function of P_{SG}, P_{GFM}, P_{GFL} and load.

These datasets have been used for the purpose of training as mentioned; the nature of the loss function that is accomplished when training the presented trained model is shown in Fig. 8. The loss function seems to have a dramatic drop until it reaches around 300 epochs, which occurs as the number of epochs increases. After 400 epochs, the loss function seems to be minimized and moving toward stable values, even though minor variations may still be noticed. Similarly, Fig. 9 presents the performance of training and validation via the use of the regression approach. After looking at Figures 8 and 9, one can conclude that the trained model that is shown has a good level of performance for the datasets and circumstances that are considered.

13
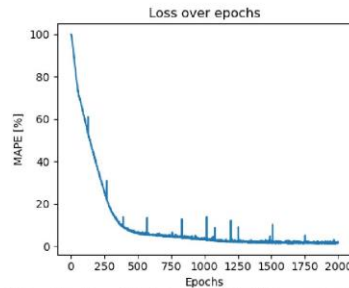
**Fig. 8.** Loss function of the trained model with increasing Epochs.
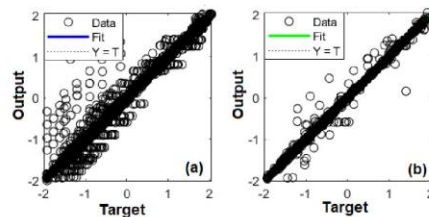
Fig. 9. Normalized regression plots for P_{GFL} (a) training, and (b) validation.

5.2. Online testing

In the context of offline training and online testing, offline training refers to the process of training a model using collected datasets, and online testing refers to the process of evaluating the model under new conditions that have not been seen before; both are complementary processes. Offline training, as is covered in the previous sub-section, entails training a model using data obtained by conducting simulations in MATLAB/ Simulink. After the presented model has been trained, it is taken to test on random data by running simulations in an environment that combines the capabilities of Python and Simulink. This makes it possible to evaluate how well the model works with data that has not been seen before and to see how it reacts to a variety of different scenarios. In this study, a random fraction of the system's total load is varied at regular intervals of one second, and the resulting effects on the system are analyzed. To make an observation, the online testing is carried out for one minute; the responses can be seen in Fig. 10.

The responses include total load, frequencies, terminal voltages, and generated powers for these three power-generating technologies. In addition, the reward function is also included to analyze the system's performance. With the change in load, the power-generating technologies tried to manage the supply-demand balance by increasing or reducing the generations. However, there are some constraints (as given in Equations 7–13) that the generators must follow. With the change in load, the frequency seems to be fluctuating, but the frequency deviation is observed as being under the standard limit as per the Nordic grid code. Similarly, the voltage deviation for GFM and GFL seems small, but that for SG seems quite higher during a sudden load change. Talking about the generated power from these three power-generating technologies, these technologies must follow constraints while increasing or decreasing the generations, and they are dependent on the availability of the sources; the main role seems to be played by the GFL to maintain the system balance. Finally, based on the conditions made for reward, as in sub-section 4.2, the environment provides the regular reward to DQN, which is also considered and shown in Fig. 10.

Fig. 11 illustrates the distribution of the power generated through the power-generating technologies with respect to load when online testing is carried out for a period of one minute. As was previously mentioned, the load varies at a random rate within an interval of one second. Fig. 11(a-c) presents the distribution of the generated power from these three power-generating technologies in order to meet the demand and keep the system secure. Among the power generation technologies, the GFL seems to be the most diverse and reliable for providing energy since it supplies power throughout crucial periods. It is possible to notice it in Fig. 12, where the distribution of GFL seems to be rather diverse in relation to load.

14
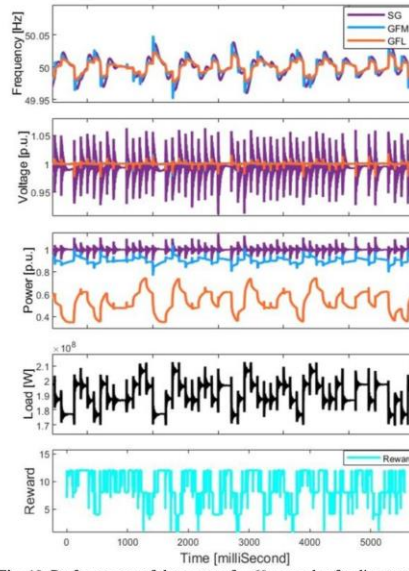
Fig. 10. Performances of the system for 60 seconds of online testing.
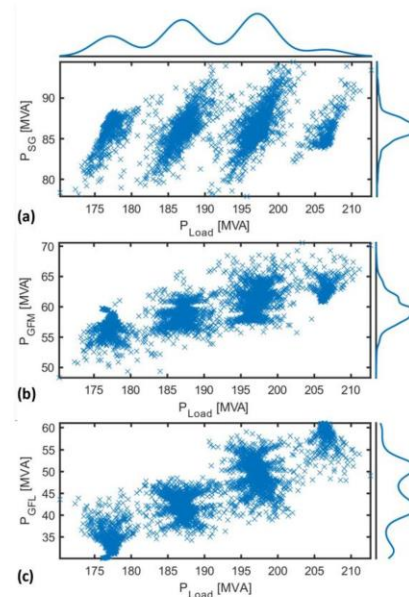

Fig. 11. Distribution of generations from three power-generating technologies with load for 60 seconds of online testing. The curve at the top and right sides indicate the density of the continuous distributions.
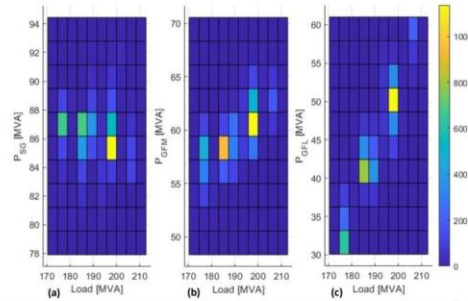
Fig. 12. Bivariate histogram of generations from three power-generating technologies with respect to total load.

Fig. 13 and Fig. 14 serve as empirical benchmarks for assessing the robustness of a power system through the lens of SS, an attribute intricately linked to the operational security of modern power systems. The SS is a measure of a grid's ability to uphold stable voltage levels amidst disturbances; a high SS denotes a strong grid, a characteristic reflective of a resilient and robust system, whereas a low SS points to a weak grid, susceptible to voltage instability [50]. The graphs in Fig. 13 illustrate the distribution of SCL values at the POIs for three different power-generating technologies. These SCL measurements, derived from the ratio of pre-fault voltage to total system impedance, are critical in signifying the SS at each POI. In the context of Fig. 13, the SCL values are observed to be consistently above the 1.6 pu threshold, with a majority clustering above 1.9 pu, thereby exceeding the minimum SCL indicative of a strong grid. Such high values of SCL are emblematic of a robust grid capable of mitigating voltage disturbances and ensuring secure operation, particularly in an online setting where the system is dynamically exposed to real-time changes in load and generation patterns. Likewise, Fig. 14 reinforces the findings of Fig. 13 with a similar pattern of SCL distribution across the POIs. The sustained high SCL values in both figures imply that the power system under analysis possesses substantial fault levels, hence a remarkable SS. This robust SS is critical in a power system that integrates a higher proportion of IBRs. IBRs are known to contribute less to fault currents, thereby typically leading to a reduced SS. However, the data presented suggest that the SGs within the system are providing sufficient fault current contributions to maintain a high level of SS, which is vital for the stability and security of the power system. The consistently high SCL values across both figures highlight not only the resilience of the grid but also the efficacy of the model used to simulate and ensure secure power system operation. Thus, these figures are indicative of a power system that is well-equipped to handle the dynamic challenges posed by modern power system demands, indicating the reliability of the underlying security assessment model.
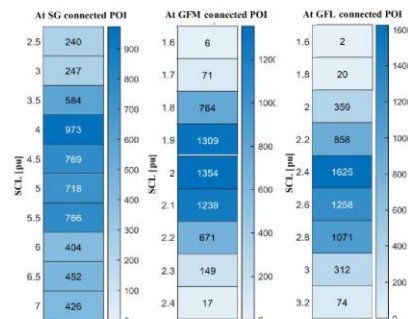

Fig. 13. Values of SCLs at the POIs connecting (a) SG, (b) GFM, and (c) GFL, for 60 seconds of online testing with 10-millisecond resolutions

16
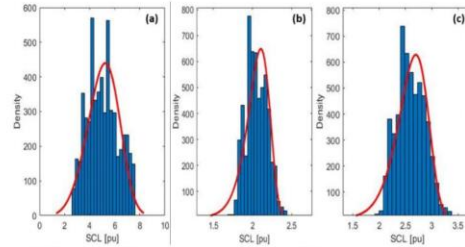
Fig. 14. Density function of SCLs at the POIs connecting (a) SG, (b) GFM, and (c) GFL, for 60 seconds of online testing.

5.3. Overview of the results

Based on the case study and the DRL model described in this paper, the key insights are summarized in the points below:

a. **Frequency and voltage stability:** The system's frequency response has proven to be exceptionally stable, with observed variations remaining within a narrow band of ±0.05 Hz. Terminal voltage stability, which is a vital sign of electrical robustness, maintained commendable consistency with deviations contained within ±2% for GFM and GFL technologies. The SGs showed marginally higher voltage fluctuations but stayed comfortably within the broader acceptable range of ±10%. These results collectively demonstrate the system's inclination to counter potential threats, ensuring continuous and stable power delivery.

b. **Generation constraints and system resilience:** The power-generating technologies, in their pursuit to match supply with demand, particularly under varying load conditions, followed closely to the constraints. The GFL, in particular, emerged as an adaptable and reliable source of energy, efficiently adjusting its output in response to the grid's demands. This behavior accentuates the system's inherent resilience and its ability to operate securely under varying conditions.

c. **SS and SCL:** Utilizing SCL as an indicator of the power system's strength has provided key insights. The consistently high SCL values (>1.6 pu), especially at the SG's POI (>2.5 pu), highlight the system's resilience. Such high values indicate the system's robustness, its capacity to handle disturbances, and its capability to mitigate potential risks associated with short circuits.

d. **DRL and system performance:** The consistent rewards obtained in the DRL model, serve as a testament to the system's devotion to secure operational parameters. These rewards, aligned with the system's stability and security goals, exemplify how the proposed DRL-based approach inherently tends towards configurations that promise system security.

e. **Operational overview with online testing:** The system showcased representative adaptability in satisfying randomly varying loads, signifying its readiness to handle unforeseen disturbances. This operational state reassures the system's capability to maintain a secure and stable environment.

To summarize, the findings from the considered case studies have robustly demonstrated the capability of the proposed DRL-based approach to enhance and ensure power system stability and security. It presents a promising avenue for contemporary grid management, aligning with the global mandate for secure, resilient, and sustainable power systems.

6. DISCUSSION

The rapid transformation across various industries has underscored the pivotal role of electricity as a fundamental pillar of modern society. With growing concerns about environmental sustainability, the escalating adoption of RESs has become vital. This shift is evidenced by the substantial rise in the proportion of RESs within the global electricity generation mix. However, this transition to RESs, particularly IBRs, has introduced unprecedented complexities and challenges to power system operation, planning, and economics. The evolving dynamics of power systems demand innovative approaches to address issues related to frequency control, voltage regulation, fault management, and other critical factors.

To bridge the gap between traditional power system methodologies and the sophisticated demands of modern converter-dominated power systems, this paper introduces a DRL-based approach. The central problem addressed is the secure and optimal management of power-generating technologies, specifically GFM and GFL, within the context of converter-dominated power systems. As the adoption of RESs accelerates, understanding and efficiently managing the energy-mix proportion becomes crucial to ensure stable power system operation.

The presented methodology employed in this study utilizes the hybrid approach in applying DQN to power system operations, integrating offline training to enhance real-time decision-making efficiency. This hybrid approach effectively addresses the computational complexities inherent in model-based simulations, enabling both efficient and precise estimation of the proportions of different power-generating technologies. The innovative use of a framework, combining MATLAB/Simulink and Python libraries, for offline training and online testing enhances the practical applicability and real-world pertinence of this approach.

The results of the research highlight the efficacy of the presented methodology in accurately determining the energy-mix proportion, crucial for the secure operation of converter-dominated power systems. Through experimental evaluations on the IEEE-9 bus system, which integrates GFM, GFL, and SG technologies, the model demonstrated its proficiency in optimizing power

generation across a spectrum of energy sources. The study's application of the SCL as a robustness indicator proved valuable in evaluating power system security. The model demonstrated dynamic responsiveness to varying load conditions, efficiently balancing supply and demand while adhering to operational constraints. Furthermore, the GFM and GFL technologies showcased their adaptability and reliability in the face of load fluctuations, substantiating their viability in modern power system management.

This paper, while pioneering in its approach and presenting substantial insights, acknowledges certain limitations. The study, fixed in the IEEE-9 bus system, serves as a representative model but might not condense the complexities inherent to larger, real-world power systems. The complexity and varied nature of these systems might introduce additional challenges, something this analysis does not completely address. Additionally, while the research highlights the advantages of employing AI techniques, primarily due to their potential computational efficiency, a direct comparison with model-based or other traditional approaches has not been performed to substantiate this claim. This leaves a gap in empirically validating the assumed computational benefits. Moreover, certain potential technical impediments, especially concerning real-time deployment and application, remain unexplored in the present methodology.

Building on the foundation laid by this paper, there is a prolific ground for subsequent research. One immediate extension would be the inclusion of larger, more complex power systems to validate the scalability and effectiveness of the DQN algorithm. Further experimental studies comparing AI methods with traditional approaches, focusing on computational efficiency and resource optimization, would be indispensable. Expressing the integration of cutting-edge AI techniques or hybrid models that synergize DRL with other optimization strategies could unearth solutions for enhanced power system stability and efficacy. The DRL framework presented here showcases enormous promise for tangible applications within actual power systems. Its proficiency in determining energy-mix proportion and strengthening power system security is in line with the surging demand for flexible and resilient solutions in a landscape dominated by converters. Harnessing the knowledge and breakthroughs shared in this paper, stakeholders in power systems – from operators to planners – can devise innovative strategies to adeptly navigate the complexities accompanied by RESs and IBRs, steering us towards a greener, more secure energy horizon.

7. CONCLUSION

This paper advances the field of power system management by introducing a novel DRL-based approach for optimizing power-generating technologies in converter-dominated power systems. Through the application of the DQN approach and the utilization of the online SCL as a robustness metric, this research provides valuable contributions to both theory and practice. The experimental results demonstrate the DQN's efficacy in estimating energy-mix proportions and securely operating power systems under real-world conditions. While acknowledging its limitations, this research paves the way for future investigations into the integration of advanced AI techniques for power system optimization and operation. The findings highlight the potential for a more sustainable and efficient energy landscape through the strategic implementation of DRL-based methodologies.

REFERENCES

[1]   H. Ritchie and M. Roser, "Electricity Mix," Our World in Data, 2022. [Online]. Available: https://ourworldindata.org/electricity-mix

[2]   A. Shrestha and F. Gonzalez-Longatt, "Frequency stability issues and research opportunities in converter dominated power system," *Energies,* vol. 14, no. 14, p. 4184, 2021. [Online]. Available: https://www.mdpi.com/1996-1073/14/14/4184.

[3]   A. Shrestha and F. Gonzalez-Longatt, "Parametric sensitivity analysis of rotor angle stability indicators," *Energies,* vol. 14, no. 16, p. 5023, 2021.

[4]   A. Sajadi, R. W. Kenyon, and B.-M. Hodge, "Synchronization in electric power networks with inherent heterogeneity up to 100% inverter-based renewable generation," *Nature communications,* vol. 13, no. 1, pp. 1-12, 2022.

[5]   B. P. Heard, B. W. Brook, T. M. Wigley, and C. J. Bradshaw, "Burden of proof: A comprehensive review of the feasibility of 100% renewable-electricity systems," *Renewable and Sustainable Energy Reviews,* vol. 76, pp. 1122-1133, 2017.

[6]   T. Van Cutsem and C. Vournas, *Voltage stability of electric power systems.* Springer Science & Business Media, 1998.

[7]   T. Ananthapadmanabha, A. Kulkarni, M. Pujar, H. Pradeep, and S. Chetan, "Rotor angle stability analysis of a distributed generator connected to distribution network," *Journal of Electrical and Electronics Engineering Research,* vol. 2, no. 5, pp. 107-113, 2010.

[8]   Z. A. Obaid, L. M. Cipcigan, L. Abrahim, and M. T. Muhssin, "Frequency control of future power systems: reviewing and evaluating challenges and new control methods," *Journal of Modern Power Systems and Clean Energy,* vol. 7, no. 1, pp. 9-25, 2019.

[9]   Y. Cheng, R. Azizipanah-Abarghooee, S. Azizi, L. Ding, and V. Terzija, "Smart frequency control in low inertia energy systems based on frequency response techniques: A review," *Applied Energy,* vol. 279, p. 115798, 2020.

[10]   M. Kosmecki *et al.*, "A Methodology for Provision of Frequency Stability in Operation Planning of Low Inertia Power Systems," *Energies,* vol. 14, no. 3, p. 737, 2021.

[11]   S. Martinez Romero *et al.*, "Grid Integration Requirements for Variable Renewable Energy," The World Bank, 2019.

[12]   J. Rocabert, A. Luna, F. Blaabjerg, and P. Rodriguez, "Control of power converters in AC microgrids," *IEEE transactions on power electronics,* vol. 27, no. 11, pp. 4734-4749, 2012.

[13]   A. D. Paquette, M. J. Reno, R. G. Harley, and D. M. Divan, "Sharing transient loads: Causes of unequal transient load sharing in islanded microgrid operation," *IEEE Industry Applications Magazine,* vol. 20, no. 2, pp. 23-34, 2013.

18

[14] H. Xin, Y. Wang, X. Liu, B. Tang, G. Yu, and L. Huang, "How Many Grid-Forming Converters do We Need? A Perspective From Power Grid Strength," *arXiv preprint arXiv:2209.10465,* 2022.

[15] L. Huang *et al.*, "Grid-synchronization stability analysis and loop shaping for PLL-based power converters with different reactive power control," *IEEE Transactions on Smart Grid,* vol. 11, no. 1, pp. 501-516, 2019.

[16] B. Shakerighadi *et al.*, "An overview of stability challenges for power-electronic-dominated power systems: The grid-forming approach," *IET Generation, Transmission & Distribution,* vol. 17, no. 2, pp. 284-306, 2023.

[17] F. F. Ardakani, S. B. Mozafari, and S. Soleymani, "Scheduling energy and spinning reserve based on linear chance constrained optimization for a wind integrated power system," *Ain Shams Engineering Journal,* vol. 13, no. 3, p. 101582, 2022.

[18] Z. Tang, Y. Liu, L. Wu, J. Liu, and H. Gao, "Reserve model of energy storage in day-ahead joint energy and reserve markets: A stochastic UC solution," *IEEE Transactions on Smart Grid,* vol. 12, no. 1, pp. 372-382, 2020.

[19] Y. Zuo, Z. Yuan, F. Sossan, A. Zecchino, R. Cherkaoui, and M. Paolone, "Performance assessment of grid-forming and grid-following converter-interfaced battery energy storage systems on frequency regulation in low-inertia power grids," *Sustainable Energy, Grids and Networks,* vol. 27, p. 100496, 2021.

[20] M. N. Acosta Montalvo, "Intelligent frequency control for the secure operation of modern power system," PhD, University of Southeastern Norway, 103, 2021.

[21] Y. Gu and L. Xie, "Early detection and optimal corrective measures of power system insecurity in enhanced look-ahead dispatch," *IEEE Transactions on Power Systems,* vol. 28, no. 2, pp. 1297-1307, 2012.

[22] Y. Gu and L. Xie, "Stochastic look-ahead economic dispatch with variable generation resources," *IEEE Transactions on Power Systems,* vol. 32, no. 1, pp. 17-29, 2016.

[23] C. Tang *et al.*, "Look-ahead economic dispatch with adjustable confidence interval based on a truncated versatile distribution model for wind power," *IEEE Transactions on Power Systems,* vol. 33, no. 2, pp. 1755-1767, 2017.

[24] L. Xie, Y. Gu, X. Zhu, and M. G. Genton, "Short-term spatio-temporal wind power forecast in robust look-ahead power system dispatch," *IEEE Transactions on Smart Grid,* vol. 5, no. 1, pp. 511-520, 2013.

[25] A. Shrestha *et al.*, "Peer-to-peer energy trading in micro/mini-grids for local energy communities: A review and case study of Nepal," *IEEE access,* vol. 7, pp. 131911-131928, 2019.

[26] T. B. Malla, A. Bhattarai, A. Parajuli, A. Shrestha, B. B. Chhetri, and K. Chapagain, "Status, Challenges and Future Directions of Blockchain Technology in Power System: A State of Art Review," *Energies,* vol. 15, no. 22, p. 8571, 2022.

[27] M. A. Yassin, A. Shrestha, and S. Rabie, "Digital twin in power system research and development: Principle, scope, and challenges," *Energy Reviews,* p. 100039, 2023.

[28] M. M. Hossain and C. Peng, "Cyber–physical security for on-going smart grid initiatives: a survey," *IET Cyber-Physical Systems: Theory & Applications,* vol. 5, no. 3, pp. 233-244, 2020.

[29] T. Krause, R. Ernst, B. Klaer, I. Hacker, and M. Henze, "Cybersecurity in power grids: Challenges and opportunities," *Sensors,* vol. 21, no. 18, p. 6225, 2021.

[30] D. E. A. Mansour *et al.*, "Applications of IoT and digital twin in electrical power systems: A comprehensive survey," *IET Generation, Transmission & Distribution,* 2023.

[31] A. Marahatta, Y. Rajbhandari, A. Shrestha, S. Phuyal, A. Thapa, and P. Korba, "Model predictive control of DC/DC boost converter with reinforcement learning," *Heliyon,* vol. 8, no. 11, 2022.

[32] Y. Rajbhandari *et al.*, "Impact study of temperature on the time series electricity demand of urban nepal for short-term load forecasting," *Applied System Innovation,* vol. 4, no. 3, p. 43, 2021.

[33] A. Shrestha, B. Ghimire, and F. Gonzalez-Longatt, "A Bayesian model to forecast the time series kinetic energy data for a power system," *Energies,* vol. 14, no. 11, p. 3299, 2021.

[34] S. Afzal, H. Mokhlis, H. A. Illias, N. N. Mansor, and H. Shareef, "State-of-the-art review on power system resilience and assessment techniques," *IET Generation, Transmission & Distribution,* vol. 14, no. 25, pp. 6107-6121, 2020.

[35] H. Raoufi, V. Vahidinasab, and K. Mehran, "Power systems resilience metrics: A comprehensive review of challenges and outlook," *Sustainability,* vol. 12, no. 22, p. 9698, 2020.

[36] M. Panteli, P. Mancarella, D. N. Trakas, E. Kyriakides, and N. D. Hatziargyriou, "Metrics and quantification of operational and infrastructure resilience in power systems," *IEEE Transactions on Power Systems,* vol. 32, no. 6, pp. 4732-4742, 2017.

[37] M. Gol, A. Abur, and F. Galvan, "Metrics for success: Performance metrics for power system state estimators and measurement designs," *IEEE Power and Energy Magazine,* vol. 10, no. 5, pp. 50-57, 2012.

[38] D. Wu, G. Li, M. Javadi, A. M. Malyscheff, M. Hong, and J. N. Jiang, "Assessing impact of renewable energy integration on system strength using site-dependent short circuit ratio," *IEEE Transactions on Sustainable Energy,* vol. 9, no. 3, pp. 1072-1080, 2017.

[39] TransGrid, "National Electricity Rules change proposal: Efficient management of system strength on the power system," Australian Energy Market Operator (AEMO), Australia, 2020. [Online]. Available: https://www.aemc.gov.au/sites/default/files/documents/erc0300_rule_change_request_pending.pdf

[40] I. H. Sarker, "Data science and analytics: an overview from data-driven smart computing, decision-making and applications perspective," *SN Computer Science,* vol. 2, no. 5, p. 377, 2021.

[41] I. H. Sarker, M. H. Furhad, and R. Nowrozy, "Ai-driven cybersecurity: an overview, security intelligence modeling and research directions," *SN Computer Science,* vol. 2, pp. 1-18, 2021.

[42] A. S. Zamzam, X. Fu, and N. D. Sidiropoulos, "Data-driven learning-based optimization for distribution system state estimation," *IEEE Transactions on Power Systems,* vol. 34, no. 6, pp. 4796-4805, 2019.

[43] J. D. Lara, R. Henriquez-Auba, D. Ramasubramanian, S. Dhople, D. S. Callaway, and S. Sanders, "Revisiting Power Systems Time-domain Simulation Methods and Models," *arXiv preprint arXiv:2301.10043,* 2023.

[44] L. Fan, Z. Miao, P. Shah, P. Koralewicz, V. Gevorgian, and J. Fu, "Data-driven dynamic modeling in power systems: A fresh look on inverter-based resource modeling," *IEEE Power and Energy Magazine,* vol. 20, no. 3, pp. 64-76, 2022.

[45] E. Davis and G. Marcus, "The scope and limits of simulation in automated reasoning," *Artificial Intelligence,* vol. 233, pp. 60-72, 2016.

[46] Y. Maccarana, A. Panza, G. Maroni, L. Sarto, M. F. Carta, and S. Reggiani, "Comparison of model-based and data-driven approaches for modeling energy and comfort management systems, with a case study," in *2019 IEEE International Conference on Environment*

19

and Electrical Engineering and 2019 IEEE Industrial and Commercial Power Systems Europe (EEEIC/I&CPS Europe), 2019: IEEE, pp. 1-6.

[47] A. Shrestha, Y. Rajbhandari, and F. Gonzalez-Longatt, "Day-ahead energy-mix proportion for the secure operation of renewable energy-dominated power system," *International Journal of Electrical Power and Energy Systems,* vol. 155, no. 109560, 2024, doi: 10.1016/j.ijepes.2023.109560.

[48] P. M. Anderson and A. A. Fouad, *Power system control and stability.* John Wiley & Sons, 2008.

[49] Nordel, "Nordic Grid Code 2007 (Nordic collection of rules)," 2007. [Online]. Available: https://eepublicdownloads.entsoe.eu/clean-documents/pre2015/publications/nordic/planning/070115_entsoe_nordic_NordicGridCode.pdf

[50] A. E. M. Commission, "National electricity amendment (managing power system fault levels) rule 2017," ed, 2017.

[51] D. Kim, H. Cho, B. Park, and B. Lee, "Evaluating influence of inverter-based resources on system strength considering inverter interaction level," *Sustainability,* vol. 12, no. 8, p. 3469, 2020.

[52] AEMO, "System Strength: System strength in the NEM explained," Australian Energy Market Operator Limited, Australia, 2020. [Online]. Available: https://aemo.com.au/-/media/files/electricity/nem/system-strength-explained.pdf

[53] AEMO, "NEM Engineering Framework," Australian Energy Market Operator, 2021. [Online]. Available: https://aemo.com.au/-/media/files/initiatives/engineering-framework/2021/nem-engineering-framework-march-2021-report.pdfs

[54] G. Murphy, J. Outram, R. Bryans, M. Bebbington, V. Outram, and M. Khaddoumi, "Real time fault level monitoring," 2019.

[55] C. J. Watkins and P. Dayan, "Q-learning," *Machine learning,* vol. 8, no. 3, pp. 279-292, 1992.

[56] L. Matignon, G. J. Laurent, and N. Le Fort-Piat, "Independent reinforcement learners in cooperative markov games: a survey regarding coordination problems," *The Knowledge Engineering Review,* vol. 27, no. 1, pp. 1-31, 2012.

[57] M. Gheisarnejad, H. Farsizadeh, and M. H. Khooban, "A novel non-linear deep reinforcement learning controller for DC/DC power buck converters," *IEEE Transactions on Industrial Electronics,* 2020.

[58] C. Cui, N. Yan, and C. Zhang, "An Intelligent Control Strategy for buck DC-DC Converter via Deep Reinforcement Learning," *arXiv preprint arXiv:2008.04542,* 2020.

[59] A. Sri, "Everything you need to know about Reinforcement Learning in 80 minutes." [Online]. Available: https://srianumakonda.medium.com/everything-you-need-to-know-about-reinforcement-learning-in-80minutes-4cd5a365e340

[60] L. Pan, Q. Cai, Q. Meng, W. Chen, L. Huang, and T.-Y. Liu, "Reinforcement learning with dynamic boltzmann softmax updates," *arXiv preprint arXiv:1903.05926,* 2019.

[61] Z.-W. Hong, S.-Y. Su, T.-Y. Shann, Y.-H. Chang, and C.-Y. Lee, "A deep policy inference q-network for multi-agent systems," *arXiv preprint arXiv:1712.07893,* 2017.

[62] T. Schaul, J. Quan, I. Antonoglou, and D. Silver, "Prioritized experience replay," *arXiv preprint arXiv:1511.05952,* 2015.

[63] W. Dabney, M. Rowland, M. Bellemare, and R. Munos, "Distributional reinforcement learning with quantile regression," in *Proceedings of the AAAI Conference on Artificial Intelligence,* 2018, vol. 32, no. 1.

[64] K. Arulkumaran, M. P. Deisenroth, M. Brundage, and A. A. Bharath, "A brief survey of deep reinforcement learning," *arXiv preprint arXiv:1708.05866,* 2017.

Estimation of the energy-mix proportion for the secure operation of converter dominated power system
Ashish Shrestha

usn.no